Reactions of long-lived lens proteins

A thesis submitted in fulfilment of the requirements for the degree of

Doctor of Philosophy

From

Save Sight Institute

School of Medicine

By

Brian Lyons

BSc (Hons)

Aug 2012

Thesis Declaration

"I hereby declare that this thesis is my own work, except where due acknowledgement is made in the thesis. To the best of my knowledge, the thesis contains no materials previously published or written by another person, or substantial proportions of material which have been accepted for the award of any other degree or diploma at The University of Sydney or any other educational institution.

I also declare that the intellectual content of this thesis is the product of my own work, except to the extent that assistance from others in the research design and conception or in style, presentation and linguistic expression is acknowledged. Any contribution made to the research by others, with whom I have worked at The University of Sydney or elsewhere, is explicitly acknowledged in the thesis.

All experiments described in this thesis were performed at the Save Sight Institute (Sydney Medical School, University of Sydney, Sydney Eye Hospital Campus, Sydney, NSW, Australia) and at Macquarie University (North Ryde, Sydney NS Australia).

Brian Lyons

Signed ……..

Date ……..

Acknowledgements

- To my supervisors Professor Roger Truscott and Professor Joanne Jamie for all their hard work, patience and guidance throughout all aspects of this project.

- To Dr Michael Friedrich, Michelle Hooi and all other members of the Truscott, Jamie and Gillies research groups for their friendship, advice and assistance with this thesis.

- To Dr Michelle Madigan for all her help and advice with preparation of this thesis.

- To Professor Mark Raftery for his help with the high resolution mass spectrometry analysis.

- To Dr Meidong Zhu and Dr Raj Devasahayam for their assistance with provision of human lens

- To Professor Peter Karusso and Dr Ann Kwan and for all their help and advice with NMR analysis and data interpretation.

- To Giovanni Crasto for his administrative help through the years.

- To Professor John McAvoy, Professor Peter McCluskey and Professor John Grigg for the support provided by the Save Sight Institute.

- To my uncle Willie for all his advice throughout university.

- To all my family and friends for putting up with me over the last 4 years.

- To my parents for all their help, support and encouragement and for believing in me.

- To Sam for all of her patience, encouragement and without whom this would not have been possible.

Publications

Sections of the work described in this thesis have been reported in the following publications:

1. Lyons, B., Jamie, J., Truscott, R.J.W., *Spontaneous Cleavage of Proteins at Serine Residues.* International Journal of Peptide Research and Therapeutics, 2011: p. **1-5**.

2. Truscott, R.J.W., Mizdrak, J., Friedrich, M., Hooi, M., Lyons, B., Jamie, J., Davies, M., Wilmarth, P., and L. David, *Is protein methylation in the human lens a result of non-enzymatic methylation by S-adenosylmethionine?* Experemental Eye Research, 2012. **99**: p. 48-54.

3. Su, S.P., B. Lyons, M. Friedrich, J.D. McArthur, X. Song, D. Xavier, J.A. Aquilina, and R.J. Truscott, *Molecular signatures of long-lived proteins: Autolytic cleavage adjacent to serine residues.* Aging Cell, 2012. **10.1111/j.1474-9726.2012.00860.x [doi]**.

4. Lyons, B., Kwan, A., Jamie, J., Truscott, R.J.W., *Age-dependent modification of proteins: N-terminal racemisation.* FEBS, **10.1111/febs.12217 [doi]**. (In Press)

Conference presentations

The abstract on which you are First Author has been accepted as a **Paper Presentation** at ARVO's 2012 Annual Meeting, Translational Research: Seeing the Possibilities, May 6-10, 2012, in Fort Lauderdale, Florida.

Program number: 3663

Abstract title: Reactions Responsible for the Degradation of Aged Human Lens Proteins

Author Block: Brian Lyons[1], Joanne Jamie[2], Roger Truscott[1]. [1]Save Sight Institute, Sydney University, Sydney, Australia; [2]Department of Chemistry and Biomolecular Sciences, Macquarie University, Sydney, Australia.

Introduction: Long-lived proteins, including those found in the lens, undergo numerous modifications as a result of prolonged exposure to physiological conditions, however the details of several of these reactions remain to be elucidated. These age-related modifications contribute to deterioration in health and fitness. One such major modification is racemisation, although the mechanism is not well understood.

Methods: Peptides were exposed to prolonged incubation at 37°C, as well as to elevated temperatures, at pH 7 and the products characterised using MALDI mass spectrometry, ESI mass spectrometry and NMR spectroscopy. One peptide examined, PFHSPS, is based on a sequence known to be modified in human αB-crystallin. All peptides had a C-Terminal Tyr added to aid detection by HPLC.

Results: Incubation of peptides PFHSPSY, PAHSPSY, PEHSPSY, PKHSPSY, resulted in facile racemisation of the N-terminal amino acid. Typically between 15 and 40% racemisation was observed after 2 weeks at 60°C.Incubating PFHSPSY under physiological conditions (37°C) resulted in ~5% racemisation after 8 weeks. AFHSPSY showed less N-terminal racemisation. Other modifications, for example, truncation of the peptides by loss of amino acid residues from the N-terminus were also observed.

Conclusions: Some reactions of long-lived proteins can be mimicked using exposure of peptides to elevated temperatures. The ramifications of N-terminal racemisation for protein structure and function are as yet unknown, although its impact will probably vary depending on the particular protein. In terms of susceptibility to enzymatic proteolysis, it is likely that having a D-amino acid at the N-terminus will inhibit cleavage of long-lived proteins by exopeptidases.

This thesis is dedicated to

my mum and dad

my family

my partner Sam

Abstract

The human lens contains the highest protein concentration of any tissue in the body, yet there is no protein turnover. As a result, proteins found in the centre of the lens (the nucleus) are present for a lifetime. This tissue can therefore be used to examine major posttranslational events that take place in long-lived proteins. Age-dependent deterioration of long-lived proteins in humans may have wide-ranging effects on health, fitness and diseases of the elderly [1]. To a large extent, denaturation of old proteins appears to result from the intrinsic instability of certain amino acids, however these reactions are incompletely understood.

In this thesis, to understand more about these reactions, the breakdown of peptides was studied under controlled conditions, typically at physiologically relevant pHs and with elevated temperatures used to promote the reaction. Significant truncation of long-lived proteins has been shown to occur in the aged human lens. In the case of α-crystallin, one notable feature of the sequences of two of the most abundant truncations (αA 67-80 and αB 1-18) was that sites of cleavage were adjacent to Ser residues. While the truncation of proteins at Asp/Asn residues *via* the formation of a succinimide ring has been well characterised, our understanding of the processes that enable truncation at Ser is incomplete. The first part of this thesis aimed at understanding the mechanisms behind this truncation. A secondary aim was to understand the mechanism behind the age-related racemisation of Ser residues seen in the lens, and determine if it occurs via a mechanism analogous to that seen with Asp residues.

Model peptides based on the sequence of known Ser truncation sites in human α-crystallin were exposed to elevated temperatures at physiological pH. Non-enzymatic truncation at the N-terminus of Ser, similar to that seen in the aged-lens was demonstrated. A range of additional factors were also examined for their ability to promote truncation. The role of the Ser hydroxyl group was investigated and found to play an important role in truncation at Ser. Interestingly Ser racemisation was also observed under these conditions, and it occurred regardless of the presence of a free or

blocked Ser hydroxyl group. This was at odds with our initial hypothesis that both racemisation of Ser and truncation the N-terminal side of Ser might be a linked process, occurring *via* formation of a cyclic tetrahedral intermediate.

Another possible source of Ser racemisation was investigated by examining the potential of phosphoser (pSer) residues to form dehydroalanine (DHA) *via* beta elimination. While DHA was generated from a model peptide at physiological pH, the results in this thesis did not find any evidence of water adding to the double bond, thus ruling it out as a possible explanation for Ser racemisation in the lens. However the observed formation of DHA at physiological pH does provide a potential explanation for the extensive non-covalent cross linking seen in aged lens proteins.

The second part of this thesis examined a range of modifications that can occur at a peptide N-terminus. Approximately 70% of soluble proteins in eukaryotic cells have an acetylated α amino group. One proposed role of this is that it protects the protein from a range of N-terminal modifications. However following age-related internal truncations, such as those observed at the N-terminus of Ser and other known truncations, the resulting protein fragments (with free amino groups) could then be subject to N-terminal degradation.

Using model peptides based on human lens crystallin sequences, facile racemisation of N-terminal residues incubated under physiological conditions was demonstrated. It was shown to occur across a range of N-terminal residues, buffers and temperatures. Unexpectedly the racemisation rate of L-residues was almost twice that of D-residues but the reasons for this are as yet unclear. A novel mechanism to explain these findings, involving the formation of a Schiff base has been proposed. Racemisation of the N-terminal residue was also shown to render the peptides resistant to amino peptidase degradation, suggesting a protective role could be provided by this modification.

The prevalence of this modification in the humans lens was then demonstrated using the integral membrane protein Aquaporin 0 (AQP0). By the age of 68, 13% of the N-terminal Met residue of

AQP0 had racemised in the cortex, increasing to 28% in the nucleus which is the oldest part of the lens.

Other N-terminal modifications studied included the degradation of model peptides *via* sequential loss of their N-terminal residues. Again it was shown to occur at physiological conditions using model peptides based on crystallin sequences, however further investigation revealed that it was more prominent in phosphate buffer. One potential mechanism involves phosphate buffer acting as a nucleophile. It is worth noting that phosphate buffer is present in the human lens and that this may still be a biologically relevant degradation process. Aged proteins demonstrating sequential loss of amino acid residues or "laddering" have been described in the literature [2].

The potential for proteins to degrade *via* loss of two amino acids at a time through a cyclic diketopiperazine (dkp) from the N-terminus was also investigated. A range of factors were considered and it was shown to be another potential degradation pathway for long-lived proteins which have a free amino termini. Peptides that have a penultimate Pro residue were particularly prone, with significant dkp formation occurring even at physiological temperatures. For peptides without a penultimate Pro, dkp formation was still observed for a range of peptides, but elevated temperatures were required.

The final part of this thesis detailed the isolation and characterisation of a novel UV filter found in the lens of the thirteen-lined ground squirrel. The structure of this UV filter is of interest due to the lens of the thirteen-ground squirrel having a similar UV filter profile to that of the human lens. Characterisation by mass spectrometry and NMR spectroscopy revealed the likely structure to be an *N*-acetylated 3OH Kynurenine adduct with the incorporation of a proline. A potential structure has been proposed involving the formation of an imine bond between the proline and the 3OH Kynurenine.

Table of Contents

Abbreviations

The following abbreviations are used throughout the text:

1D	One-dimensional
2D	Two-dimensional
3-OHKyn	3-Hydroxykynurenine
ACN	Acetonitrile
Amu	Atomic mass unit
AQP0	Aquaporin-0
COSY	Correlation spectroscopy
Da	Dalton
DHA	Dehydroalanine
Dkp	Diketopiperazine
EDTA	Ethylenediaminetetraacetic acid
ESI-MS	Electrospray-ionisation mass spectrometry
GSH	Reduced glutathione
HCl	Hydrochloric acid
HEPES	[4-(2-hydroxyethyl)piperazin-1-yl]ethanesulfonic acid
HMBC	Heteronuclear multiple bond coherence
HPLC	High pressure liquid chromatography
HSQC	Heteronuclear single quantum correlation
Kyn	Kynurenine
LAP	Leucine amino peptidase
LC-MS	Liquid chromatography mass spectrometry
m/z	Mass-to-charge ratio
MALDI	Matrix-assisted laser desorption ionisation
MES	2-(N-morpholino)ethanesulfonic acid
MS	Mass spectrometry
MS/MS	Tandem mass spectrometry
MW	Molecular weight
NaOH	Sodium hydroxide
NMR	Nuclear magnetic spectroscopy
NOESY	Nuclear overhauser effect spectroscopy
PE	Phenylethylamine
ppm	Parts per million
pSer	Phosphorylated Ser
PTMs	Post-translational modifications
ROESY	Rotational nuclear overhauser effect spectroscopy
RT	Retention time
TES	2[[1,3-dihydroxy-2-(hydroxymethyl)propan-2-yl]amino]ethanesulfonic acid
TOCSY	Total correlated spectroscopy
TOF	Time of flight
α-crystallin	Alpha crystallin

β-crystallin	Beta crystallin
γ-crystallin	Gamma crystallin
δ	Chemical shift

1 Chapter 1: Introduction

1.1 Overview

The human lens contains the highest protein concentration of any tissue in the human body, yet there is no protein turnover [1]. This means that the protein found in the centre of the lens (nucleus) is present for an entire lifetime. As a result, it is subject to numerous age-related modifications. Many of these modifications have been documented and studied, however it is likely many more remain to be elucidated. Additionally, the mechanisms behind some of these age-related modifications (such as truncation at the N-terminus of Ser) are not yet understood. The broad aim of this thesis was to use model peptides based on human lens protein sequences to investigate some of these modifications in an attempt to be better understand the mechanisms behind them. Potential new age-related modifications were also examined. This literature review section summarises some of the major components of the human lens as well as the age-related degradations that are known to occur that enable the findings outlined in this thesis to be put in context.

1.2 Implications of eye health

It was estimated that in 2012 there were 733 million people living with low vision or blindness worldwide, costing close to $3 trillion (US) dollars per year when all associated costs are included [3]. In Australia, the total health care cost of treating vision related disease was $2.58 billion (Aus) dollars in 2009, with over half a million people suffering from vision loss [4]. These costs are predicted to rise significantly by 2020 due to the increased ageing of the population [3, 4]. Numerous diseases can affect vision, including macular degeneration, retinopathy, glaucoma and cataract. Of these, cataract is the most common cause of blindness [5, 6] with an estimated 45 million people suffering from the disease globally. A study in 2005 by the Australian Institute of

Health and Welfare stated that in 2004 almost 1.5 million Australians aged 55 or over suffered from an untreated cataract [7].

Cataract is a cloudiness or opacification of the lens of the eye that can diminish visual acuity and visual function [8]. The most common form of cataract is age-related nuclear cataract (ARNC), which is responsible for 48% of world blindness [6, 9]. Surgical removal of the lens *via* phacoemulsification and intraocular lens implantation remains the only proven treatment for cataract [10], but this relatively costly procedure is beyond the means of many in the developing world [11, 12].

As people in the world live longer, the number of people with cataract is growing [3, 13]. Cataract and other vision diseases are placing a large financial strain on health budgets around the world, at a time when they can least afford them. It has been estimated that delaying cataract development by 10 years would decrease the need for cataract surgery by 45% [14]. Research into the fundamental causes of these age-related conditions is essential so that eventually non-surgical, cost effective treatment options can be developed.

1.3 Anatomy of the eye

The human eye (Figure 1-1) is the organ of sight. Covering its outermost layer is the cornea and the sclera. The cornea is a transparent viscoelastic tissue at the front of the eye. It contributes to the image-forming process by refracting light entering the eye. Covering the remainder of the outside of the eye is a tough white sheath called the sclera. The pupil is the opening in the iris through which light enters the eye. It can contract and expand, moderating the amount of light that enters the retina. The iris sits in front of the pupil and is a thin circular colored structure, which is responsible for adjusting the size of the pupil and preventing light scattering.

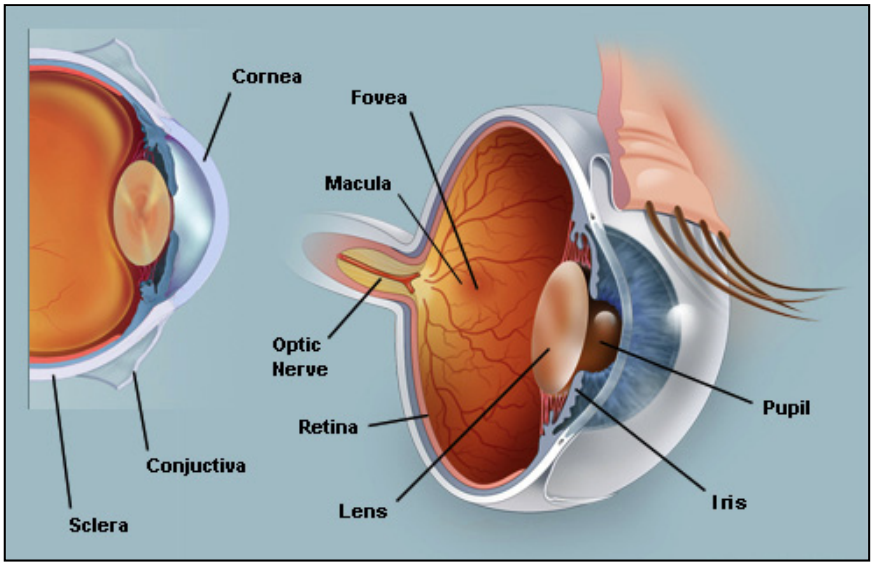

Figure 1-1: Diagram of the Human Eye. Adapted from [15].

The lens is a transparent tissue situated behind the iris and the pupil, and is held in place by zonular fibres attached to the ciliary body (Figure 1-2). Surrounding the iris and lens is the aqueous humour and behind the lens is the vitreous humour. The aqueous humour maintains intraocular pressure and provides nutrients, while the vitreous humour provides growth factors and also acts as a shock absorber. The retina is located at the back of the eye. It contains photosensitive elements (rods and cones) that convert light into nerve impulses that are then sent to the brain along the optic nerve.

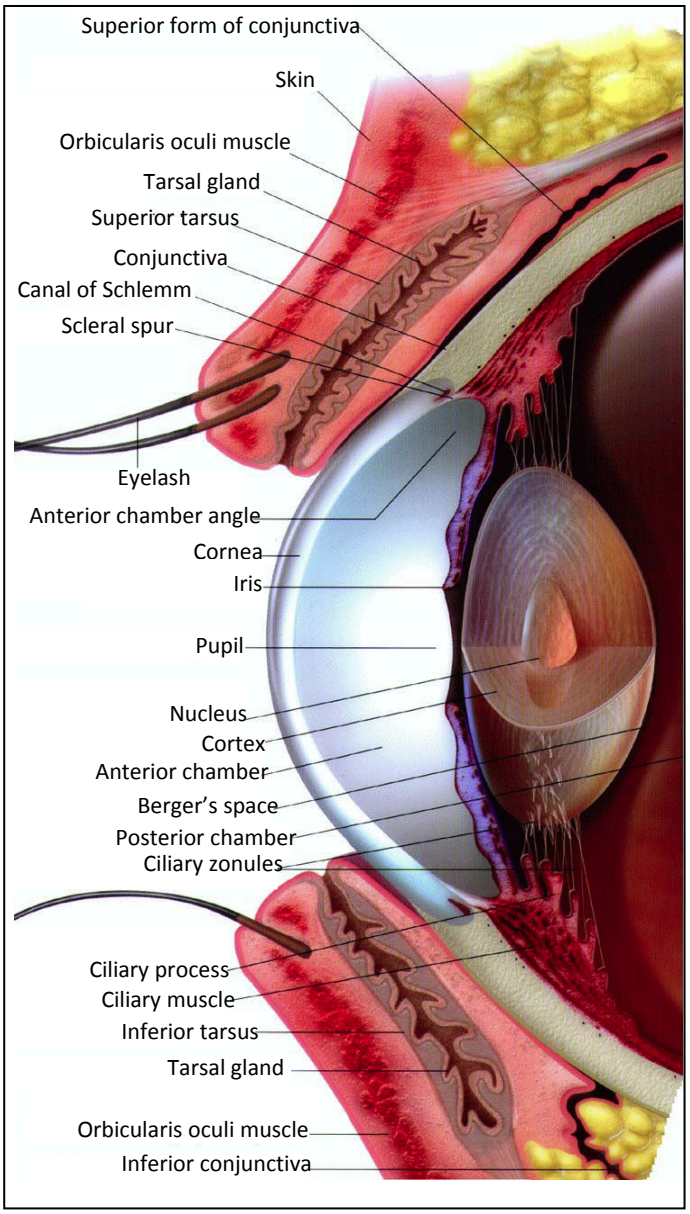

Figure 1-2: Detailed side view of the Human Eye. Adapted from [16].

1.4 Anatomy of the lens

The human lens is a biconvex avascular organ that is transparent and highly refractive (Figure 1-2). It is situated at the front of the eye between the anterior and vitreous body, suspended by zonular fibres. Oxygen and other nutrient requirements diffuse through the lens capsule from the surrounding fluids [17]. The lens is enclosed by a thin transparent, elastic and semi-permeable membrane known as the lens capsule [18]. A diagram of the lens is shown Figure 1-3.

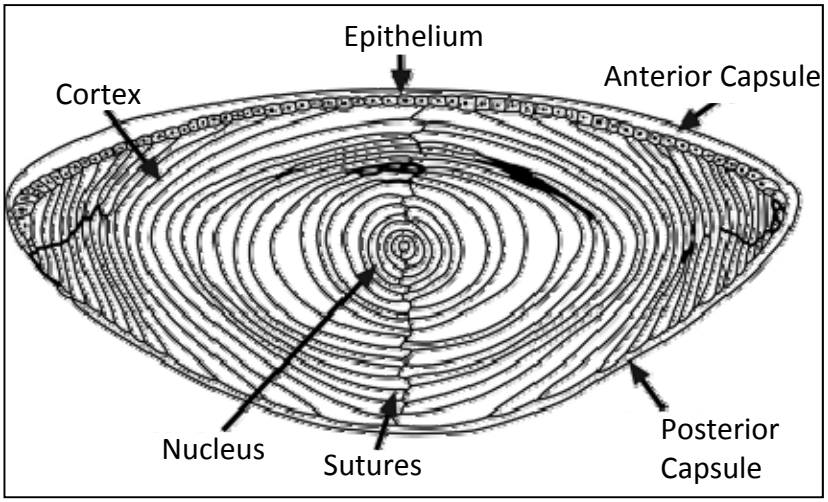

Figure 1-3: Diagram of human lens. Adapted from [19]

The lens is composed of a single layer of epithelial cells located at the anterior surface and a mass of elongated fibre cells that extend from the anterior to posterior poles. It continues to grow throughout life with fibre cells continuously laid down layer upon layer. At birth there are approximately 1.6 million fibre cells, whereas by age 80 there are almost 3.5 millions cells [20]. The terminal differentiation and aging of lens fibre cells are marked by dramatic morphological changes [21]. As new cells arise on the outside of the lens, older cells lose their organelles and fuse to form a syncytium [20, 22]. A consequence of this growth pattern is that in the differentiated fibre cells there is no protein turnover [23, 24]. Given that proteins do not diffuse between fibre cells, the centre of a human lens (nucleus) contains the original proteins that were synthesised during embryogenesis [18].

1.5 Lens accommodation

Accommodation refers to the ability of the lens to change shape in order to bring objects into focus [25]. Helmholtz elucidated the basic principles in 1855 [26]. He stated that contraction of the ciliary muscle causes a reduction in zonular tension that allows the lens to increase its curvature. This decreases the lens equatorial diameter while increasing its thickness, enabling it to focus. Strenk *et al*. [27] have confirmed this using high resolution Magnetic Resonance Imaging (MRI) to

demonstrate that if the pull of the zonule is relaxed for near vision, the equatorial diameter of the lens diminishes (Figure 1-4). This results in the lens becoming thicker in the middle with both surfaces becoming more curved.

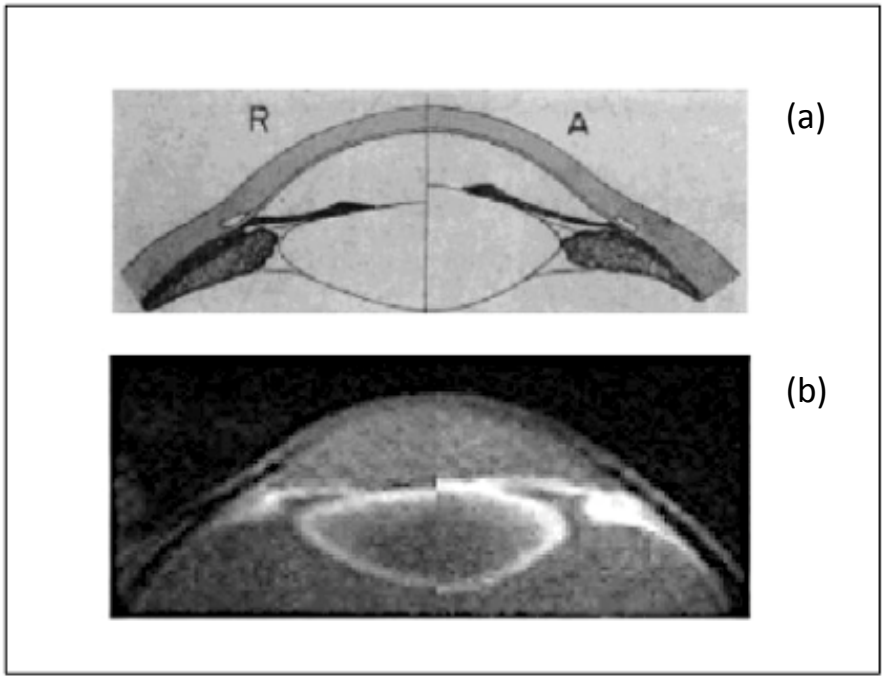

Figure 1-4: The original drawing by Helmholtz demonstrating his theory of accommodation is shown in (a), where the left half shows relaxed accommodation and the right half shows the increase in lens thickness and the decrease in the equatorial diameter after ciliary muscle contraction. A composite of 2 MRI scans illustrating the same thing is shown in (b). Diagram b adapted from Strenk *et al*. [27].

1.6 Lens protein composition

The human lens contains approximately 65% water and 35% protein by weight [28, 29]. Crystallins are the predominant protein in the lens and account for over 90% of total protein content [30, 31]. These crystallins are present in the lens at a concentration of approximately 400 mg/ml [28, 32]. They are water soluble proteins that can form relatively stable and durable structures. [33]. In healthy lenses they are uniformly packed, due to the short range interactions between lens crystallins [33, 34], and maintain the transparency of the lens. Their high protein concentration allows the necessary refractive index to be achieved [34, 35]. Crystallins are divided into 2 major families: α-crystallins and βγ-crystallins.

1.6.1 α-Crystallins

α-Crystallins are the most abundant protein family in the human lens, accounting for approximately 40% of all lens proteins [36]. They are high molecular weight proteins that exist as aggregates of about 800 kDa [37]. α-Crystallins consist of two related subunits αA (acidic) and αB (basic), which have a 57% sequence homology [38]. The 3-dimensional (3D) reconstruction of αB-crystallin by electron microscopy is shown in Figure 1-5 .It reveals a sphere-like structure with large openings to the interior of the protein.

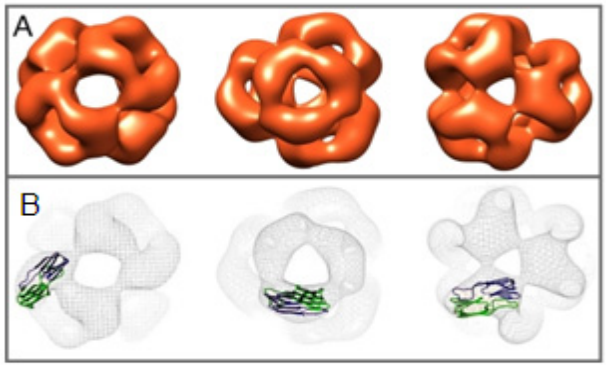

Figure 1-5: 3D reconstruction of the surface representation of αB-crystallin by electron microscopy (A). Superposition of the ribbon representation of the dimeric α-crystallin domain of Hsp16.5 from M. Jannaschii (B). The α crystallin domain is conserved in αB crystallin and Hsp16.5. Adapted from Peschek *et al.* [39].

The ratio of αA- to αB-crystallin varies with age and region of the lens. In a foetal lens it is approximately 2:1, but it changes to 3:1 by middle age [40, 41]. αA-Crystallin is found mainly in the lens, although trace amounts have been found in other tissue [42]. αB-Crystallin is considered a more ubiquitous protein, occurring in the lens, heart, brain and other tissues [43, 44]. In addition to being structural and refractive proteins, both αA- and αB-crystallins are members of the small heat shock protein super family [45], containing a consensus sequence of 80 – 100 residues that is common to all the heat shock proteins. In this role, they function as molecular chaperones by binding and stabilising denatured and unfolded proteins [46, 47]. Due to the polydispersive size distribution of both the natural and recombinant α-crystallins, crystallisation of the entire vertebrate

α-crystallin has to date been unsuccessful [30]. However, the partial crystal structure of human αB-crystallin has recently been determined [48, 49] and is shown in Figure 1-6.

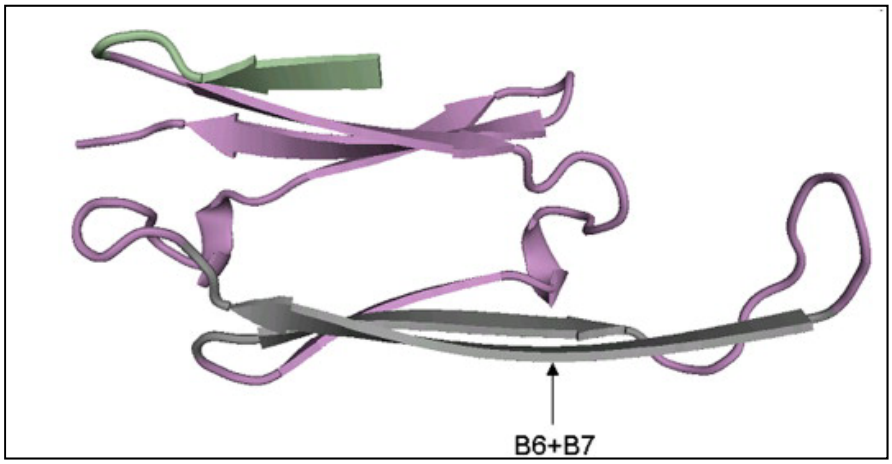

Figure 1-6: The α-crystallin domain of human αB (plum ribbon) with the sequence equivalent of β2 strand in green, the β5 and β6 + β7 strands in gray and the intervening residues (construct residues 42–49) in plum. Adapted from [49].

1.6.2 β - and γ- crystallins

β- and γ-crystallins are the two other major structural proteins in the lens [30]. They are closely related and are often referred to as the β/γ super family. β/γ-Crystallins are genetically distinct from α-crystallins, and their expression suggests an evolutionary divergence between the two families [50]. They are built from four homologous Greek key motifs organised into two domains [51]. The crystal structure of dimeric truncated βB1-crystallin, highlighting the subunits intramolecular domain pairing, is shown in Figure 1-7.

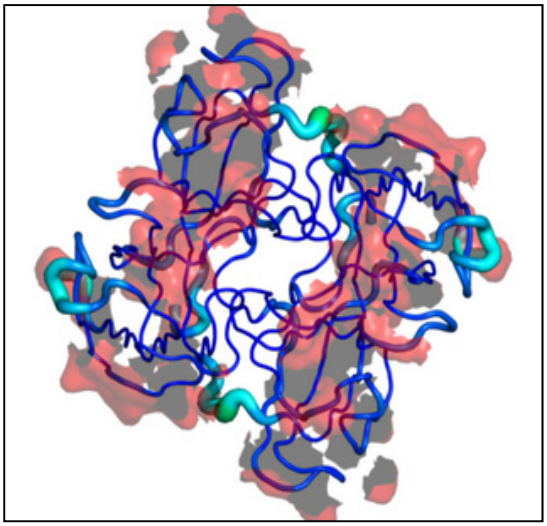

Figure 1-7: Crystal structure of dimeric truncated β1-crystallin. Adapted from [52].

The main sequence difference between β- and γ-crystallins is that β-crystallins have *N*-terminal extensions compared with γ-crystallins which do not. The basic β-crystallins also have an additional *C*-terminal extension [30]. β-Crystallins also exist as aggregates of between 40,000 and 200,000 whereas γ-crystallin is a monomer [47, 53]. The β-crystallins consist of basic (βB1, βB2, βB3) and acidic (βA1, βA2, βA3 and βA4) polypeptides [40]. βB1 and βB3 are primarily found in the lens nucleus in early fibre development, while βB2 is found in all regions of the human lens [40]. The basic β-crystallin genes are fibre cell specific, however the acidic β-crystallin genes are found in both the nucleus and the cortex of the lens [40, 54]. The γ-crystallin family is comprised of seven proteins (γA, γB, γC, γD, γE, γF, γS). γA-F are very similar, having a high degree of sequence homology, whereas γS differs significantly both in sequence and time of expression [55]. Only γC-, γD- and γS-crystallins have been detected in the human lens [56].

1.6.3 Lens enzymes

While crystallins make up over 90% of all lens proteins, lenses also contain a wide variety of enzymes including superoxide dismutase (SOD), glyceraldehyde 3-phosphate dehydrogenase and glucose-6-phosphate dehydrogenase. Studies have shown however, that as we age only inactive versions of

these enzymes exist in the centre of the adult lens [57-59]. In contrast, it has been shown that in the outer region of the lens there is no measurable age-dependent decline in the capacity of enzymes to synthesise lactate or glutathione across a wide age range from youth to old age [60].

1.7 Lens membrane composition

Membranes of the adult human lens are some of the most saturated, ordered membranes in the human body. Unlike most bio-membranes, lens membranes contain a high proportion of lipids associated with proteins such as α-crystallin and aquaporin-0 (AQP0), which reduces their mobility [61]. Figure 1-8 highlights the major structural differences between a typical membrane and a lens membrane. Additionally the age-related membrane changes observed appear to be greater than for any other membrane [61, 62].

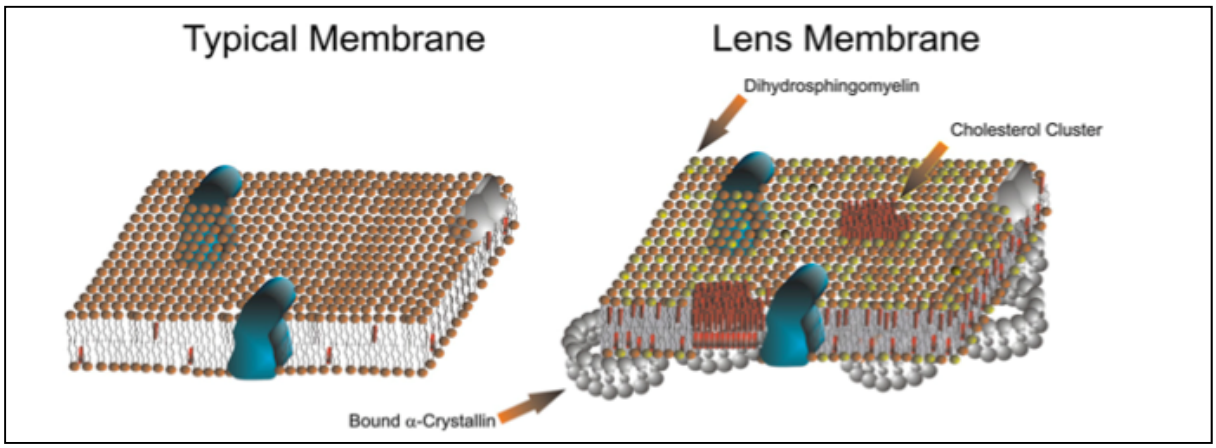

Figure 1-8: Comparison of a typical membrane (left) with lens membrane (right). In the lens membrane most of the lipids are associated with proteins such as α-crystallin and AQPO, which restrict their mobility. Adapted from Borchman *et al* [61].

1.7.1 Phospholipids

The major phospholipid in the human lens is dihydrosphingomyelin, accounting for 60% of lipid content [61, 63, 64]. It has been suggested that this may confer resistance to oxidation, allowing membranes to stay clear for longer [65]. In contrast to the typical Singer fluid mosaic membrane model [66], most lens lipids are associated with proteins, which limits their mobility. Unlike most

other major organs, the lenses of different species have very different phospholipid content [67-69]. A correlation between the relative growth rate of the lens and the amount of phosphatidylcholine has been demonstrated with a high growth rate being associated with a high level of phosphatidylcholine [67]. The other major phospholipids found in the human lens are sphingomyelins, phosphatidylcholines, phosphatidylethanolamine and phosphatidylserines [69].

The amount of some phosphoplipids in the lens has been shown to vary with age. In the first four decades of life, glycerophospholipids (with the exception of lysophosphatidylethanolamines) decline rapidly, such that by age 40, their content became negligible [62]. The concentration of sphingomyelins and dihydrosphingomyelins remain unchanged over the whole life span [62].

1.7.2 Membrane proteins

The fibre cells of the lens are interconnected through extensive gap junctions. These membrane junctions allow fluxes of small solutes and water to move between inner cells and peripheral cells, where the majority of transmembrane transport takes place. The other major lens membrane proteins include AQP0, membrane intrinsic protein (P-20) and the lens integral membrane protein 2 (LIM2).

1.7.2.1 Aquaporin-0

Aquaporin-0 (AQP0) is a 28 kDa protein with six transmembrane domains. It is the most abundant integral membrane protein in the lens and accounts for over 50% of all membrane protein [70, 71]. One function of AQP0 is to facilitate flow of water across the membrane in response to osmotic gradients [72]. Figure 1-9 illustrates how AQP0 may aid Connexin-50 (CX50) in the formation of gap junctions by functioning as an adhesion molecule and pulling the plasma membranes of apposing cells closer. Possibly as a result of this, more CX50 connexins on the cell surface are able to dock with their apposing counterparts from neighbouring cells to form functional gap junction channels.

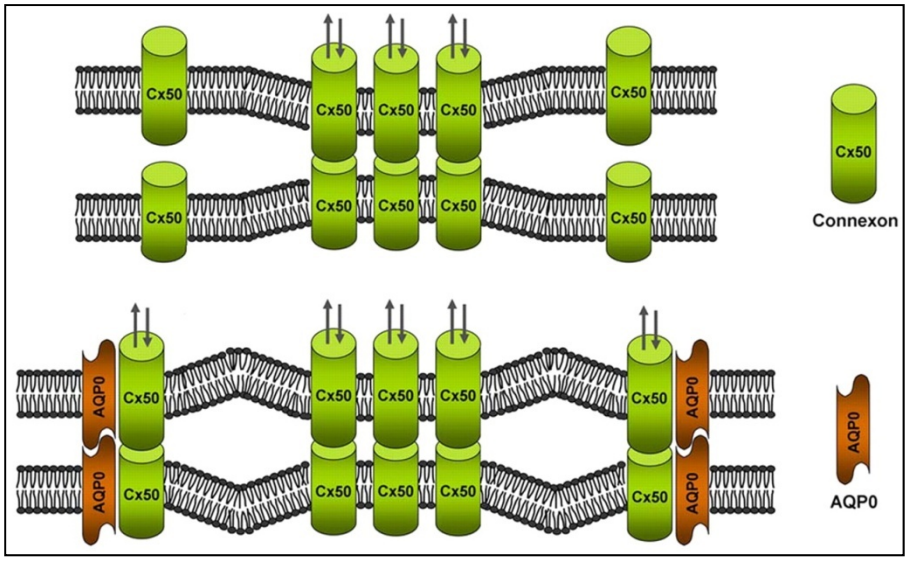

Figure 1-9: Schematic model illustrating the enhancement of CX50-mediated intercellular communication by AQP0 in the lens fibres. Connexins oligomerise to form half-intercellular channels, called connexons which form the intercellular channels [73]. The top section shows a lens membrane with no AQP0 and the bottom shows it with AQP0. Adapted from Liu [74].

AQP0 has widespread distribution throughout lens fibres, but is absent in lens epithelial cells. It has approximately 40 times lower water permeability than other aquaporins such as AQP1 [75, 76] and as a result it has been suggested that AQP0 might be involved in regulating the resistance of the paracellular pathway, rather than in cell membrane water permeability [77, 78]. Recent studies, however, have demonstrated that AQP0 water conductance can double under mildly acidic conditions, similar to those found in the core of the lens [77, 79, 80]. The factors that prompt AQP0 to form membrane junctions are still under investigation [80].

Mutated AQP0 has been associated with hereditary cataract in humans [81], however, the mechanism linking the loss of AQP0 function and cataract are not yet understood. Some proposed mechanisms include the loss of AQP0 facilitated fibre-fibre adherence [82] and impaired fibre cell dehydration [83]. AQP0 is also subject to extensive age-related truncation [84, 85], deamidation [84, 86] and phosphorylation [84].

1.7.2.2 Lens Integral membrane protein 2

Lens integral membrane protein 2 (LIM2) is the second most abundant protein in lens fibre cell membranes. Although the post-translational glycosylation pattern supports the view that LIM2 has four transmembrane domains [87], alternative non-tetraspan topologies have also been proposed [88, 89]. While its exact purpose is unknown, the suggested roles for LIM2 include cell junction formation [90], fibre cell adhesion [91] and occlusion of extracellular space between fibres [92].

1.7.2.3 Connexins

Connexins are a family of intercellular gap junction channels used to transport metabolites, ions and water in the lens [93]. Connexins oligomerise to form half-intercellular channels, called connexons which interact across a narrow extracellular space ("gap") to form the complete intercellular channels [73]. They have four *trans*-membrane domains with three intracellular regions (the *N* terminus, a cytoplasmic loop and the *C*-terminus) and two extracellular loops (E1 and E2) [94]. The lens connexin family contains at least three different proteins (CX43, CX46 and CX50). CX43 is mainly expressed in lens epithelial cells [95]. A structural diagram of CX50 is shown in Figure 1-10. CX46 is expressed in the lens fibre cells and is essential for lens transparency [96]. CX50 is found in both epithelial and fibre cells and is important for both cell growth and transparency [97]. The diverse gap junction channels formed by CX46 and CX50 are important for the differentiation, elongation and maturation of lens fibre cells [98].

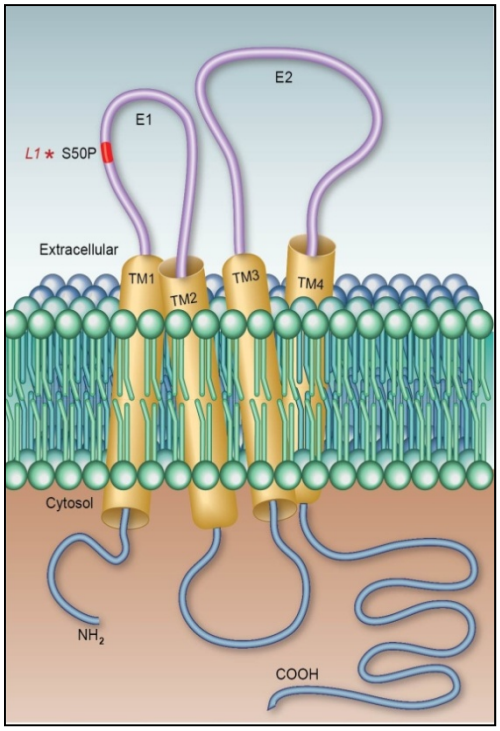

Figure 1-10: Diagram of CX50: The *trans*-membrane domains of CX50 are labelled TM1-4. The extracellular loops are labelled E1 and E2. Adapted from Fleisham *et al*. [99].

1.7.3 Cytoskeletal proteins

The lens cytoskeleton is comprised of actin-containing microfilaments, microtubules and at least two different intermediate filament (IF) protein networks [100]. One of these networks is based on an IF protein, vimentin, and the other is based on a beaded filament co-polymer of filensin and phakinin. Actin is predominantly seen along the fibre plasma membrane, whereas vimentin is present in both the undifferentiated lens epithelium as well as the differentiating fibre cells [101, 102]. Their exact roles are still being investigated. A role in accommodation has been suggested by Kibbelaar *et al*. [103] and Ramaekers *et al*. [104] have suggested they may play a role in fibre cell elongation. Filensin and phakinin are unique to differentiated lens fibre cells and mutations of these proteins have been linked to cataract formation [100, 105].

1.8 UV filters

The human lens contains a family of tryptophan-derived UV filter compounds, that improve vision by absorbing shorter light wavelengths and preventing them from reaching the retina [106]. UV filters are continuously biosynthesised in the lens from L-tryptophan (Trp) *via* the kynurenine pathway [107, 108]. The major UV filter compound found in the human lens is L-3-hydroxykynurenine O-β-D-glucoside (3OHKG), followed by 4-(2-amino-3-hydroxyphenyl)-4-oxobutanoic acid O-β-D-glucoside (AHBG), L-kynurenine (Kyn) and L-3-hydroxykynurenine (3OHKyn) [109-113]. The structures of some of the major UV filters found in the human lens are shown in Figure 1-11.

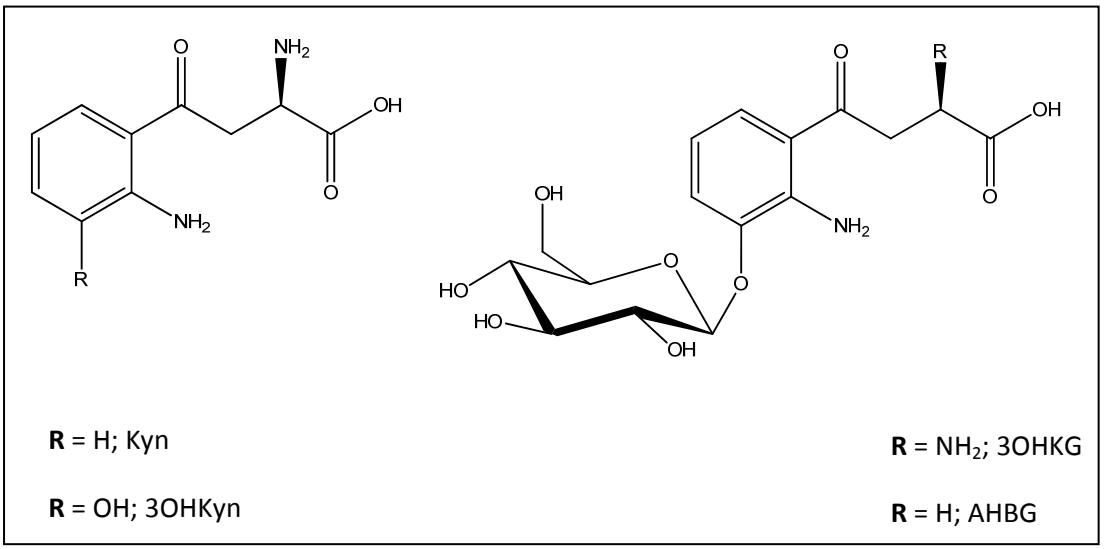

Figure 1-11: Structure of some of the major UV filters found in the human lens

Due to their rapid fluorescent decay, UV filters are capable of processing UV light *via* a non-destructive pathway [114, 115]. Following light absorption, UV filters are promoted to an electronic excited state, which undergoes a rapid and efficient physical quenching process within picoseconds [116]. This results in the regeneration of the original ground-state formation without the generation of reactive oxygen species. 3OHKG, Kyn and 3OHKyn have been shown to be unstable under

physiological conditions and can undergo a number of age-related degradations that are discussed later in this chapter.

1.9 Age-related modifications in lens proteins

A summary of some of the modifications discussed here can be seen in Figure 11-1.

1.9.1 Racemisation

Age-related racemisation has been shown to occur in long lived proteins such as those found in the human lens [117-119] and this may lead to loss of biological integrity [118, 120, 121]. Asp is the most easily racemised amino acid, with Asp151 in human αA crystallin as well as Asp36 and Asp62 in human αB crystallin showing extensive age-related racemisation in the lens [122]. Glu, Ser and Thr residues have also been shown to racemise with age in the human lens [117]. While the process of Asp racemisation is relatively well understood and occurs *via* a succinimide ring (Figure 1-13) formation [123-125], the mechanism of racemisation of other amino acids remains to be elucidated. One potential mechanism which occurs via base catalysed alpha proton loss and re-addition is outlined in Figure 1-12.

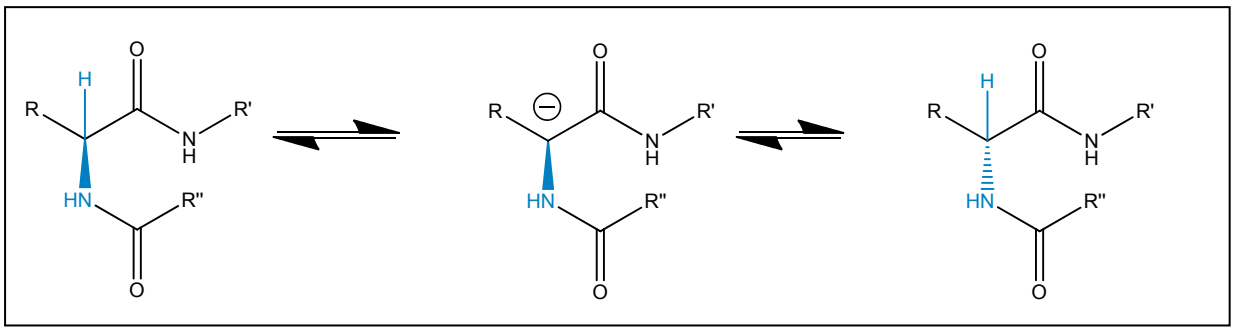

Figure 1-12: Amino acid racemisation *via* base catalysed alpha proton loss and re-addition. (R represents the amino acid side chain. R' and R'' represent the rest of the protein).

1.9.2 Truncation

Recent publications [126-128] have described the presence of shortened forms of crystallins in aged lenses and it is estimated that in the human lens approximately ~45-55% of all α-crystallin is truncated by old age [129]. As the centre of the lens is almost completely devoid of active enzymes [58-60, 130], these abundant truncations are likely the result of non-enzymatic processes [131]. Truncation from the *C*-terminal region of α-crystallin has been hypothesised to be a causative mechanism in the formation of increased amounts of high molecular weight aggregates found in mature and cataractous lenses [129]. Truncated α-crystallins have been shown to have reduced chaperone activity [37, 132, 133]. Additionally truncated β-crystallins have decreased solubility, which may also be associated with cataract formation [134].

αA-Crystallin undergoes major age-related truncations [37] with Asp / Asn (αA 1-101, 1-151) and Ser (αA 1-168, 1-169, 1-172) being the most commonly truncated residues in human lens proteins [135-137]. Truncation at Asn is generally accepted to occur non-enzymatically *via* an imide ring formation [125], but the mechanisms by which Ser and other amino acids truncate is unknown [138].

1.9.3 Deamidation

Deamidation of Asp is a common non-enzymatic post translational modification in aging proteins [132, 139, 140]. Due to the change in local charge that results, it could affect both the structural and functional integrity of a protein[132]. The deamidation occurs *via* the formation of the same succinimide mechanism [125] responsible for the racemisation of Asn (Figure 1-13). *In vivo* age-dependent deamidations have been shown to occur in several crystallins e.g. Asn101 in human αA-crystallin [125].

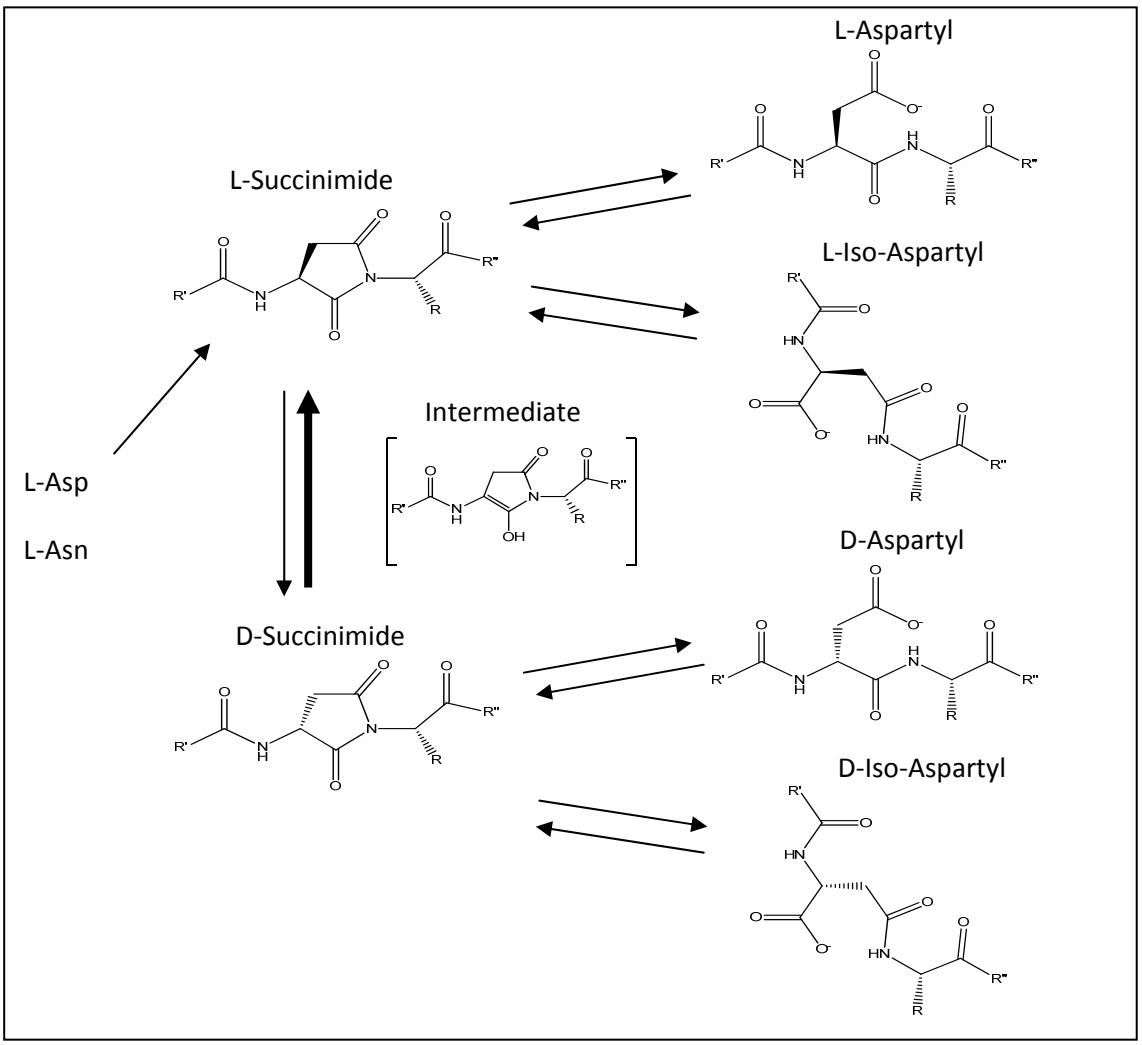

Figure 1-13: Spontaneous formation of peptide succinimides and racemised products from aspartyl and asparaginyl residues. (R' and R'' = rest of protein).

1.9.4 Phosphorylation

Phosphorylation involves the addition of a phosphate group to a Ser or less commonly to a Thr or Tyr. This leads to structural changes that could affect the function and stability of the protein. Phosphorylation at Ser19, Ser45 and Ser59 of αB-crystallin and Ser122 of αA-crystallin has been detected in lens samples of various ages including from young adults [141].

The effect of phosphorylation is still being investigated and conflicting reports exist. One study by Kamei *et al.* found that just one phosphorylation site reduced the chaperone-like activity of αB-crystallin by about 30% [142], whereas an *in vivo* study by Martinus [143] *et al.* showed that the

phosphorylated forms of αA- and αB-crystallins had better chaperone-like ability than their respective non phosphorylated forms (Figure 1-14).

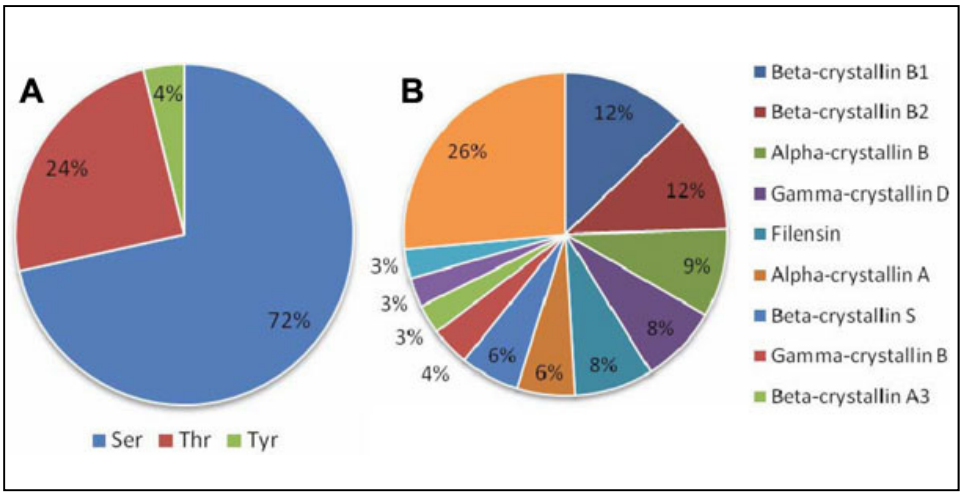

Figure 1-14: (a) Ratio of amino acids phosphorylated in normal lens proteins, (b) proportions of the identified proteins with phosphorylation. Adapted from Huang *et al.* [144].

1.9.5 Oxidation / reduction in glutathione levels

Glutathione (GSH) is the major antioxidant in the lens. It functions by scavenging reactive oxygen species such as hydrogen peroxide [145] thus helping to maintain lens transparency [145, 146]. GSH also promotes the antioxidant properties of vitamin C and vitamin E by maintaining these nutrients in a reduced state [147, 148]. It is synthesised in the lens epithelium and outer cortex by the enzymes γ-glutamylcysteine synthetase and glutathione synthetase from the amino acids glutamic acid, cysteine and glycine [145]. The concentration of GSH has been demonstrated to decrease with age [149], with levels in the cortex decreasing by 7% per decade and those in the nucleus decreasing by 10% per decade.

Oxidative stress in lenses typically leads to the loss of protein sulfhydryl groups, and oxidation of methionine residues. The concentration of proteins damaged by oxidative processes is significantly higher in cataractous lenses compared to normal transparent lenses [150]. This increase in oxidised proteins is now widely accepted as a hallmark of age-related nuclear cataract (ARNC) [151, 152],

with in excess of 90% of sulfhydryl groups and approximately 50% of methionine residues oxidised in advanced ARNC [153, 154].

1.9.6 Glycosylation

Age-related glycosylation of lens proteins can occur *via* the Maillard reaction. Arginine or lysine residues react with sugars such as glucose to form cross-linked proteins that contain a high concentration of yellow chromophores and UVA fluorophores [155]. These advanced glycation endproducts (AGEs) have been linked to protein aggregation and cataract formation [156, 157]. It should be noted that reactive products can arise from breakdown of ascorbate.

1.9.7 Protein aggregation

While lens proteins are relatively durable, the combination of age and the many post translational modifications detailed above eventually leads to aggregation and precipitation [158]. This can lead to impairment of lens light refraction, and ultimately to loss of sight as a result of cataract formation [151, 159]. In younger lenses, α-crystallins, as a member of the small heat shock protein (sHSP) family, bind to partially folding proteins preventing their precipitation [46]. However, as there is no protein turnover in the lens, it contains a finite amount of α-crystallin and once it is all used aggregation increases rapidly [160, 37].

1.9.8 UV filter modification

UV filters are intrinsically unstable under physiological conditions and undergo extensive changes with age. The levels of the free UV filters 3OHKyn , Kyn and 3OHKG decrease in the human lens by approximately 12% per decade from the ages of 20 to 80 years [107]. The human lens becomes increasingly colored and fluorescent [107, 161] and this results, in part, from the covalent attachment of these UV filters to lens proteins[106]. The way in which this occurs is detailed in Figure 1-15. The UV filters undergo spontaneous non-enzymatic deamination to yield α,β-

unsaturated carbonyl compounds which can then react with nucleophilic species in the lens through Michael addition [107, 162]. Reaction with protein side chains is particularly favored because the lens has the highest protein concentration of any human tissue. 3OHKG has been shown to bind covalently to crystallins *in vivo* [106] and 3OHKyn can react with crystallins *in vitro* forming cross-linked products with features characteristic of those observed in age-related nuclear cataract lenses [163-165].

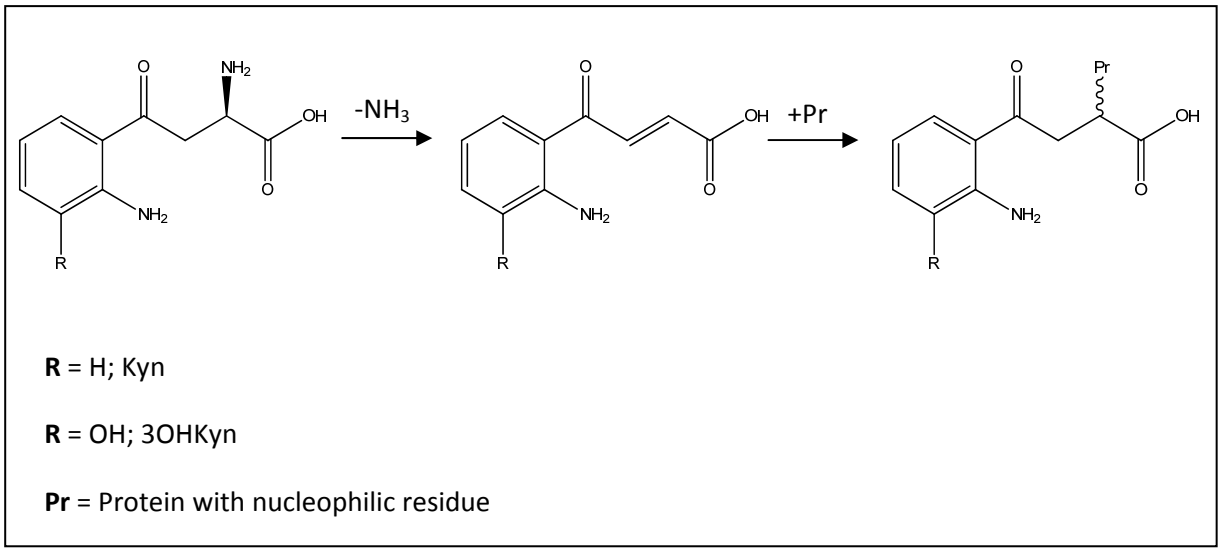

Figure 1-15: Age-related modification of UV filters.

Interestingly the UV filters present in the lens of the thirteen- lined ground squirrel have an N-acetyl group attached to the amino group [166]. This stabilises the UV filters, preventing the deamination outlined in Figure 1-15 [166] and preventing the formation of protein cross links *via* this pathway.

1.10 Eye conditions associated with aging

1.10.1 Presbyopia

Presbyopia is the inability to focus on objects that are close to the eye. Accommodative loss begins during childhood and is a gradual process that occurs over decades, with presbyopia affecting almost everyone by middle age [167]. While several theories exist, the exact mechanisms behind presbyopia are still not fully understood [168]. Continuous growth of the lens within a fixed eye volume has been proposed as a cause by *Strenk et al*. [25]. Harocopos *et al.* have suggested that age-dependent liquefaction of the vitreous may be the cause [169]. A study by Heys *et al*. [170] described a 1000-fold difference in the lens nuclear stiffness from youth to old age, which would have significant implications for lens accommodation. This agrees with work published by Glasser *et al*. who noted that intact lenses extracted from donor eyes aged 50 or greater were unable to change shape when forces similar to those found in the eye were applied [171].

Studies by Koretz and Bron *et al.* have described how it is the oldest part of the lens, the nucleus, that predominantly changes shape when the eye focuses [31, 172]. Given that presbyopia occurs at middle age, it is likely that the mechanisms that protect the lens prior to this point are no longer occurring. It has been shown by age 40 no free α-crystallin can be detected in the centre of the lens [173]. This depletion of free α-crystallin by around middle age, and therefore minimal molecular chaperone ability available to prevent protein denaturation in the lens, has been proposed as a reason why presbyopia becomes evident at this time [168]. Recent studies by Sheppard *et al* [174] have reported that while age-related morphological changes do occur in the human ciliary muscle, these changes do not appear to compromise ciliary muscle contraction during accommodation, even in presbyopes.

Heat has also been suggested as an important factor in presbyopia. Studies by Schwartz have shown that the lens temperature is sensitive to ambient temperature [175]. Miranda *et al.* performed an

epidemiological study comparing the average ambient temperature with the onset of presbyopia and determined that presbyopia developed at a later age at lower ambient temperatures [176].

1.10.2 Barrier formation

As the lens is avascular, the transport of metabolites is dependent on diffusion. However, at middle age a barrier forms (Figure 1-16) at the nucleus / cortex interface with the resulting lack of antioxidants in the centre of the lens causing an increase in the amount of post translational modification [131, 177, 178]. It also explains why high levels of protein oxidation can be present in the lens nucleus of cataract lenses despite normal GSH levels in the cortical tissue.

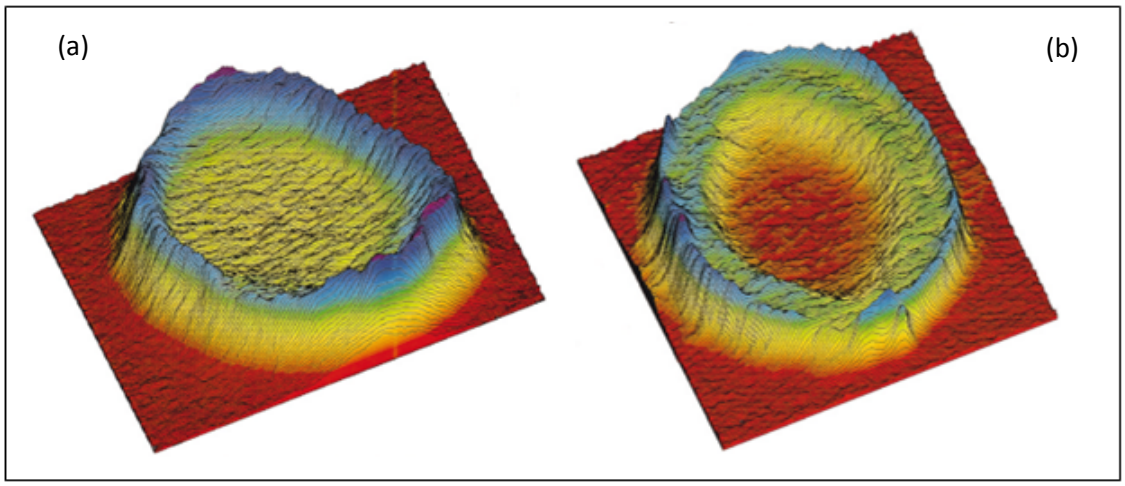

Figure 1-16: An autoradiograph of axial sections of (a) 19 year old lens and (b) 56 year old lens, both having been incubated with radio labelled cysteine which shows the barrier to diffusion that develops with age. Adapted from Sweeney *et al.* [177].

1.10.3 Cataract

Cataracts are typically classified into three main types depending on their location. Cortical cataracts, which are the most common cataract in younger people, are defined by an opacity confined to the outer lens shell. The most common cataract in people over 65 is age-related nuclear cataract (ARNC) where the opacity first appears in the centre of the lens [179]. The least commonly observed cataract is a posterior subcapsular cataract, which can be found in the outermost layers of

the cortex at the posterior pole. A system devised by Pirie is often used to classify cataract (Figure 1-17). Types II to V are nuclear cataracts of increasing severity with type 1 referring to a cortical cataract. Cortical cataracts have an opacity in the outer region of the lens and nuclear cataracts have an opacity in the inner region of the lens [17]. Many cataracts contain a mixture of both types. Additional cataract classifications methods include the Lens Opacities Classification System III (LOCS III)[180] and the Oxford Clinical Cataract Classification [181].

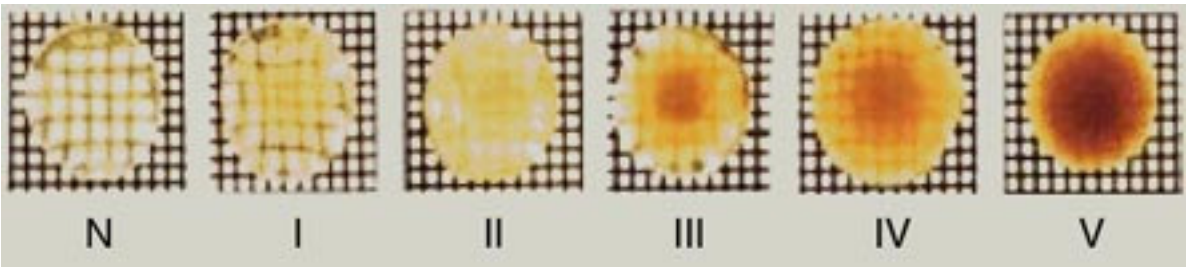

Figure 1-17: Pirie classification of cataracts. Adapted from Pirie et al. [182].

Aging is by far the greatest risk factor for ARNC [183, 184]. Other factors include diabetes, UV light, smoking and alcohol consumption [183, 185]. Surgical removal of the lens *via* phacoemulsification and intraocular lens implantation is the modern treatment for cataract [10]. The procedure involves the use of an ultrasonic probe, which emulsifies the lens while leaving most of the lens capsule intact, enabling it to be removed without the need for a large incision. It has largely superseded intracapsular extraction (ICCE) which is still a cataract removal procedure sometimes used in less developed countries [186].

1.11 Aims

The research presented in this thesis was divided into three sections (A, B and C) each with specific aims.

Section A:

As already described, long-lived proteins in the human lens undergo numerous changes as a result of prolonged exposure to physiological conditions, with truncation being a common modification in aged lenses. Since enzyme activity is absent in the nuclei of adult human lenses [57-60], many cleavages appear to be non-enzymatic (i.e. spontaneous), however little is known about the specific processes involved. With regards to truncation of α-crystallins, one notable feature of the sequences of two of the most abundant peptides (αA 67-80 and αB 1-18) in the lens is that sites of cleavage are on the N-terminal side of Ser residues [128, 187]. It is likely these truncations are therefore a result of non-enzymatic reactions involving Ser.

Aims:

(1) To use model peptides that mimic cleaved regions of α-crystallins, to replicate truncation at the N-terminal side of Ser.
(2) To propose a mechanism for truncation on the N-terminal side of Ser residues

Section B:

While investigating model peptides for Section A, a number of side reactions were observed. Most of these involved modification at the peptide N-termini. This section deals with the characterisation of these modifications as well as investigating if they could be potential degradation pathways for long-lived proteins such as those found in the human lens.

The majority of long-lived proteins in the human lens have an N-terminal acetyl group. This protects them from a range of N-terminal degradations. For this reason the model peptides used in Section A

contained an N-terminal acetyl group to prevent these modifications and enable focus on truncation at internal Ser residues. However in the lens, following N-terminal Ser truncation (Section A), and other documented age-related truncations such as at Asn residues, the resulting peptide fragments all have free amino terminals and could be subject to further degradation *via* some of the modifications outlined in this section.

Aim:

To use model peptides derived from human crystallin sequences, with free amino terminal groups to investigate the spontaneous N-terminal modifications which were observed in Section-A

Section C:

Animals commonly used for scientific research such as the rat and the mouse are considered poor models for lens research because they are short-lived and can see UV light [188]. In addition, their crystallins and lens structures are significantly different from that of humans and other primates [151]. The thirteen-lined ground squirrel was previously found by the Giblin research group to contain similar Trp-derived UV filters found in the human lens and has been proposed as a more appropriate animal model [166]. In addition to the UV filters found in humans, the squirrel lens contains a major UV filter that is unidentified. This section focused on the characterisation of this novel UV filter.

Aim

To purify the unknown UV filter using semi-preparative HPLC and determine its structure using a variety of spectroscopic and analytical techniques.

2 Chapter 2: Materials and Methods

2.1 Materials

This section covers the Materials used in all chapters.

2.1.1 Chemicals

The following chemicals were purchased from Sigma-Aldrich (St. Louis, MO, U.S.A)

- NaH_2PO_4
- HEPES [4-(2-hydroxyethyl)piperazin-1-yl]ethanesulfonic acid
- TES 2[[1,3-dihydroxy-2-(hydroxymethyl)propan-2-yl]amino]ethanesulfonic acid
- MES 2-(N-morpholino)ethanesulfonic acid
- Marfeys regent (N_α-(2,4-dinitro-5-fluorophenyl)-L-alaninamide)
- TFA (Chromosolv HPLC grade)
- NaOH pellets
- HCl (37% - reagent grade)

Na_2HPO_4 was purchased from Amresco (Solon, OH, U.S.A) and acetonitrile (HPLC grade) was purchased from Merck (Whitehouse station, NJ, U.S.A)

2.1.2 Custom peptides

All peptides were synthesised by GL Biochem (Shanghai) Ltd at 95% purity. Prior to dispatch they were analysed by HPLC and ESI Mass spectrometry and shown to be within specification.

2.2 General Methods (Chapters 4 to 8)

Most of the experiments in this thesis involved the use of a number of standard procedures and rather than repeat them in each chapter they are described here. A typical experiment involved:

(1) Incubating model peptides under various conditions (Section 2.21)

(2) Purification of the products (Section 2.22)

(3) Characterisation of the products (Section 2.23)

(4) Quantification of the products (Section 2.24)

(5) Data analysis (Section 2.25)

Any modification to these procedures will be referred to in the relevant chapters.

2.2.1 Peptide incubations

For incubating peptides three temperatures were typically used.

(1) 37 °C to replicate physiological temperature (**Incubation-A**)
(2) 60 °C to accelerate the reaction rate (**Incubation-B**)
(3) 85 °C for peptides that were stable at 60 °C (**Incubation-C**)

"All peptides were incubated in triplicate (1 mg/ml) using one of the following three protocols unless otherwise stated. As custom peptides are expensive a concentration of 1mg / ml was chosen as it enabled approximately 10 time points to be taken while still leaving enough for purification and subsequent analysis of the products formed. Phosphate buffer was chosen for most incubations as it suitably mimics intercellular conditions [189] ".

Incubation-A (37 °C)

Incubations were carried out in a Labshop MC-20AIC Incusafe® incubator (set to 37 °C) and 2 ml Eppendorf Safe Lock ® tubes were used to prevent evaporation. Peptides were incubated in triplicate (1 mg/ml) in 100 mM phosphate buffer pH 7.4. Aliquots (20 µl) were taken at T=0, week 1, week 2, week 5 and week 11 and analysed by HPLC (Section 2.24: Method-C). The degradation products were purified by semi-preparative HPLC (Section 2.22: Method-A) and characterised using HPLC standards, ESI Mass Spectrometry and NMR spectroscopy, as detailed in Section 2.23. In all cases the temperature was checked with a thermometer at regular intervals to ensure accuracy.

Incubation-B (60 °C)

Incubations were carried out in an SEM oven (set to 60 °C) and 2ml Eppendorf Safe Lock ® tubes were used to prevent evaporation. Peptides were incubated in triplicate (1 mg/ml) in 100 mM phosphate buffer pH 7.4. Aliquots (20 µl) were taken at T=0, day-2, day-7 and day 14 and analysed by HPLC (Section 2.24: Method-C). The degradation products were purified by semi-preparative

HPLC (Section 2.22: Method-A) and characterised using HPLC standards, ESI Mass Spectrometry and NMR spectroscopy, as detailed in Section 2.23. In all cases the temperature was checked with a thermometer at regular intervals to ensure accuracy.

Incubation-C (85 °C)

Incubations were carried out in a Polaron oven (set to 85 °C) and 2 ml glass screw-top vials specially designed to withstand high temperatures were used. Peptides were incubated in triplicate (1 mg/ml) in 100 mM phosphate buffer pH 7.4. Aliquots (20 µl) were taken at T=0, day-2, day-7 and day-14 and analysed by HPLC (Section 2.24: Method-C). The degradation products were purified by semi-preparative HPLC (Section 2.22: Method-A) and characterised using HPLC standards, ESI Mass Spectrometry and NMR spectroscopy, as detailed in Section 2.23. In all cases the temperature was checked with a thermometer at regular intervals to ensure accuracy.

Buffers

To maintain a constant pH, all incubations were carried out in buffered solutions made using 18 Ω Millipore grade water. All buffers used in this thesis are detailed below. Unless otherwise stated, 100 mM phosphate buffer pH 7.4 was used.

Phosphate Buffer

200 mM stock solutions of Na_2HPO_4 (28.39 g/L) and NaH_2PO_4 (23.96 g/L) were prepared. To make 100 ml of 100 mM phosphate buffer (pH 7.4) 40.5 ml of the 200 mM Na_2HPO_4 solution and 9.5 ml of the 200 mM NaH_2PO_4 solution were combined and the pH was checked using a calibrated pH meter. If necessary, the pH was adjusted using 1 M NaOH or 1 M HCl and the buffer was then made up to 100 ml using Millipore water.

HEPES Buffer

To make 100 mM HEPES buffer (pH 7.4) 2.38 g of 2-[4-(2-hydroxyethyl)piperazin-1-yl]ethanesulfonic acid was dissolved in 50 ml Millipore water. The pH was adjusted to 7.4 using 1 M NaOH and the solution was made up to 100 ml.

TES Buffer

To make 100 mM TES buffer (pH 7.4) 2.29 g of 2-[[1,3-dihydroxy-2-(hydroxymethyl)propan-2-yl]amino]ethanesulfonic acid was dissolved in 50 ml Millipore water. The pH was adjusted to 7.4 using 1 M NaOH and the solution was made up to 100 ml.

MES buffer

To make 100 mM MES buffer (pH 5.4) 1.95 g of 2-(N-morpholino)ethanesulfonic acid was dissolved in 50 ml Millipore water. The pH was adjusted to 5.4 using 1 M NaOH and the solution was made up to 100 ml.

Tris buffer

To make 50 mM Tris buffer (pH 8.5) 0.605 g of 2-amino-2-hydroxymethyl-propane-1,3-diol was dissolved in 50 ml water. The pH was adjusted to 8.5 using 0.1 M HCl and made up to 100 ml

Boric Acid buffer

To make 100 mM boric acid buffer (pH 9.9) 0.618 g of boric acid was dissolved in 50 ml water. The pH was adjusted to 9.9 using 0.1 M NaOH and made up to 100 ml.

2.2.2 Purification of Incubation products

Following incubation of a peptide, isolation of the products was usually required. This was done using semi-preparative HPLC as follows:

HPLC Settings

A Shimadzu prominence HPLC system controlled by Shimadzu Class VP software equipped with a UV-Vis detector (SPD-20A) and a fraction collector (FRC-10a) was used. Purification of the peptides was achieved using a Phenomonex Kinetex (100 mm x 4.6 mm I.D) 2.6 µm 100 Å C-18 column at ambient temperature and eluents were monitored at 280 nm and 216 nm.

HPLC Method: (Method-A)

The gradient was 0% B (0.1% TFA) to 60% B (0.1% TFA in acetonitrile) over 110 minutes followed by 10 minutes equilibrating back to starting conditions (0% B). The fraction collector was set to collect all peaks of interest.

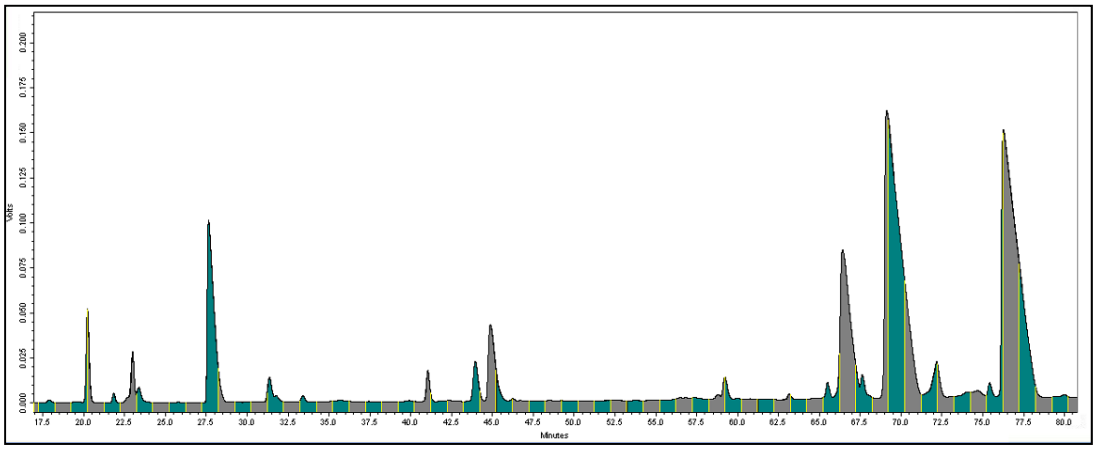

Figure 2-1: A typical HPLC trace of sample purification by semi-preparative HPLC (280 nm). The alternating colours reflect the fractions that were collected.

2.2.3 Characterisation of Incubation products

Following purification by semi-preparative HPLC, the isolated peptides were lyophilised and then analysed using a number of analytical techniques.

(1) MALDI mass spectrometry

(2) ESI Mass spectrometry

(3) Chiral amino acid HPLC analysis

(4) NMR spectroscopy

(1) MALDI Mass spectrometry

MALDI-MS analysis was performed using a Shimadzu (Nakagyo-ku, Kyoto, Japan) Axima TOF^2 mass spectrometer used in reflection positive ion mode. Peptides were prepared in α-cyano-4-hydroxycinnamic acid (8 mg/mL) in 80% (v/v) acetonitrile, 0.1% (v/v) TFA.

(2) ESI Mass spectrometry

Peptides with a molecular weight below ~500 dalton are difficult to analyse by MALDI due to saturation by matrix ions signals in this mass region [190]. These peptides were analysed by ESI Mass spectrometry as follows. Samples were re-suspended in 50% (v/v) acetonitrile, 0.5% (v/v) formic acid and analysed in positive ion mode using a Micromass Q-TOF2 equipped with a nanospray source. For MS/MS analysis, ions were subjected to a range of collision energies (typically between 10–25 eV).

(3) Chiral HPLC amino acid analysis (Method B)

Chiral HPLC analysis was based on a modified version of that described by Goodlett et al. [191] which enables resolution of many D- and L- amino acids by reversed phase HPLC. It was used to check the peptide incubations for evidence of amino acid racemisation.

Sample derivatisation for chiral HPLC

Peptides were first hydrolysed in 6 M HCl at 110 °C for 6 hours and then lyophilised. They were then dissolved in 100 µl of 1 M sodium carbonate (pH 8) and 5 µl of Marfey's reagent (N_α-(2,4-Dinitro-5-fluorophenyl)-L-alaninamide) in acetone) was added. The sample was incubated for 1 hour at 40 °C

and quenched by adding 50 µl of 2 M HCl. Between 1 µl and 10 µl of this mixture was analysed by HPLC as detailed below. A small amount of racemisation did occur as a result of the acid hydrolysis, consistent with the findings of Hooi et al [117].

A Shimadzu prominence HPLC system controlled by Shimadzu Class VP software equipped with a UV-Vis detector (SPD-20A) was used. Separation of the amino acids was achieved using a Kinetex (100 mm x 4.6 mm I.D) 2.6 µm C-18 HPLC column at 60 °C and was monitored at 340 nm. The gradient was 0% B (0.1% TFA) to 45% B (0.1% TFA in acetonitrile) over 50 minutes followed 10 minutes at 100%B to wash the column and 10 minutes at 0%B to equilibrate the column to starting conditions. Amino acid standards (D and L) were incubated in Marfeys's reagent (as above) and analysed to determine the retention times of each amino acid stereoisomer complex, and these were compared to those found in the peptide samples. A sample chromatogram showing part of the resolution of D- and L- amino acids is shown in Figure 2-2.

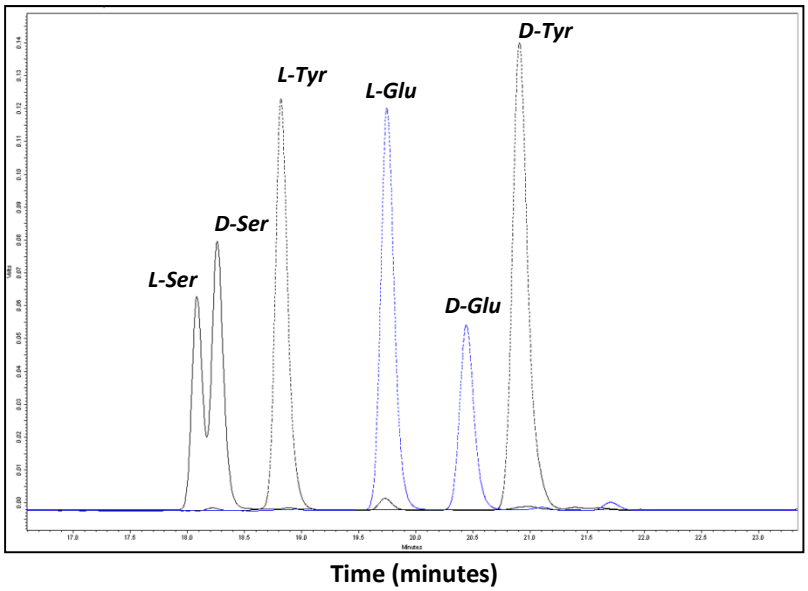

Figure 2-2: Sample HPLC trace (340nm) for three amino acids demonstrating resolution between D and L stereoisomers.

(4) NMR spectroscopy

NMR spectroscopy was used to determine the structure of selected purified peptides.

Methods

Samples were made up in 50 mM Phosphate buffer pH 7.4 containing 1 mM DSS(4,4-dimethyl-4-silapentane-1-sulfonic acid) as an internal reference and 10% D_20. Spectra were acquired at 25 °C on a Bruker Avance III 800-MHz narrow-bore NMR spectrometer equipped with a high-resolution cryogenic TCI probe-head. All experiments were carried out at 298 K. Water suppression was achieved using pulsed-field gradients and the WATERGATE sequence [192].A reduced volume Shigemi D_2O matched NMR tube (100 µl) was used. The following NMR experiments were acquired using standard Bruker pulse sequences: 1D ^{1}H, 2D ^{1}H-TOCSY, 2D ^{1}H-ROESY, 2D ^{13}C-^{1}H HSQC and ^{13}C-^{1}H HMBC.

2.2.4 Quantification of incubation products

Once an unknown degradation product had been characterised the next step was to quantify how much of it formed during the incubation. To do this a standard of each of the newly characterised peptide was obtained. A standard curve (generated as detailed below) was then used to convert the HPLC peak area of each peptide to the number of moles present.

Standard curve

An accurately weighed standard of each peptide was made up (1 mg/ml). Varying amounts were injected in duplicate into the HPLC using Method-C (Section 2.24). For peptides containing a Tyr residue, the absorbance at 280 nm was recorded. For all other peptides the absorbance at 216 nm was used. The results of each replicate were then averaged and the number of moles represented by

each absorbance unit was then calculated. A sample calculation for the peptide SFHSPSY is shown in Table 2-1.

Table 2-1: SFHSPSY standard curve data.

Amount injected	**2 µg**	**5 µg**	**10 µg**	**20 µg**
Peak Area Abs Rep-1 (280 nm)	133.15	333.85	666.01	1338.44
Peak Area Abs Rep-2 (280 nm)	132.55	332.6	666.22	1337.51
Average	132.85	333.25	666.11	1337.97
Peak Area Abs (280 nm) / 1 µg	**66.42**	**66.64**	**66.61**	**66.89**

It was calculated that:

1 µg of SFHSPSY had an absorbance (280 nm) of 66.64 milli absorbance units per second (mAU*S).

1 µg of SFHSPSY = 1.21308E-09 moles.

1 Abs unit of SFHSPSY at 280nm corresponded to 1.8133E-11 moles.

This value was then used to calculate the number of moles of SFHSPSY in any incubation. A graph of the above data demonstrating linearity across the range of concentrations is shown in Figure 2-3. Similar standard curves were generated for all peptides used in this thesis.

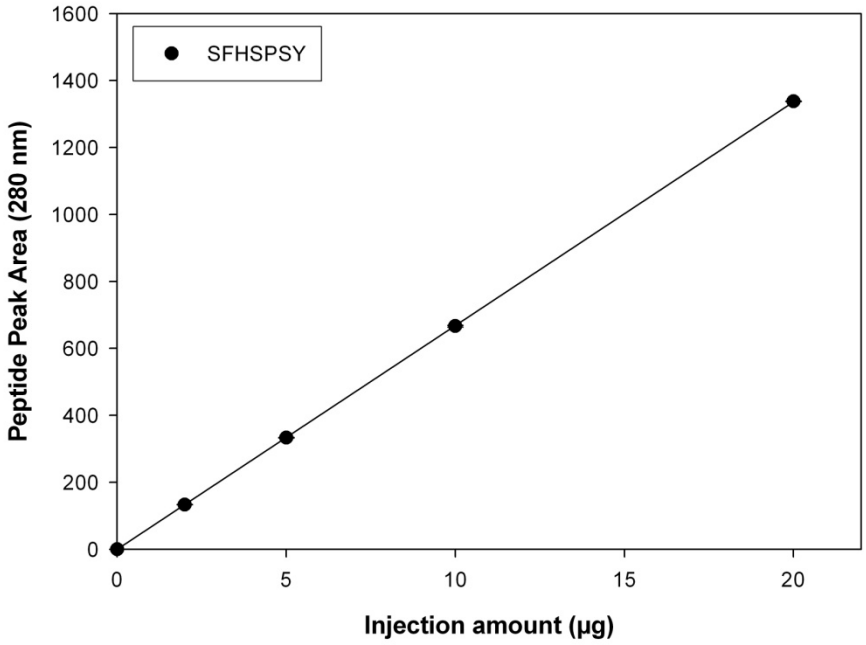

Figure 2-3: Standard curve of SFHSPSY relating peak area at 280 nm to amount injected (µg).

HPLC quantification

HPLC quantification was used to calculate the peak area of each peptide present in an incubation at a given time. Incubations were typically done in triplicate and the average peak area of each triplicate was used. The standard deviation of the average was plotted as error bars. Based on the results from the standard curves the number of moles of each peptide could then be calculated. Depending on the level of separation required, one of two HPLC methods (Method-C or Method-D) was used to quantify the various peptide incubations.

METHOD-C

An Agilent 1100 HPLC system controlled using Chemstation software and equipped with a photo diode array (PDA) detector was used. Incubations were monitored at 280 nm and 216 nm. Separation of the peptides was achieved using a Jupiter Proteo 4 µm 90 Å column (150 mm x 4.6 mm I.D) at 40 °C. The gradient was 0% B (0.1% TFA) to 60% B (0.1% TFA in acetonitrile) over 25 minutes

followed by 2 minutes at 60% B with a flow rate of 1ml/min Figure 2-4. The column was equilibrated at 0% B for 10 minutes at the end of each run.

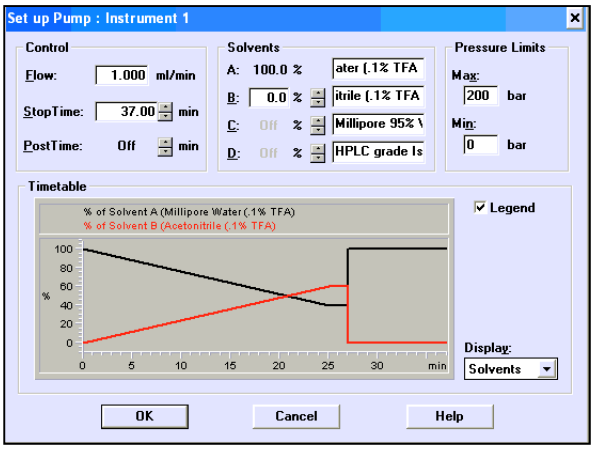

Figure 2-4: HPLC parameters for Method-C.

Method-D (Extended Gradient)

For incubations where Method-C did not provide sufficient separation of all analytes, an extended 2-hour method (Method D) was used. The gradient was 0% B (0.1% TFA) to 25% B (0.1% TFA in acetonitrile) over 100 minutes, increasing to 60% B over another 5 minutes and then held at 60% for a further 5 minutes. The column was equilibrated back to starting conditions (0% B) for 10 minutes at the end of the run (Figure 2-5). All other parameters were as in Method-C.

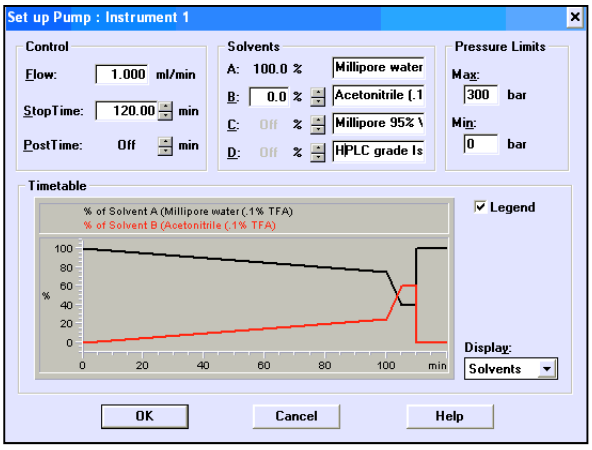

Figure 2-5: HPLC parameters for Method-D.

2.2.5 Data Analysis

There were 2 main types of graph used in this thesis.

(1) Comparison of the appearance of one peptide(moles) and the disappearance of another(moles)

(2) Percentage of each peptide that had undergone a specific modification.

(1) Appearance of one peptide and disappearance of another

Figure 2-6 shows a HPLC chromatogram from day-x of sample peptide incubation. It shows Peptide-A has partially degraded to Peptide-B. Standard curve data was used to convert the peak area of each peptide to moles. This enabled calculation of the number of moles of each peptide present at each time point. Where incubations were carried out in duplicate or triplicate, the number of moles of each was averaged and the standard deviation expressed with error bars. A sample graph showing the disappearance of Peptide-A and the appearance of Peptide-B is shown in Figure 2-7.

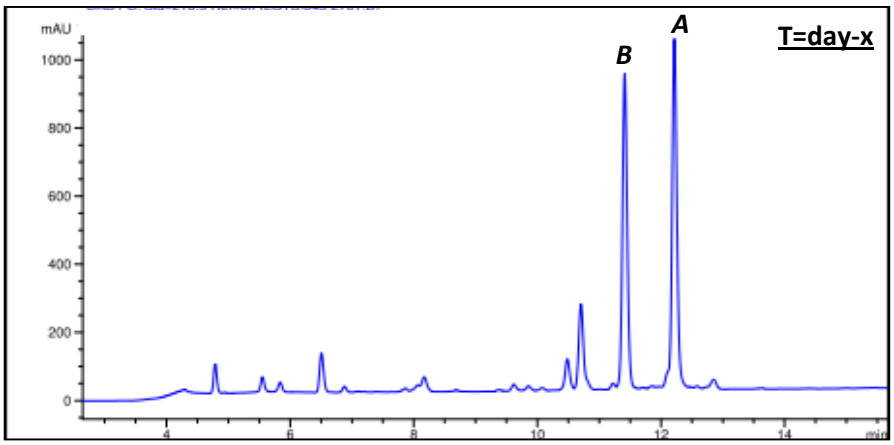

Figure 2-6: HPLC trace (216 nm) of a sample peptide incubation at the day-x time point.

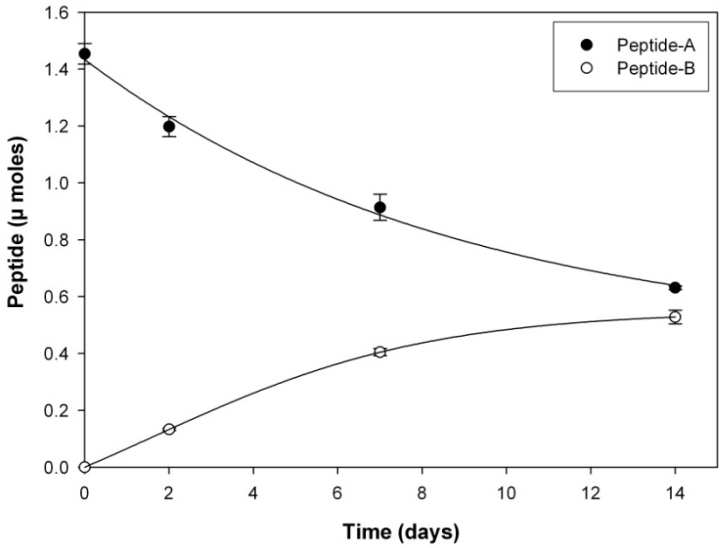

Figure 2-7: Sample graph with error bars showing the appearance of Peptide-A and disappearance of Peptide-B (µ moles).

(2) Percentage of an intact peptide that has degraded to another peptide

Consider two peptides (Peptide-A and Peptide-B) which are incubated separately and degrade to Peptide-C. In order to compare the rate of formation of Peptide-C in each peptide the following calculations are performed:

(1) Using a standard curve and the peak area at T=0, the total number of moles present in each incubation was calculated (Figure 2-8).

(2) The number of moles of Peptide-C present at each time point is then calculated in a similar manner

(3) The percentage conversion of each peptide to FHSPSY is calculated as:

$$\frac{\text{Moles of Peptide-C at day-x}}{\text{Moles of Peptide (A or B) at T=0}} \text{ X } 100$$

(4) The percentage of Peptide-C at each time point is then plotted in Figure 2-9.

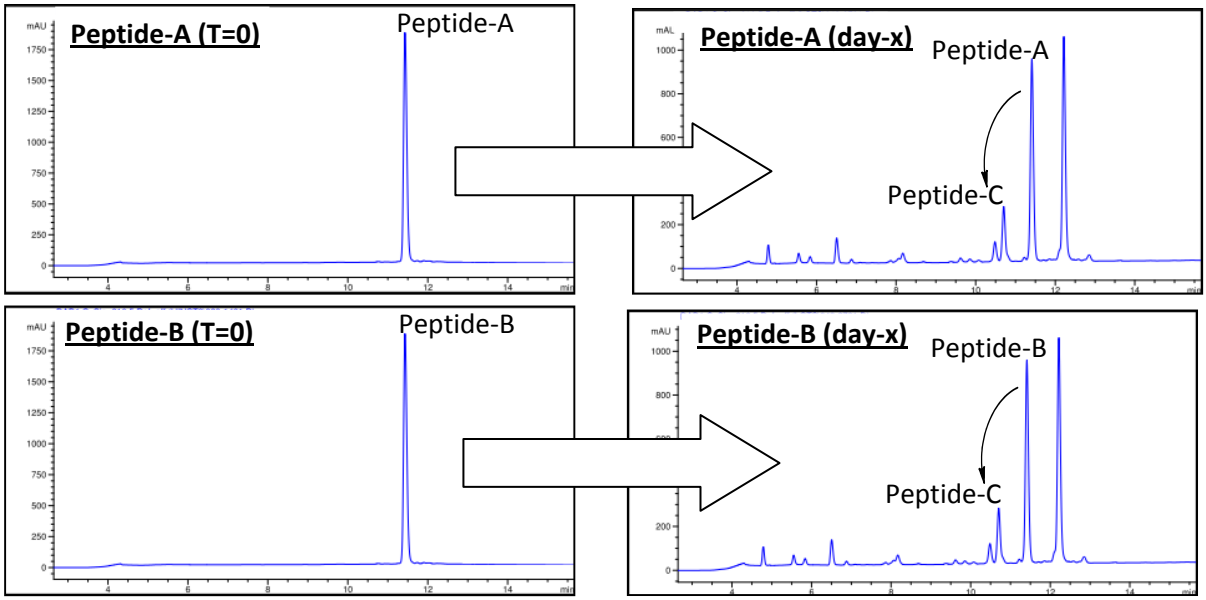

Figure 2-8 : HPLC traces (280 nm) showing the degradation of PFHSPSY and SFHSPSY to FHSPSY.

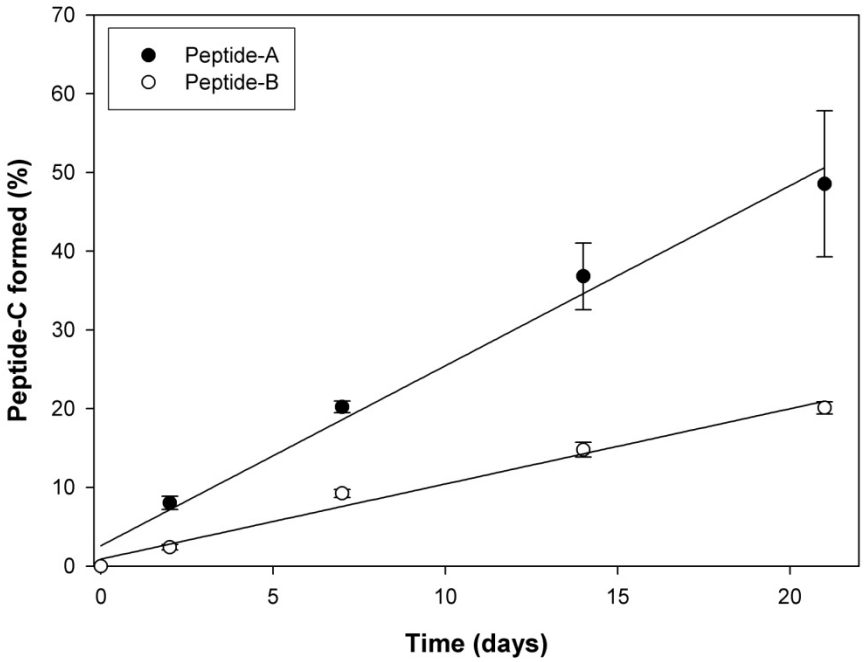

Figure 2-9: Comparison of the percentage of Peptide-A and Peptide-B that formed Peptide-C with respect to time.

2.3 Isolation of AQP0 from human lens and analysis (Chapter 7)

Isolation of AQP0 from human lens and digestion with trypsin

The N-terminal tryptic peptide of AQP0 was purified using methods based on those of Schey et al. [86]. Briefly, five lens pairs (age range 67-69 years) which had been stored at -80 °C were dissected into two regions (Nucleus) and (Cortex) using a 6 mm trephine. Each was homogenised in 6 M guanidine HCl in Tris pH 8.0 to dissolve the water soluble and water insoluble proteins. Following homogenisation the tubes were centrifuged at 16,000 G and the supernatant was removed. This process was repeated a further four times. Then the pellets were homogenised with water and centrifuged. This process was also repeated four more times and then the pellets were freeze dried. The resulting cell membrane was dissolved in 50 mM ammonium carbonate buffer pH 8 and 20 µg trypsin was added. The tubes were incubated at 37 °C for 16 hours and then freeze dried. Prior to digestion it is important to note that the cell membrane was deliberately not delipidated. This meant that only the N-terminal of AQP0, which protrudes from the membrane, should be cleaved rather than the whole of AQP0 as well as other intrinsic membrane proteins, which would complicate the sample.

Purification of AQP0 tryptic peptides by HPLC

Synthetic standards of MWELR and (D-Met)WELR were run by HPLC using Method-B (Section 2.2.2). The retention time of MWELR was 47.7 minutes and the retention time of (D-Met)WELR was 50.9 minutes (Figure 2-10).

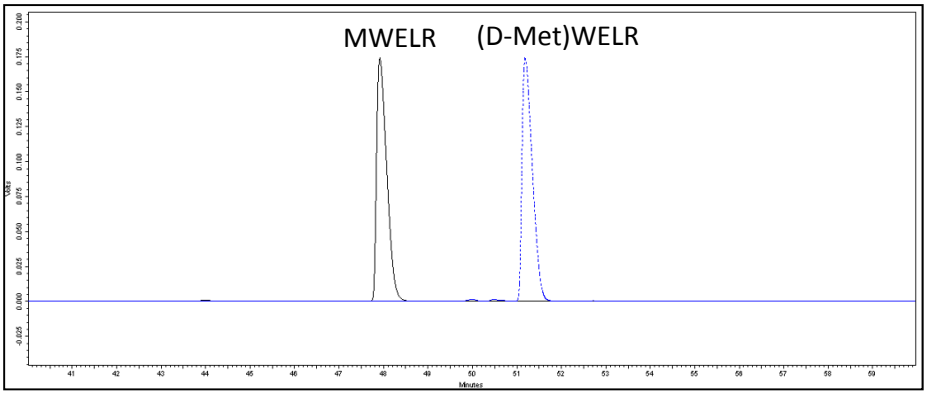

Figure 2-10: Separation of MWELR and (D-Met)WELR by HPLC.

A sample of the tryptic digest of the lens membrane was then injected into the HPLC using the same method as the synthetic standards. The fractions corresponding to the retention times of MWELR and (D-Met)WELR were collected and lyophilised. To add a second level of purification the lyophilized samples were then re-injected into the HPLC which was this time setup with methanol as solvent B instead of acetonitrile. Methanol was chosen to enable better purification of the desired AQP0 peptides as the peptides present in the fractions collected from the acetonitrile HPLC run would have very different elution profiles in methanol . With Methanol as solvent B the retention time of MWELR was 72.05 minutes and the retention time of (D-Met)WELR was 76.89 minutes. The fractions corresponding to the retention times of MWELR and (D-Met)WELR were collected.

Analysis by MALDI MS/MS mass spectrometry

MALDI-MS analysis was performed using a Shimadzu (Nakagyo-ku, Kyoto, Japan) Axima TOF2 mass spectrometer used in reflection positive ion mode. Peptides were prepared in α-cyano-4-hydroxycinnamic acid (8 mg/ml) in 80% (v/v) acetonitrile, 0.1% (v/v) TFA.

Analysis by ESI MS/MS mass spectrometry

High voltage (1800 V) was applied to a low volume tee (Upchurch Scientific) and the column tip positioned ~ 0.5 cm from the heated capillary (T=250 °C) of a LTQ FT Ultra (Thermo Electron, Bremen, Germany) mass spectrometer. Positive ions were generated by electrospray and the LTQ

FT Ultra operated in data dependent acquisition mode (DDA). A survey scan *m/z* 350-1750 was acquired in the FT ICR cell (resolution = 100,000 at *m/z* 400, with an accumulation target value of 1,000,000 ions). Up to the 6 most abundant ions (>3,000 counts) with charge states > +2 were sequentially isolated and fragmented within the linear ion trap using collisionally induced dissociation with an activation q = 0.25 and activation time of 30 ms at a target value of 30,000 ions. *m/z* ratios selected for MS/MS were dynamically excluded for 30 seconds.

Analysis by ESI LC- MS/MS mass spectrometry.

Nano-Liquid chromatography (nano-LC) was performed using an Ultimate 3000 HPLC and autosampler system (Dionex, Amsterdam, Netherlands). Samples were injected into a fritless nanoLC column (75 µ x ~10 cm) containing C-18 media (3 µ, 200 Å Magic, Michrom]. Peptides were eluted using a linear gradient according to the conditions in the Table 2-2, over 50 min, at a flow rate of 0.25 µL /min. Mobile phase A consisted of 0.1% formic acid in H_2O, while mobile phase B consisted of acetonitrile : H_2O (8:2) with 0.1% formic acid.

Table 2-2: LC-MS Gradient.

Time (min)	%B
0.0	2.0
4.0	5.0
34.0	45.0
35.0	90.0
36.0	90.0
37.0	2.0
50.0	2.0

Standards of MWELR and (D-Met)WELR were run to determine the retention time of each peptide. Then the tryptic digests of AQP0 isolated from the human lens samples were injected and the relative response factor of each peptide was determined by MS / MS as per above.

Degradation with Leucine amino peptidase

(L-Met)WELR and (D-Met)WELR were incubated with 1 µg leucine amino peptidase (LAP) in 50 mM Tris pH 8.5 at 30 °C (100 µg / 100 µl). Aliquots (20 µl) were taken at regular intervals and analysed by HPLC (Section 2.24 Method-C). The percentage of each peptide remaining with respect to time was plotted.

Chemical degradation

(L-Met)WELR and (D-Met)WELR were incubated (1 mg/ml) in 100 mM phosphate buffer pH 7.4 at 60 °C. Aliquots (20 µl) were taken at regular intervals and analysed by HPLC (Section 2.24 Method-C). The percentage of each peptide remaining with respect to time was plotted.

2.4 UV filter isolation and characterisation (Chapter 10)

Extraction of the UV filters from lenses of the thirteen-lined ground squirrel was done by members of the Giblin research group as follows:

Adult thirteen-lined ground squirrel s were obtained from TLS Research (Bloomington, IL,USA) with ethical approval from the Oakland University Institutional Animal Care and Use Committee, protocol #04081. The gender of the animals was not determined. Since the animals were wild-trapped, their exact ages were not known. The supplier has estimated ages of 1–3 years. Following euthanasia of the animals, lenses (27 mg wet wt. each) and retinas were removed from the eyes (the retinas were used in a separate study by another investigator). UV filters were extracted by homogenising each lens in 0.3 ml of 100% (v/v) ethanol, leaving at room temperature for 1 h, centrifuging for 10 min at 12 000 xg and re-extracting two times in 0.3 ml 80% (v/v) ethanol and treated as above. The supernatant was observed to be pale yellow in colour, and the precipitated protein was white. The supernatants were pooled and lyophilised. The dried extracts were then couriered to Australia.

HPLC purification

Combined extracts from 18 thirteen-lined ground squirrel lenses were dissolved in 0.1% TFA in Millipore water and UV-X was purified using semi-preparative HPLC (Method-A) as outlined in Section 2.2.2. The HPLC trace was monitored at 360 nm.

High resolution MS and MS/MS mass spectrometry

High-mass-accuracy analysis and MS/MS fragmentation was performed using an LTQXL Orbitrap Fourier Transform mass spectrometer operating in positive (electrospray) mode. Prior to analysis the system was calibrated and shown to be within an error of 2 ppm.

NMR analysis

NMR analysis was done as per Section 2.23

Hydrolysis of UV-X with HCl

UV-X was dissolved in 100 µl 6N HCl and incubated in a sealed glass vial at 100 °C. Samples (20 µl) were taken at T=0 and T= 2.5 hours and lyophilized. Samples were dissolved in 100 µl water, lyophillised again and analysed by HPLC as per Method-B (Section 2.2.4).

Synthesis of N-acetyl 3OH Kyn

N-acetyl 3OHKyn was generated as per the literature [166]. Briefly, acetic anhydride was added in a two-fold molar excess over 3OHKyn in 400 mM sodium phosphate buffer, pH 7.4 and it was incubated for 30 min at 37 °C. Both mono- and di-acetylated products were obtained and the correct mono acetylated adduct was purified by HPLC using the retention time of the *N*-acetyl 3OHKyn isolated from the thirteen-lined ground squirrel as a reference.

Synthesis of proposed novel UV filter structure (UV-X)

N-Acetyl 3OHKyn was incubated in 100 mM phosphate buffer pH 7.4 in the presence of excess (20 equiv) L-Pro to determine if an imine could be formed between the L-Pro amine and the ketone carbonyl of *N*-Acetyl 3OHKyn. A control which did not contain any L-Pro was also incubated. The incubation was then monitored by HPLC for the presence of an adduct that matched the retention time of UV-X.

3 Chapter 3: Section-A Overview (Reactions of Ser)

3.1 Introduction

Long-lived proteins such as the crystallins in the lens undergo numerous changes as a result of prolonged exposure to physiological conditions. Major modifications to such long-lived proteins include racemisation [117-119], deamidation [123, 132, 141, 193-195] and truncation [126, 127, 196-198]. Because the centre of the adult human lens contains no active enzymes [58, 59], it is likely that many of these processes are non-enzymatic in nature.

3.1.1 Serine truncation

In the case of α-crystallin, one notable feature of the sequences of two of the most abundant peptides (αA 67-80 and αB 1-18) is that sites of cleavage are adjacent to the N-terminal of Ser residues [128, 187]. Since enzyme activity is absent in the nuclei of adult human lenses [58-60, 198, 199], it is likely such cleavages result from spontaneous reactions involving Ser. While the truncation of peptides at the N-terminal of Asn residues *via* the formation of a succinimide ring [200] has been well characterised, our understanding of the processes that enable truncation at Ser is incomplete. One possible mechanism involves an *N*-*O*-acyl shift analogous to that seen in intein formation [201], followed by ester hydrolysis (Figure 3-1).

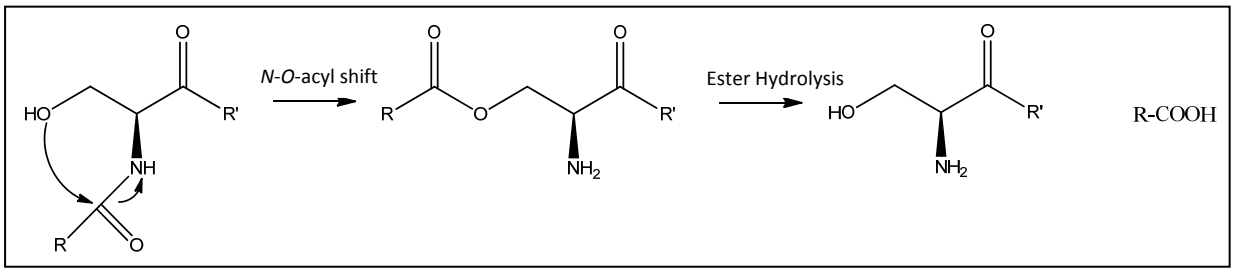

Figure 3-1: Potential mechanism to explain truncation on the N-terminal side of Ser residues. (R and R' represent the rest of the protein).

3.1.2 Serine Racemisation

Ser residues in human lens proteins have also been shown to racemise with age [117]. With the exception of Asp / Asn residues, which primarily racemise *via* an internal succinimide ring formation [202], racemisation of all other amino acids is thought to occur *via* a carbanion intermediate [203]. This involves the base catalysed removal of the hydrogen atom attached to the α-carbon resulting in a negatively charged planar carbanion intermediate being formed. Re-addition of a proton then occurs on either side of the carbanion to form the D- and L- enantiomer.

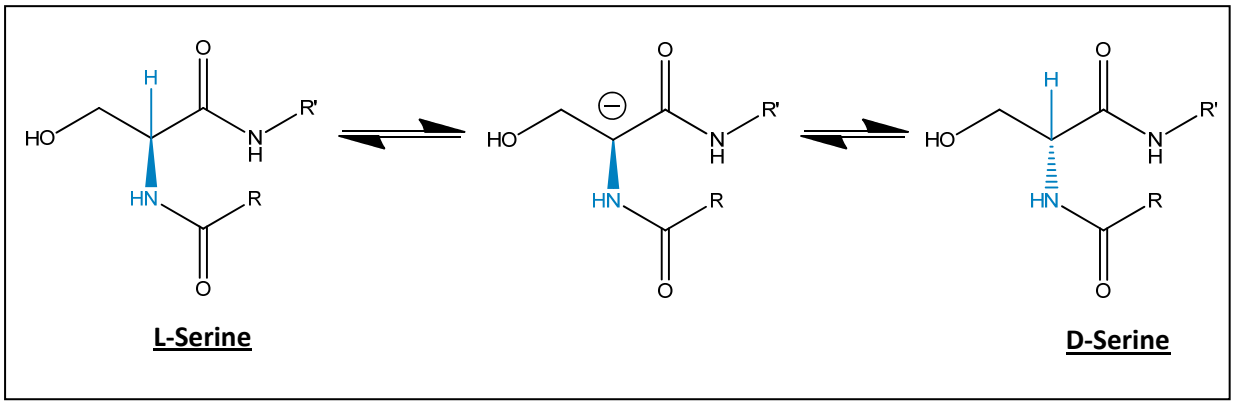

Figure 3-2: Racemisation of amino acids (using Ser as an example) *via* base catalysed alpha proton loss and re-addition. (R and R' represent the rest of the protein). Removal of alpha proton typically requires use of a strong base but under some conditions in the cell it could occur at physiological pH.

In relation to racemisation of Ser, another mechanism similar to the Asp / Asn one, involving the nucleophilic attack of the Ser hydroxyl on the neighboring amide bond *via* formation of a cyclic tetrahedral intermediate could be envisaged (Figure 4-3).

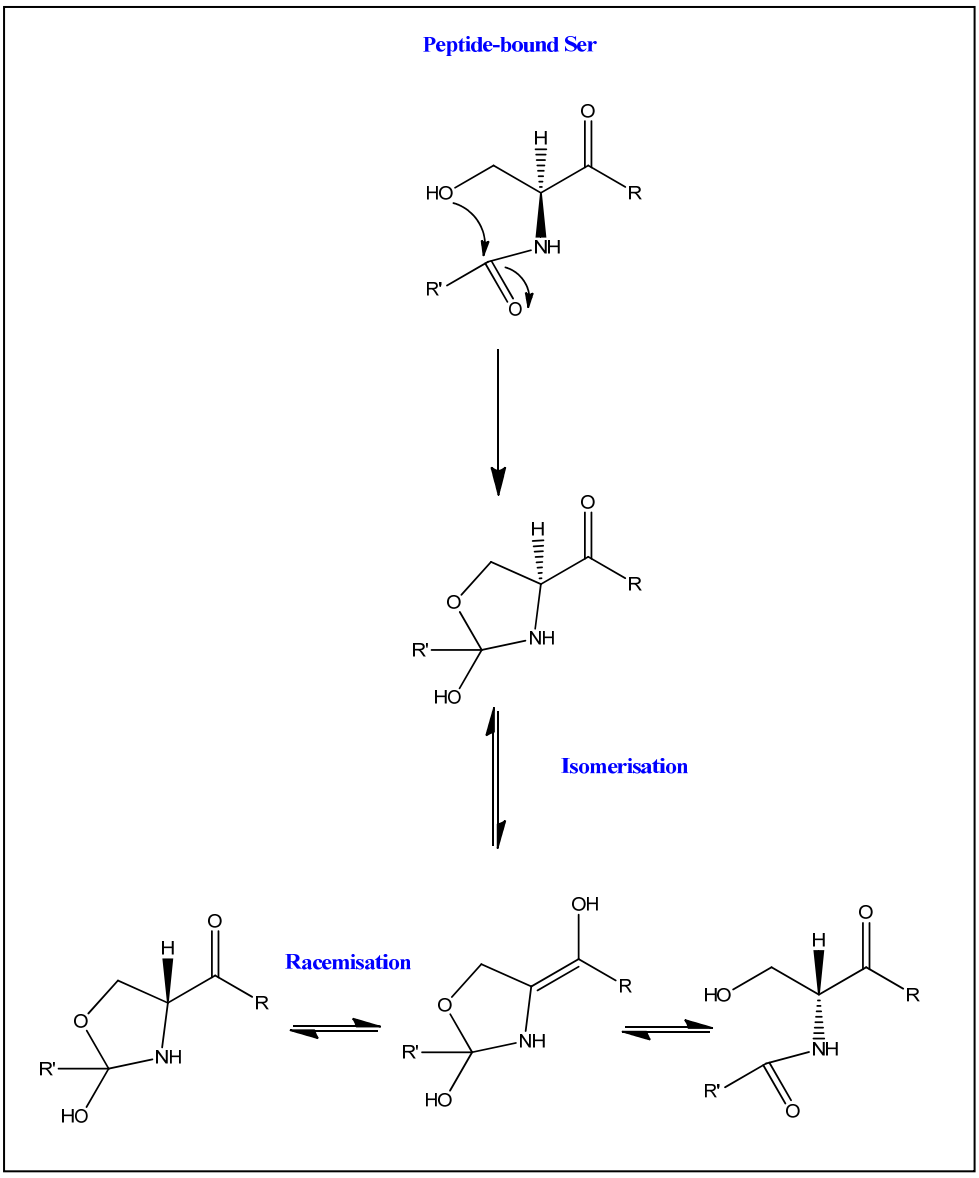

Figure 3-3: Possible mechanism for racemisation of peptide-bound Ser racemisation involving the nucleophillic attack of the Ser hydroxyl on the neighboring peptide bond and formation of a cyclic tetrahedral intermediate. (R and R' represent the rest of the protein).

3.1.3 Use of model peptides

Most of the experiments in this thesis use model peptides based on human lens protein sequences where age-related modifications are known to occur. It should be noted that in the lens secondary structure may influence the prevalence of these modifications but this is outside the scope of this thesis. Additionally while both inter-protein modifications such as cross-linking [2, 204] and intra protein modifications such as truncation[128], racemisation[205] etc have been shown to occur in the human lens with age, this thesis will only focus on intra-protein reactions.

4 Chapter 4: Chemical reactions of Ser

4.1 Aim

The aim of this chapter was to see if it were possible to replicate truncation at N-terminal of Ser using peptides incubated under physiological conditions. A secondary aim was to determine if Ser racemisation and truncation at the N-terminal side of Ser occur *via* a linked mechanism.

4.2 Model peptides based on known sites of Ser truncation in the lens

A notable feature of the sequence of one of the most abundant truncated peptides (αB-crystallin 1-18) found in the aged human lens, is that it is formed *via* cleavage on the N-terminal side of a Ser residue [128, 187]. A peptide PFHSPSY based on this sequence (αB 16-21) was therefore synthesised. The location of this sequence in a 3D model of bovine αB crystallin is shown in Figure 4-1. In the aged lens this truncation occurs on the N-terminal side of Ser 19 (equivalent to Ser 4 in the model peptide) [128, 187].

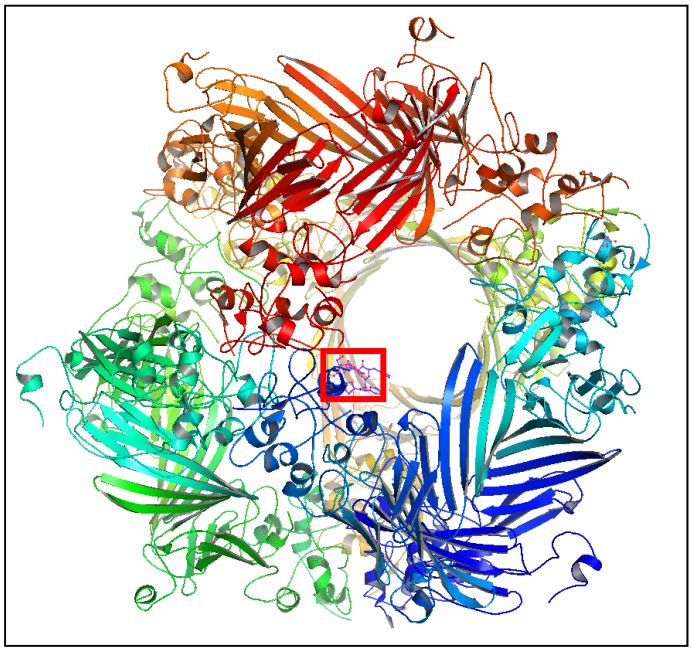

Figure 4-1: 3D model of Bovine αB crystallin modified to show the location of PFHSPS. Adapted from Braun et al [206]

PFHAPAY is a control peptide where both Ser residues have been replaced with Ala. Both peptides were incubated in triplicate at 60 °C pH 7.4 and characterised as per Incubation-B (Section 2.2.1).

4.2.1 Results and Discussion

A HPLC trace of the PFHSPSY incubation day-3 time point is shown in Figure 4-2.

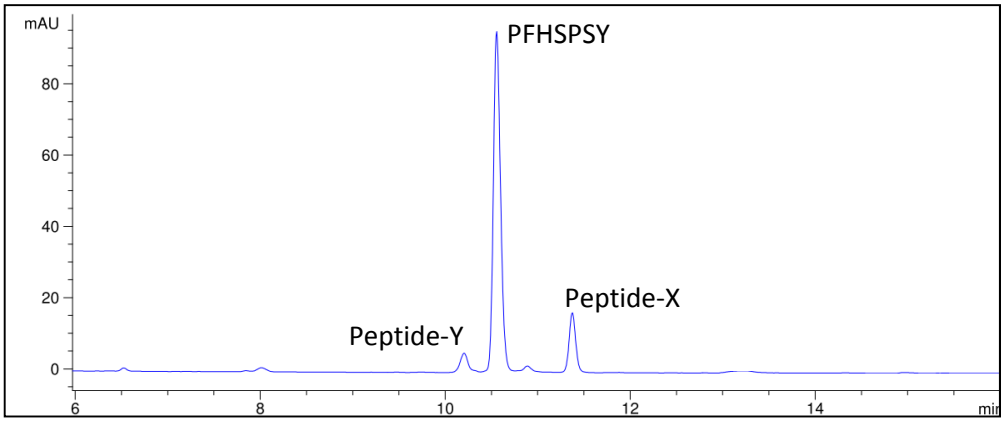

Figure 4-2: A HPLC trace (280 nm) showing the presence of Peptide-X and Peptide-Y, following incubation of PFHSPSY for 3 days at 60 °C. PFHSPSY was incubated in 100 mM phosphate buffer pH 7.4. At T=0 only a peak for PFHSPSY was observed.

The unexpected major products (Peptide-X and Peptide-Y) were modifications unrelated to truncation at the N-terminal of Ser. Similar peptides were also observed for PFHAPAY (Figure 4-3). Their characterisation (using a range of analytical techniques) as modifications occurring at the peptide N-terminus is discussed at length in Chapter 7 and Chapter 8. However due to the degradation of PFHSPSY and PFHAPAY, these model peptides proved unsuitable for their intended purpose of examining Ser cleavage and other options were investigated.

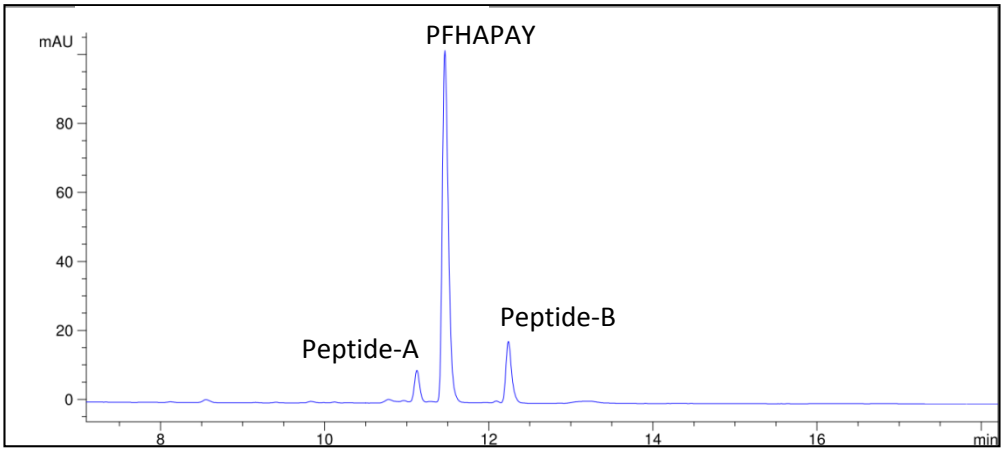

Figure 4-3: A HPLC trace (280 nm) showing the presence of Peptide-A and Peptide-B, following incubation of PFHAPAY for 3 days at 60 °C. PFHAPAY was incubated in 100 mM phosphate buffer pH 7.4. At T=0 only a peak for PFHAPAY was observed.

4.3 Model peptides based on the αB-crystallin sequence (60 °C)

To investigate if an N-terminal acetyl group could prevent the modifications observed in Section 4.2, a shorter model peptide Ac-SPSY was examined. A peptide where the Ser residues was replaced with Ala (Ac-APAY) was used as a control. Both peptides were incubated in triplicate (1 mg/ ml) at 60 °C pH 7.4 as per Incubation-B (Section 2.2.1).

4.3.1 Results and Discussion

HPLC traces showing the effects of incubating Ac-SPSY and Ac-APAY for 3 weeks at 60 °C is shown in Figure 4-4 and Figure 4-5 respectively.

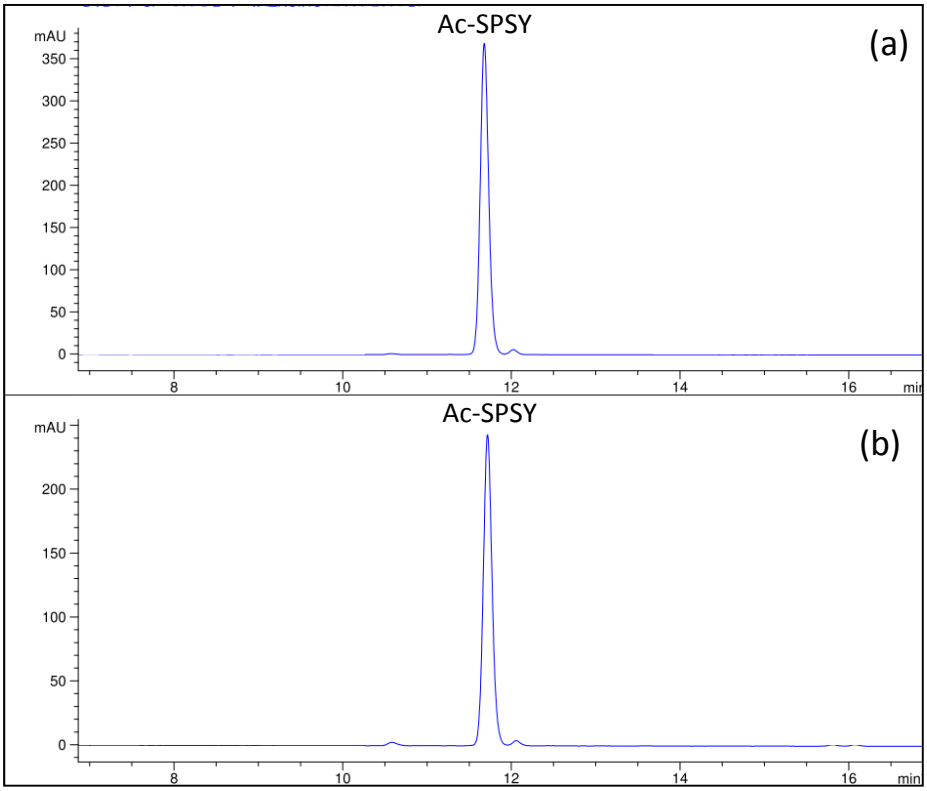

Figure 4-4: HPLC trace (280 nm) comparing Ac-SPSY at (a) T=0 and (b) 3 weeks.

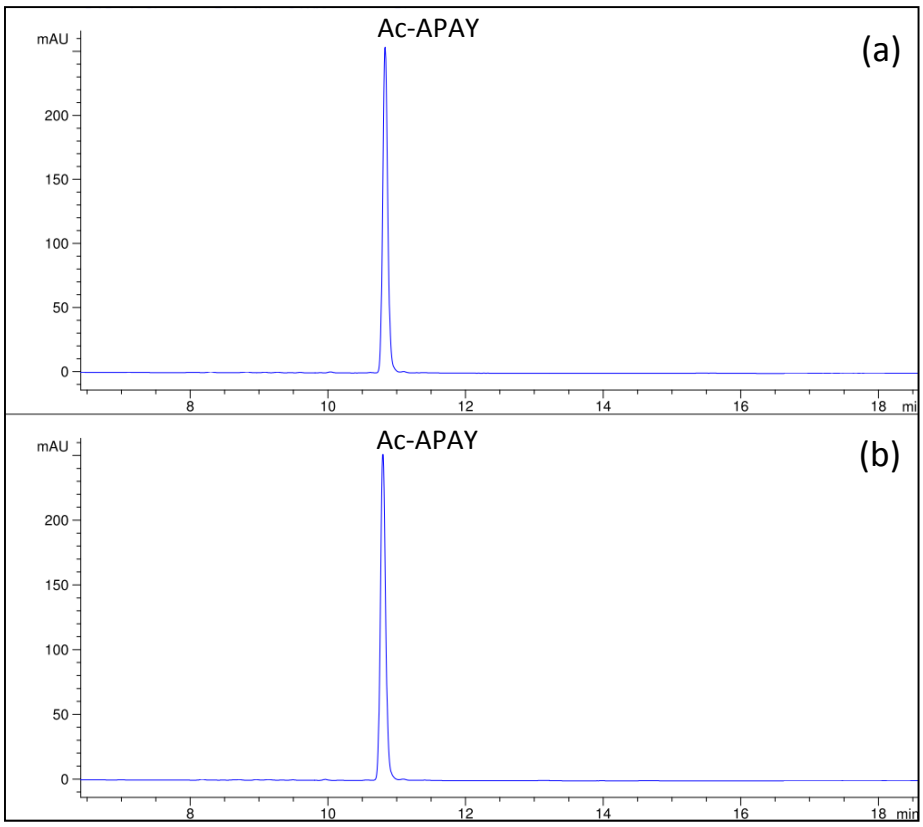

Figure 4-5: HPLC trace (280 nm) comparing Ac-APAY at (a) T=0 and (b) 3 weeks.

As can be seen in Figure 4-3 and Figure 4-5 there is no evidence of any major modification occurring, including the modifications seen in Section 4.1. So while it appears that an N-terminal acetyl group does prevent these modifications, it is also apparent that these model peptides do not show evidence of truncation at the N-terminal of Ser under these conditions. Repeating the experiment at a higher temperature was deemed necessary (Section 4.4).

4.4 Model peptides based on the αB-crystallin sequence (85 °C)

4.4.1 Method

Ac-SPSY and Ac-APAY were incubated at a higher temperature of 85 °C, pH 7.4 and products characterised as per Incubation-C (Section 2.2.1).

4.4.2 Results and Discussion

Figure 4-6 shows HPLC traces of the day-14 time points of each incubation.

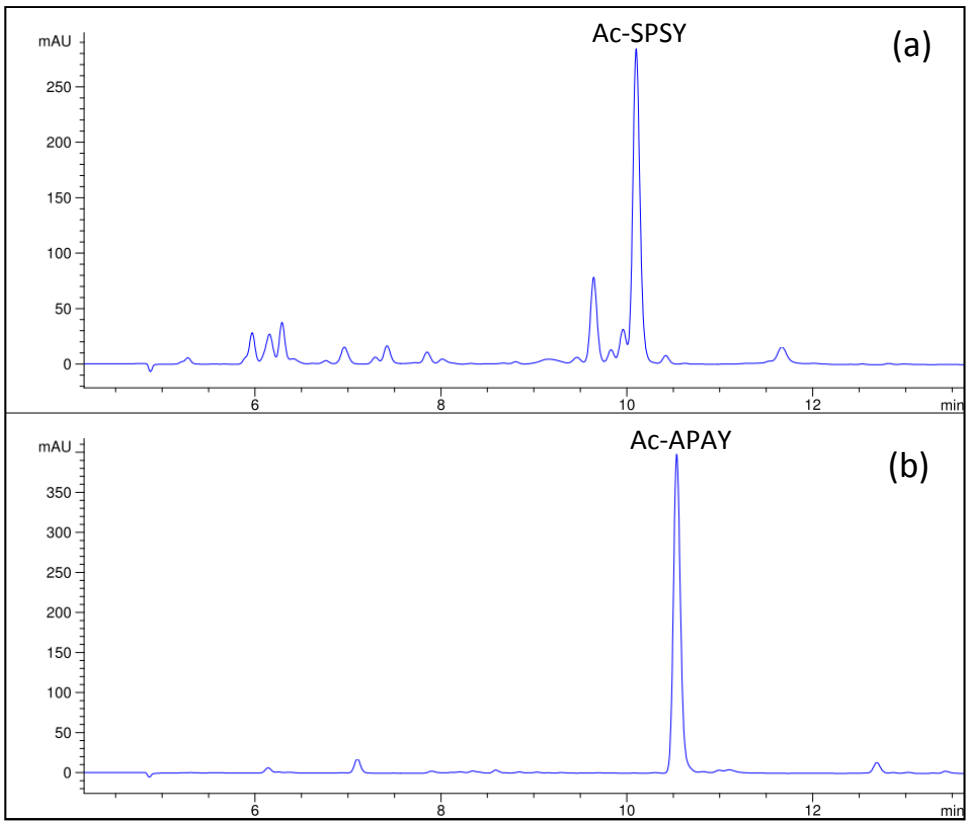

Figure 4-6: HPLC traces (280 nm) of day-14 time point following incubation of (a) Ac-SPSY and (b) Ac-APAY at 85 °C. Peptides were incubated in 100 mM phosphate buffer pH 7.4.

As can be seen above, after 14 days incubation at 85 °C Ac-APAY was relatively stable (~95% intact based on peak area) whereas Ac-SPSY showed significant degradation (~50% intact). The percentage of each peptide remaining with respect to time is shown in (Figure 4-7).

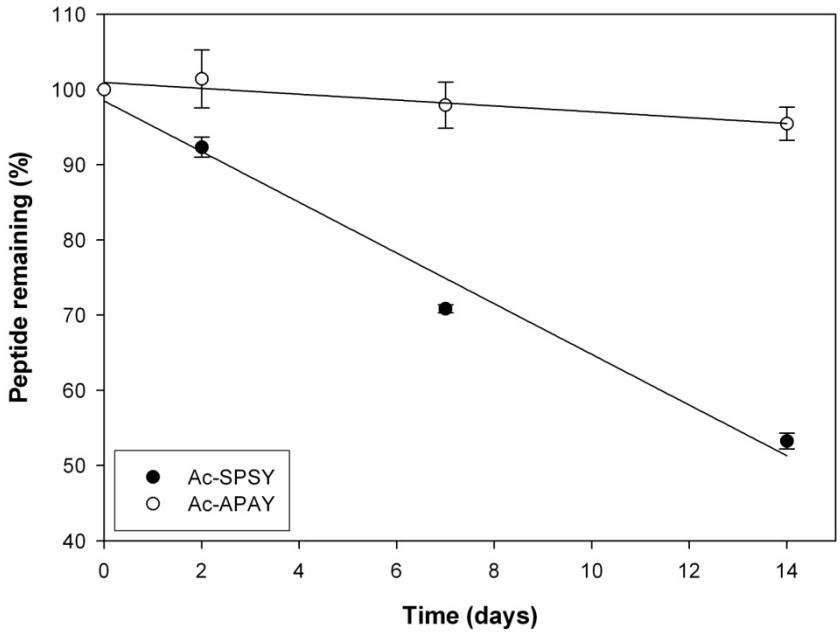

Figure 4-7: Percentage of Ac-SPSY and Ac-APAY remaining with respect to time. Peptides were incubated in 100 mM phosphate buffer pH 7.4 at 85 °C. Percentage values were calculated as the amount (moles) of each peptide present with respect to time compared to the amount of each peptide present at T=0.

A semi-preparative HPLC trace showing the isolation of the degradation products formed following incubation of Ac-SPSY at 85 °C is shown in Figure 4-8.

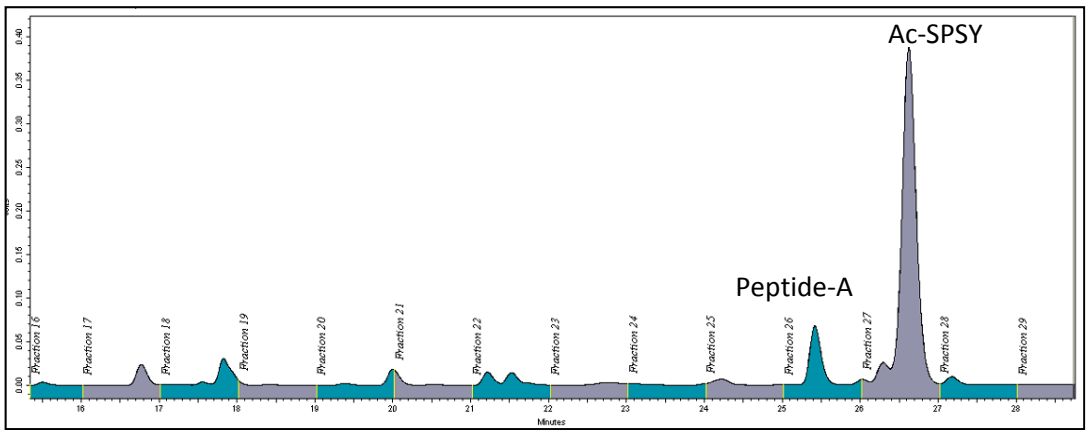

Figure 4-8: HPLC trace (280 nm) showing the purification by semi-preparative HPLC of the Ac-SPSY incubation. The alternating colours represent the fractions collected. Ac-SPSY was incubated in 100 mM phosphate buffer pH 7.4 at 85 °C for 2 weeks.

Truncation at the N-terminus of Ser

If truncation at the N-terminus of Ser similar to that seen in aged lens protein was occurring then two truncated peptides should be observed:

The use of HPLC standards confirmed the presence of SY indicating that truncation at the N-terminal of Ser occurred in Ac-SPSY. However incubation of SY under similar conditions (Section 6.8) found it spontaneously formed a diketopiperazine and, as a consequence of further breakdown, racemised and sequence inverted peptides. These processes are discussed in more detail in Chapter 6 but this made it unsuitable to use for quantifying the amount of N-terminal Ser truncation. A peptide with a retention corresponding to Ac-SP was also detected, but analysis of this peak by photo diode array (PDA) detection revealed that in addition to absorbing at the expected 216 nm it also absorbed at 280 nm. The most likely explanation of this is that another degradation peptide co-eluted with Ac-SP and this made it unsuitable to use for quantifying the amount of N-terminal Ser truncation.

Racemisation of a Ser residue

Analysis by MALDI mass spectrometry revealed the most abundant product, Peptide-A (Figure 4-9) had the same molecular weight as Ac-SPSY despite a different HPLC retention time (Table 4-1).

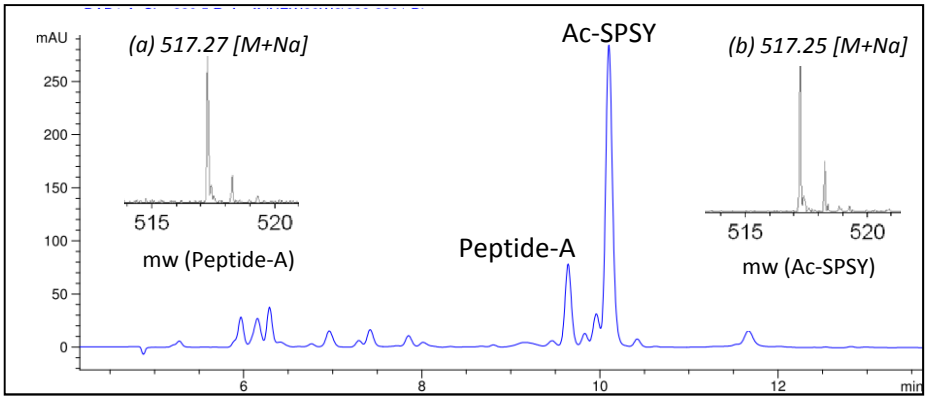

Figure 4-9: HPLC trace (280 nm) of the day-14 time point showing the major product (Peptide-A) formed following incubation of Ac-SPSY at 85 °C. Ac-SPSY was incubated in 100 mM phosphate buffer pH 7.4.The molecular weights (mw) of (a) Peptide-A and (b) Ac-SPSY, calculated my MALDI mass spectrometry are shown as inserts.

Table 4-1: Summary of MALDI mass spectrometry results.

Peptide	Mw	Retention time
Ac-SPSY	517.27 $[M+Na]^{1+}$	11.95
Peptide-A	517.25 $[M+Na]^{1+}$	11.34

Racemisation of one of more of amino acid residues is one possibility that could explain this. To test for racemisation, Ac-SPSY and Peptide-A were hydrolysed with HCl and subjected to chiral amino acid analysis using Marfey's reagent as per Section 2.23. This revealed that Peptide-A contained ~50% L-Ser and ~50% D-Ser, indicating that one of the Ser residues had racemised (Figure 4-10a). The results showed no evidence of racemisation of any other residues in either peptide.

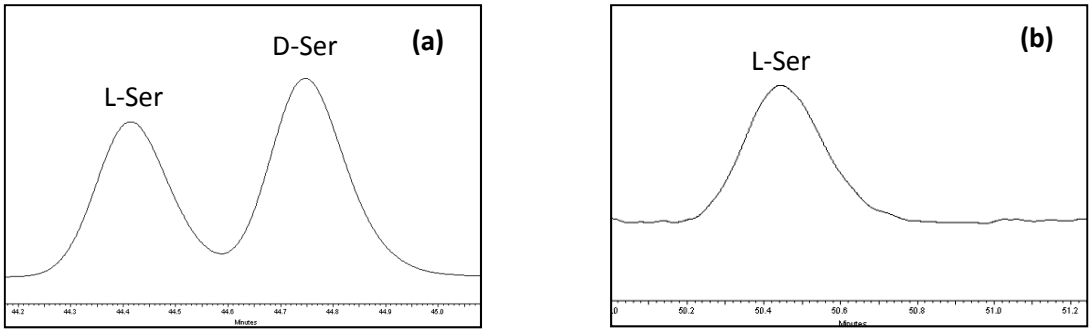

Figure 4-10: Chiral HPLC analysis of the hydrolysis products of (a) Ac-SPSY and the major (b) Peptide-A.

A standard of Ac-SP(D-Ser)Y was synthesised and compared to Peptide-A. While it was shown to have the same HPLC retention time as Peptide-A (Figure 4-11) indicating racemisation of Ser 3, the possibility that it was Ser 1 which racemised cannot be ruled out.

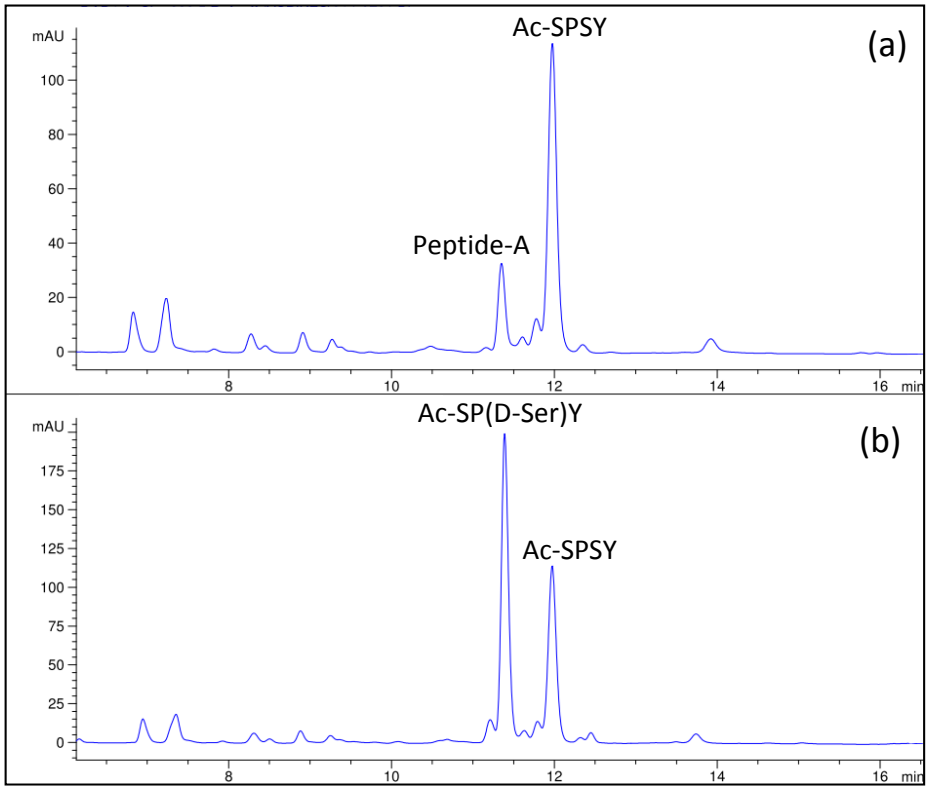

Figure 4-11: (a) HPLC analysis (280 nm) of Ac-SPSY day-14 time point showing the unknown peptide (Peptide-A) and (b) the same time point spiked with a standard of Ac-SPS(D-Ser)Y.

Standard curves for Ac-SPSY and Ac-SP(D-Ser)Y were generated as detailed in the Materials and Methods Chapter and these were used in combination with the HPLC time point data to calculate the number of moles of Ac-SPSY that underwent racemisation at Ser. An example of the standard curve for Ac-SPSY is shown in Figure 4-12.

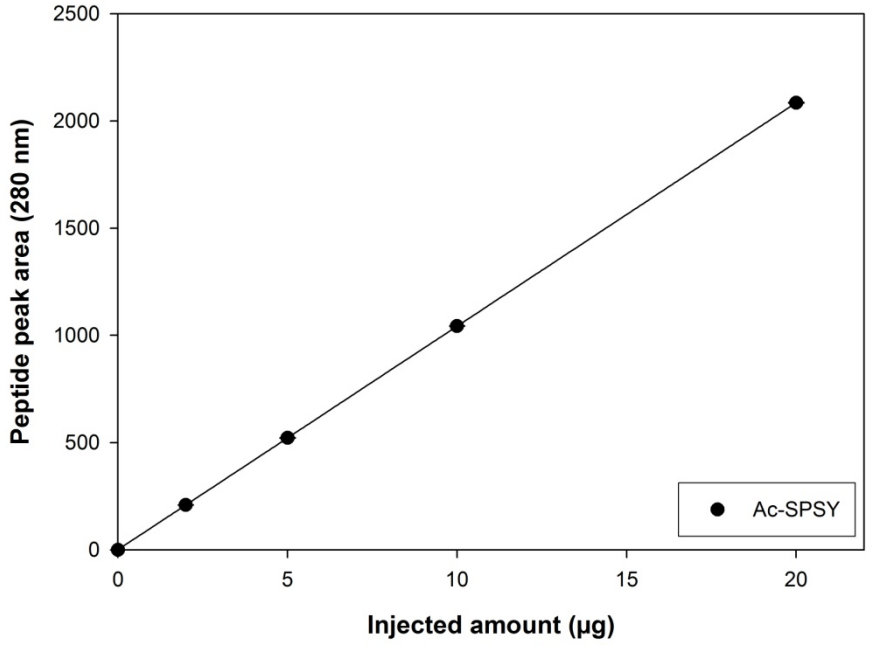

Figure 4-12: Standard curve for Ac-SPSY relating peak area at 280 nm to peptide amount (µg).

The number of moles of Ac-SPSY that underwent racemisation at Ser is shown in Figure 4-13.

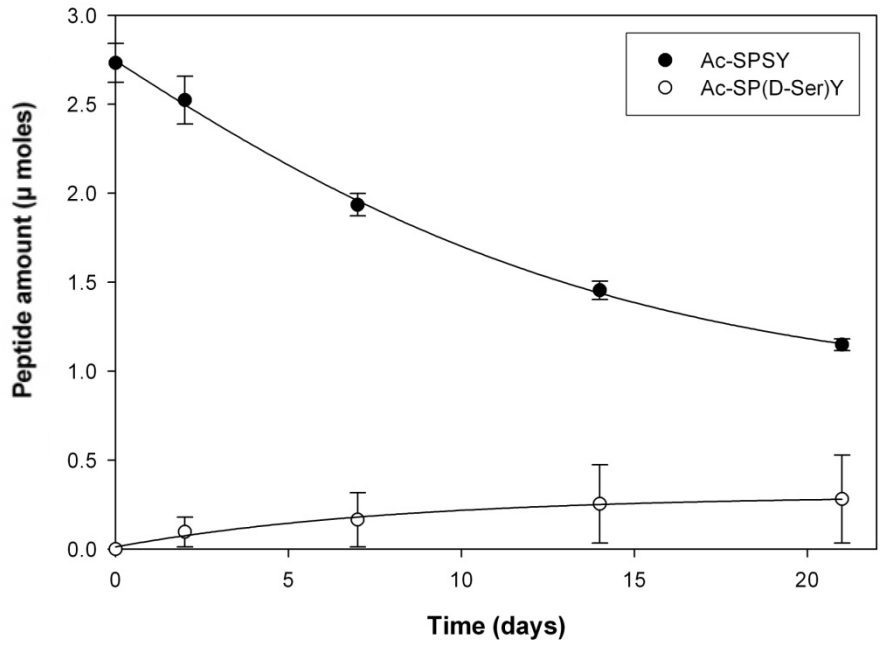

Figure 4-13: Time course showing (a) loss of Ac-SPSY and appearance of probable Ac-SP(D-Ser)Y. Ac-SPSY was incubated in 100 mM phosphate pH 7.4 at 85 °C.

As can be seen in Figure 4-14, approximately 14% of a Ser residue (assumed to be Ser 3) in Ac-SPSY was shown to racemise following incubation for 3 weeks at 85 °C. No racemisation of any residue in the control was observed.

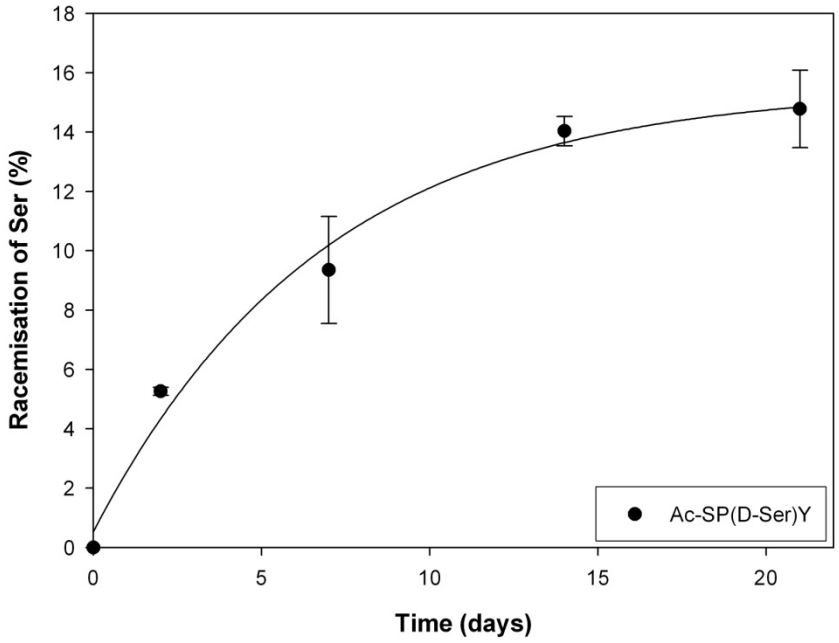

Figure 4-14: Percentage of Ser that racemised when Ac-SPSY was incubated at 85 °C. Ac-SPSY was incubated in 100 mM phosphate buffer pH 7.4. Percentage values were calculated as the amount (moles) of Ac-SP(D-Ser)Y present with respect to time compared to the amount of Ac-SPSY present at T=0.

4.5 Simple model peptides

Section 4.4 demonstrated that a peptide containing a Ser residue, degraded faster and racemised faster than a non-Ser containing control peptide. However due to the instability of SY and the co-elution of other modified peptides with Ac-SP it was not possible to accurately determine if the degradation was due to truncation at the N-terminal of Ser.

To investigate this, the following two simple model peptides were compared.

(1) Ac-FSY

(2) Ac-FS(O-Me)Y

Both incorporate an N-terminal acetyl group to prevent the N-terminal degradations that will be discussed in Section-B of this thesis. Aromatic residues with differing UV absorbance profiles were chosen at the N- and C- terminals to aid with characterisation of any degradation products. The key difference between the two peptides is that Ac-FS(O-Me)Y contains a blocked Ser alcohol (OH) group as highlighted in Figure 4-15. The purpose of this was to examine if the Ser alcohol group plays a role in either racemisation or peptide degradation *via* truncation at the N-terminal side of Ser residues. Both peptides were incubated in triplicate (1 mg/ml) at 85 °C pH 7.4 and characterised as per Incubation-C (Section 2.2.1).

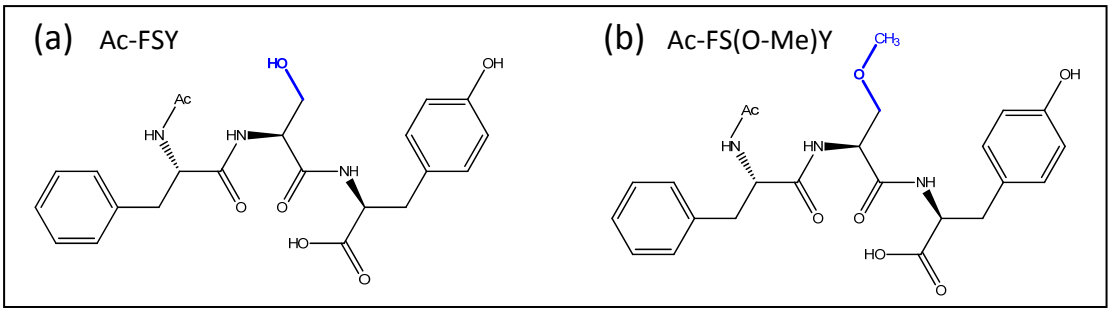

Figure 4-15: Structure of (a) Ac-FSY and (b) Ac-FS(O-Me)Y.

4.5.1 Results and Discussion

Characterisation

An example of the manner in which the degradation products of the Ac-FSY incubation were purified by semi-preparative HPLC is shown in Figure 4-16.This process was repeated to characterise the products of the Ac-FS(O-Me)Y incubation.

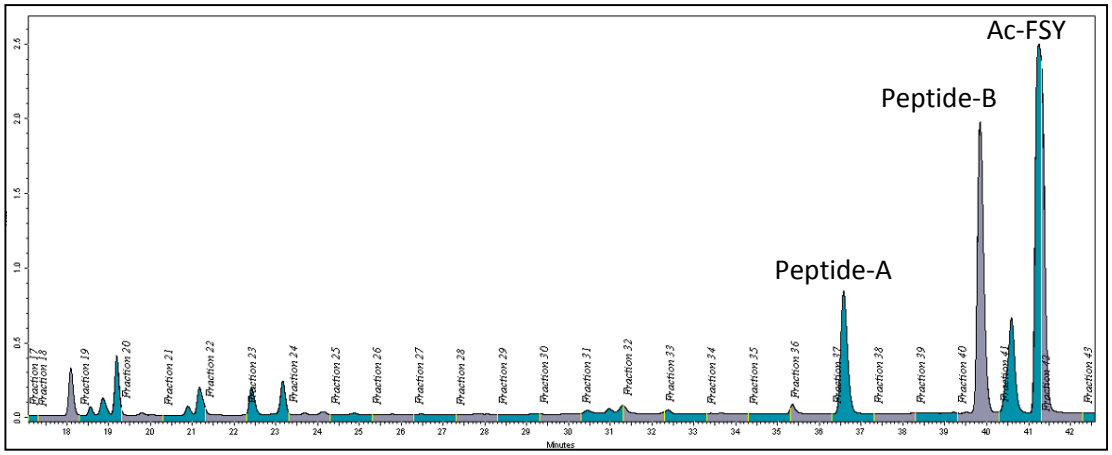

Figure 4-16: HPLC trace (257 nm) showing the semi-preparative purification of the major degradation products formed when Ac-FSY was incubated at 85 °C. Ac-FSY was incubated in 100 mM phosphate buffer pH 7.4 for 2 weeks.

Truncation at the N-terminus of Ser

If truncation at the N-terminus of Ser was occurring then the peptides detailed in Table 4-2 should be observed.

Table 4-2: Peptide truncation products.

Peptide	Ser truncation products
Ac-FSY	Ac-F + SY
Ac-FS(O-Me)Y	Ac-F + S(O-Me)Y

The use of synthetic HPLC standards suggested the presence of SY and other SY degradation products in the incubation of Ac-FSY and of S(O-Me)Y and its corresponding degradation products in the incubation of Ac-FS(O-Me)Y (Figure 4-17). This provided an indication that truncation at the N-terminal of Ser had occurred. Separate incubation of SY and S(O-Me) confirmed that they rapidly degrade *via* diketopiperazine formation resulting in racemised and sequence inverted peptides. These degradations are discussed in more detail in Chapter 6 but this made them unsuitable for monitoring the rate of truncation at the N-terminal side of Ser. For this reason the rate of formation of Ac-F was used to compare the rate of N-terminal Ser truncation.

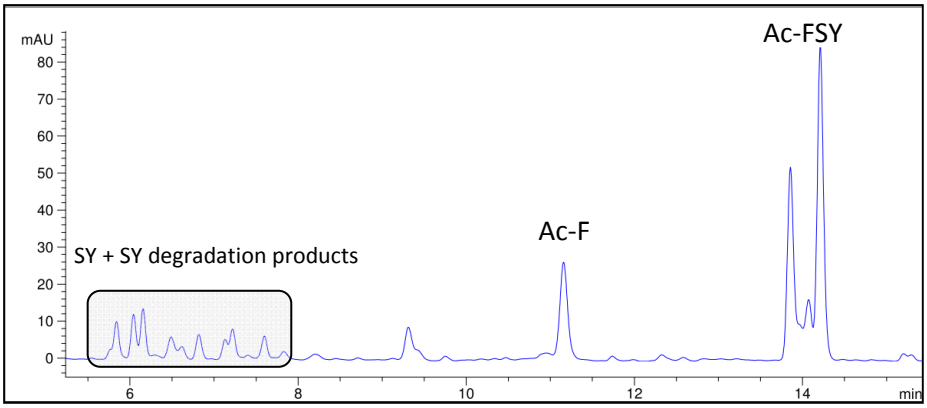

Figure 4-17: Ac-FSY day-14 HPLC spectra (280 nm).

The formation of Ac-F in both incubations was suggested by the appearance of a peak at 46 minutes that had an absorbance at 257 nm but not at 280 nm. The lack of absorbance at 280 nm is evidence that this peptide does not contain a Tyr residue (Figure 4-18).

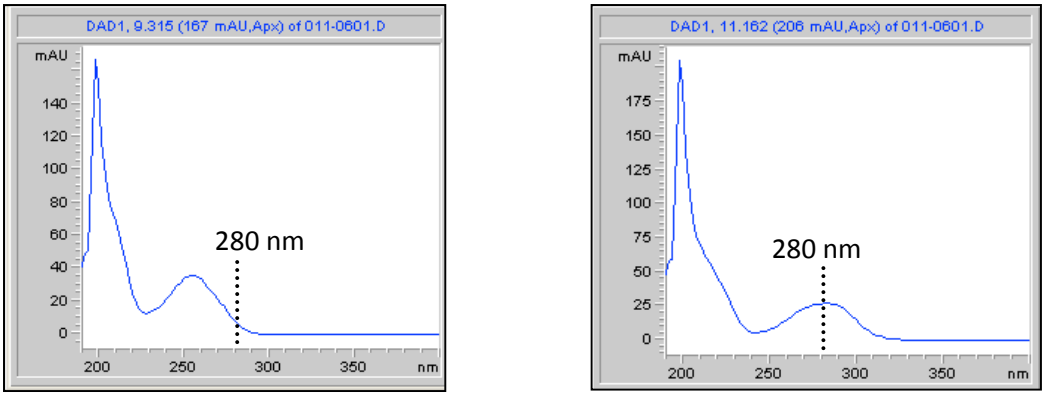

Figure 4-18: PDA analysis of (a) Ac-F and (b) Ac-FSY. Peptides with a Tyr residue (Ac-FSY) absorb strongly at 280 nm whereas Ac-F, which has a Phe residue but no Tyr, has a peak absorbance of 257 nm.

Further evidence supporting the assignment of Ac-F as a product of the incubations was obtained by spiking time point samples of Ac-FSY and Ac-FS(O-Me)Y with a standard of Ac-F and showing that it co-eluted. An example of the HPLC trace (257 nm) of Ac-FSY day 14 time point spiked with Ac-F is shown in Figure 4-19.

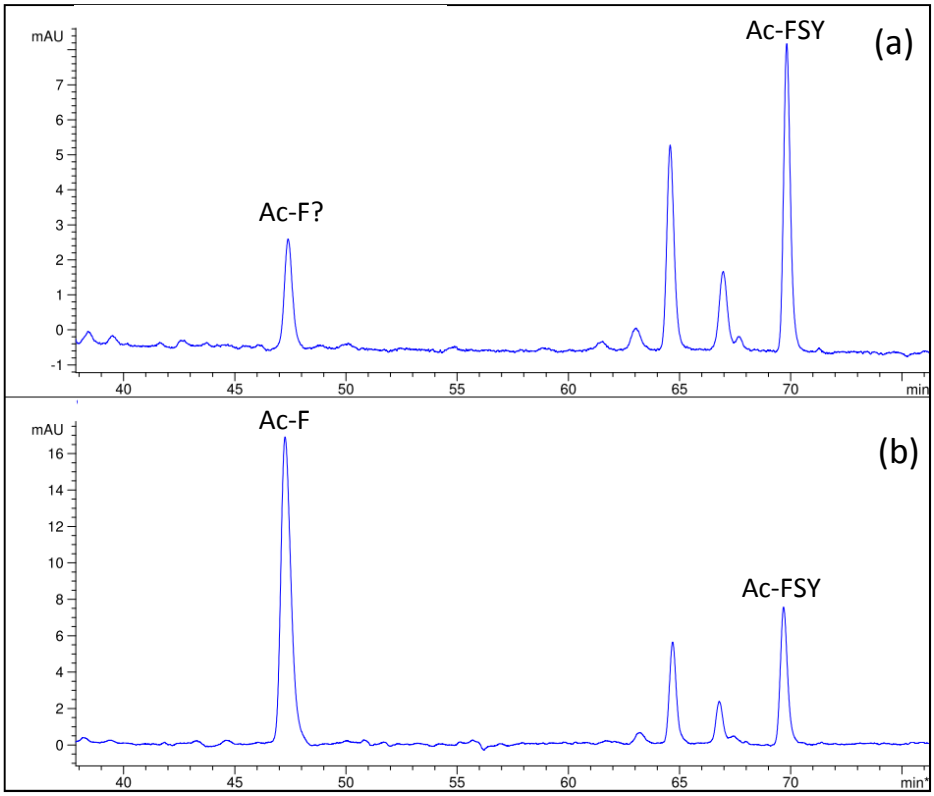

Figure 4-19: HPLC trace (257 nm) of (a) Ac-FSY day-14 incubation time point, (b) Ac-FSY day-14 incubation time point spiked with a standard of Ac-F.

Quantification

Standard curves for each peptide were generated as detailed in the Materials and Methods Chapter and these were used to calculate the number of moles of each peptide that truncated at the N-terminal of Ser forming Ac-F. An example of the standard curve for Ac-FSY is shown in Figure 4-20.

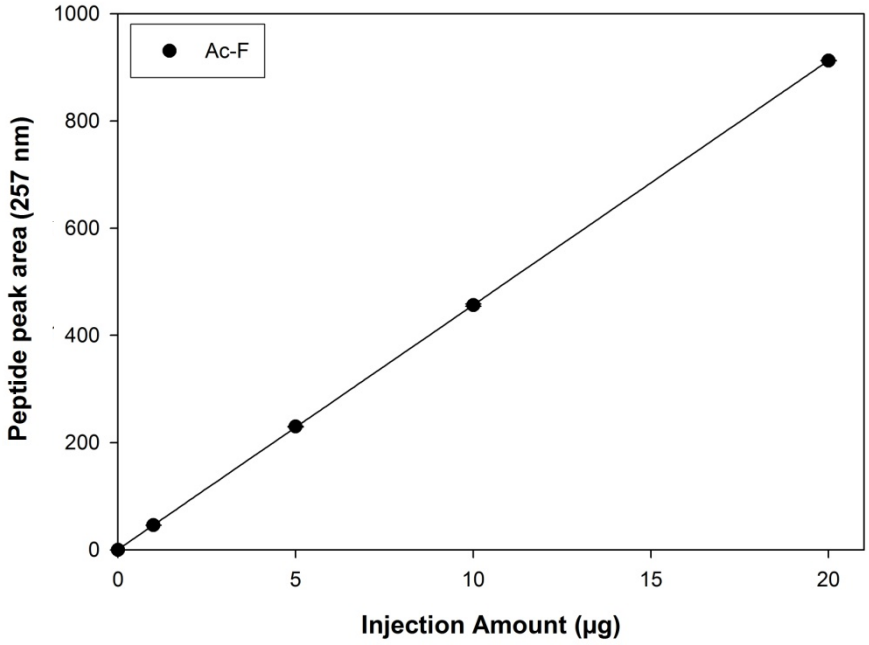

Figure 4-20: Standard curve of Ac-F relating peak area at 257 nm to peptide amount (µg).

The time course of truncation at the N-terminal of Ser (amount of Ac-F formed) in each incubation is shown in Figure 4-21.

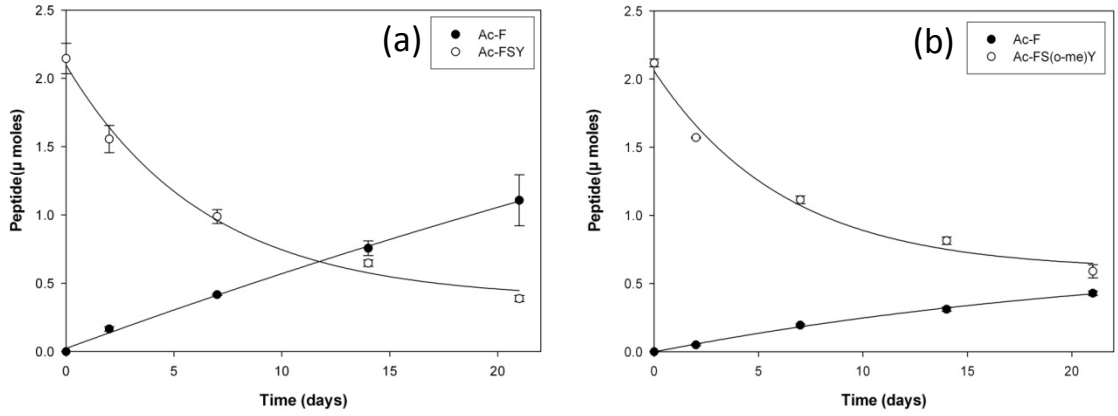

Figure 4-21: Time course showing (a) Loss of Ac-FSY and appearance of Ac-F, (b) Loss of Ac-FS(O-Me)Y and appearance of Ac-F. Peptides were incubated in 100 mM phosphate buffer pH 7.4 at 85 °C.

To compare the rate of N-terminal Ser truncation between the two peptides, the percentage conversion of each peptide to Ac-F was calculated (Figure 4-22).

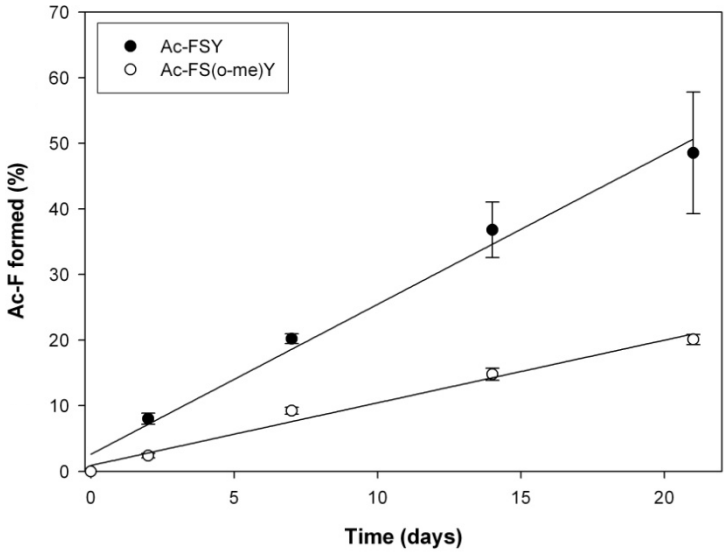

Figure 4-22 : Percentage of Ac-FSY and Ac-FS(O-Me)Y that truncated forming Ac-F. Peptides were incubated in 100 mM phosphate buffer pH 7.4 at 85 °C. Percentage values were calculated as the amount (moles) of each peptide which formed Ac-F with respect to time compared to the amount of each peptide present at T=0.

The data shows that Ac-FSY truncated at approximately double the rate of Ac-FS(O-Me)Y indicating that the presence of a free Ser OH group increased the rate peptide bond cleavage.

Racemisation at Serine

The Ser truncation products discussed above were not the major modification products observed in these incubations (Figure 4-19a). Analysis by MALDI mass spectrometry revealed the major product of both incubations had the same molecular weight as their respective intact peptides but a different retention time by HPLC (Table 4-3).

Table 4-3: Comparison of the molecular weight and HPLC retetion times of the major degradation products and intact peptides from each incubation.

Peptide	Mw	Retention time
Ac-FSY	480.30 $[M+Na]^{1+}$	64.9
Major degradation product	480.26 $[M+Na]^{1+}$	69.8

Peptide	Mw	Retention time
Ac-FS(O-Me)Y	494.22 [M+Na]	66.3
Major degradation product	494.26 [M+Na]	71.5

Figure 4-23 highlights this using a HPLC trace (280nm) of the Ac-FSY incubation showing that Peptide-B has a different retention time but the same molecular weight as Ac-FSY. A similar peptide was the major product formed in the Ac-FS(O-Me)Y incubation.

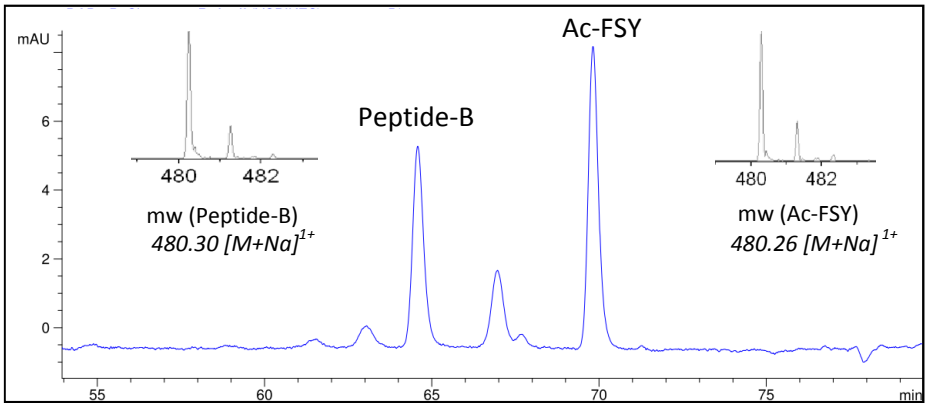

Figure 4-23: HPLC trace (280 nm) showing the formation of an unknown degradation product (Peptide-B) formed following the incubation of Ac-FSY at 85 °C. The molecular weight (mw) of Peptide-B calculated by MALDI mass spectrometry is shown in the insert and matched that of Ac-FSY.

This suggested racemisation of one or more of the amino acids was occurring. Chiral HPLC amino acid analysis of the hydrolysis products of Ac-FSY (Figure 4-24a) using Marfey's reagent (Section 2.2.3) revealed no evidence of D-Ser or other D-amino acids. Conversely analysis of Peptide-B (Figure 4-24b) showed it contained predominantly D-Ser.

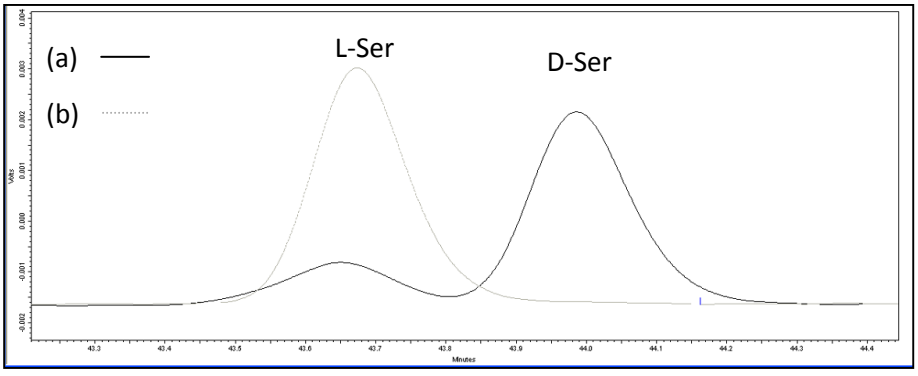

Figure 4-24: Chiral HPLC amino acid analysis of hydrolysis products of (a) Ac-FSY and (b) Peptide-B.

Similar results were obtained for Ac-FS (O-Me)Y and its suspected racemised peptide. No evidence of racemisation of Phe or Tyr was detected in any of the peptides analysed.

Standards of Ac-F(D-Ser)Y and Ac-F(D-Ser-O-Me)Y were synthesised and it was confirmed they had the same HPLC retention times as the putative racemised peptides. An example of a HPLC trace of the Ac-FSY day-14 time point spiked with Ac-F(D-Ser)Y is shown in Figure 4-25. The UV absorbance profile of each peptide is also overlaid.

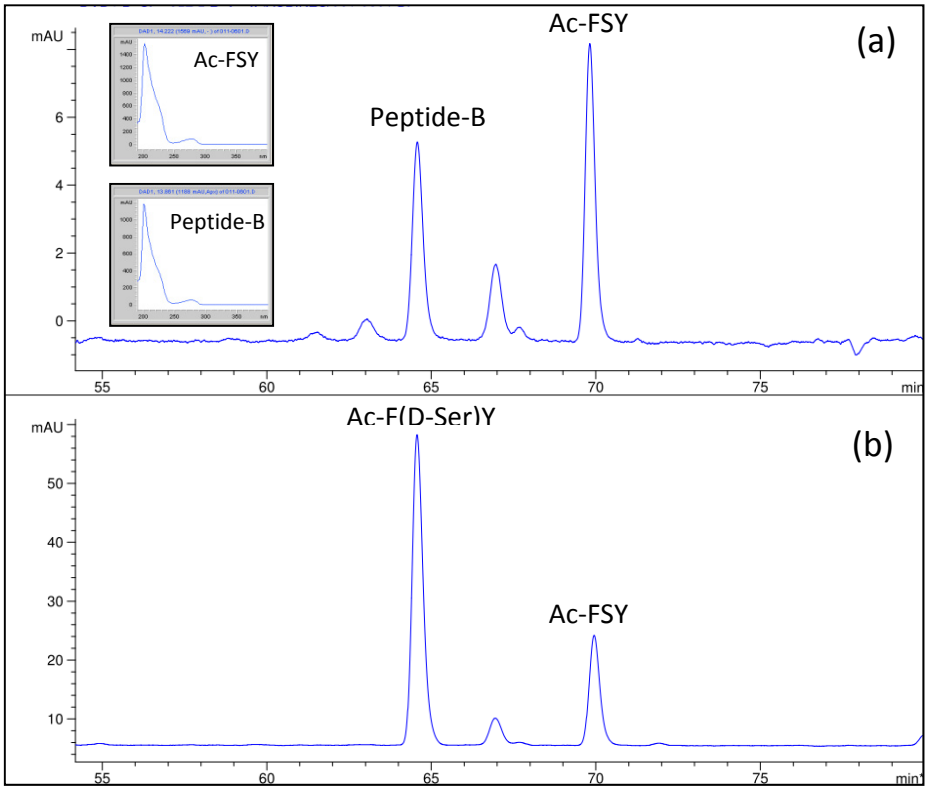

Figure 4-25: (a) Ac-FSY day-14 HPLC spectra (280 nm) and (b) Ac-FSY day-14 HPLC spectra (280 nm) spiked with a standard of Ac-F(D-Ser)Y. The UV absorbance profile of Ac-FSY and Peptide-B is also overlaid.

An expanded region (250 nm to 300 nm) of the UV absorbance profile of Ac-FSY and Peptide-B is shown in Figure 4-26.

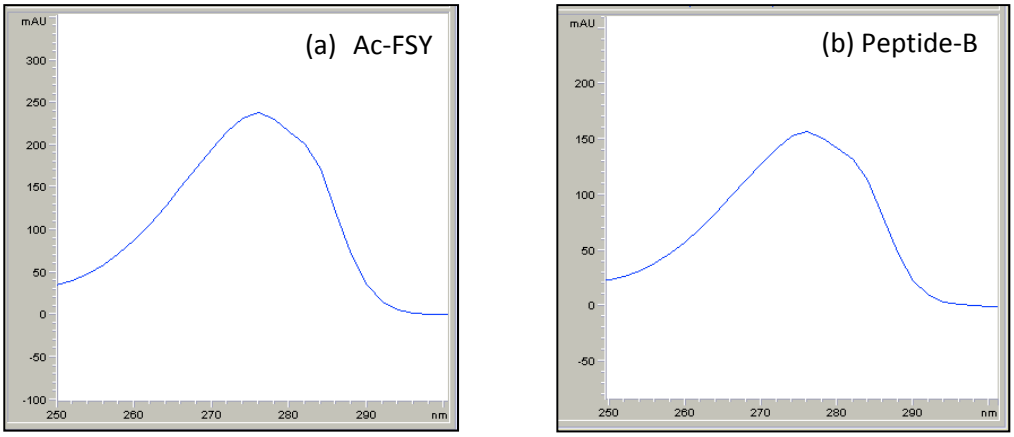

Figure 4-26: Expanded region (250 nm to 300 nm) of the UV absorbance profile of (a) Ac-FSY and (b) Peptide-B

Standard curves for each peptide were generated as detailed in the Materials and Methods Chapter and these were used to calculate the number of moles of each peptide that racemised at the Ser residue. The rate of disappearance of the intact peptide and appearance of the Ser racemised peptide for both incubations was plotted in Figure 4-27. The observed plateau in the rate of formation of the racemised peptides is likely due to degradation *via* other processes.

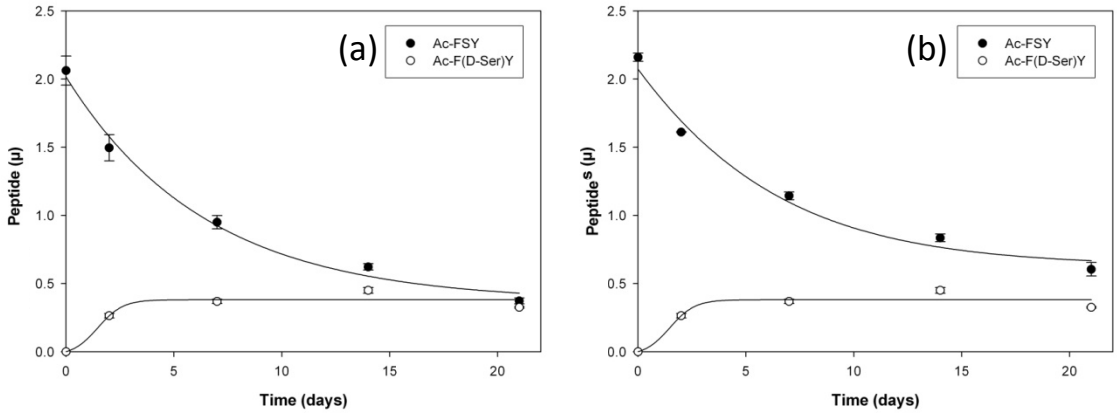

Figure 4-27: Time course showing (a) Loss of Ac-FSY and appearance of Ac-F(D-Ser)Y, (b) Loss of Ac-FS(O-Me)Y and appearance of Ac-F(D-Ser-O-Me)Y. Peptides were incubated in 100 mM phosphate buffer pH 7.4 at 85 °C.

To compare the rate of Ser racemisation in Ac-FSY and Ac-FS(O-Me)Y the percentage of each peptide that racemised with respect to time was plotted in Figure 4-28.

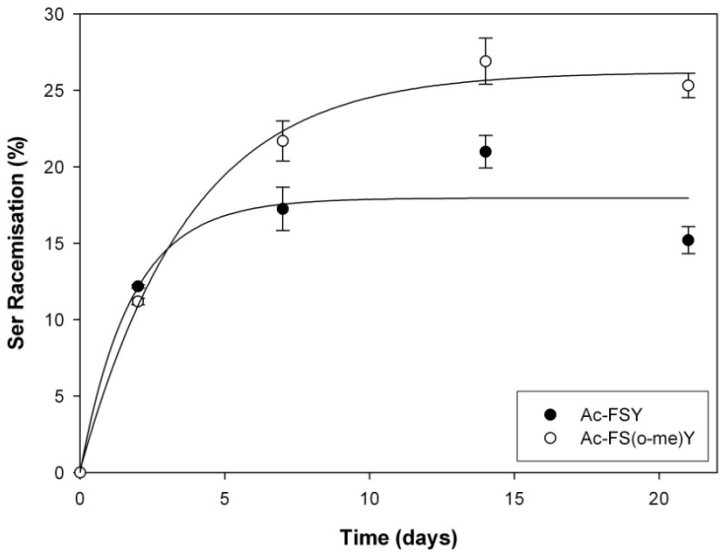

Figure 4-28: Percentage of Ser racemisation when Ac-FSY and Ac-FS(O-Me)Y were incubated at 85 °C. Peptides were incubated in 100 mM phosphate buffer pH 7.4 at 85 °C. Percentage values were calculated as the amount (moles) of each peptide which formed D-Ser with respect to time compared to the amount of each peptide present at T=0.

Surprisingly Ser racemised faster in Ac-FS(O-Me)Y, which has a blocked Ser OH, than in Ac-FSY which has a free OH. However, Figure 4-22 demonstrated that due to the presence of a free Ser OH, Ac-FSY truncates faster than Ac-FS(O-Me)Y at the N-terminal of Ser. Further evidence for this is also observed in Figure 4-28 where the racemised product of Ac-FSY rises initially at a similar rate to Ac-FS(O-Me)Y but then begins to fall. This is likely the result of truncation at the N-terminal side of Ser as per Figure 4-22. These observations may help to explain the apparently slower rate of Ser racemisation seen in Ac-FSY than in Ac-FS(O-Me)Y.

An important thing to note is that a free Ser alcohol group increased the rate of truncation at the N-terminal of Ser, but did appear to influence the rate of Ser racemisation. If both racemisation and truncation were occurring *via* a common mechanism then Ac-FS(O-Me)Y should have shown little racemisation. The O-Me derivative cannot form the cyclic tetrahedral intermediate. These results suggest that under the conditions outlined above, truncation at the N-terminus of Ser and racemisation are separate, i.e. not linked processes. So while a free OH group may be important for the N-terminal truncation of Ser it seems apparent that a different process e.g. direct abstraction of the α proton is responsible for Ser racemisation under these conditions.

4.6 *N*-α-acetyl peptides based on a known site of truncation site at Ser

Having demonstrated that Ser truncation and Ser racemisation can occur at physiological pH using simple tripeptides, the next step was to see if a known Ser truncation site in a lens crystallin could also be reproduced. Ac-PFHSPSY is based on the αB-crystallin sequence (16-21). In the aged human lens it has been shown to truncate at Ser 19 (i.e. Ser 4 in the model peptide) [128, 187]. Ac-PFHAPAY was synthesised as a control peptide where both Ser residues were replaced with Ala. Both incorporate an N-terminal acetyl group to prevent the degradations that will be discussed in this thesis in Section B. Tyr was added at the C-terminal to aid HPLC detection. Both peptides were incubated at 85 °C and characterised as per Incubation-C (Section 2.2.1).

4.6.1 Results and Discussion

The time-course of the degradation of Ac-PFHSPSY and Ac-PFHAPAY is shown in Figure 4-29. As can be seen from the graph, Ac-PFHSPSY is less stable than the control (Ac-PFHAPAY) under these conditions. However this does not necessarily mean this is the result of truncation at either Ser residue.

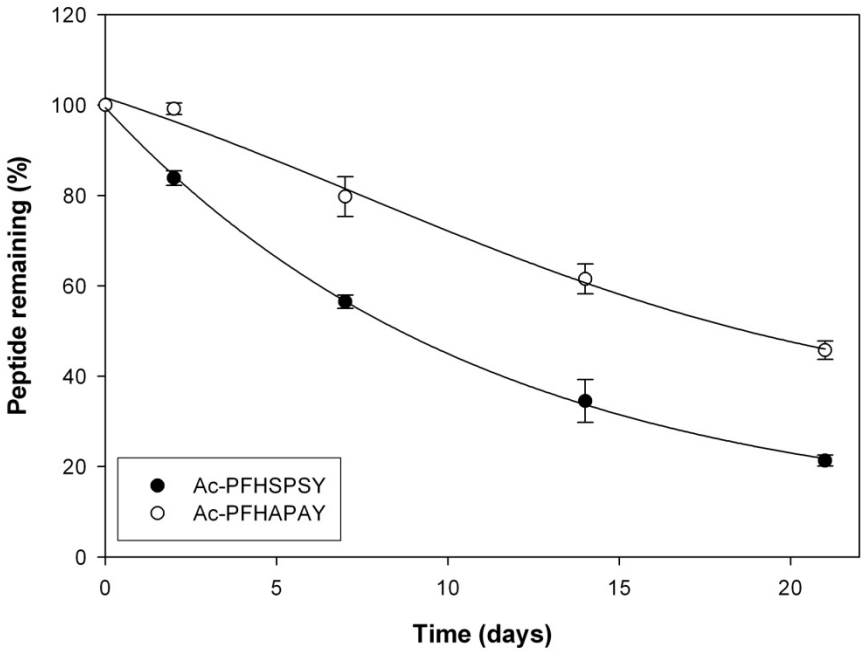

Figure 4-29: Time course of degradation of Ac-PFHSPSY and Ac-PFHAPAY when incubated in 100 mM phosphate buffer pH 7.4 at 85 °C. Percentage values were calculated as the amount (moles) of each peptide which remained with respect to time compared to the amount of each peptide present at T=0.

If truncation on the N-terminal side of Ser were occurring similar to that seen in the lens, then Ac-PFH and SPSY should be formed. Chapter-6 will demonstrate that SPSY is unstable due to a penultimate Pro residue rendering it highly susceptible to further degradation *via* diketopiperazine formation. For this reason the amount of Ac-PFH formed was used to calculate the amount of truncation at the N-terminal of Ser following incubation of Ac-PFHSPSY. Analysis of the degradation products present in each incubation by HPLC and MALDI mass spectrometry confirmed the presence of Ac-PFH in the Ac-PFHSPSY incubation but not in the Ac-PFHAPAY incubation (Figure 4-30).

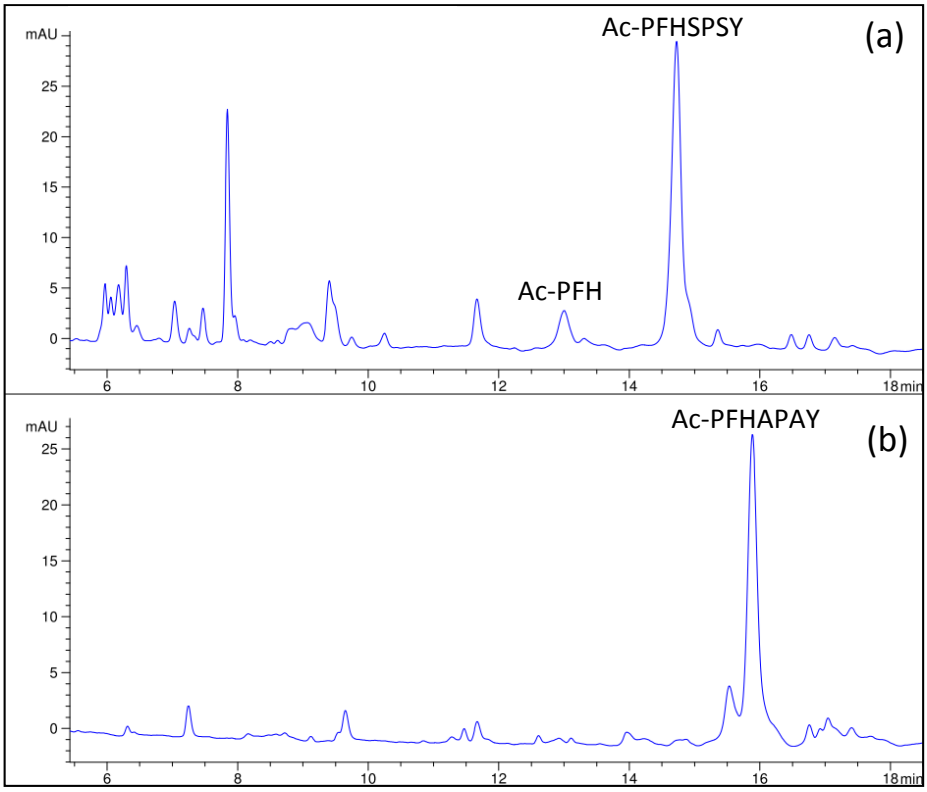

Figure 4-30: HPLC traces (257 nm) of the day-7 time points following incubation of (a) Ac-PFHSPSY and (b) Ac-PFHAPAY at 85 °C. Peptides were incubated in 100 mM phosphate buffer pH 7.4 at 85 °C.

To calculate the number of moles of Ac-PFH that formed, standard curves of each peptide were generated as detailed in the Materials and Method chapter. An example of the standard curve for Ac-PFHSPSY is shown in Figure 4-31. It should be noted that while the peak area of Ac-PFH (257 nm) in Figure 4-30 appears small compared to the other degradation products this is due the fact that most other degradations contain a Tyr residue and this absorbs more strongly than Phe at this wavelength.

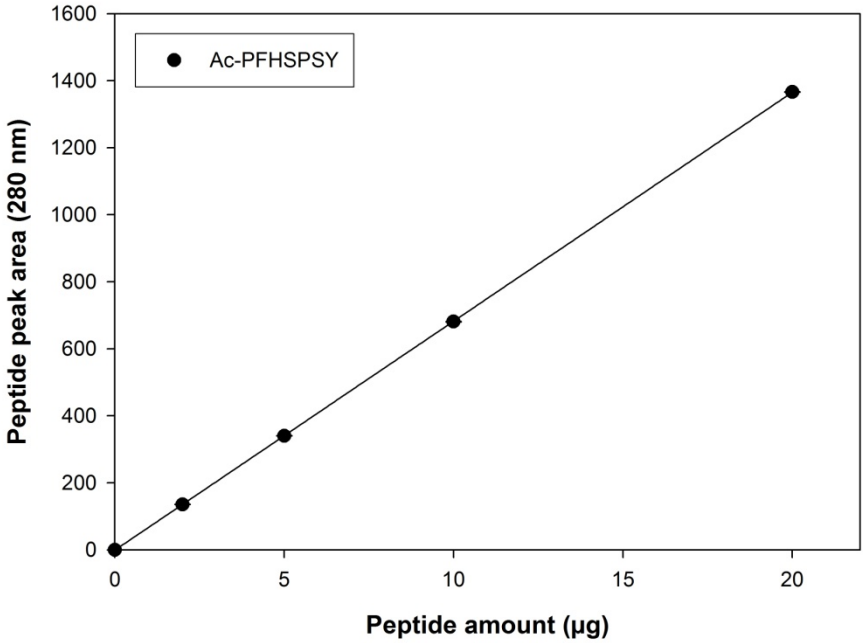

Figure 4-31: Standard curve for Ac-PFHSPSY relating peak area at 280 nm to peptide amount injected (µg).

The time course of the disappearance of Ac-PFHSPSY and appearance of Ac-PFH is shown in Figure 4-32 (a). Figure 4-32 (b) shows that while some degradation of Ac-PFHAPAY occurred no Ac-PFH was detected.

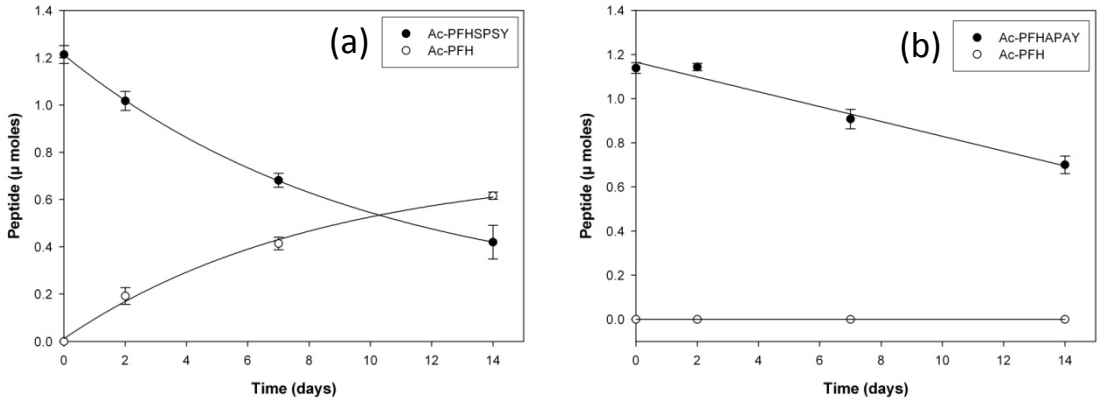

Figure 4-32: Time course graphs showing (a) loss of Ac-PFHSPSY and appearance of Ac-PFH, (b) loss of Ac-PFHAPAY and Ac-PFH formed. Peptides were incubated in 100 mM phosphate buffer pH 7.4 at 85 °C.

Figure 4-33 highlights that after 14 days incubation at 85 °C, approximately 50% of the Ac-PFHSPSY truncated at Ser forming Ac-PFH whereas there was no evidence of the analogous truncation in the control (Ac-PFHAPAY).

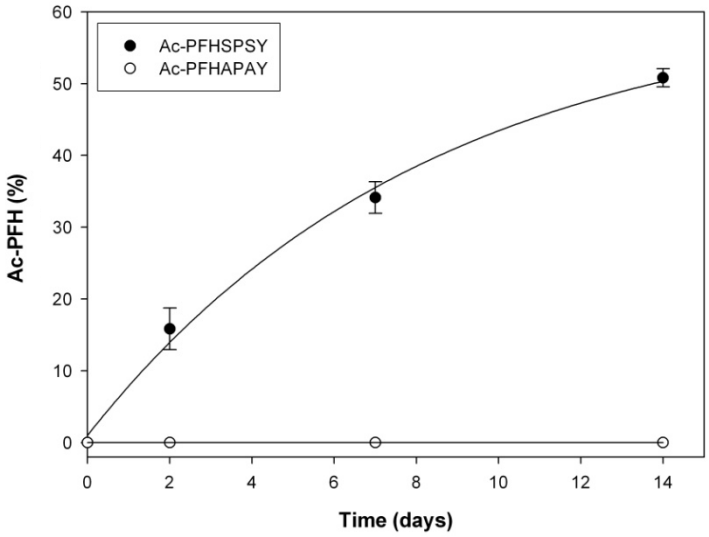

Figure 4-33: Percentage of each peptide (Ac-PFHSPSY, Ac-PFHAPAY) that truncated at the N-terminal of Ser forming Ac-PFH. Peptides were incubated in 100 mM phosphate buffer pH 7.4 at 85 °C. Percentage values were calculated as the amount (moles) of each peptide which truncated to Ac-PFH with respect to time compared to the amount of each peptide present at T=0.

These results indicated that Ac-PFHSPSY degraded at a faster rate than the Ser-free peptide (Ac-PFHAPAY). The formation of Ac-PFH as the major degradation product is evidence that truncation at the N-terminal side of Ser, at the analogous point seen in the aged human lens, can be replicated using a model peptide. It could be argued that Ac-PFH may be generated *via* other processes, such as sequential C-terminal degradation but the fact that Ac-PFHAPAY did not form any Ac-PFH suggests this is not the case. It is also important to note that Ser-related truncation is certainly not the only degradation occurring as indicated by the significant loss of both peptides over time.

4.7 Acidic conditions

While truncation at the N-terminus of Ser and racemisation of Ser were both observed in previous sections, incubation at relatively high temperatures (85 °C) for extended periods was required. This

experiment aimed to investigate if racemisation or truncation could be observed under less extreme conditions by using an acidic pH. Acidic conditions should promote an *N*-*O*- acyl shift [207], potentially leading to increased truncation at the N-terminal of Ser *via* the mechanism outlined in Section 3-1 if this mechanism is valid. Ac-PFHSPSY and Ac-PFHAPAY were incubated at pH 7.4 and pH 5.4 both at 60 °C and characterised as per Incubation-B (Section 2.2.1). pH 5.4 approximates that found inside the cell lysosome which is a membrane-bound organelle containing acid hydrolase enzymes that break down waste materials and cellular debris [208, 209].

The characterisation of the degradation products formed in each incubation was carried out in a similar manner to Section 4.6. Figure 4-34 shows that Ac-PFH was present in the Ac-PFHSPSY (pH 5.4) incubation suggesting truncation on the N-terminal side of Ser is occurring. There was no evidence of any Ac-PFH forming in the Ac-PFHSPSY (pH 7.4) incubation or in the Ac-PFHAPAY control incubation at pH 5.4 or pH 7.4. This is in agreement with previous experiments done in Section 4.2 where no truncation of Ac-SPSY was seen at 60 °C. These results suggest that acidic conditions increased the rate of truncation at the N-terminal side of Ser, possibly due to an increased rate of *N*-*O*-*a*cyl shift at this pH, as demonstrated by Johansson et al [207].

As per Section 4.6 it should be noted that while the peak area of Ac-PFH (257 nm) in Figure 4-34(a) appears small compared to the other degradation products, this is due the fact that most other degradation products contain a Tyr residue and this absorbs more strongly than Phe at this wavelength. A standard curve of Ac-PFH was used to relate its absorbance at 257 nm to the amount formed in the incubation. The time course of the percentage of each peptide that truncated to Ac-PFH is shown in Figure 4-35.

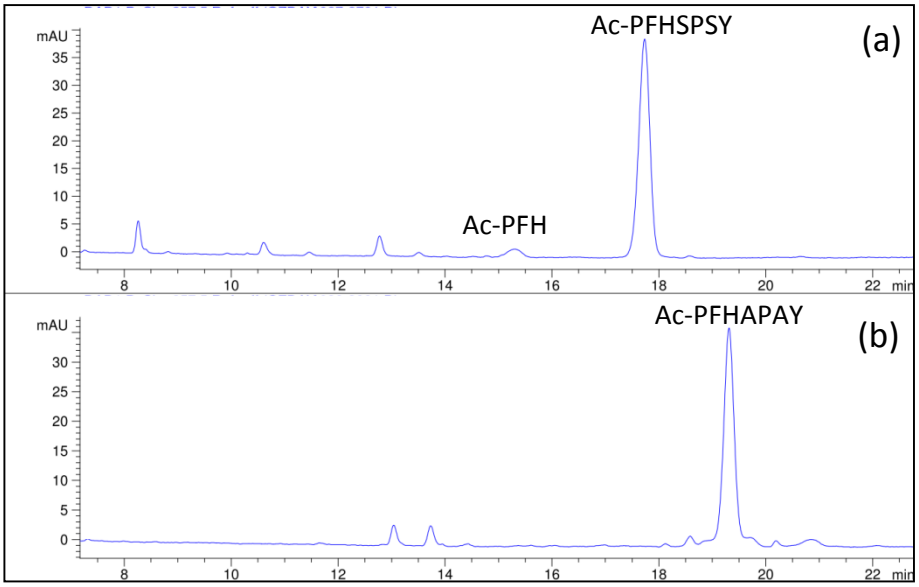

Figure 4-34: HPLC traces (257 nm) of day-35 time point from incubation of (a) Ac-PFHSPSY and (b) Ac-PFHAPAY in MES buffer pH 5.4 at 60 °C. Both peptides remained completely intact when incubated at pH 7.4 at 60 °C.

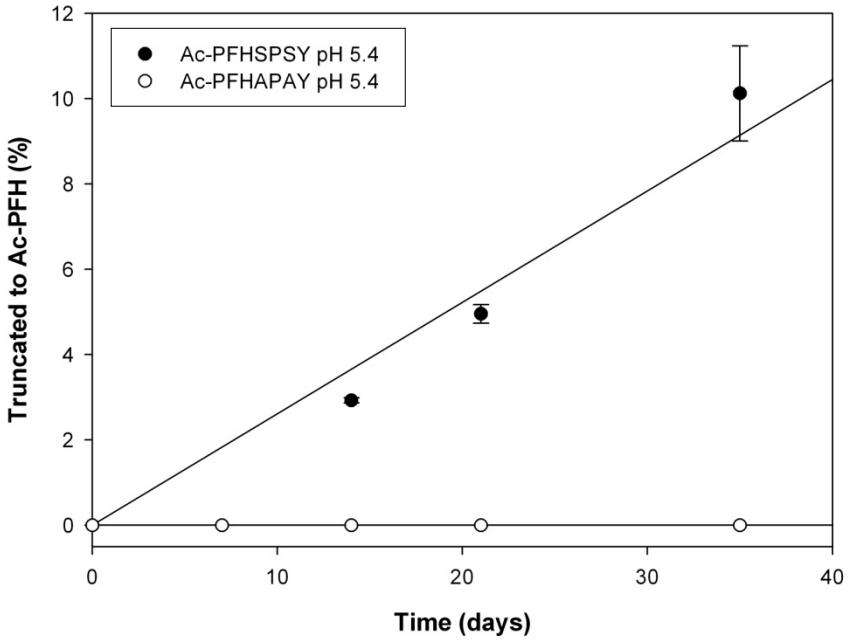

Figure 4-35: Percentage of each peptide (Ac-PFHSPSY, Ac-PFHAPAY that truncated at the N-terminal side of Ser forming Ac-PFH following incubation at pH 7.4 and pH 5.4. Peptides were incubated in 100 mM MES buffer (pH 5.4) and 100 mM phosphate buffer (pH 7.4) at 60 °C. Both peptides remained completely intact when incubated at pH 7.4 at 60 °C. Percentage values were calculated as the amount (moles) of each peptide which truncated to Ac-PFH with respect to time compared to the amount of each peptide present at T=0.

4.8 Basic residues

Another possible way to increase the rate of truncation at the N-terminal of Ser may be to increase the nucleophilicity of the Ser OH group, thus promoting the *N*-*O*-acyl shift proposed to be involved in the truncation. It was proposed that incubating model peptides in a buffer containing an excess of guanidine HCl, which is a base, that this may increase the nucleophilicity of the Ser OH resulting in increased truncation at the N-terminal side of Ser. To test this, a peptide (Ac-FSY) known to be stable at pH 7.4 and 60 °C was incubated (in triplicate) in the presence of a high concentration of guanidine HCl and characterised as per Incubation-B (Section 2.2.1). A control containing no guanidine HCl was also incubated.

4.8.1 Results and Discussion

A HPLC trace overlaying the day-14 time points from both incubations is shown in Figure 4-36. As can be seen by the fact that both traces are identical, the guanidine HCl did not have any effect.

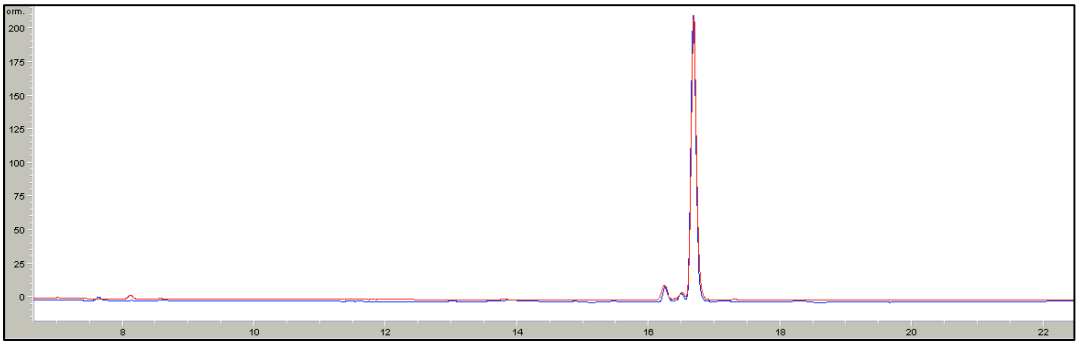

Figure 4-36: Overlay of day-14 time-point HPLC trace (280 nm) of Ac-FSY with and without addition guanidine HCl.

4.9 Metal Ions

A study by Reddy et al. [210] demonstrated a marked increase in the rate of racemisation of free and bound Ala in the presence of metal complexes. Metals are known to be present in the human lens [211] and as a result could be involved in the age-related racemisation of Ser residues seen in long-lived lens proteins. A model peptide (Ac-FSY) previously shown to be stable at 60 °C pH 7.4 was incubated in triplicate with 1 mM $CuSO_4$ to investigate if the presence of the metal ions would

promote racemisation of the Ser residues. A control of Ac-FSY, which did not contain any $CuSO_4$ was also incubated.

4.9.1 Results

A HPLC trace of Ac-FSY day-21 time-point and Ac-FSY + 1 mM CuSO4 day-21 time point is shown in Figure 4-37. In both incubations the peptide is almost completely intact with no evidence of Ser racemisation or any other degradation.

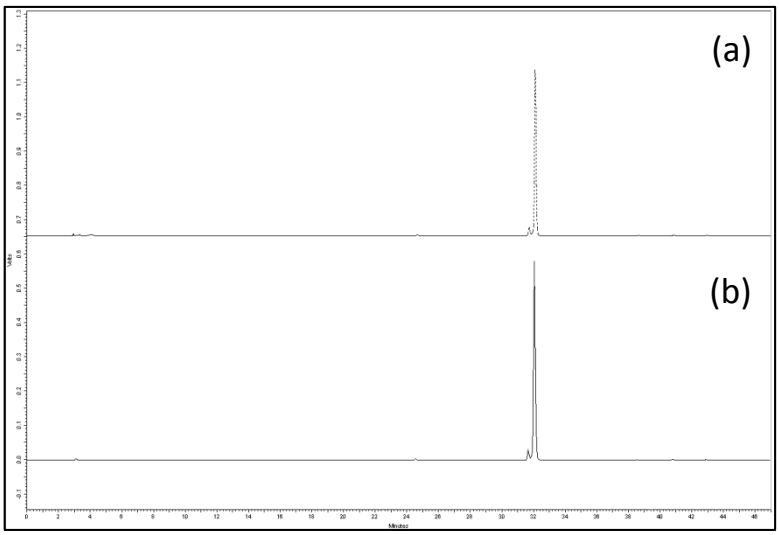

Figure 4-37: HPLC trace (280 nm) of (a) Ac-FSY day-21 time point and (b) Ac-FSY + 1mM $CuSO_4$ day-21 time point.

4.10 Phosphorylation as a potential contributor to Ser racemisation

Phosphorylation plays a major role in the regulation of various bio-signalling pathways that control metabolic processes and cellular functions [144]. Phosphoserine can undergo β-elimination leading to the formation of dehydroalanine (DHA) [212, 213]. Recent studies have speculated this DHA adduct is subject to further modification such as the addition of the lens oxidant glutathione[213]. Analysis of both cataractous and normal human lenses, has shown the accumulation of DHA

crosslinks in both the water-soluble and the water-insoluble proteins with histidinoalanine (HAL) and lanthionine(LAN) as the major adducts [204, 214].

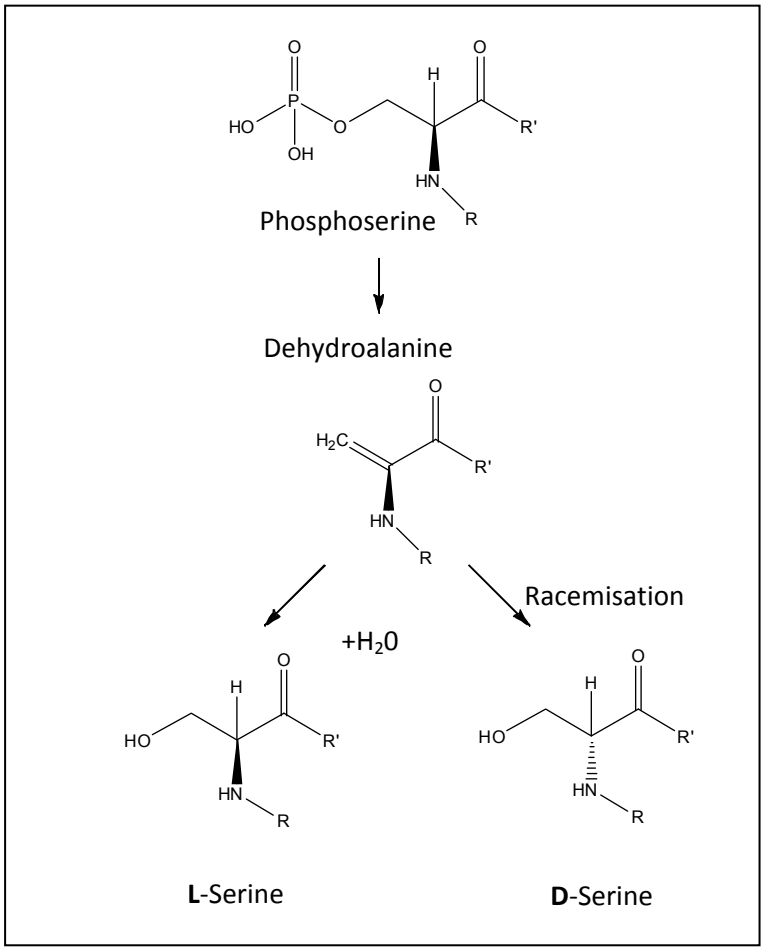

Figure 4-38: Proposed mechanism for Ser racemisation based on a dehydroalanine intermediate. (R and R' represent the rest of the protein).

In the case of phosphoserine residues (designated as pSer), should DHA form, it could also potentially revert to a Ser residue by addition of water across the double bond, resulting in an equal chance of D or L Ser being formed (Figure 4-38).This may be another mechanism to explain the age-related racemisation of Ser residues seen in long-lived lens proteins. Another implication of DHA residues is their potential ability to react with thiol groups such as cysteine and glutathione [213].

There is also the possibility for amino groups of proteins containing for example, Lys or His residues to react, forming cross links between two proteins (Figure 4-39).

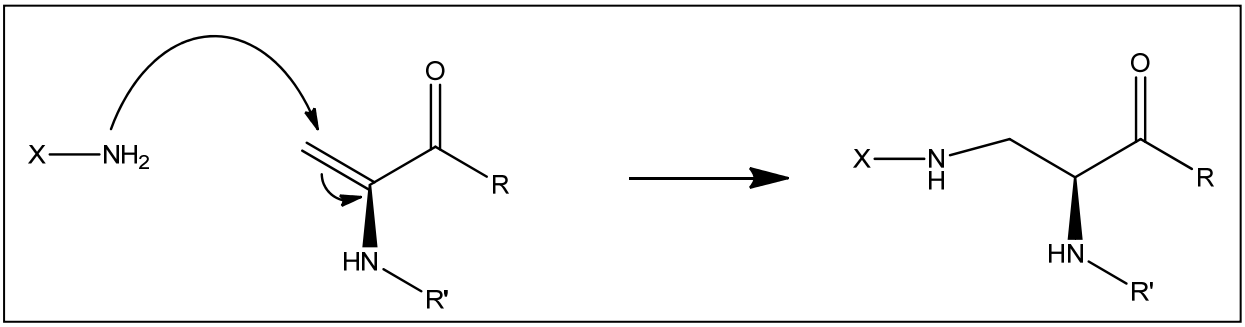

Figure 4-39: One mechanism of formation of cross links involving DHA. (R and R' represent the rest of the Peptide-1, X = amino group of a peptide or protein eg Lys).

Previous studies, under alkaline conditions have demonstrated that the loss of a phosphate group from Ser residues could proceed *via* β-elimination, resulting in the formation of a DHA intermediate [215]. The aim of this section was to investigate if this could be replicated at physiological pH and hence be applicable in the human lens. Prior to this it was deemed important to first demonstrate that it could occur under the high pH conditions outlined in the literature. Proteins can be phosphorylated by several proline-directed kinases [216], and the peptide (Ac-YAPSW) used for this study is based on a lens crystallin sequence (αB 57-60) known to contain a pSer residue [141, 217]. It is also the major phosphorylation site in αB-crystallin in the brains of patients with Alexander's disease[218]. A DHA residue, should it form, is a Michael acceptor and would be prone to nucleophillic addition [219]. Phenylethyalmine (PE) has been previously used as a nucleophillie to react with DHA residues [220], and it was chosen for a similar role in this study (Figure 4-40).

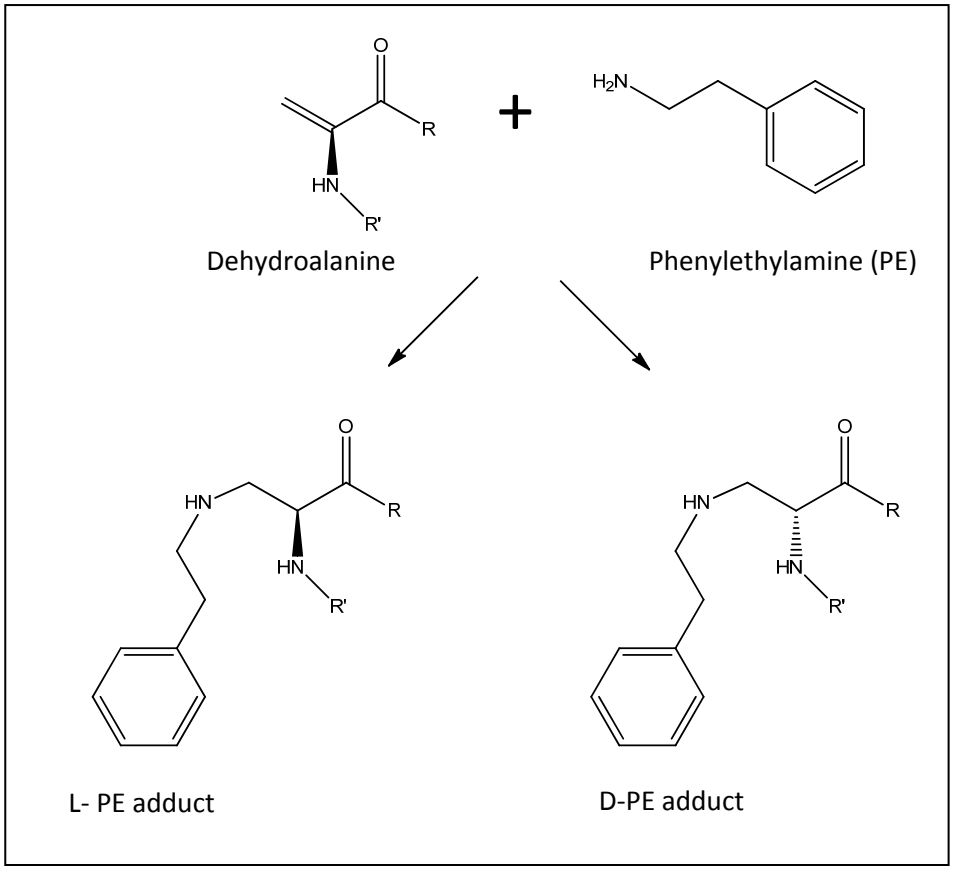

Figure 4-40: Addition of phenylethylamine to dehydroalanine results in the formation of two isomers in a 1:1 ratio. (R and R' represent the rest of the peptide)

Formation of this adduct would provide evidence of a DHA residue which may otherwise prove too unstable / reactive to isolate and characterise. Based on the condition used by Byford et al. [215] ,the peptides Ac-YAPSW and Ac-YAP(pSer)W were incubated in 100mM NaOH at room temperature in the presence of 10 equiv of PE. Controls without any PE were also incubated.

4.10.1 Results and Discussion

Figure 4-41 compares the HPLC trace of pH 13 incubation of Ac-YAP(pSer)W with and without PE. Analysis of the modified peptides, which occurred by MALDI mass spectrometry, revealed that both incubations formed a peptide with a molecular weight that corresponded to Ac-YAPSW – 18 Da. One possibility that explains this change in molecular weight is the β elimination of a phosphate group from Ser resulting in the formation of a DHA residue.

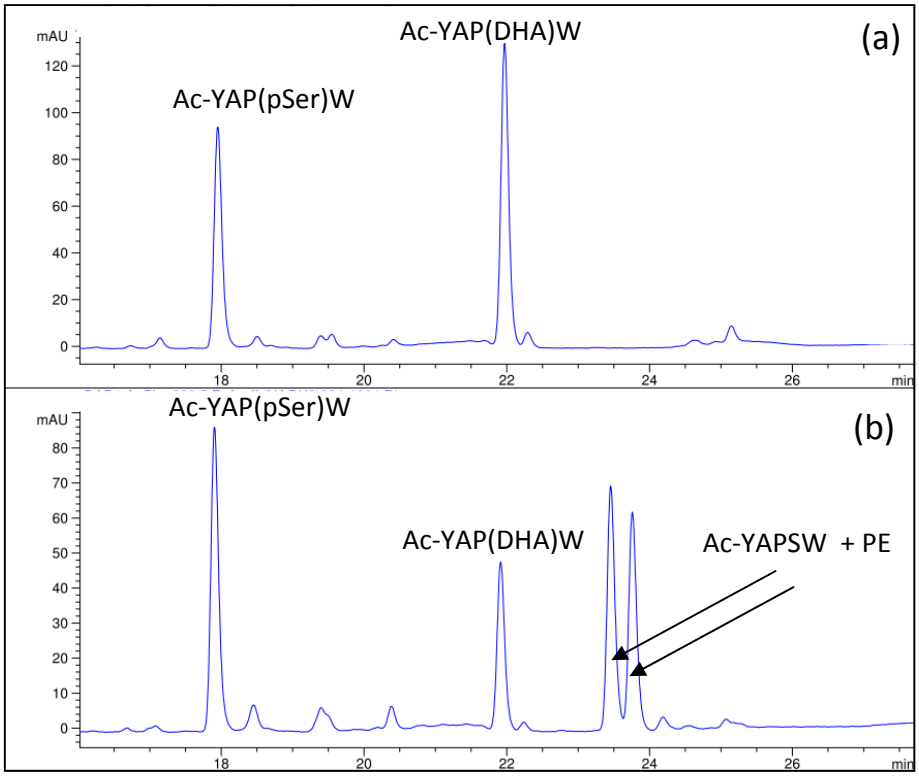

Figure 4-41: HPLC traces (280 nm) of the day-4 time point following incubation of (a) Ac-YAP(pSer)W and (b) Ac-YAP(pSer)W + 10 equiv PE at 30 °C in 100mM NaOH. Peptides were assigned based on the combination of analysis by MALDI mass spectrometry and HPLC retention times.

The incubation containing PE also contained significantly less of the "DHA peptide" compared to the incubation without PE, supporting the notion that DHA had reacted with PE. Should PE add to the DHA residue, it should form a D- and L- substituted product in the ratio of 1:1, which appears to be the case as indicated by the two peaks (Figure 4-41). Due to its double bond, DHA residues have an increased absorbance band in the 241 nm region. Detection at this wavelength has therefore in previous studies to quantify the amount of DHA formed [215]. Figure 4-42 compares the HPLC traces of the day-1 time point of Ac-YAP(pSer)W at 241 nm and 280 nm. The relative peak area of the assumed "DHA peptide" compared to the Ac-YAPSW peak area was observed to increase at 241 nm compared to 280 nm. Given that the only residues present in Ac-YAPSW that should absorb at either 280 nm or 241 nm are Trp and Tyr, and that these are also present in both peptides, a reasonable explanation of the increase peak ratio is the formation of a DHA residue.

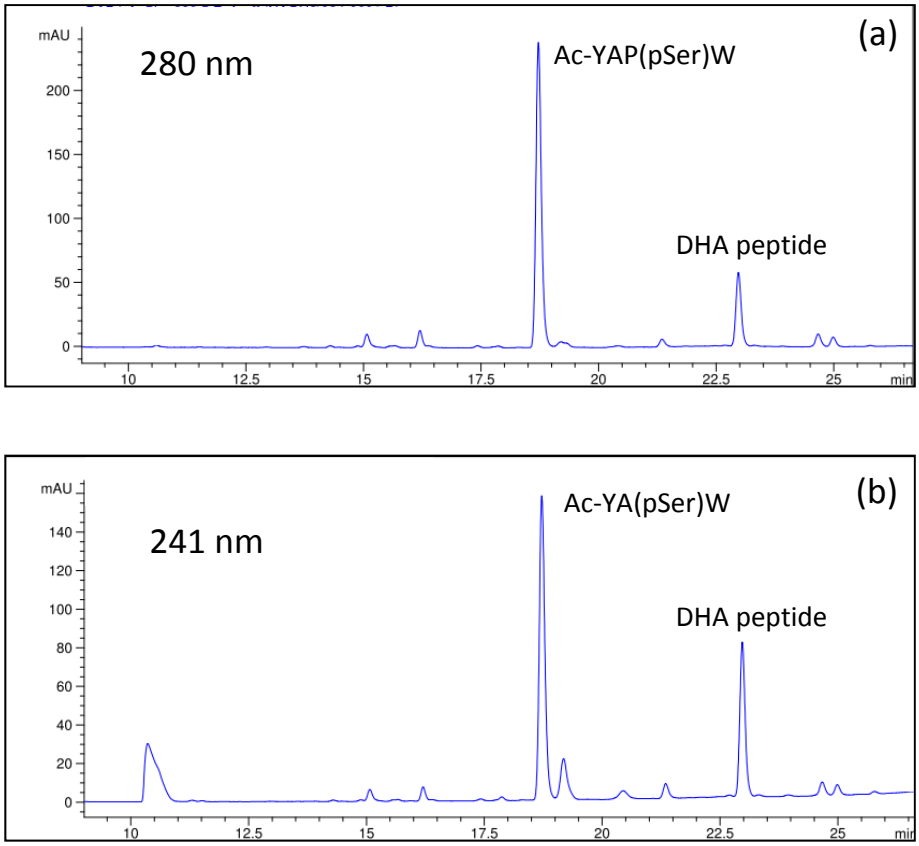

Figure 4-42: HPLC traces of the day-1 time point showing that the relative peak area of the assumed "DHA peptide" compared to the Ac-YAP(pSer)W peak area was observed to increase at 241 nm compared to 280 nm

The assumed "Ac-YAP(DHA)W peptide" and "Ac-YAPSW-PE peptide" were isolated by semi-preparative HPLC and analysed by MALDI Mass spectrometry (not shown) and NMR spectroscopy. Figure 4-43 compares a selected region of the ^{1}H NMR spectra from synthetic standards of Ac-YAPSW and Ac-YAP(pSer)W to the isolated Ac-YAP(DHA)W peptide. While they are all similar, there are two key differences which distinguish them. The DHA peptide contains two singlets at 5.66ppm and 5.63ppm (DHA in Figure 4-43) which corresponds to the expected literature chemical shift of a DHA residue [221]. Additionally the NH (* in Figure 4-43) which presumably corresponds to the peptide bond NH of the Ser / pSer / DHA residue is seen to shift while all others remained essentially the same.

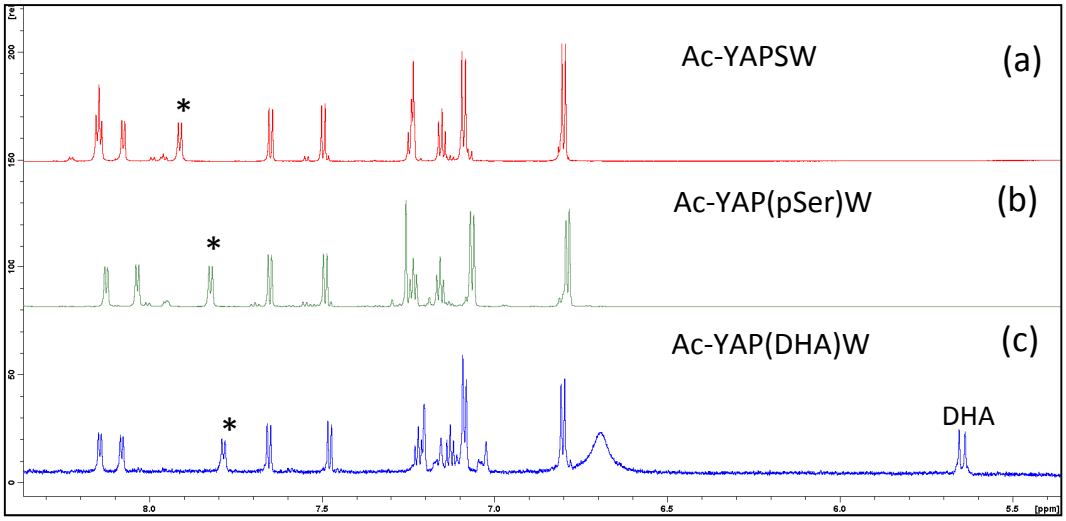

Figure 4-43: Selected region of ^{1}H NMR spectra of (a) Synthetic standard of Ac-YAPSW, (b) synthetic standard of Ac-YAP(pSer)W and (c) Ac-YAP(DHA)W isolated from incubation. (*) = NH corresponding to Ser / pSer / DHA residue. (DHA) = Characteristic peaks for a DHA residue.

Figure 4-44 compares a selected region of the ^{1}H NMR spectra from the above three peptides (Ac-YAPSW, Ac-YAP(pSer)W and Ac-YAP(DHA)W) with that of one of the two isolated Ac-YAPSW-PE adducts. The peaks indicated by (*) correspond to additional aromatic protons, presumably due to the PE adduct. Additionally the two singlets at 5.66ppm and 5.63ppm which correspond to the expected literature chemical shift of a DHA residue are not present in the Ac-YAPSW-PE adduct. These results strongly indicate that the adducts isolated from the above incubations are Ac-YAP(DHA)W and Ac-YAPSW-PE adducts.

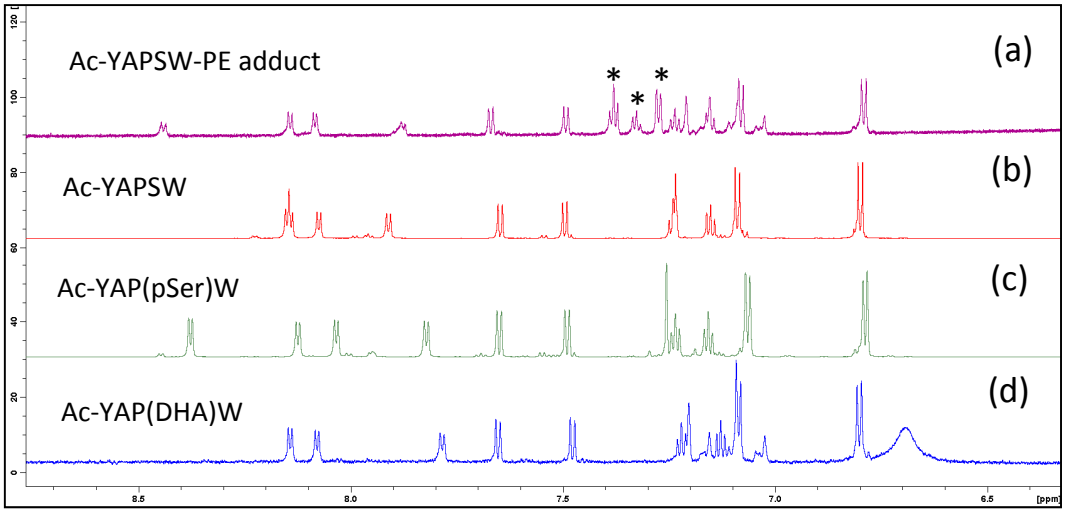

Figure 4-44: Selected region of ^{1}H NMR spectra of (a) Ac-YAPSW-PE adduct, (b) Ac-YAPSW, (c) Ac-YAP(pSer)W and (d) Ac-YAP(DHA)W. (*) = Additional aromatic protons present in PE adduct.

Figure 4-45 compares the HPLC trace of the incubation of Ac-YAPSW with and without the addition of PE. Analysis of the modified peptides that formed revealed that in both incubations a modified form of the peptide with a molecular weight and HPLC retention time corresponding to DHA formation was produced. Additionally, the incubation containing the PE formed two peptides, each matching the molecular weight of a PE having added to the DHA residue. Significantly, less Ac-YAP(DHA)W formed from Ser than from pSer, which is as expected from the literature [215].Interestingly the retention time of Peptide-X matched that of Ac-YAP(D-Ser)W, indicating racemisation of Ser may be occurring. As there was no corresponding peak formed from Ac-YAP(pSer)W, which forms much greater amounts of DHA, it is assumed that this is due to base catalysed racemisation of Ser rather than due to addition of water to the DHA residue.

In summary, under alkaline conditions, both Ac-YAPSW and Ac-YAP(pSer)W were shown to form a DHA peptide that readily reacted with PE (when present) forming diastereomeric modified peptides in a 1:1 ratio.

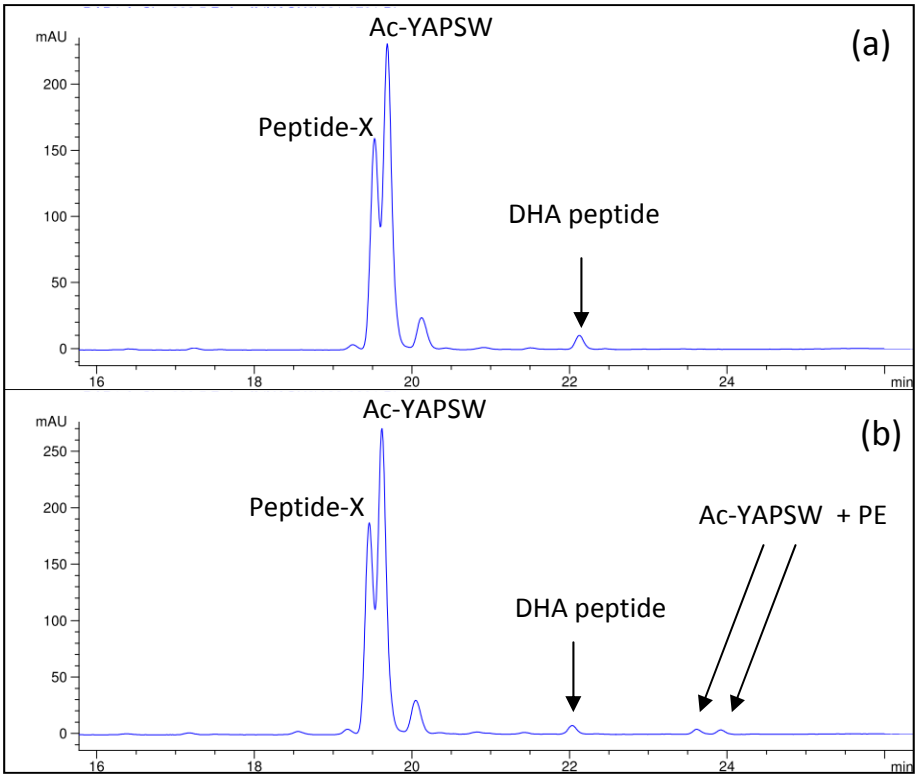

Figure 4-45: HPLC traces (280 nm) of the day-4 time point following incubation of (a) Ac-YAPSW and (b) Ac-YAPSW + 10 equiv PE at at 30 °C in 100mM NaOH. Peptides were assigned based on the combination of analysis by MALDI mass spectrometry and HPLC retention times.

4.11 Investigations at pH 7.4

While DHA was readily formed in the previous experiment, the use of an alkaline pH was required. In order to determine if the formation of DHA could play a role in the age-related racemisation of Ser residues, the previous experiment was repeated at physiological pH. Ac-YAPSW and Ac-YAP(pSer)W were incubated in duplicate (1 mg/ml) in the presence of 0.1 equiv of PE, at 60 °C and physiological pH (7.4) as per Table 4-4. Controls that did not contain any PE were also incubated and used as a comparison. Due to the basicity of PE and its potential effect on buffer pH, significantly less PE had to be added to these incubations.

Table 4-4: Peptide incubations.

Serine	Ac-YAPSW Ac-YAPSW + PE (0.1 Equiv)	pH 7.4 [1] pH 7.4 [1]
Phosphoserine	Ac-YAP(pSer)W Ac-YAP(pSer)W + PE (0.1 Equiv)	pH 7.4 [1] pH 7.4 [1]

1 = Phosphate buffer (100 mM)
2 = Boric acid buffer (100 mM)

4.11.1 Results and Discussion

Figure 4-46 shows the HPLC traces from the day-15 incubation of Ac-YAPSW and Ac-YAP(pSer)W at physiological pH. As can be seen, Ac-YAPSW was stable under these conditions, but Ac-YAP(pSer)W formed two products. Isolation and analysis of these products by MALDI mass spectrometry revealed molecular weights corresponding to Ac-YAPSW (indicating loss of the Ser phosphate group and reformation of the Ser alcohol) and Ac-YAPSW – 18 Da (indicating the loss of the Ser phosphate group plus an additional loss of 18 Da, which suggests the formation of a DHA peptide). Comparison of each of the proposed DHA and Ac-YAPSW peptides formed in the incubation, with standards of the DHA peptide (obtained from Section 4.10) and Ac-YASPW (synthetic standard) revealed matching retention times and PDA absorbance profiles. Due to the small amount of the DHA peptide produced, analysis by NMR spectroscopy was not possible.

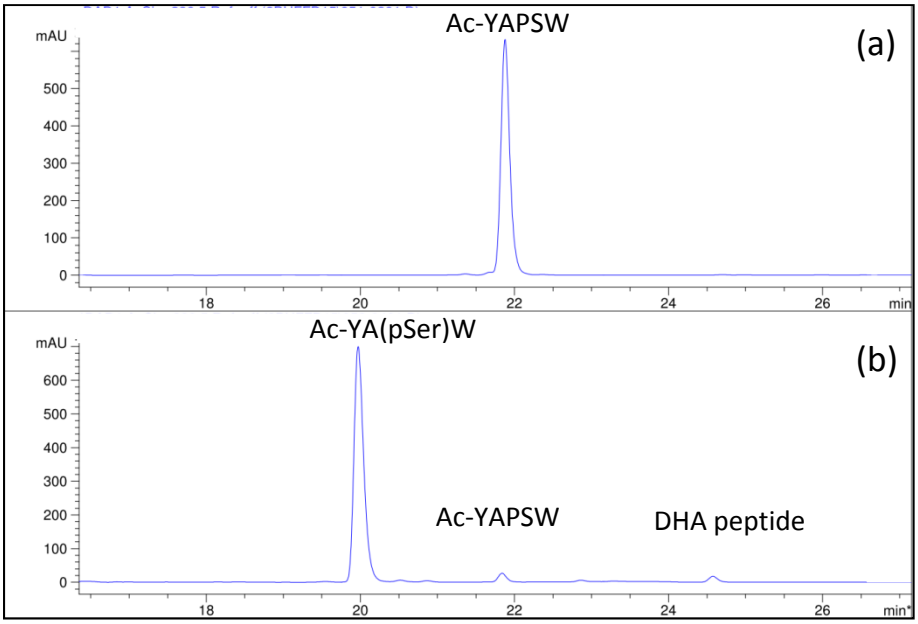

Figure 4-46: HPLC traces (280 nm) of the day-15 time point following incubation of (a) Ac-YAPSW and (b) Ac-YAP(pSer)W at 60 °C in 100mM phosphate buffer.

If Ac-YAP(pSer)W were forming Ac-YAPSW *via* addition of a water molecule across the DHA double bond then it would be expected that Ac-YAPSW and Ac-YAP(D-Ser)W would form in equal amounts, as seen for the addition of PE in Section 4.10. A synthetic standard of Ac-YAP(D-Ser)W was spiked into an Ac-YAP(pSer)W incubation time point and analysed by HPLC. As can been seen in (Figure 4-47) it is possible to resolve Ac-YAPSW from Ac-YAP(D-Ser)W by HPLC suggesting that if it was forming in the above incubation it should be seen by HPLC.

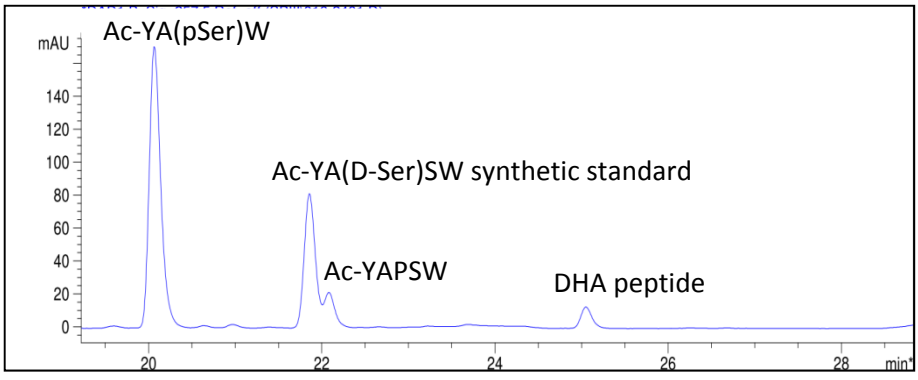

Figure 4-47: HPLC trace (280 nm) of the day-15 time point of Ac-YAP(pSer)W spiked with a synthetic standard of Ac-YAPS(D-Ser)W.

Unlike the incubations at pH 13, incubation of Ac-YAPSW and Ac-YAP(pSer)W at pH 7.4 with PE showed essentially the same results as the incubations that did not contain PE, i.e. no PE adduct was formed. There are a number of possibilities to explain this. The most likely one is the reduced amount of DHA formed at this pH, combined with the reduced amount of PE present. Another possibility is that the addition of the PE amino group to the DHA residue does not occur readily at this pH. Further work on this matter is planned.

In summary, at physiological pH, Ser residues did not show evidence of DHA formation where as pSer residues did. At the start of this section it was proposed that addition of a water molecule to DHA could be one explanation for racemisation of Ser residues. The results of these experiments suggest that this is not the case. While pSer residues did lose a phosphate group when incubated at physiological pH, there was no evidence of any D-Ser formation, which rules out addition of water to DHA as the cause.

As DHA was shown to form from pSer residues at physiological pH this open up the possibility of it occurring in long-lived proteins. Studies have shown that the prevalence of pSer groups in dentin phosphoproteins , which are long lived proteins found in teeth, decreases significantly with age [222, 223]. Additionally the location of phosphorylated residues in some of the major long lived lens proteins has recently been characterised [224, 225]. Should the loss of phosphate groups from these proteins proceed in a similar manner to the model peptide studied in this experiment, then it is certainly conceivable that significant amount of DHA residues could result. Reaction of these DHA residues with thiols and amines could then lead to protein cross linking as per [204, 214].

4.12 Conclusions

In this chapter, peptides based on human lens αB-crystallin sequences known to truncate on the N-terminus side of Ser were examined. Incubation at 60 °C and physiological pH did not result in significant degradation. However when the temperature was raised to 85 °C both truncation of internal Ser residues at the N-terminus of Ser and racemisation of Ser was observed. While 85 °C is a relatively high temperature to expose peptides to, it is worth considering that some long-lived proteins (such as those at the centre of the human lens) are exposed to 37 °C for an entire life-time.

The role of the Ser hydroxyl group was investigated and found to play an important role in truncation. Interestingly Ser racemisation occurred regardless of the presence or absence of a free Ser hydroxyl group. This finding was inconsistent with our initial hypothesis that both racemisation of Ser and truncation the N-terminal side of Ser might be linked processes, occurring *via* formation of a cyclic tetrahedral intermediate. It now appears likely that they occur by separate processes. As the Ser hydroxyl group does not appear to play a role in racemisation it is likely that it is the result of simple α proton abstraction and re-addition.

A range of other factors were investigated to see if truncation at the N-terminal of Ser could be promoted at lower temperatures. Despite some literature precedence the use of a base such as guanidine HCl or a metal ion such as Cu, did not have a significant effect. Acidic pH (5.4) was the only condition under which truncation at the N-terminal of Ser could be observed at 60 °C. This still has biological relevance as a comparable pH (~5) is found in the cell lysosome [208].

The use of phosphorylated Ser residues was also examined as a potential source of D-Ser. Incubation of peptides containing Ser or pSer residues, at room temperature (pH 13) showed the formation of DHA, which is consistent with other studies in the literature. More importantly, the formation of DHA from a pSer residue was demonstrated at physiological pH. While the use of elevated temperature (60 °C) was required, given the decades that pSer residues would be exposed to

physiological pH in the human lens, it is certainly conceivable that significant amounts of DHA could form. There was also no evidence of any addition of a water molecule to DHA residues, suggesting that it is not a rational explanation for Ser racemisation. However due to the ability of DHA residues to react with amino or thiol groups it is certainly a potential source of protein cross links within long-lived proteins.

5 Chapter 5: Section-B Overview (N-terminal modifications)

In this section of the thesis, three reactions involving the N-terminus of peptides that occurred while investigating model peptides for Section A will be discussed in separate chapters, as detailed below.

- Diketopiperazine formation (Chapter-6)
- N-Terminal racemisation (Chapter -7)
- N-Terminal truncation (Chapter-8)

5.1 Introduction

Long-lived proteins are found at many sites in the human body including the brain [226, 227], the heart [228], and the lens[1, 30]. As a result of prolonged exposure to physiological conditions these proteins undergo numerous age-related changes. Major modifications to such long-lived proteins include racemisation [118, 119, 226, 229, 230], deamidation [123, 141, 193-195] and truncation [126, 127, 196, 197]. In the human lens crystallins are the predominant protein family accounting for over 90% of total protein [30, 31]. Because the centre of the adult human lens contains no active enzymes [59, 231], it is likely that many of these processes are non-enzymatic in nature.

Numerous studies have demonstrated that significant crystallin truncation occurs with age [37, 135-137]. It is estimated that 45-55% of α-crystallin is truncated by old age [129] and extensive fragmentation of several subunits including αA, αB and βB1 have been found even in young lenses [40, 232, 233]. The proposed mechanism behind one such truncation (that next to Ser) has already been investigated in Section A. While the exact implications of these truncations are still under investigation, fragments of α-crystallin isolated from the human lens have been shown to promote crystallin aggregation rather than the preventative role of the precursor [128]. Additionally N-terminally truncated βB1 has been shown to behave differently from native βB1 crystallin [132].

Major lens proteins, α- and β-crystallin, are N-terminally acetylated [234]. It has been suggested that N-acetylation of proteins in higher organisms is an evolutionary process to protect against degradation of proteins *via* the N-terminal [235]. However, the γ-crystallins and other lens proteins such as aquaporin-0 are not N-terminally acetylated and could be subject to N-terminal degradations. Additionally, age-related protein truncation results in generation of new peptides that have unprotected α amino groups (Figure 5-1), and these could therefore be subject to N-terminal modifications.

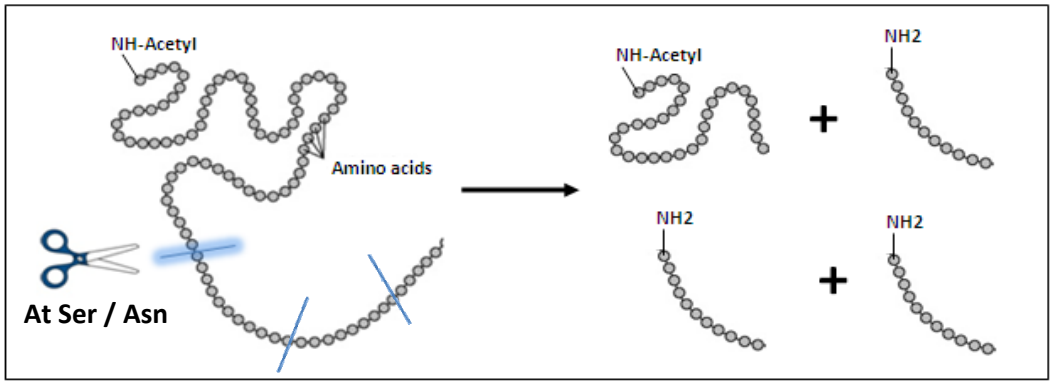

Figure 5-1: Schematic diagram showing crystallin truncation leading to new peptide fragments with free amino terminal groups.

The general approach of Chapters 6 to 8 was to incubate peptides at physiological pH, characterise the products, then examine some of the factors that promote these modifications and determine if they could potentially occur in long-lived proteins. The challenge in studying these N-terminal modifications is that they are often competing reactions and are difficult to study in isolation. The rate of each process is also sequence dependent and the products themselves are unstable. These multiple degradation products can significantly complicates accurate quantification. For example, a peptide that undergoes N-terminal racemisation is often subject to degradation *via* DKP as well as truncation of the N-terminal amino acid, making accurate quantification of the racemised peptide a challenge.

6 Chapter 6: Diketopiperazine (dkp) formation

6.1 Introduction

Incubation of model peptides (Chapter 4) resulted in a number of side reactions occurring. One such process was the loss of a cyclic diketopiperazine (dkp) from the N-termini of the peptides. While the use of model peptides incorporating an N-terminal acetyl group was successful in preventing this modification, it was deemed of interest to investigate some of the factors involved in dkp formation and its potential relevance to long-lived proteins. Dkp formation from peptides (Figure 6-1) involves nucleophilic attack of a peptide N-terminal amino group on the amide carbonyl between the second and third amino acid residues, resulting in the formation of a cyclic lactam and a truncated peptide [236]. This intramolecular aminolysis reaction occurs in aqueous solution [237, 238] with peptides having Pro as the penultimate *N*-terminal residue being particularly prone to degradation *via* this pathway [236]. This is due to high propensity of Pro to form a *cis* peptide bond with the preceding residue, which promotes the cyclisation reaction [239].

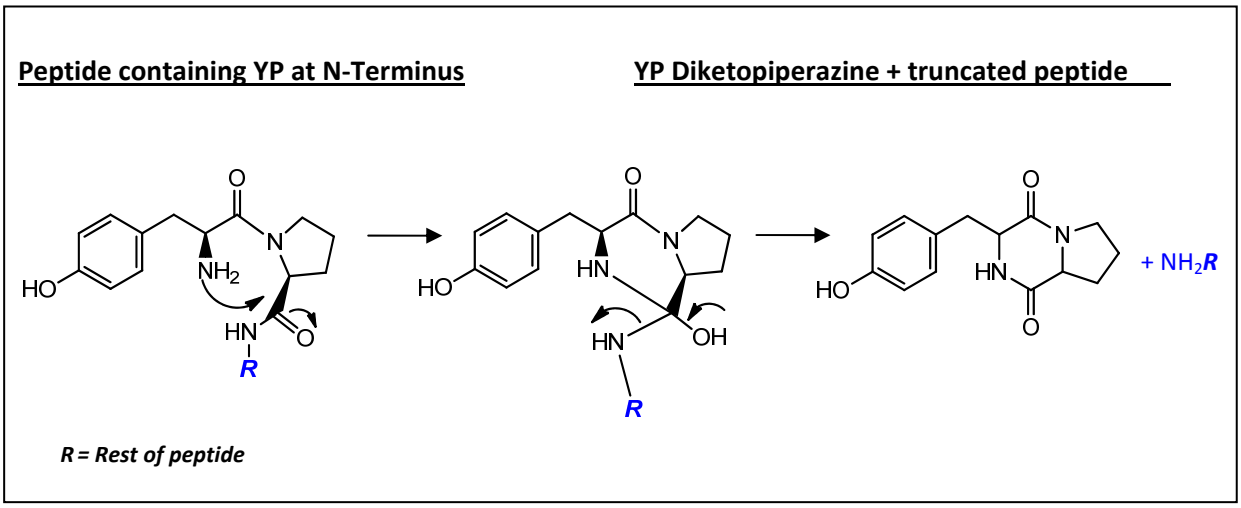

Figure 6-1: Mechanism of dkp formation.

Although the formation of a dkp has been shown to be a side reaction in peptide synthesis [240, 241], to our knowledge it has been little studied as a decomposition pathway of peptides at pH 7 and has not been studied as a degradation pathway of long-lived proteins. Dkp formation has gained renewed interest of late with reports by several groups highlighting issues with storage of protein pharmaceuticals including human growth hormone (HGH) which were degraded *via* dkp formation [242-244]. Given that long-lived proteins such as those in the lens are exposed to physiological conditions for decades, it is reasonable to propose that some might also be subject to degradation *via* dkp formation.

In the lens most proteins (e.g. crystallins) have an N-terminal acetyl group which protects them from dkp formation. However, due to the extensive age-related truncation of lens protein [128, 163, 245], many peptide fragments are formed in the aged lens that have a free amino termini. One premise of this chapter is that these peptide fragments could be subject to further degradation *via* sequential dkp formation. Model peptides were used to investigate factors that could influence the formation of dkp.

6.2 Aim:

The aim of this chapter was to investigate the factors which influence the formation of a dkp and to demonstrate if it could potentially occur in long-lived proteins such as those found in the lens.

6.3 Dkp formation

Many sites of truncation have been observed in aged lens protein [128, 163, 245]. One of the most abundant is at Ser 19 in αB-crystallin [128]. Unlike most crystallins, which have an N-terminal acetyl group and hence cannot degrade *via* dkp formation, the resulting truncated peptides have free amino termini (Figure 6-2) and are subject to further N-terminal degradation.

SPSY, a model peptide based on the sequence of the remaining truncated peptide from αB-crystallin (19-21) was used to investigate if this sequence could be prone to further degradation *via* dkp formation. A *C*-terminal Tyr was added to aid HPLC detection at 280 nm. Due to the inability of *N*-terminally acetylated peptides to form a dkp, Ac-SPSY was used as a control. Peptides (Ac-SPSY and SPSY) were incubated (in triplicate) at 60 °C pH 7.4 and characterised as per Incubation-B (Section 2.2.1).

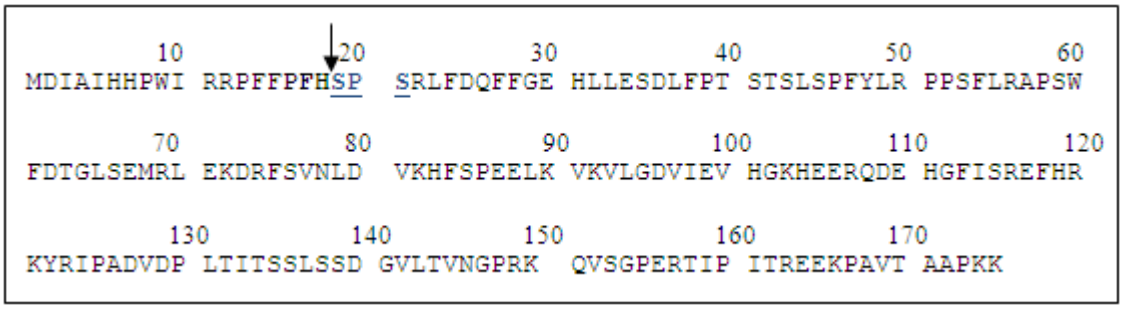

Figure 6-2: Sequence of human αB-crystallin. The site of cleavage in older human lenses is shown with an arrow and the peptide region examined in this investigation is underlined.

If degradation *via* dkp formation was occurred then the peptides in Table 6-1 should be observed. The loss of SP (dkp) from SPSY is also shown mechanistically in Figure 6-3.

Table 6-1: Degradation products of Ac-SPSY and SPSY.

Peptide	Proposed degradation products
Ac-SPSY	Dkp formation not possible
SPSY	SP(dkp) + SY

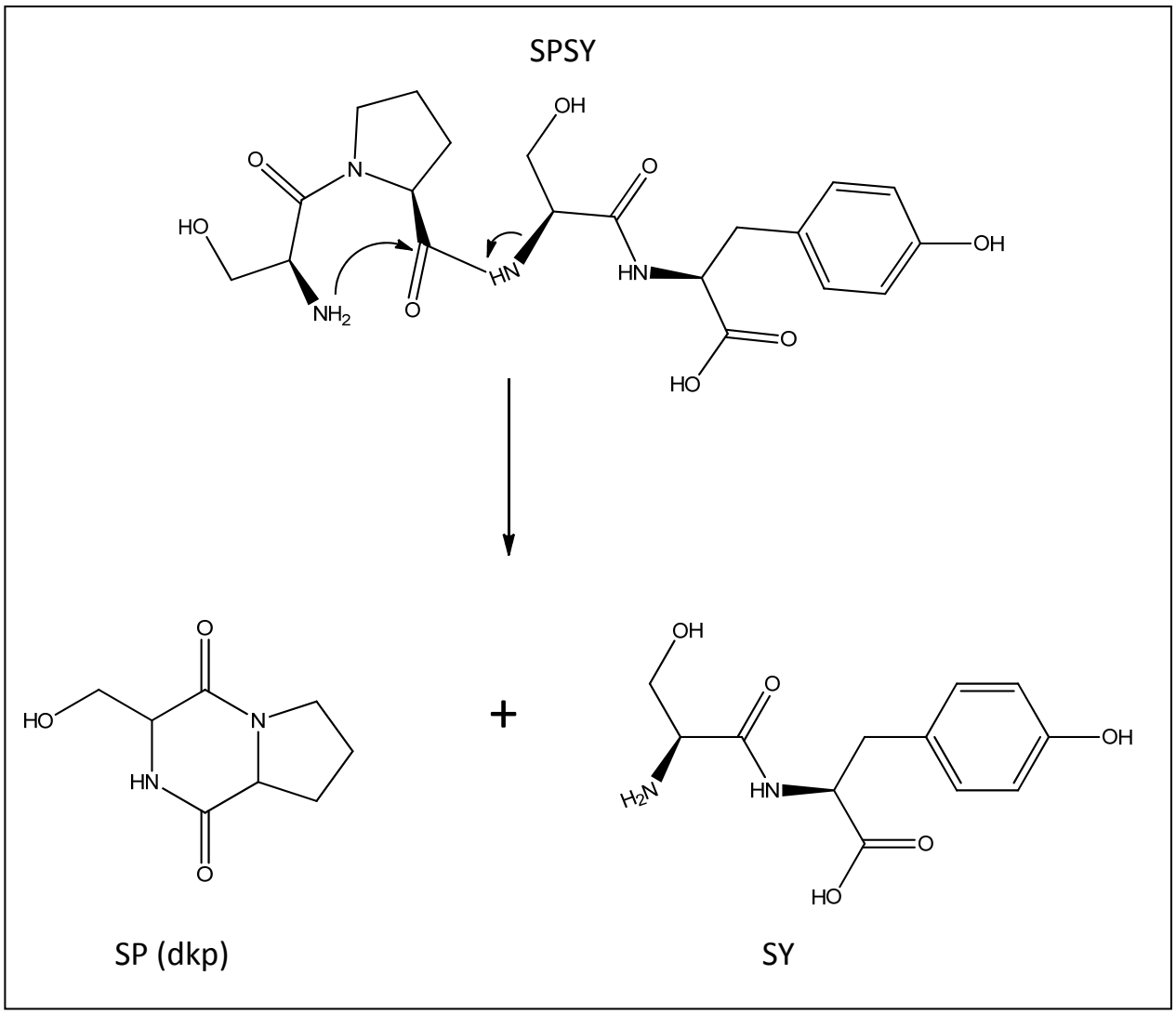

Figure 6-3: Mechanism showing the formation of SP (dkp) and SY from SPSY.

6.3.1 Results and Discussion

Characterisation

A sample HPLC trace of SPSY after 3 days incubation at 60 °C is shown in Figure 6-4.

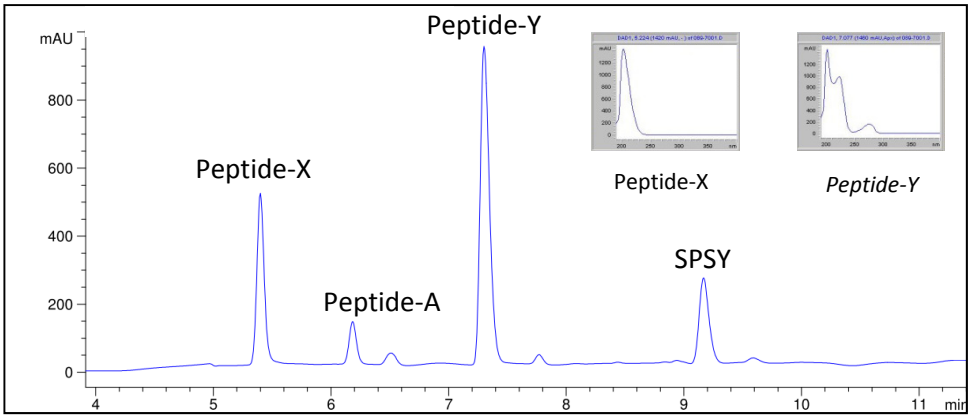

Figure 6-4: HPLC trace (216 nm) of SPSY day 3 time point showing the multiple products formed following incubation at 60 °C. The UV absorbance profile of Peptide-X and Peptide-Y are included as inserts. Peptides were incubated in 100 mM phosphate buffer pH 7.4.

Peptide-X (Figure 6-4) did not absorb at 280 nm indicating the loss of the Tyr residue. Analysis by ESI mass spectrometry (Figure 6-5) revealed a molecular weight of SP – 18 amu, which suggested formation of SP(dkp). The retention time of Peptide-X (Figure 6-6) matched that of synthetic SP(dkp) and it was therefore assigned as SP(dkp).

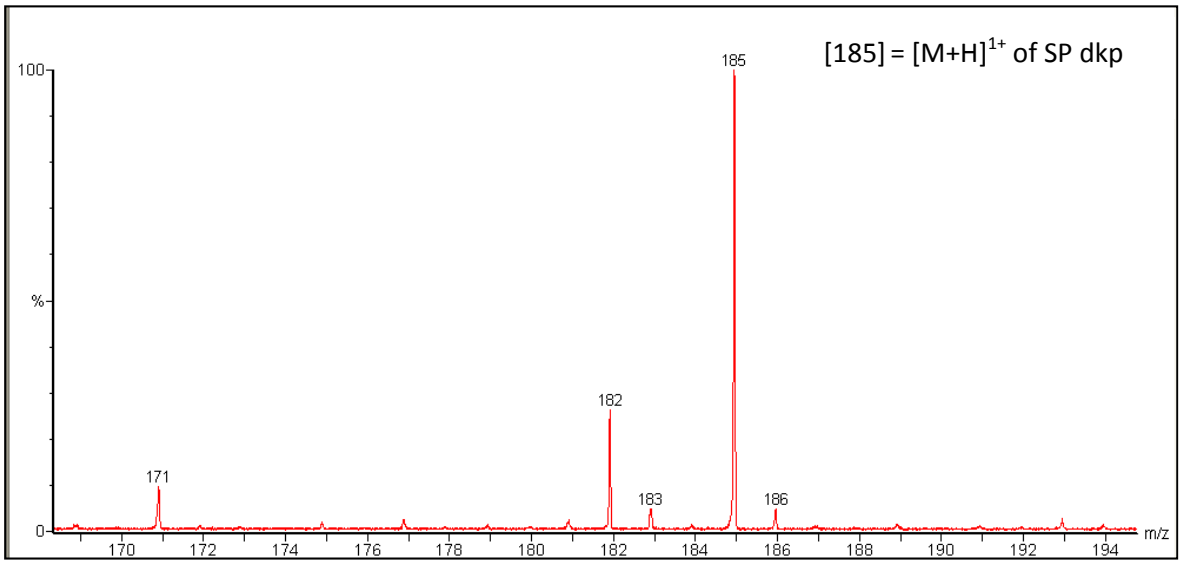

Figure 6-5: ESI Mass spectrum of Peptide-X isolated from incubation of SPSY in 100 mM phosphate buffer pH 7.4 at 60 °C for 3 days.

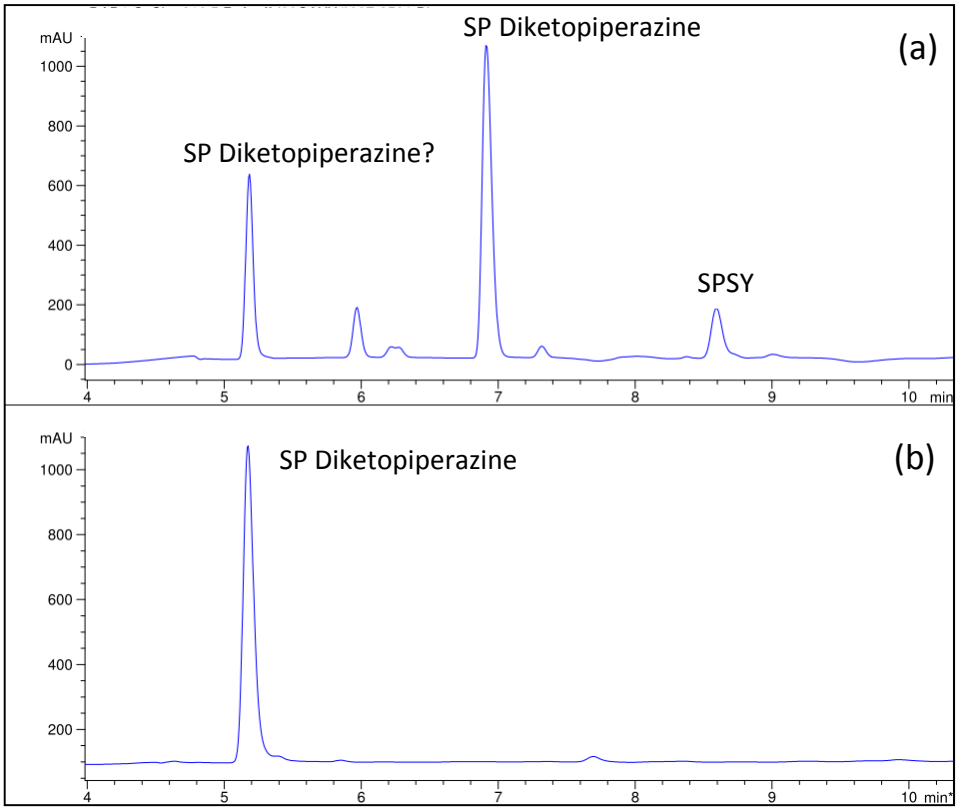

Figure 6-6: HPLC traces (216 nm) of (a) SPSY day-3 incubation time point, (b) Standard of SP dkp.

Peptide-Y did absorb at 280 nm, indicating the Tyr residue was still present. Analysis by ESI mass spectrometry revealed a molecular weight matching that of the dipeptide SY (Figure 6-7). It was compared to a synthetic HPLC standard of SY and revealed a matching retention time. Peptide-Y was assigned as SY.

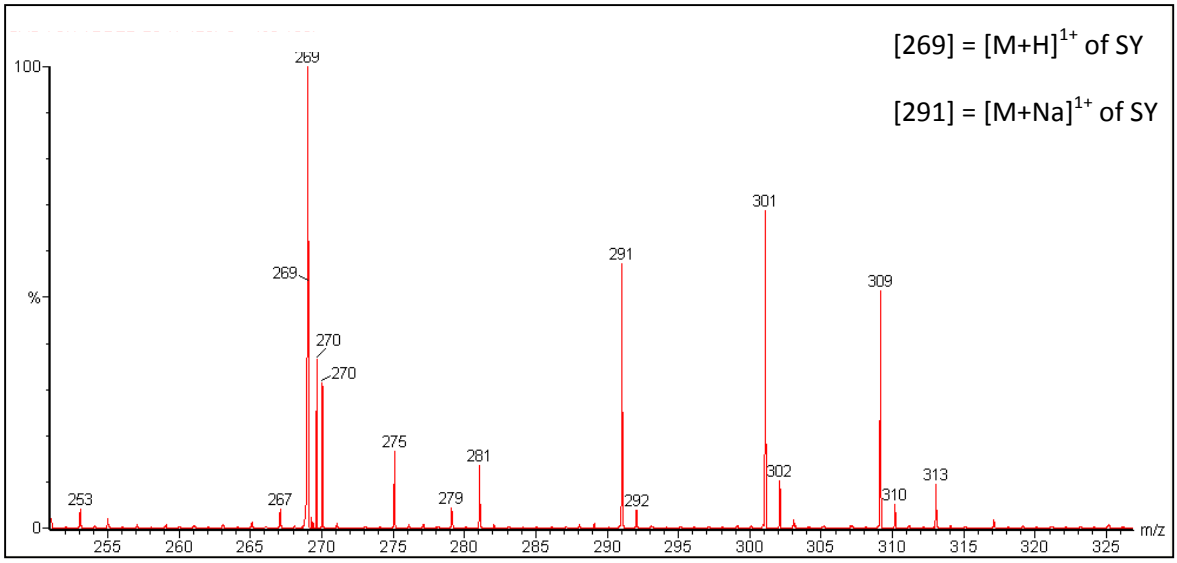

Figure 6-7: ESI Mass spectrum of Peptide-Y isolated from incubation of SPSY at 60 °C. The peptide was incubated in 100 mM phosphate buffer pH 7.4 for 3 days.

Interestingly, analyses by ESI mass spectrometry (Figure 6-8) revealed that in addition to the expected SP dkp and SY, another major degradation product was observed (Peptide-A). The molecular weight of this unknown product (Figure 6-8) matched that of SY –18 amu which would be consistent with the formation of SY dkp. As C-terminal loss of a dkp is not possible, it was suspected that SY spontaneously formed a dkp from SY under these conditions. This was investigated in Section 6.8.

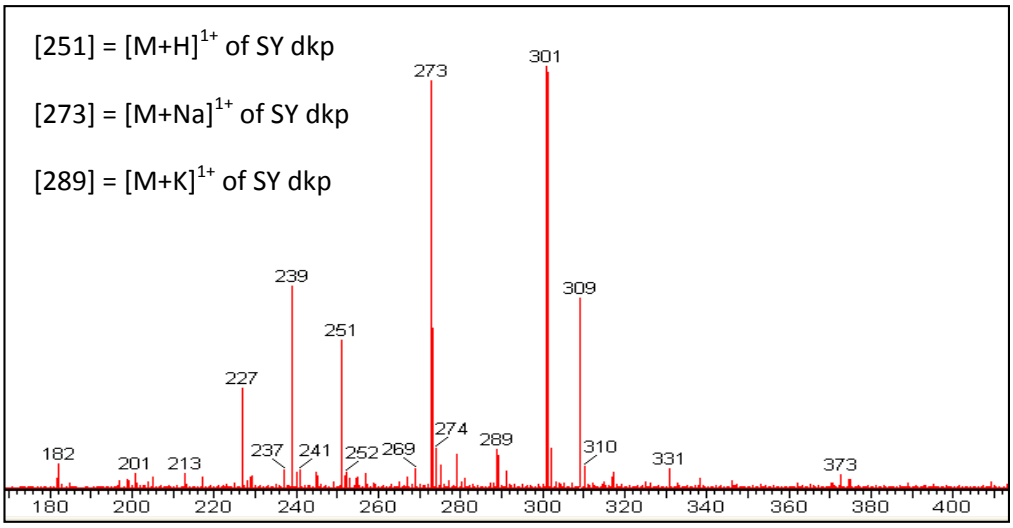

Figure 6-8: ESI Mass spectrum Peptide-A isolated by semi-preparative HPLC from incubation of SPSY at 60 °C. Peptide was incubated in 100 mM phosphate buffer pH 7.4 for 3 days.

Quantification

Figure 6-9 shows the percentage of each peptide remaining at each time point. After 3 days incubation at 60 °C, approximately 75% of SPSY had been degraded and it was completely degraded after 14 days. By contrast, Ac-SPSY remained almost completely intact.

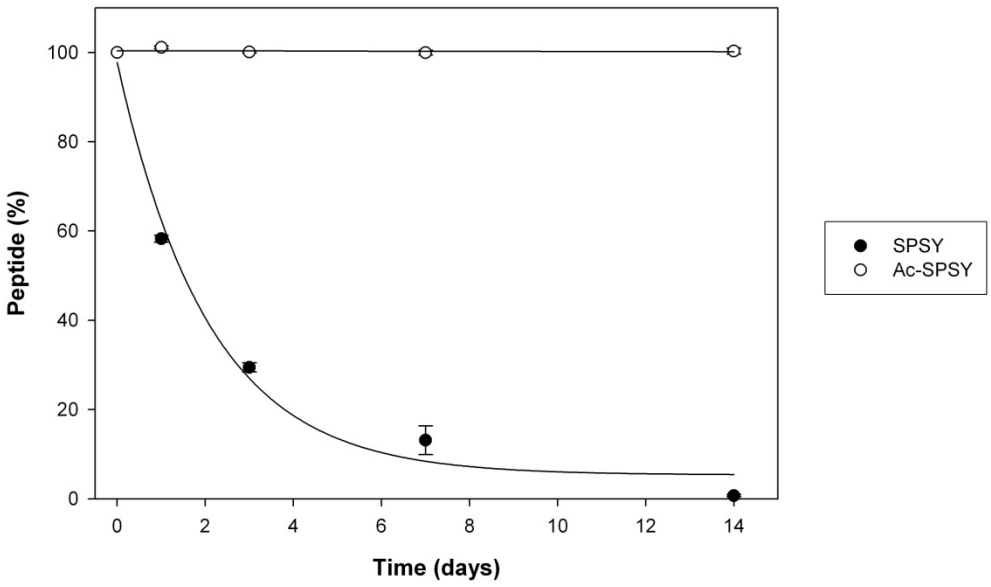

Figure 6-9: Degradation of SPSY and Ac-SPSY when incubated at 60 °C. Peptides were incubated in 100 mM phosphate buffer pH 7.4 for 2 weeks. Percentage values were calculated as the amount (moles) of each peptide remaining with respect to time compared to the amount of each peptide present at T=0.

While Figure 6-9 showed that SPSY degraded much faster than Ac-SPSY, it does not show how much was due to formation of a dkp. This was calculated by determining the amount of SP dkp present at each time point. A standard curve of SP dkp is shown in Figure 6-10. This was used to calculate the number of moles of each peptide (SPSY and Ac-SPSY) that degraded *via* dkp formation (Figure 6-11).

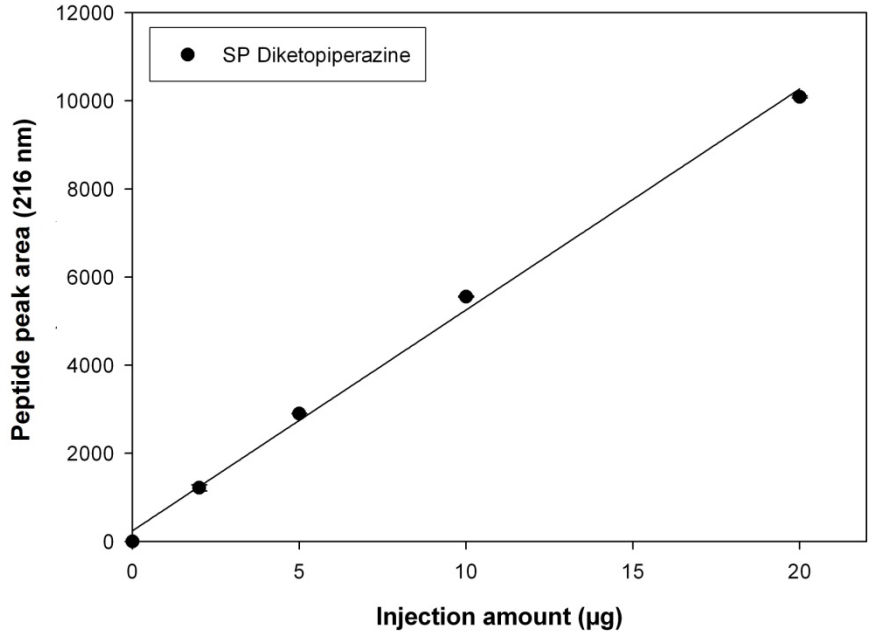

Figure 6-10: Standard curve for SP dkp relating peak area at 216 nm to peptide amount (µg).

Figure 6-11(a) shows that the number of moles of SP dkp present at day-14 is approximately equal to the number of moles of SPSY present at the beginning of the incubation (T=0). Therefore it can be concluded that SPSY almost exclusively degrades *via* dkp formation. In marked contrast, Figure 6-11(b) shows that Ac-SPSY did not form any SP dkp, or indeed any other degradation products at 60 °C.

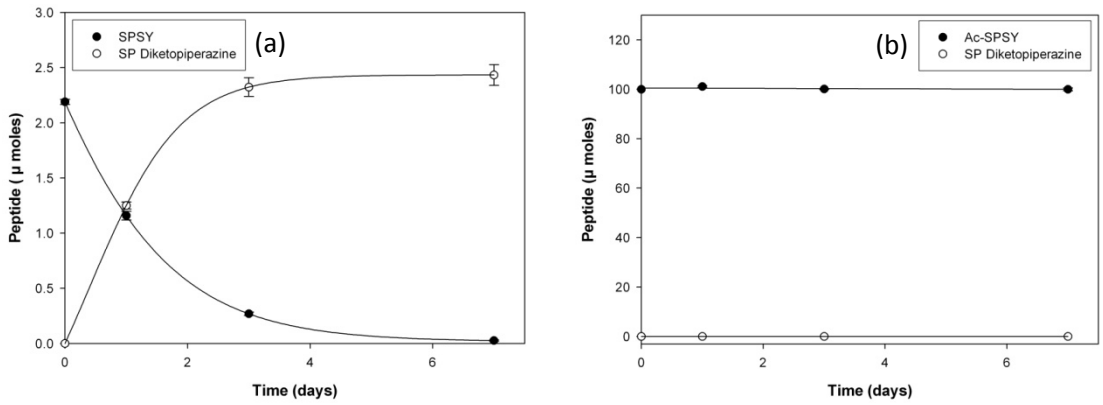

Figure 6-11: Time course showing (a) the number of moles of SPSY and SP dkp at each time point, (b) the number of moles of Ac-SPSY and SP dkp at each time point. Peptides were incubated in 100 mM phosphate buffer pH 7.4 at 60 °C.

6.4 Effect of sequence on the rate of dkp formation

The previous experiment (Section 6.3), demonstrated that a peptide based on the αB-crystallin sequence could potentially be subject to further degradation *via* loss of a dkp. However, the model peptide (SPSY) used contained a penultimate Pro residue, which is associated with an increased rate of dkp formation [236]. In this section one aim was to compare a model peptide without a penultimate Pro (SASY). Peptides (SPSY and SASY) were incubated (in triplicate) at 60 °C pH 7.4 and characterised as per Incubation-B (Section 2.2.1).

6.4.1 Results and Discussion

Figure 6-12 shows the amount of each peptide which had degraded at each time point. As per Section 6.2, 100% of SPSY was degraded by day-14, but only ~30% of SASY was degraded over the same time-frame.

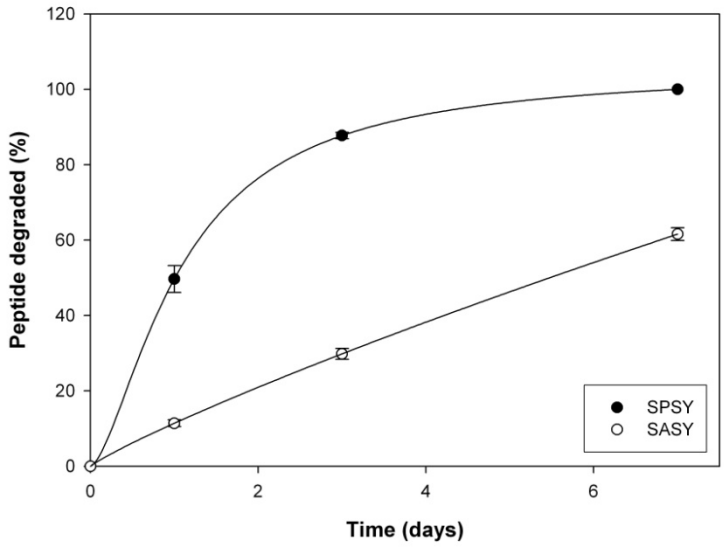

Figure 6-12: Percentage of SPSY and SPAY that degraded when incubated at 60 °C. Peptides were incubated in 100 mM phosphate buffer pH 7.4 for 1 week. Percentage values were calculated as the amount (moles) of each peptide remaining with respect to time compared to the amount of each peptide present at T=0.

The standard curves generated for SP dkp and SA dkp are shown in Figure 6-13.

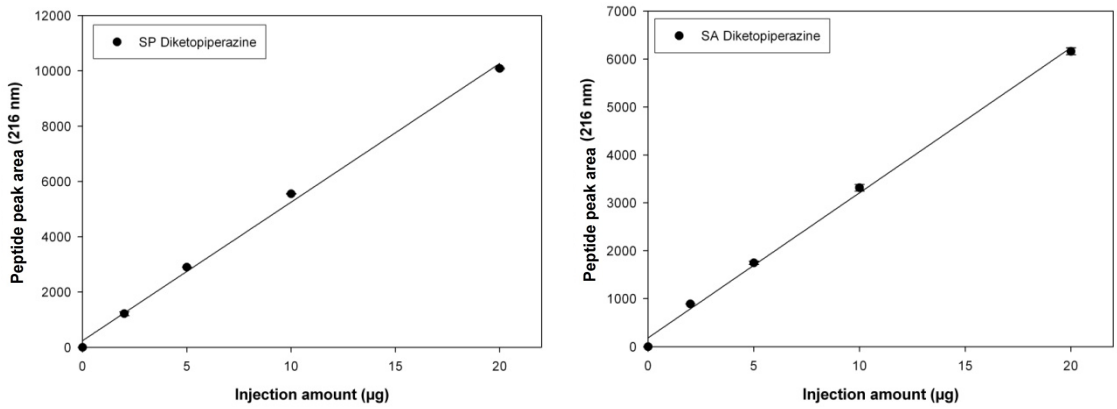

Figure 6-13: Standard curves for SP (dkp) and SA (dkp). These were used to relate the HPLC peak area at 216 nm to the number of moles present in the incubation.

These were used to calculate the number of moles of dkp that formed in each incubation (Figure 6-14).

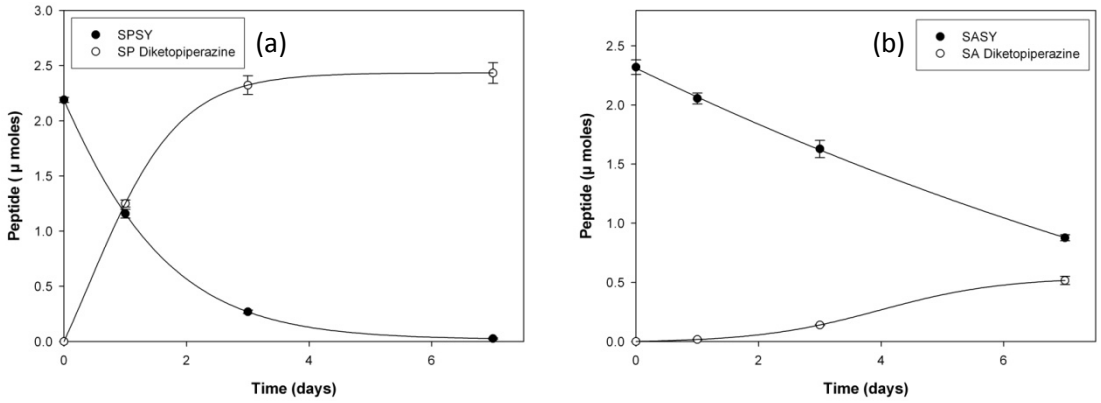

Figure 6-14: Time course showing (a) Loss of SPSY and appearance of SP dkp, (b) loss of SASY and appearance of SA dkp. Peptides were incubate in 100 mM phosphate buffer pH 7.4 at 60 °C.

Figure 6-15 shows the percentage of each peptide that degraded *via* formation of a dkp. Comparing it to Figure 6-12 reveals that while ~50% of SASY degraded by day-7, only ~15% had degraded *via* dkp formation. In contrast, ~100% of SPSY degraded *via* dkp formation. Further analysis revealed that the major modification of SASY was the formation of (D-Ser) ASY, indicating racemisation of the

N-terminal Ser residue. This will be discussed further in Chapter 7. It is proposed that for SPSY, the dkp reaction is favoured and as a result no N-terminal racemisation is observed.

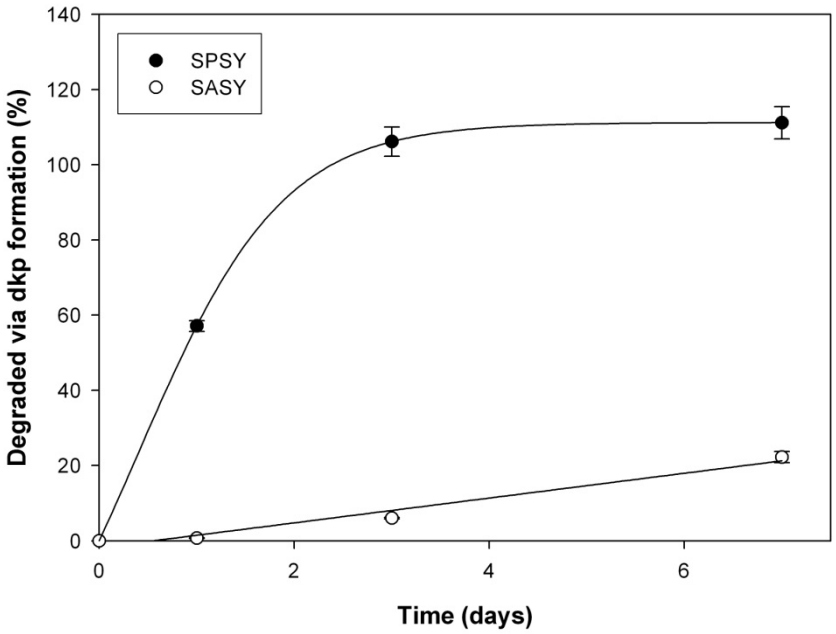

Figure 6-15: Percentage of SPSY and SPAY that degraded *via* formation of a dkp. Percentage values were calculated as the amount (moles) of each peptide which degraded *via* dkp formation with respect to time compared to the amount of each peptide present at T=0.

In conclusion, SASY does degrade *via* dkp formation, but unlike SPSY which has a penultimate Pro residue, dkp was not the major modification.

6.5 Effect of peptide length on dkp formation

To examine if these reactions could occur in proteins as well as peptides the effect of peptide length on dkp formation the model peptides YASAP, YASAAP and YASAAAP were incubated (in triplicate) at 60 °C pH 7.4 and characterised as per Incubation-B (Section 2.2.1).

6.5.1 Results and Discussion

The rate of YA (dkp) formation of each peptide was plotted with respect to time and is shown in Figure 6-16.

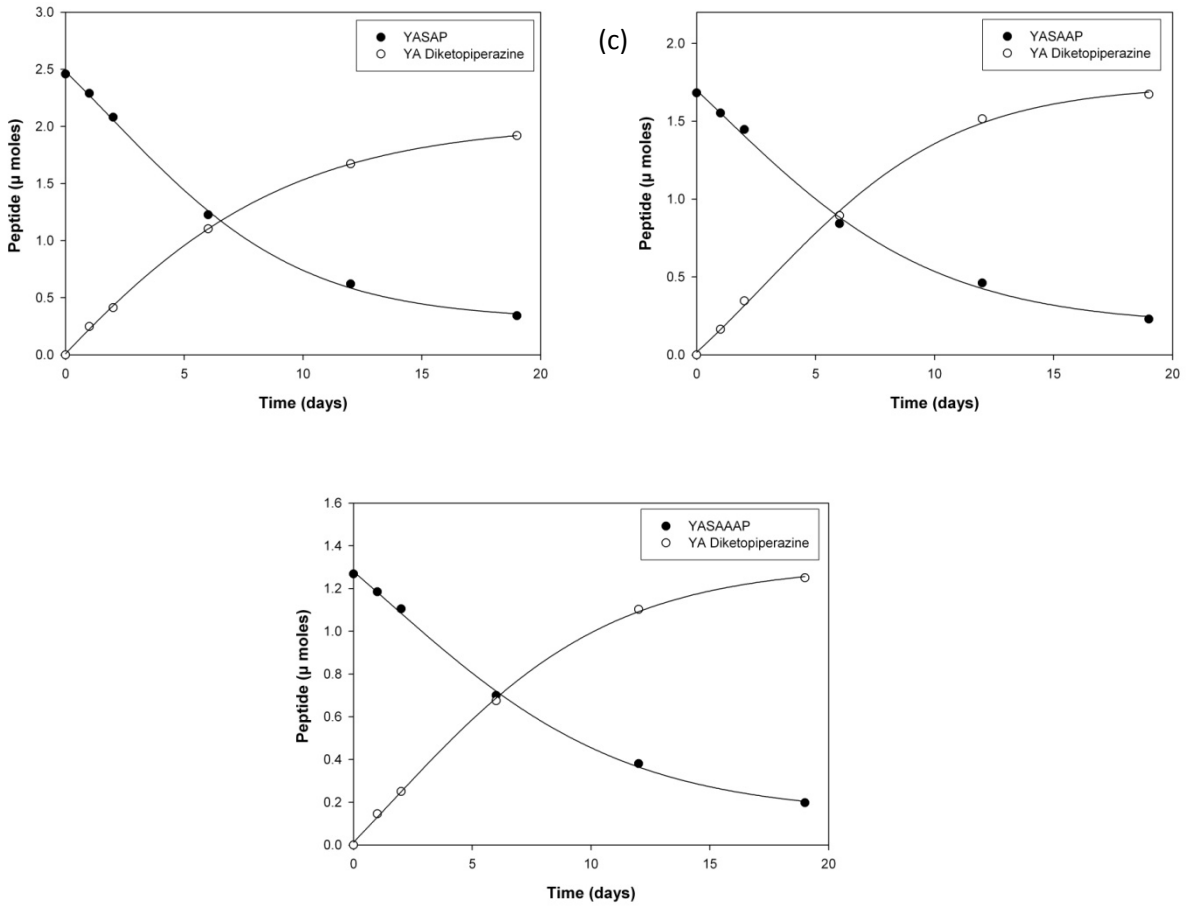

Figure 6-16: Time course showing (a) Loss of YASAP and appearance of YA dkp, (b) Loss of YASAAP and appearance of YA dkp and (c) Loss of YASAAAP and appearance of YA dkp. Peptides were incubated in 100 mM phosphate buffer pH 7.4 at 60 °C.

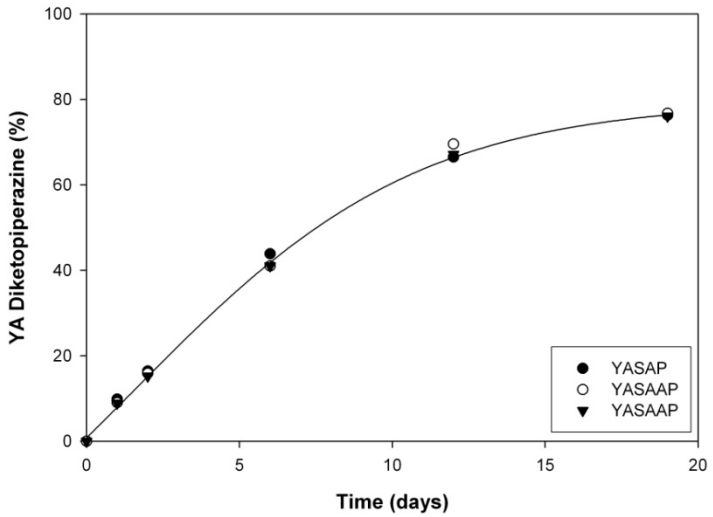

Figure 6-17: Percentage of each peptide that degraded *via* loss of a dkp. Peptides (YASAP, YASAAP and YASAAAP) were incubated at 60 °C in 100 mM phosphate buffer pH 7.4. Percentage values were calculated as the amount (moles) of each peptide which degraded *via* dkp formation with respect to time compared to the amount of each peptide present at T=0.

As can be seen from Figure 6-17, the length of the peptide chain had virtually no effect on the rate of dkp formation. YASAP, YASAAP and YASAAAP all formed a cyclic YA (dkp) at comparable rates.

6.6 Effect of buffers on dkp formation

Phosphate buffer has been shown to act as a nucleophile [246, 247] and it is possible that this affected the rate of dkp formation. To investigate the effect of buffers on the rate of dkp formation, peptide incubations were a carried out in a range of buffers, all at pH 7.4. The Good's buffers HEPES and TES were chosen for comparison. Good's buffers are characterised by low nucleophilicity and are generally regarded as being biologically inert [248].Peptides (SPSY and SASY) were incubated (in triplicate) at 60 °C pH 7.4 in each buffer (phosphate, HEPES, TES) and characterised as per Incubation-B (Section 2.2.1).

6.6.1 Results and Discussion

Figure 6-18 and Figure 6-19 show that dkp formation occurred fastest in phosphate buffer but was observed in all buffers. Unsurprisingly given their structural similarity, the rate of dkp formation in TES and HEPES was very similar.

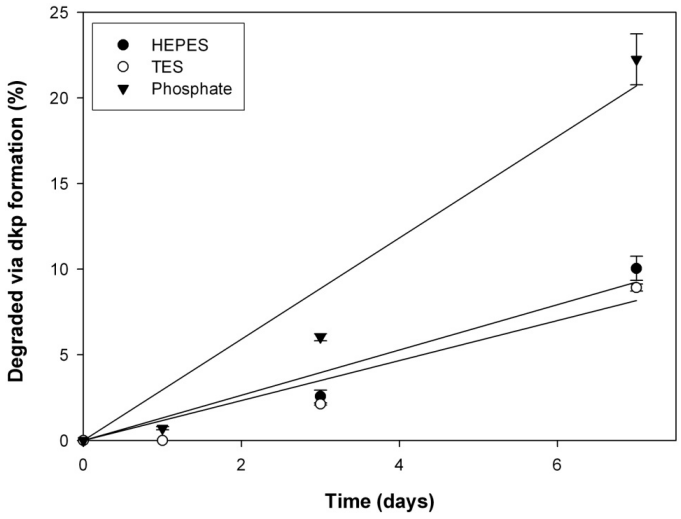

Figure 6-18: Percentage of SASY that degraded *via* formation of a dkp in HEPES, TES and Phosphate buffers. All buffers were 100 mM pH 7.4 and incubations were at 60 °C. Percentage values were calculated as the amount (moles) of each peptide which degraded *via* dkp formation as a function of time compared to the amount of each peptide present at T=0.

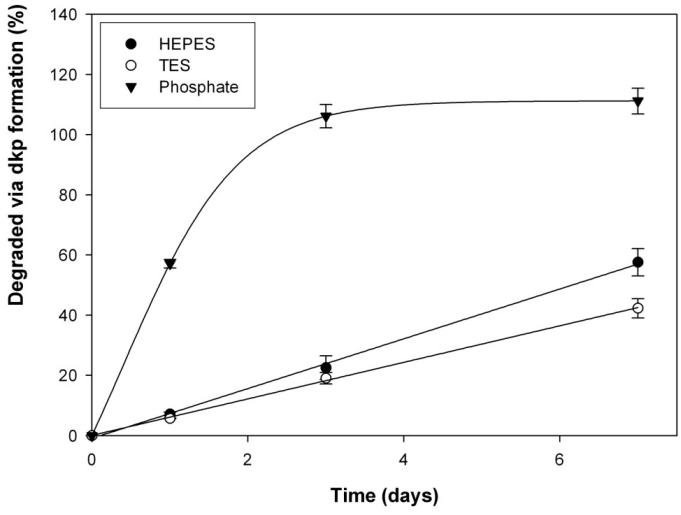

Figure 6-19: Percentage of SPSY that degraded *via* formation of a dkp in HEPES, TES and Phosphate buffers. All buffers were 100 mM pH 7.4 and incubations were at 60 °C. Percentage values were calculated as the amount (moles) of each peptide which degraded *via* dkp formation with respect to time compared to the amount of each peptide present at T=0.

The difference in rate of dkp formation between phosphate buffer and HEPES / TES buffers could be explained by a number of factors including phosphate buffer acting as a general acid and base catalyst [246]. Ion pair formation between the sulfonic acid groups of MES and TES could also potentially limit the formation of a dkp. Further work is needed but the important point is that degradation *via* dkp occurred across a range of buffers implying that long-lived lens proteins with a free amino terminal may be susceptible.

6.7 Dkp formation at physiological temperature

As the degradations being modelled in this thesis are proposed to occur over many decades to long-lived proteins in the human body [1], it was also considered important to show that these processes could occur at physiological temperature. To do this, three model peptides were chosen. SPSY was chosen based on it being a fragment of αB-crystallin (19-21) and that it has a Pro at the penultimate (2') position. SASY was chosen as a control which lacked a Pro in position 2. YPAATIPY was chosen as a longer peptide that also has a Pro in the penultimate position. Peptides (SPSY, SASY and YPAATIPY) were incubated (in triplicate) at 37 °C pH 7.4 and characterised as per Incubation-A (Section 2.2.1).

6.7.1 Results and Discussion

The standard curves generated for Section 6.5 were again used to calculate the number of moles of each peptide that degraded *via* dkp formation (Figure 6-20). As can be seen, both SPSY and YPAATIPY did degrade *via* dkp formation but SASY did not show measurable dkp production over the timeframe employed.

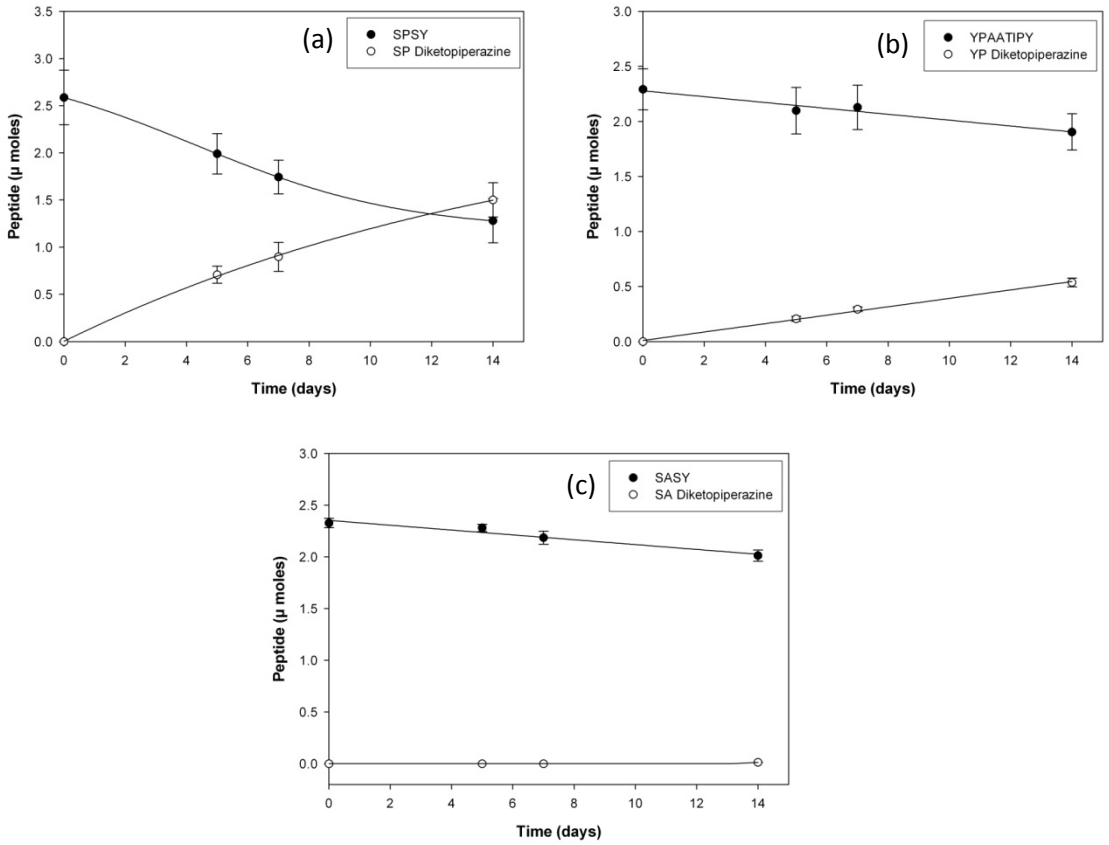

Figure 6-20: Time course showing (a) Loss of SPSY and appearance of SP dkp, (b) Loss of YPAATIPY and appearance of YP dkp and (c) Loss of SASY but no formation of any SA dkp. Peptides were incubated in 100 mM phosphate buffer pH 7.4 at 37 °C.

Figure 6-21 compares the percentage of each peptide that degraded *via* dkp formation.

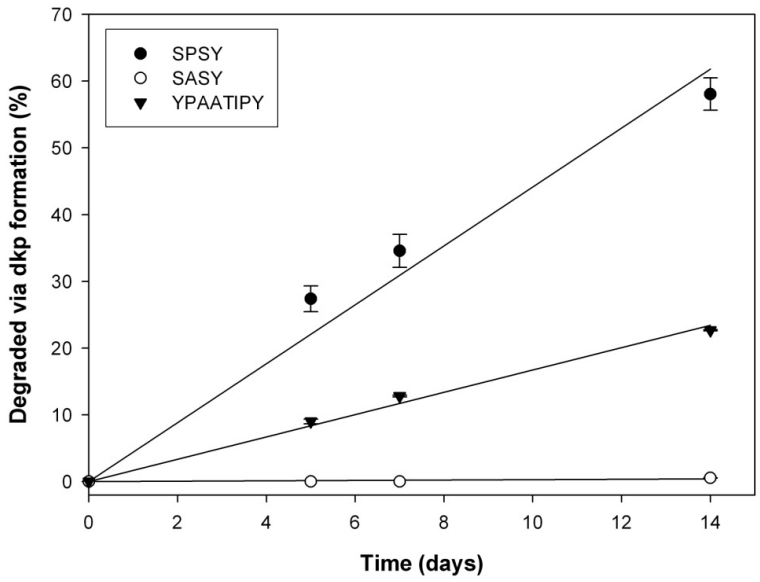

Figure 6-21: Comparison of the percentage of each peptide that degraded *via* formation of a dkp at 37 °C. Percentage values were calculated as the amount (moles) of each peptide which degraded *via* dkp formation with respect to time compared to the amount of each peptide present at T=0.

After 2 weeks incubation at 37 °C, ~50% of SPSY and ~20% of YPERTIPY has degraded *via* dkp formation. However SASY, which does not have a penultimate Pro residue, did not show evidence of degradation *via* dkp formation. Many known truncation sites in long-lived lens proteins generate a shortened protein terminating in a penultimate Pro such as αB (45-57), γS (167-178) and γS (158-173) [128, 187]. These data show that such truncated fragments should be prone to further degradation *via* loss of a dkp.

6.8 Investigation into the potential for SY to spontaneously form a dkp

Following incubation of SPSY at physiological pH (60 °C) for Section 6.3 of this thesis the expected products of SP dkp and SY were detected. However it was speculated that additional peptides which formed were the result of SY spontaneously forming a dkp, which lead to the formation of other racemised and possibly sequence-inverted peptides. This has been shown to occur in the literature by Bada et al. [249, 250]. To test this SY and (D-Ser)Y were incubated separately as per Section 6.3 and characterised as per Incubation-B (Section 2.2.1).

6.8.1 Results and Discussion

As can be seen in Figure 6-22 both incubations resulted in the formation of a number of modified peptides. Synthetic standards of SY dkp and (D-Ser)Y dkp were analysed by HPLC and found to co-elute with peaks formed in both incubations.

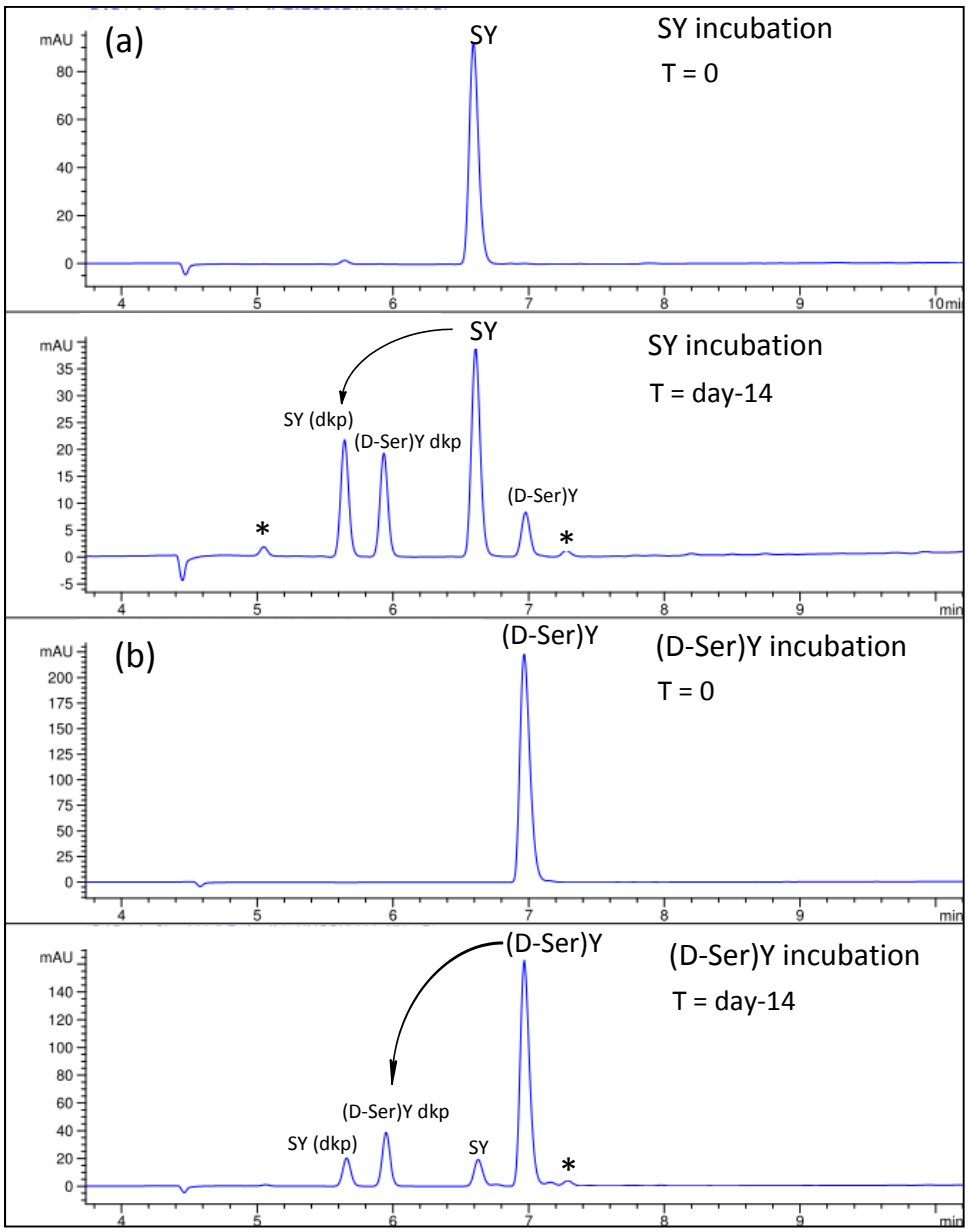

Figure 6-22: Comparison of T=0 and day-14 incubation time points of (a) SY incubation and (b) (D-Ser)Y incubation. Peaks indicated by (*) have not been assigned.

Samples of the peaks proposed to be SY dkp and (D-Ser)Y dkp were isolated and analysed by ^{1}H NMR spectroscopy (Figure 6-23). Upon formation of a dkp, an additional peptide bond NH is formed. I.e the di-peptide SY contains one NH peptide bond whereas SY dkp contains two. This can be seen in Figure 6-24. The occurrence of an additional NH signal in the ^{1}H spectra of the peaks proposed to be SY dkp and (D-Ser)Y dkp (indicated by * in Figure 6-23) supports the assignment of a dkp.

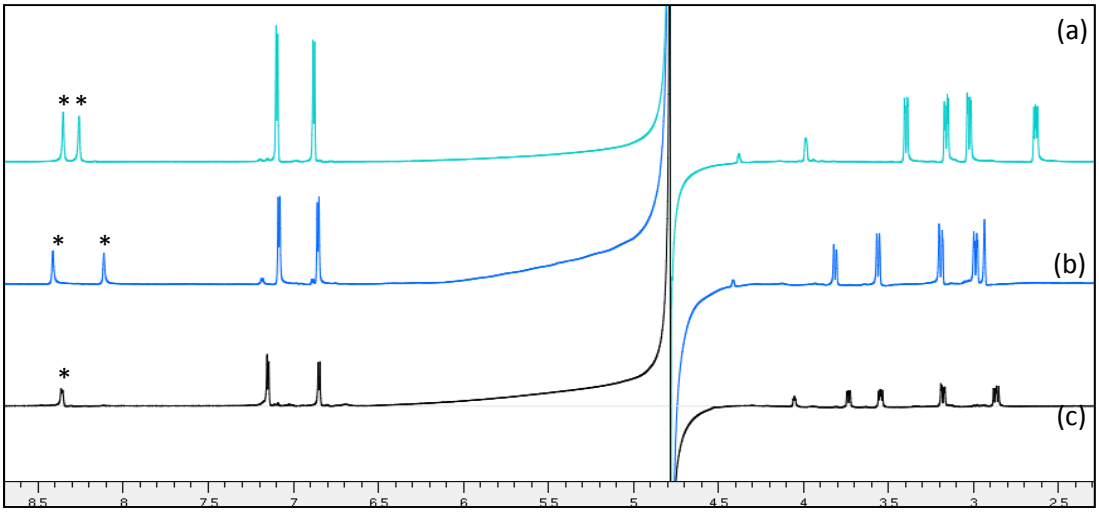

Figure 6-23: ^{1}H NMR spectrum of (a) proposed SY dkp isolated from incubation, (b) proposed (D-Ser)Y dkp isolated from incubation, SY standard (c). (*) Indicates a peak corresponding to an NH.

While both incubations formed both D- and L- forms of the dkp, the ratios varied, with SY forming a greater amount of the L- form and (D-Ser)Y forming a greater amount of the D- form. However both incubations contained both D- and L- forms of the dkp indicating that racemisation is occurring. The unidentified peaks in (indicated by * in Figure 6-22a) are speculated to be the result of sequence inversion. Interestingly the total amount of dkp formed (based on peak area) in each incubation (i.e. "SY dkp + (D-Ser)Y dkp"), varied significantly, with SY forming approximately twice as much as (D-Ser)Y. This is possibly due to steric factors, with the L-form potentially being more favourable to formation of the dkp ring. A mechanism outlining how these processes could occur is shown in Figure 6-24.

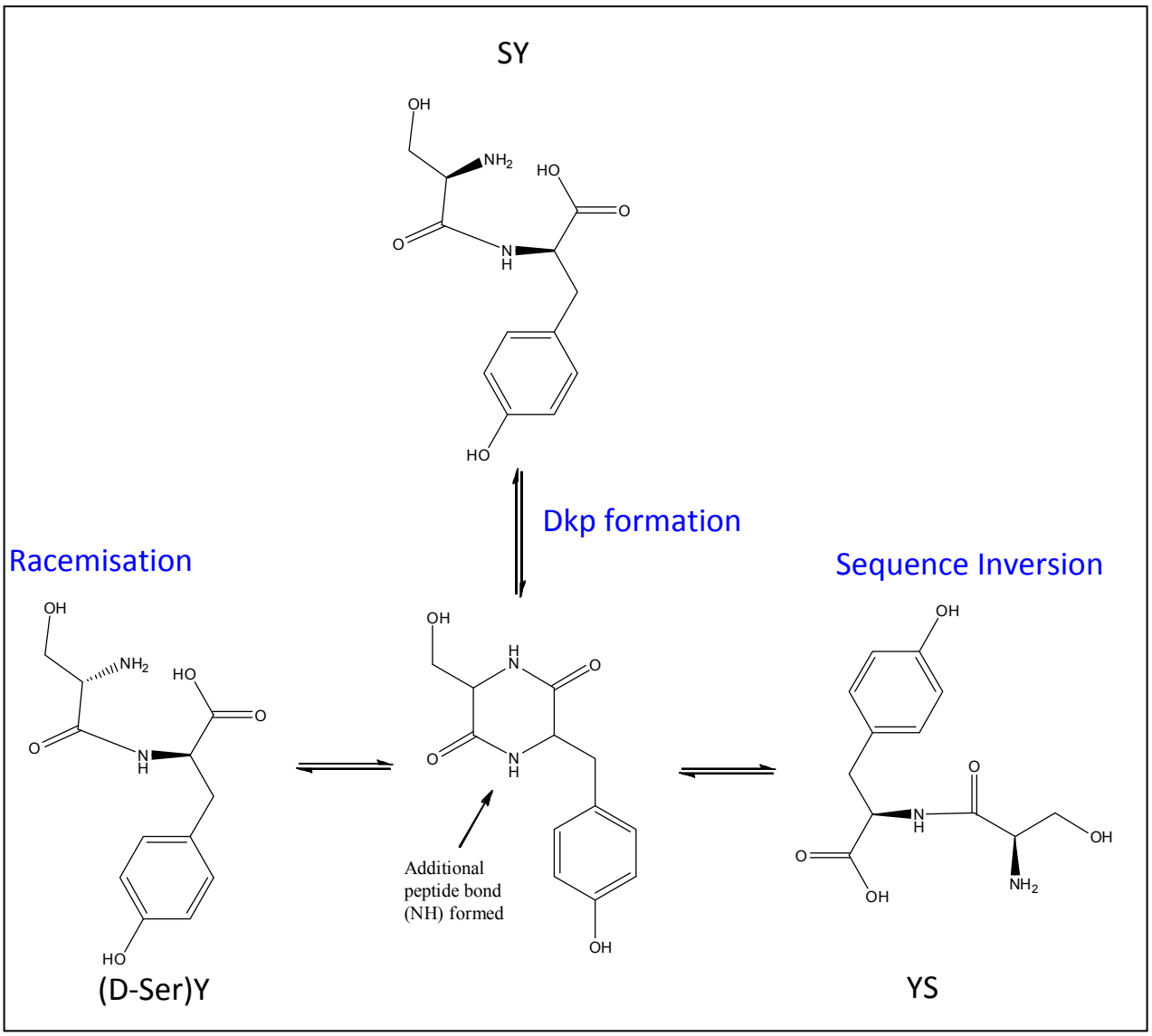

Figure 6-24: Mechanism which describes both racemisation and sequence inversion *via* formation of diketopiperazine. The formation of an additional peptide bond (NH) upon conversion to a dkp is highlighted.

The results of this simple experiment demonstrate the complexity of characterising the products of an incubation where the formation of a dkp is possible. Even with the simple dipeptide SY, the formation of 12 peptides detailed in Table 6-2 is potentially possible.

Table 6-2: Potential products which could form from SY *via* dkp formation

Potential products
SY
(D-Ser)Y
S(D-Tyr)
YS
(D-Tyr)S
Y(D-Ser)
SY dkp
YS dkp
(D-Ser)Y dkp
S(D-Tyr) dkp
Y(D-Ser) dkp
(D-Tyr)S dkp

This may explain the multiple products that are often seen by HPLC throughout this thesis.

6.9 Conclusions

This chapter explored the potential for peptides and long-lived proteins to degrade *via* the loss of an cyclic dkp from the N-terminus. Model peptides were incubated at physiological pH and elevated temperatures were used to simulate the extended periods that long lived proteins are exposed to. In the lens many known truncation sites in α-crystallin generate a shortened protein terminating in SP [128, 187] and as demonstrated in this chapter peptides with a penultimate Pro residue are particularly prone to degradation *via* dkp formation [249]. A model peptide (SPSY), based on one such truncation point (Ser 19 in αB-crystallin) was shown to be susceptible to further degradation *via* dkp formation, indicating this could be occur in the aged-lens. To examine the potential for peptides lacking a penultimate Pro to form a dkp, the peptide SASY was incubated under identical conditions and it formed a dkp at a rate approximately three times slower than SPSY.

Dkp formation was shown to occur in a range of buffers. The difference in rate between the three buffers (TES, HEPES and phosphate) is speculated to be the result of a number of factors, including

phosphate buffer as a general acid and base catalyst [246]. The key message though is that in all buffers, dkp formation did occur and this suggests its potential to occur in the aged lens.

It was conceivable that only short peptides may readily form diketopiperazines and to test this, the effect of lengthening the peptide was examined. The results indicated that peptide length up to 7 amino acids in length did not have any effect on the rate of dkp formation suggesting that it could also potentially occur in long-lived proteins

Crucially for peptides with a penultimate Pro residue, *N*-terminal truncation was also shown to occur under physiological conditions (pH 7.4 and 37 °C). Peptides without a penultimate Pro residue did not show any evidence of dkp formation, but it is possible that it could still occur in the lens over many decades. While it is likely that proteins may degrade at a slower rate than peptides [251], this data is still strong evidence that for truncated fragments with a penultimate Pro, further degradation *via* dkp formation is possible in biological systems.

7 Chapter 7: Racemisation at the N-terminus

7.1 Introduction

This chapter describes the investigation of an unexpected modification that was observed when model peptides were incubated at physiological pH (Section-4.3). Following incubation of PFHSPSY in 100 mM phosphate buffer pH 7.4 at 60 °C a major degradation product was observed. The characterisation of this modification, and its assignment as (D-Pro)FHSPSY is detailed in this chapter. Other factors in relation to this novel modification were then examined.

With the exception of Asp/Asn residues and to a lesser extent Gln/Glu, which racemise *via* an internal succinimide ring, racemisation of all other amino acids is thought to occur *via* a carbanion intermediate [203]. This is often base-catalysed. Removal of the hydrogen atom attached to the α carbon results in a negatively-charged planar carbanion intermediate being formed (Figure 7-1). Re-addition of a hydrogen ion to the carbanion results in an equal probability of either the D or the L enantiomer being formed.

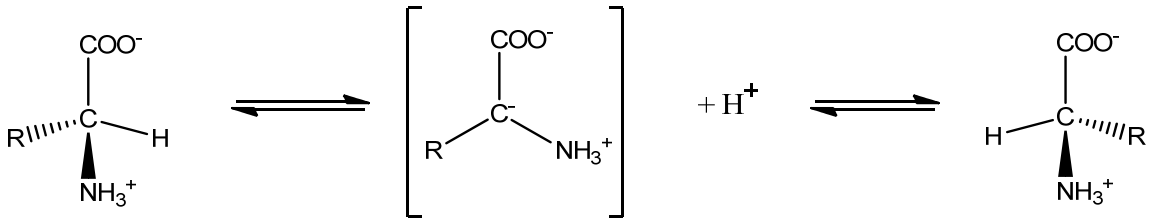

Figure 7-1: Base catalysed racemisation mechanism. Adapted from [252].

Factors known to increase the rate of racemisation include pH, temperature and, for free amino acids, enzymes that use pyridoxal phosphate [253-255]. An example of this can be seen in the food industry where protein containing foods are commonly treated with alkali in the course of preparing protein concentrates, or for destroying microorganisms, and this has been shown to lead to extensive amino acid racemisation [256, 257].

7.2 Aim

The aim of this chapter was to investigate the structure of a novel peak formed during the incubation of peptides for Section 4.3. A long-lived lens protein was also examined for evidence of this novel modification and a mechanism was proposed to explain how it occurs.

7.3 N-terminal racemisation of a model peptide

In Chapter 4 (Section 4.3), a novel product was observed when PFHSPSY (αB 16-21) was incubated at 60 °C and physiological pH. This section describes the incubation studies and subsequent spectral analysis leading to the eventual assignment of (D-Pro)FHSPSY as the major product.

7.3.1 Results and Discussion

HLPC Analysis and purification

Figure 7-2 shows a HPLC trace (280 nm) of the day-3 time point indicating formation of a major degradation product (Peptide-X).

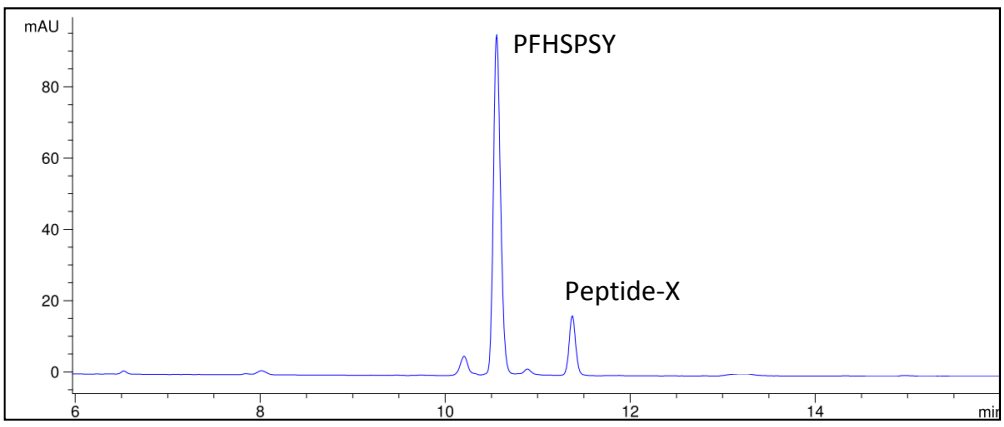

Figure 7-2: HPLC trace (280 nm) showing the formation of Peptide-X following incubation of PFHSPSY for 3 days at 60 °C. Incubation was carried out in 100 mM phosphate buffer pH 7.4.

Re-incubation of Peptide-X

Peptide-X was collected, lyophilised and incubated under identical conditions. Analysis of the products of this incubation by HPLC PDA detection and MALDI mass spectrometry revealed Peptide-X partially converted back to PFHSPSY (Figure 7-3).

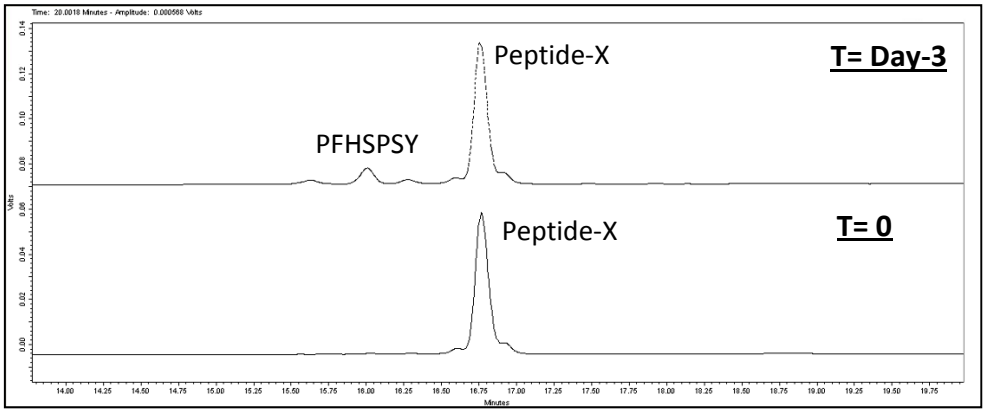

Figure 7-3: HPLC trace (280 nm) showing the formation of PFHSPSY following the re-incubation of Peptide-X. Peptide was incubated in 100 mM phosphate buffer pH 7.4 at 60 °C.

MALDI mass spectrometry

Subsequent analysis of Peptide-X by MALDI mass spectrometry (Figure 7-4) revealed that it had the same molecular weight as PFHSPSY and a matching MS/MS fragmentation pattern. It was therefore assumed to be a *cis* Pro variant of PFHSPSY.

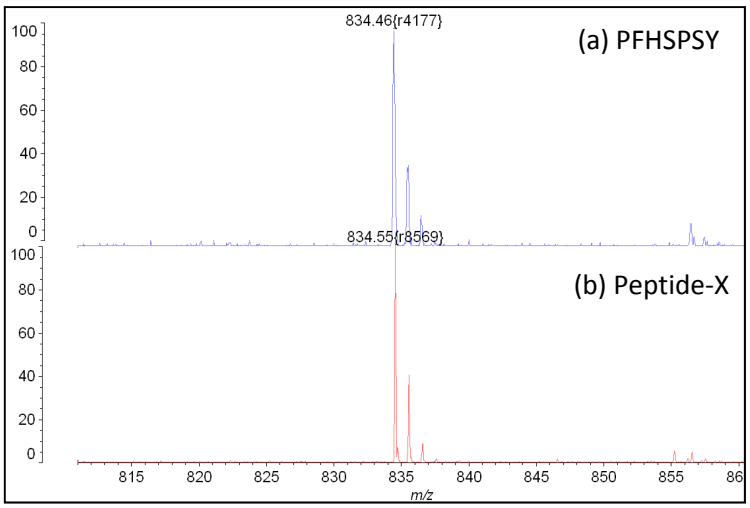

Figure 7-4: MALDI analysis of (a) PFHSPSY and (b) Peptide-X formed during incubation in 100 mM phosphate buffer pH 7.4 at 60 °C

Cis Pro

Peptides containing Pro are unique in terms of their capacity to form peptide bond conformers [258]. Peptide bonds involving Pro residues can adopt two different conformations (*cis* and *trans*), which can be simultaneously present in solution because of the low energy barriers of rotation about the peptidyl-Pro imide bond [259, 260]. This is unlike other amino acids where the enegy barrier is much greater and *cis* bonds are rarely observed.

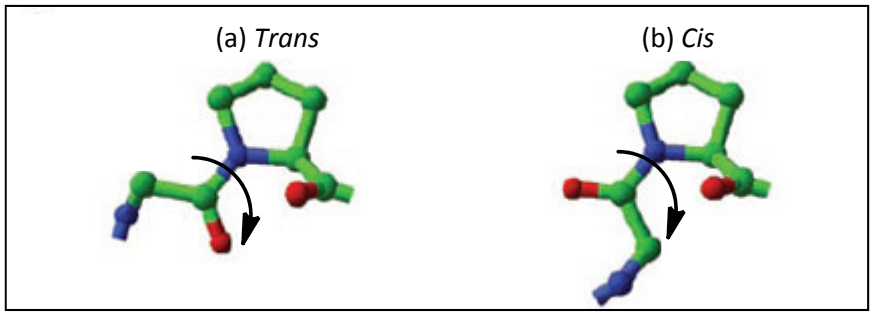

Figure 7-5: *Cis* and t*rans* Pro bond configuration. Adapted from Lu et al.[261].

^{1}H NMR spectroscopy

A comparison of the ^{1}H NMR spectra (1-4 ppm) of PFHSPSY and Peptide-X is shown in Figure 7-6 .It revealed that despite having the same molecular weight, there are differences between the two peptides, most notable the shift of the multiplet at 1.6 ppm.

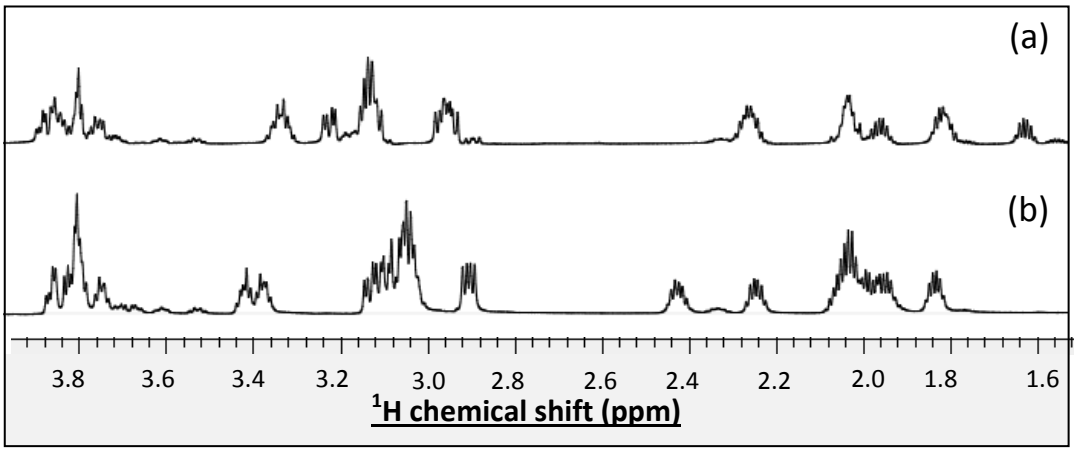

Figure 7-6: ^{1}H Proton NMR spectrum of (a) PFHSPSY and (b) Peptide-X. Samples were made up in 50 mM phosphate buffer pH 7.4 containing 1 mM 4,4-dimethyl-4-silapentane-1-sulfonic acid (DSS) and 10% D_20.

2D ROESY spectroscopy

The spectroscopic identification of a *cis*-Pro peptide bond by NMR traditionally relies upon observation of a strong $^{1}H^{\alpha}$ -$^{1}H^{\alpha}$ NOE correlation (Figure 7-7a) between the two sequential residues [262]. Due to its different orientation, a *trans*-Pro peptide bond is expected to have a 1Hα -$^{1}H^{\delta}$ NOE correlation (Figure 7-7b) between the two sequential residues.

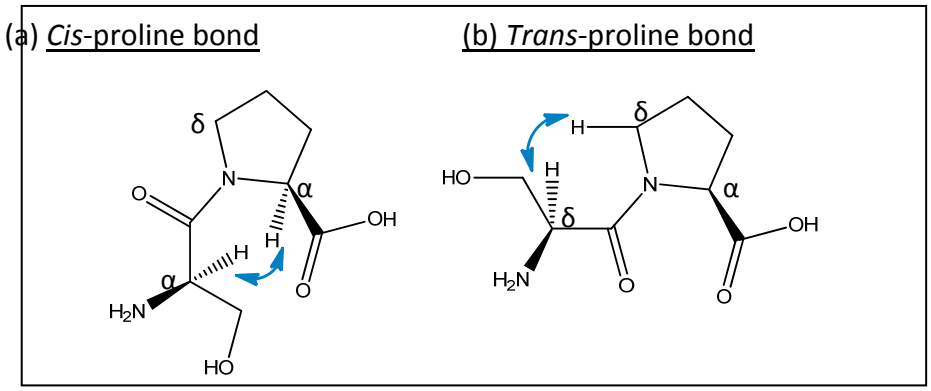

Figure 7-7: Expected NOE correlations for (a) *cis*-proline bond and (b) trans-Proline bond.

If Peptide-X was a *cis*-Pro isomer of PFHSPSY then there should be a $^{1}H^{\alpha}$ -$^{1}H^{\alpha}$ NOE correlation between the Ser 4 and the internal Pro residue (Pro 5). Analysis by 2D ROESY (Figure 7-8) did not reveal any such correlation, indicating it was unlikely that a *cis* Pro bond was present.

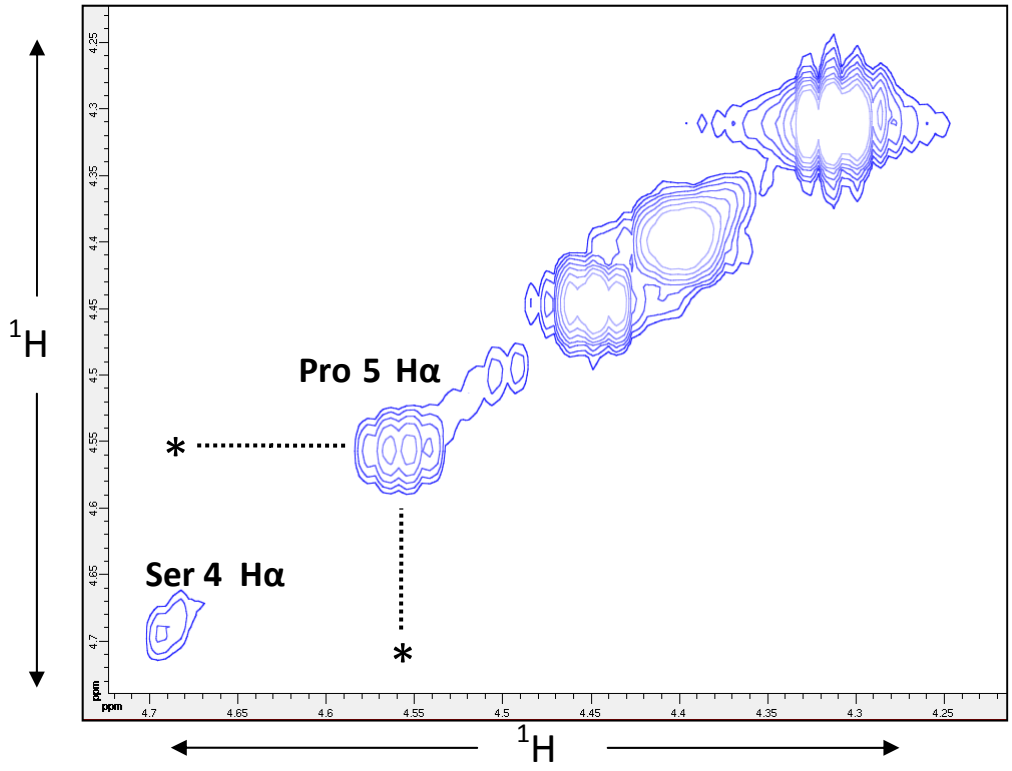

Figure 7-8: Selected region of the 2D ROESY spectrum of Peptide-X. Should a *cis* Pro bond be present then there should be cross peaks present between the Pro 5 H^{α} and the Ser 4 H^{α} (Indicated by *). As there were no cross peaks in this area it suggests that a *cis*-bond is not present in Peptide-X.

^{13}C HSQC NMR spectroscopy

It is known that NOE correlations are prone to chemical shift degeneration and artefacts originating from insufficient water suppression [263], so a ^{13}C HSQC spectrum was also obtained. Improvements in modern ^{13}C NMR sensitivity has allowed for ^{13}C HSQC spectra to provide clear Pro bond characterisation with Pro C_β and C_γ ^{13}C HSQC resonances shifting up-field by 2-3 ppm as the form alters from *trans* to *cis* [264]. As can be seen from Figure 7-9, while there are distinct changes in the ^{1}H chemical shift (indicated by the horizontal shift of the signals) there is almost no change in the C_β and C_γ ^{13}C chemical shift (vertical axis). This also suggests that Peptide-X is unlikely to be a *cis* Pro variant of PFHSPSY.

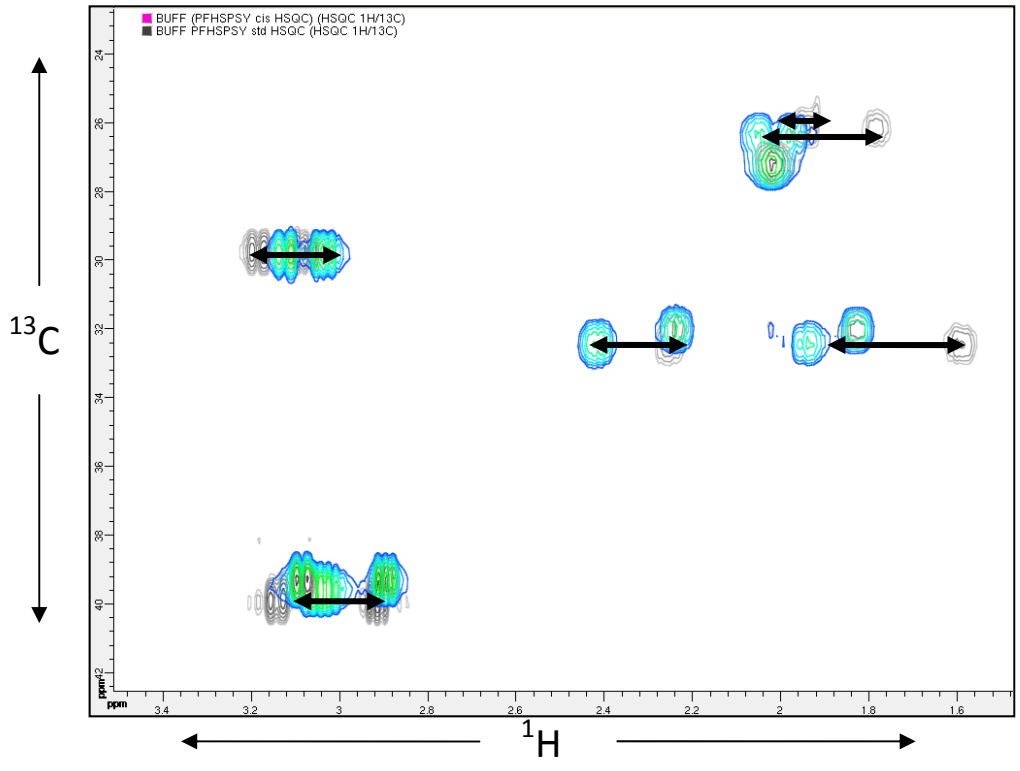

Figure 7-9: Overlay of a partial HSQC spectrum from PFHSPSY (blue) and Peptide-X (grey).

The 2D NMR signals corresponding to each amino acid residue in PFHSPSY and in Peptide-X were assigned. An example of the annotated ^{1}H TOCSY spectra of Peptide-X is shown in Figure 7-10.

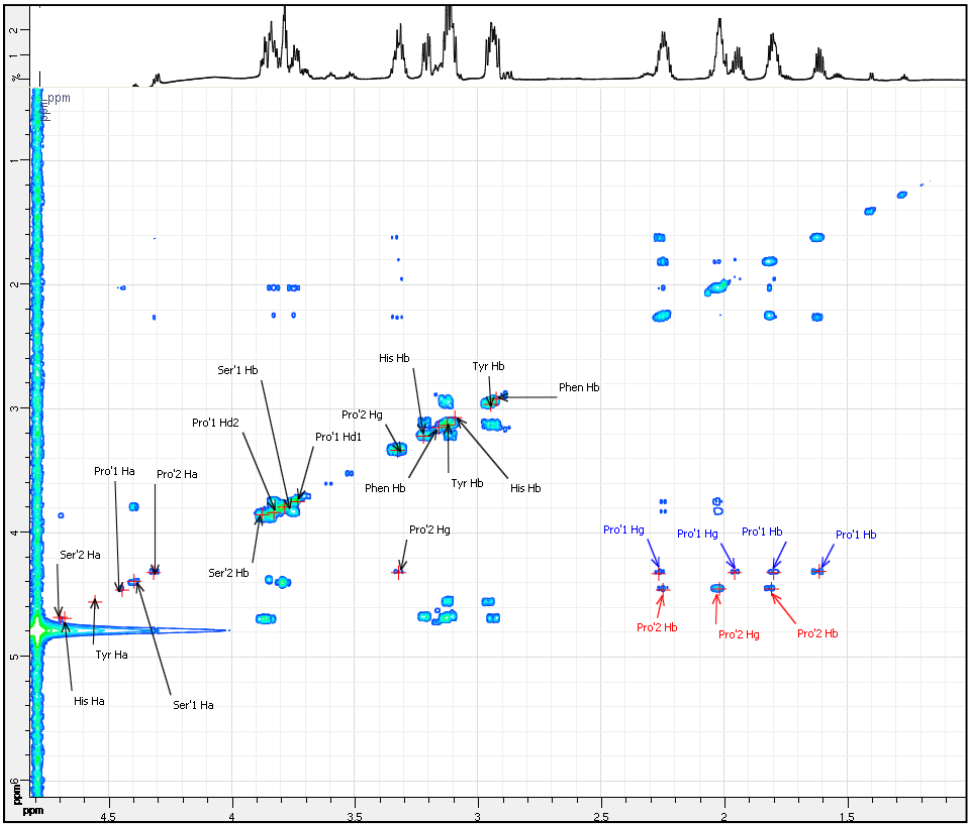

Figure 7-10: Partial TOCSY spectrum of Peptide-X showing the assignment of each signal to a corresponding amino acid residue.

Figure 7-11 highlights the region of the TOCSY NMR spectrum where the signals corresponding to the Pro residues in Peptide-X and PFHSPSY are located. The chemical shift values corresponding to the N-terminal Pro (Pro 1) in PFHSPSY and Peptide-X differed significantly, whereas the signals corresponding to Pro 5 in both peptides remained essentially the same. This suggested that Pro 1 was in a different chemical environment in the two samples and is thus likely to have undergone modification. However, the fact that the change in chemical shifts was relatively small in magnitude and that neighbouring residues were little affected suggested the modification was localised. The most likely explanation of these results was that the N-terminal of Peptide-X had undergone racemisation.

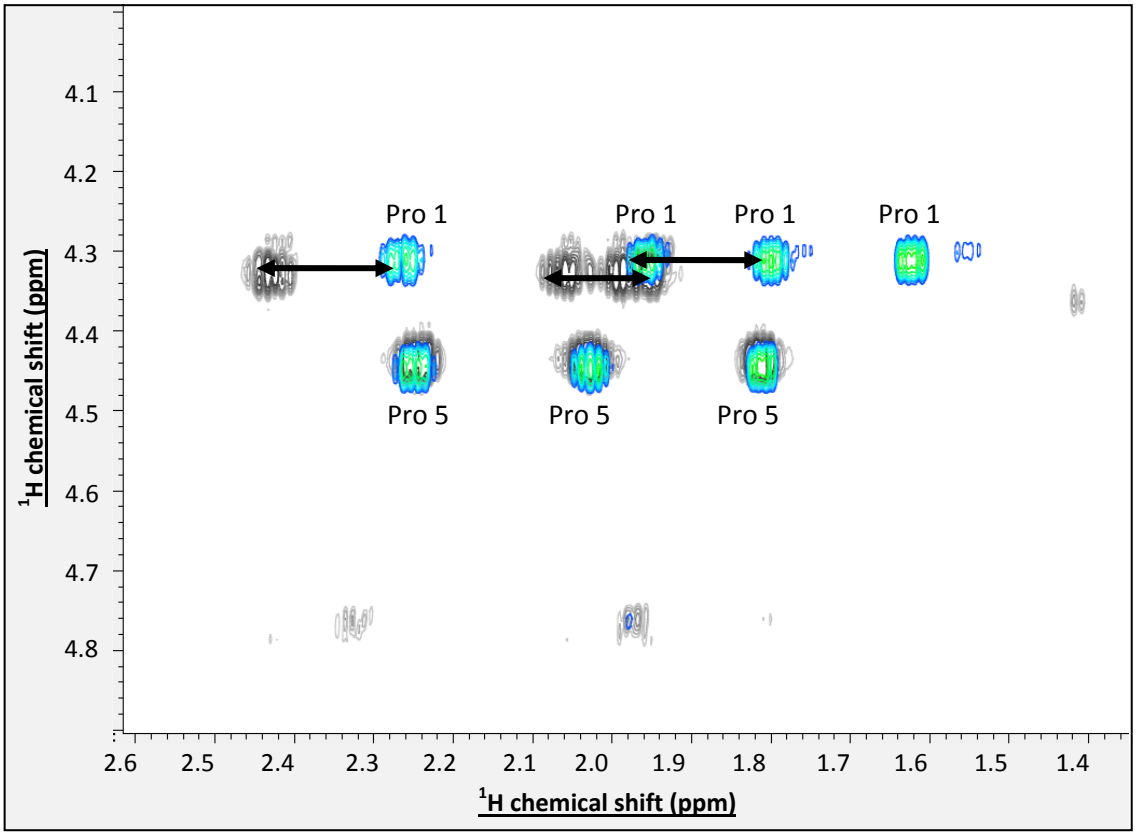

Figure 7-11: Overlay of a region of the TOCSY spectrum of PFHSPSY (Blue) and Peptide-X (Grey). The signals corresponding to the N-terminal Pro (Pro 1) vary considerably between PFHSPSY and Peptide-X where as the signals corresponding to the internal Pro (Pro 5) in both peptides remain the same.

Chiral HPLC Amino Acid Analysis

To test for racemisation, Peptide-X and PFHSPSY were hydrolysed with HCl and subjected to chiral amino acid analysis using Marfey's reagent (Figure 7-12). This revealed that Peptide-X contained ~50% L-Pro and ~50% D-Pro, indicating that one of the Pro residues had racemised. There was no evidence of racemisation of any amino acid in PFHSPSY, or any other amino acid in Peptide-X.

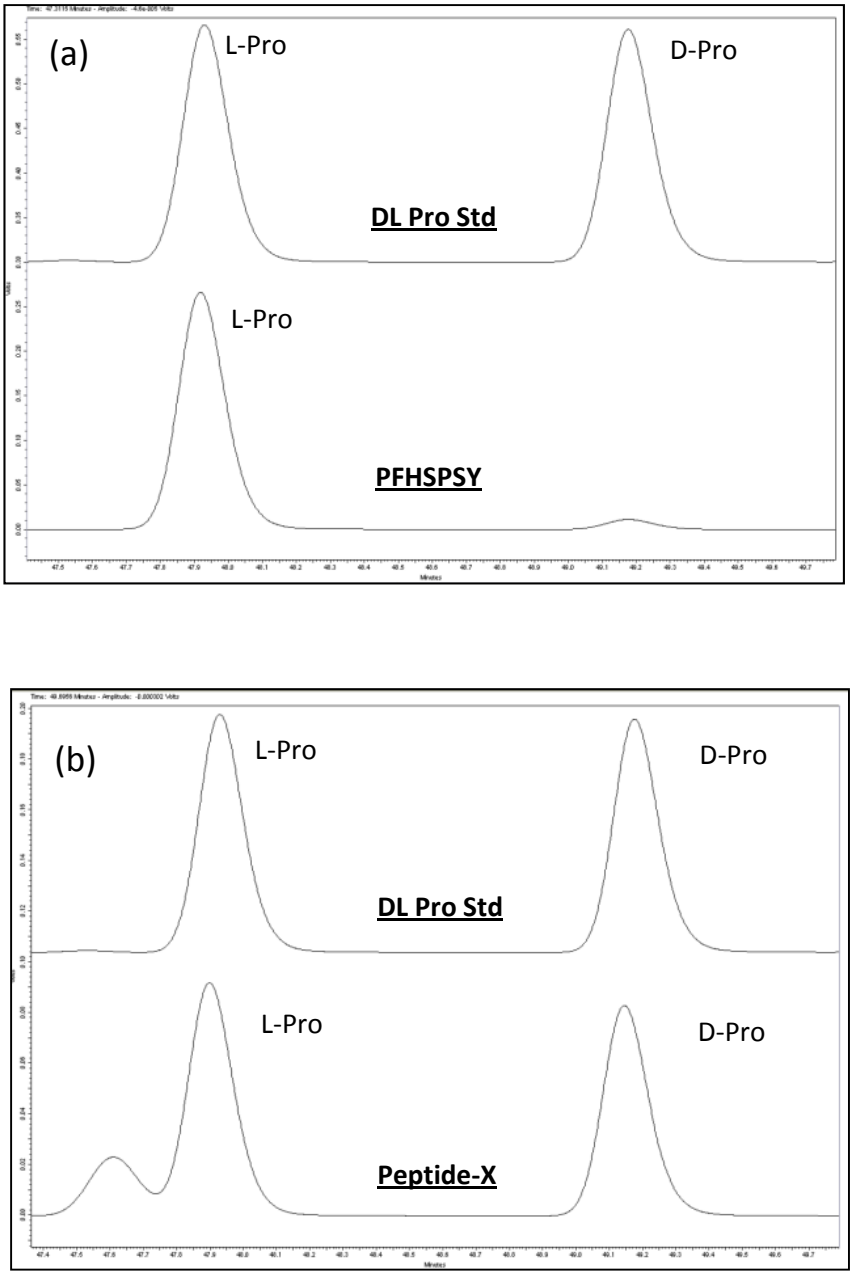

Figure 7-12: Partial spectrum from chiral HPLC analysis (340 nm), comparing the acid hydrolysis products of (a) PFHSPSY and (b) Peptide-X to a DL-Pro standard.

7.3.1.1 HPLC comparison of Peptide-X to a standard of (D-Pro)FHSPSY

Figure 7-13 shows the comparison of Peptide-X with a standard of (D-Pro)FHSPSY by HPLC. It was found to have the same retention time and also co-eluted when a sample of Peptide-X was spiked with (D-Pro)FHSPSY.

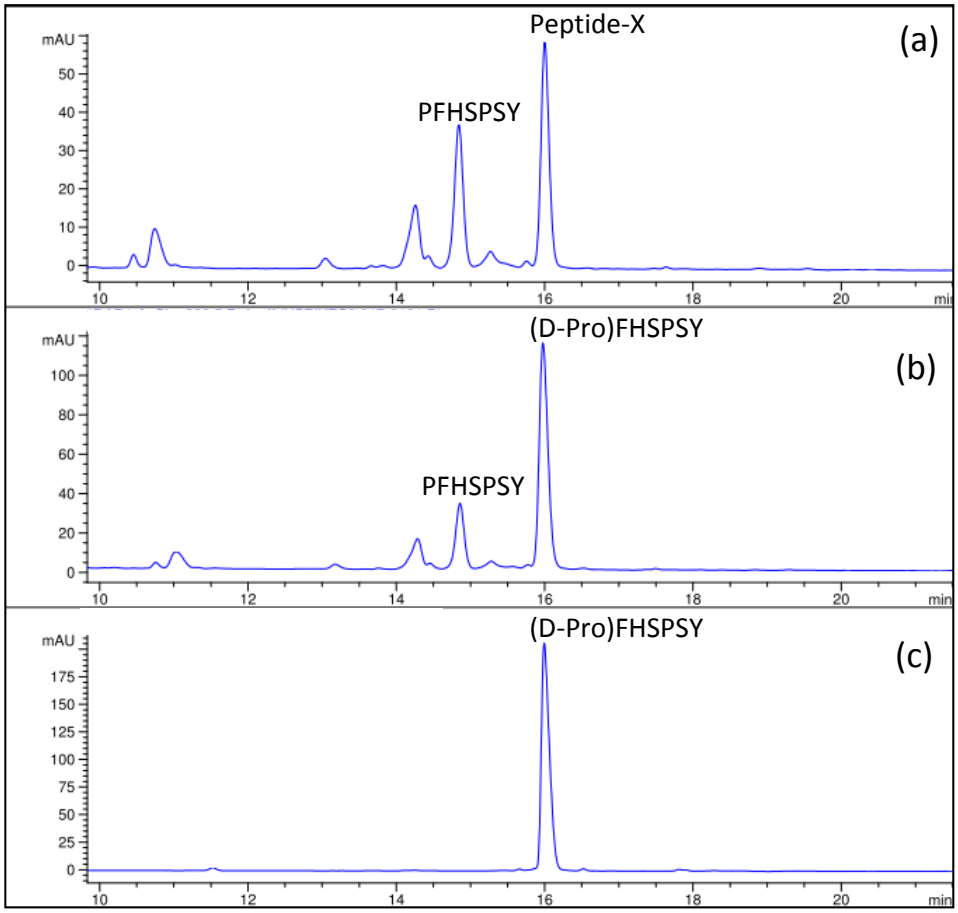

Figure 7-13: HPLC traces(280 nm) of (a) PFHSPSY day-21 time point, (b) the PFHSPSY day-21 time point spiked with (D-Pro)FHSPSY, (c) Standard of (D-Pro)FHSPSY.

NMR comparison of Peptide-X to a standard of (D-Pro)FHSPSY

Figure 7-14 shows a comparison of ^{1}H proton spectra of Peptide-X and (D-Pro)FHSPSY. As can be seen they are essentially identical. The ^{13}C HSQC spectra of both peptides were also overlaid (Figure 7-15) and shown to be identical, thus confirming the assignment of Peptide-X as (D-Pro)FHSPSY.

^{1}H spectrum (9 ppm to 1 ppm

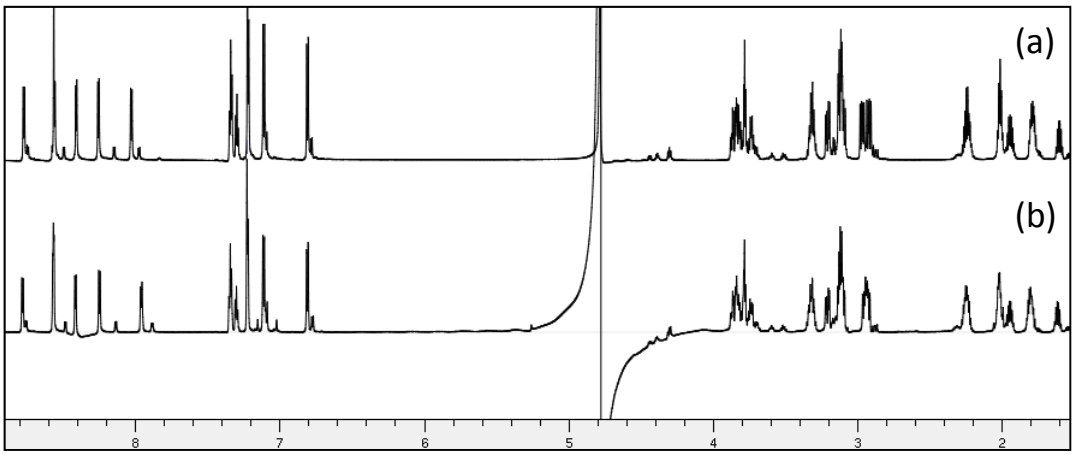

Expanded ^{1}H spectrum (1.5 ppm to 4 ppm)

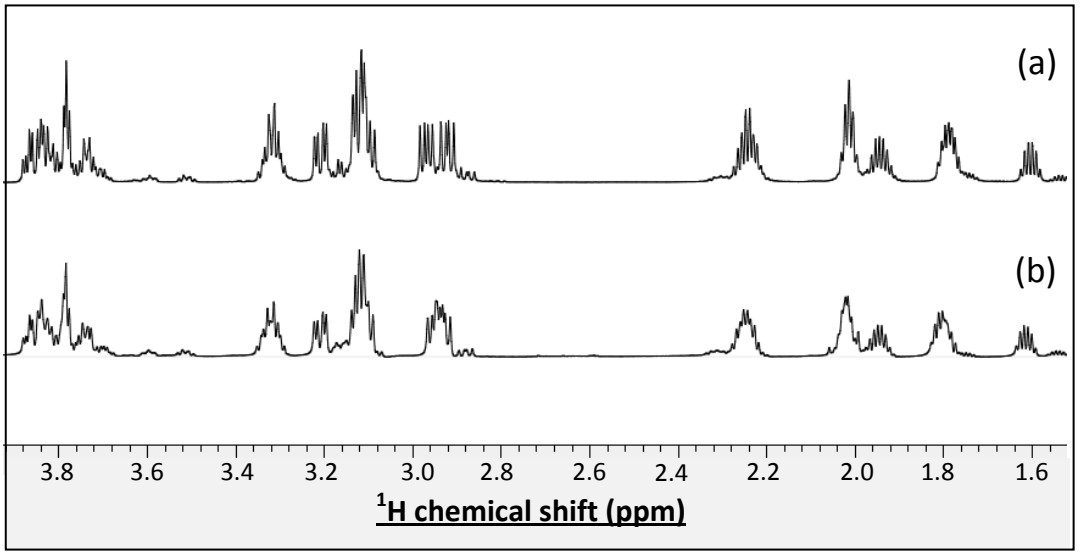

Figure 7-14: ^{1}H NMR spectrum of (a) (D-Pro)FHSPSY standard and (b) Peptide-X. Samples were made up in 50 mM phosphate buffer pH 7.4 containing 1 mM TSS and 10% D_20.

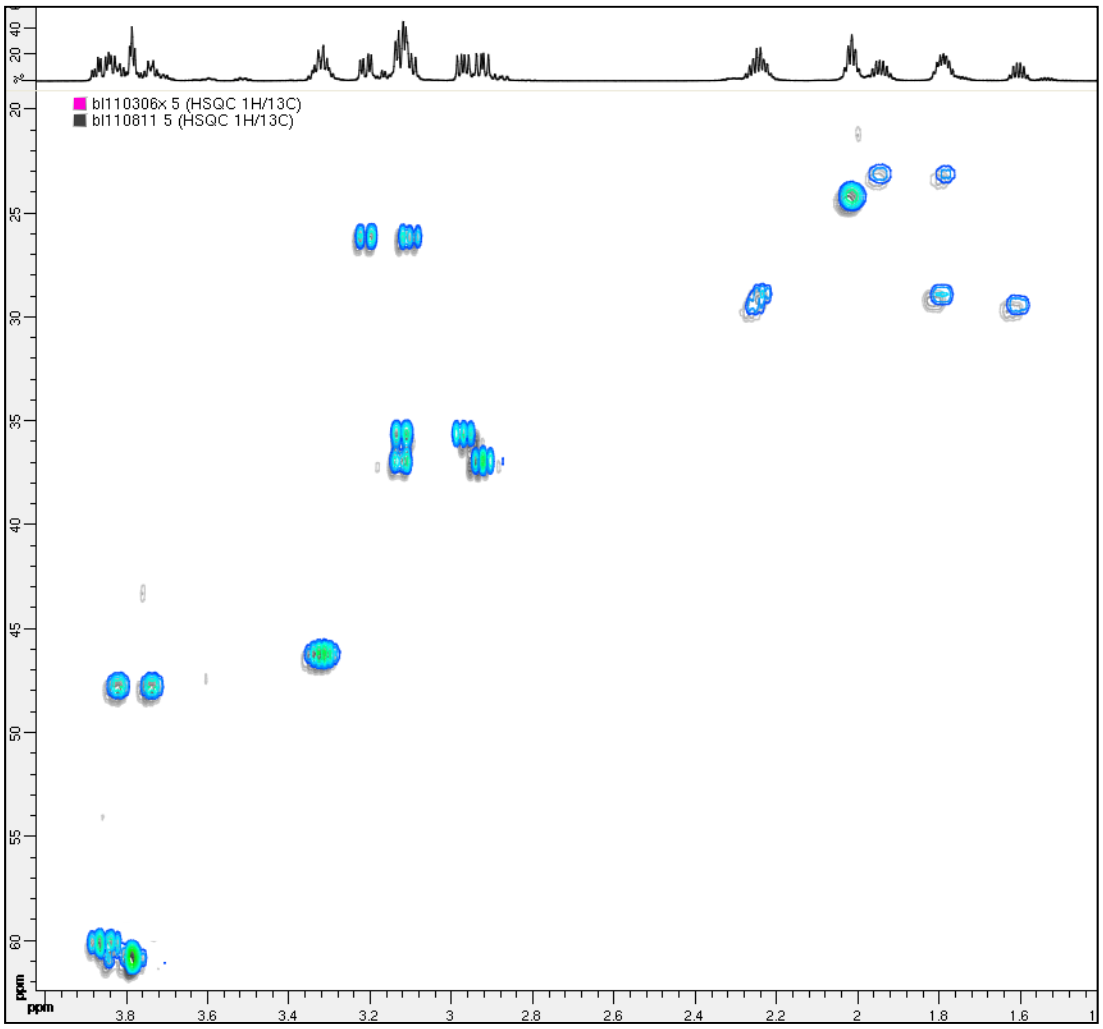

Figure 7-15: Overlay of the partial HSQC spectrum of PFHSPSY (Blue) and Peptide-X (Grey). Samples were made up in 50 mM phosphate buffer pH 7.4 containing 1 mM TSS and 10% D_20.

7.4 Effect of amino acid sequence on N-terminal racemisation (1' Position)

In the aged human lens, truncated crystallin peptides are present that contain a variety of N-terminal residues [84, 85, 126, 128]. As demonstrated in Section 7.3, a crystallin sequence-related peptide containing an N-terminal Pro can be subject to N-terminal racemisation. This section aims to expand on this finding and investigate the potential for other N-terminal residues to racemise. Three peptides (SFHSPS, PFHSPS and AFHSPS) based on αB-crystallin (αB 16-21), but with different N-terminal residues were selected. A C-terminal Tyr was added to each peptide to aid with HPLC UV

detection. An N-terminal Ser was chosen as it has been identified as a major crystallin truncation point, e.g. (αA 1-168, 1-169, 1-172) in aged lens proteins [128, 187]. A peptide containing an N-terminal Ala peptide was included as an example of the smallest amino acid that can racemise. Peptides (SFHSPSY, PFHSPSY and AFHSPSY) were incubated (in triplicate) at 60 °C in 100 mM phosphate buffer pH 7.4 as per Incubation-B (Section 2.2.1).

7.4.1 Results and Discussion

The major degradation products of each peptide were identified using methods similar to those described in Section 7.3. A sample HPLC trace of day-14 showing the formation of (D-Ala)FHSPSY from AFHSPSY is shown in Figure 7-16.

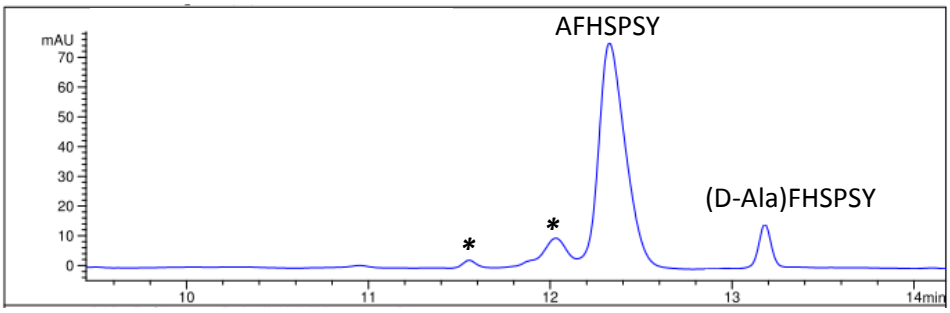

Figure 7-16: HPLC trace (280 nm) of AFHSPSY day-14 time point showing the formation of (D-Ala)FHSPSY following incubation at 60 °C. Degradation *via* other processes are shown with (*). Incubation was carried out in 100 mM phosphate buffer pH 7.4.

Standard curves for each peptide were generated and these were used in combination with the HPLC time point data to calculate the number of moles of each peptide that underwent N-terminal racemisation over time. An example of the standard curve for SFHSPSY is shown in Figure 7-17.

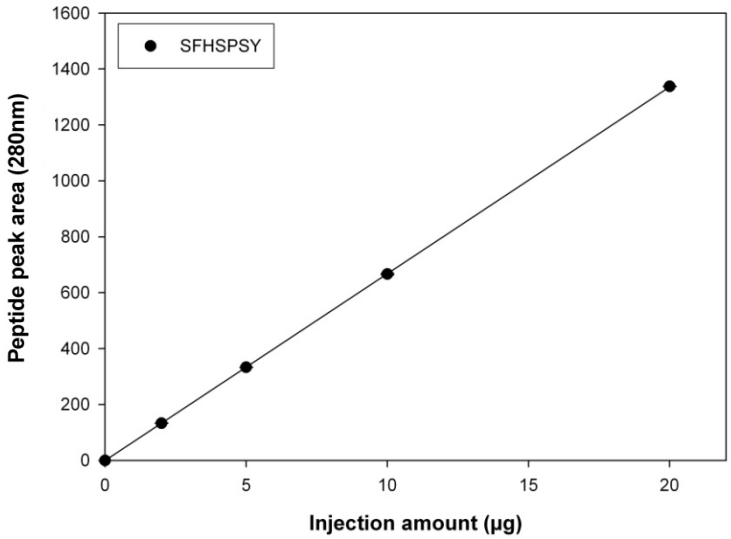

Figure 7-17: An example of a standard curve for SFHSPSY relating peak area at 280 nm to peptide amount (µg) injected onto the HPLC column.

At each time point, the results of triplicates were averaged and the rate of disappearance of the intact peptide and appearance of its N-terminal racemised adduct was plotted (Figure 7-18)

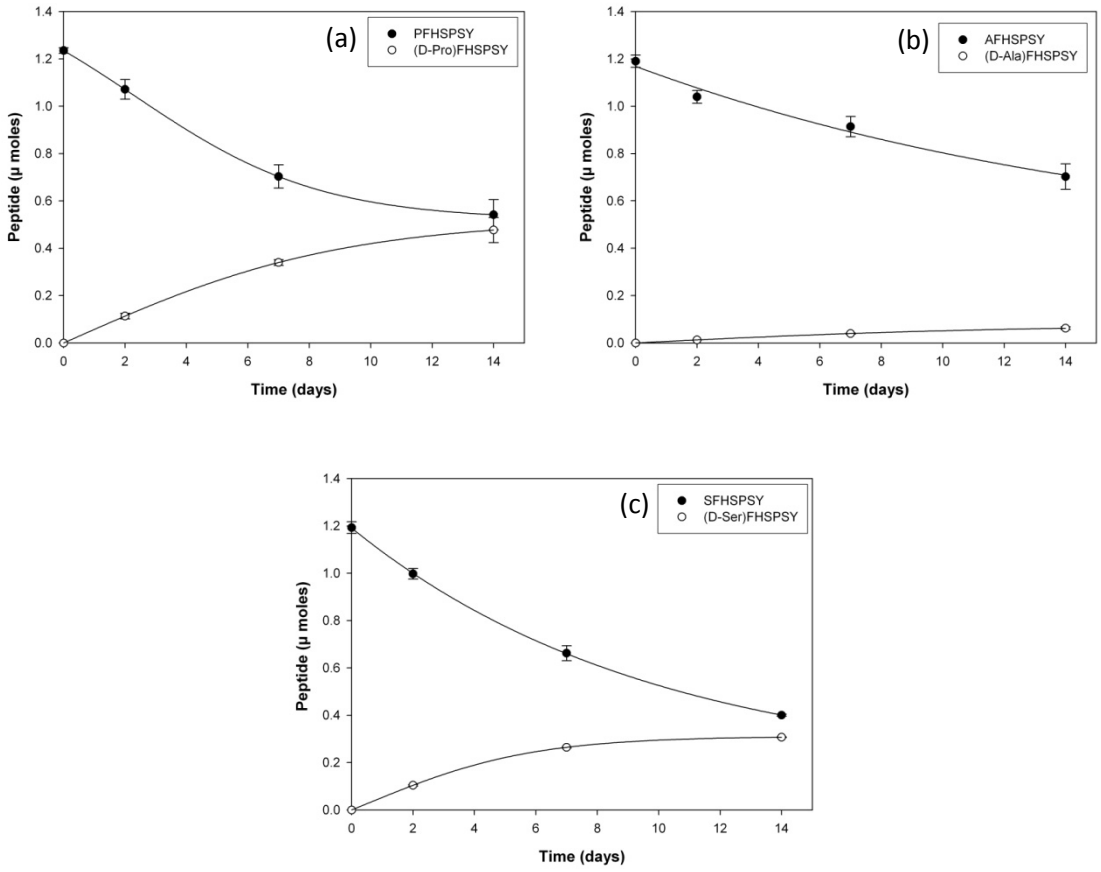

Figure 7-18: Comparison of rate of Pro, Ser and Ala N-terminal racemisation. (a) Loss of PFHSPSY and appearance of (D-Pro)FHSPSY, (b) loss of AFHSPSY and appearance of (D-Ala)FHSPSY and (c) loss of SFHSPSY and appearance of (D-Ser)FHSPSY. Peptides were incubated in 100 mM phosphate buffer pH 7.4 at 60 °C.

A comparison of the percentage conversion of each peptide to its N-terminally racemised form is shown in Figure 7-19. A substantial difference between the rates was observed. After 14 days ~38% of the N-terminal residue of PFHSPSY had racemised, compared to ~25% of the N-terminal residue of SFHSPSY and only ~5% of the N-terminal residue of AFHSPSY peptide.

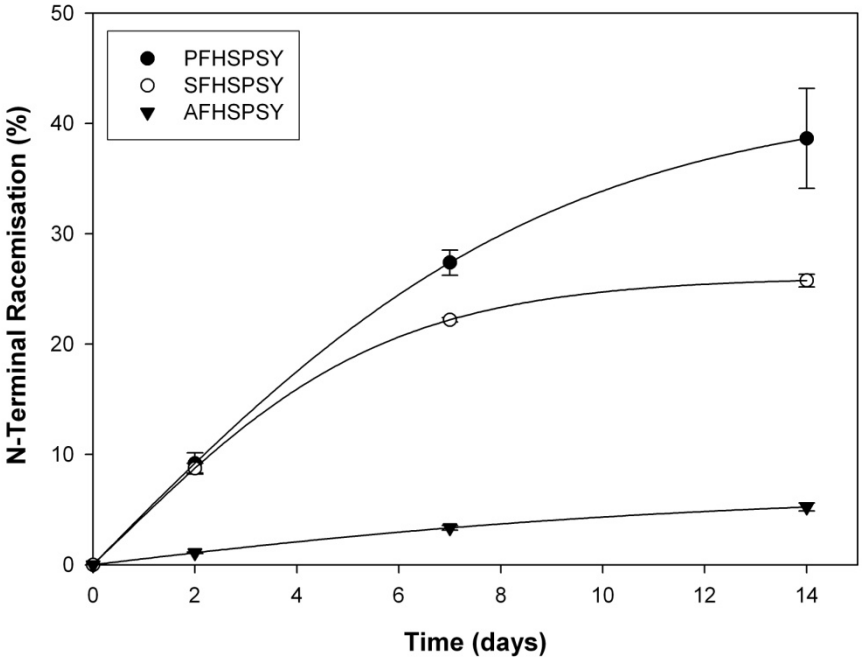

Figure 7-19: Percentage of each peptide (PFHSPSY, SFHSPSY and AFHSPSY) that underwent N-terminal racemisation. Peptides were incubated in 100 mM phosphate buffer pH 7.4 at 60 °C. Percentage values were calculated as the amount (moles) of each peptide which racemised at the N-terminal residue with respect to time compared to the amount of each peptide present at T=0.

These results show that N-terminal racemisation can occur at physiological pH, under relatively mild conditions and that the rate of racemisation varies significantly depending on the N-terminal amino acid residue.

7.5 Effect of amino acid sequence on N-terminal racemisation (2' Position)

To investigate the effect of the penultimate amino acid (denoted as 2') on the rate of N-terminal racemisation, four related peptides (Table 7-1) were examined. In each case only the residue in the 2' position was varied. The peptides (PFHSPSY, PAHSPSY, PEHSPSY and PKHSPSY) were incubated (in triplicate) at 60 °C in 100 mM phosphate buffer pH 7.4 as per Incubation-B (Section 2.2.1).

Table 7-1: Four related peptides with different penultimate residues (underlined).

Peptide	Penultimate residue
P<u>F</u>HSPSY	Aromatic
P<u>A</u>HSPSY	Neutral
P<u>E</u>HSPSY	Acidic
P<u>K</u>HSPSY	Basic

7.5.1 Results and Discussion

In each case the major products were identified using similar methods to those outlined in Section 7.3. A sample HPLC trace of PAHSPSY day-7 time point indicating N-terminal racemisation as the major degradation product is shown in Figure 7-20.

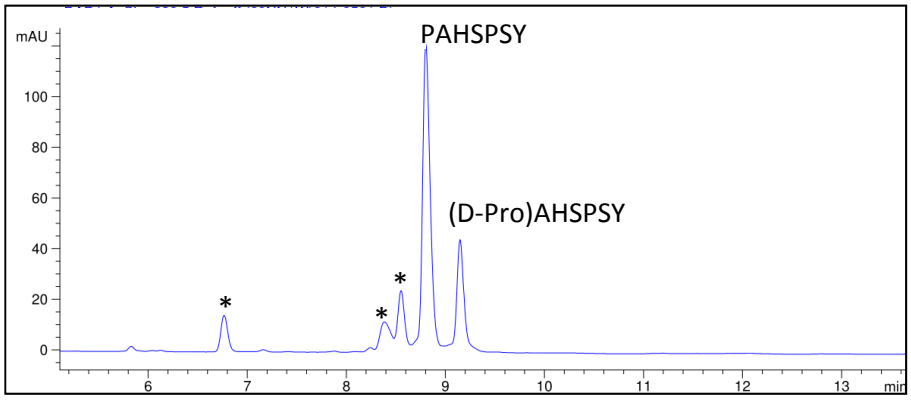

Figure 7-20: HPLC trace (280 nm) of PAHSPSY day-7 time point showing the formation of (D-Pro)AHSPSY following incubation in 100 mM phosphate buffer pH 7.4 at 60 °C. Other peptide products are shown with (*)

Standard curves for each peptide were generated and these were used in combination with the HPLC time point data to calculate the number of moles of each peptide that underwent N-terminal racemisation as a function of time. At each time point the triplicate results were averaged and the rate of disappearance of the original peptide and appearance of its N-terminal racemised product was plotted (Figure 7-21).

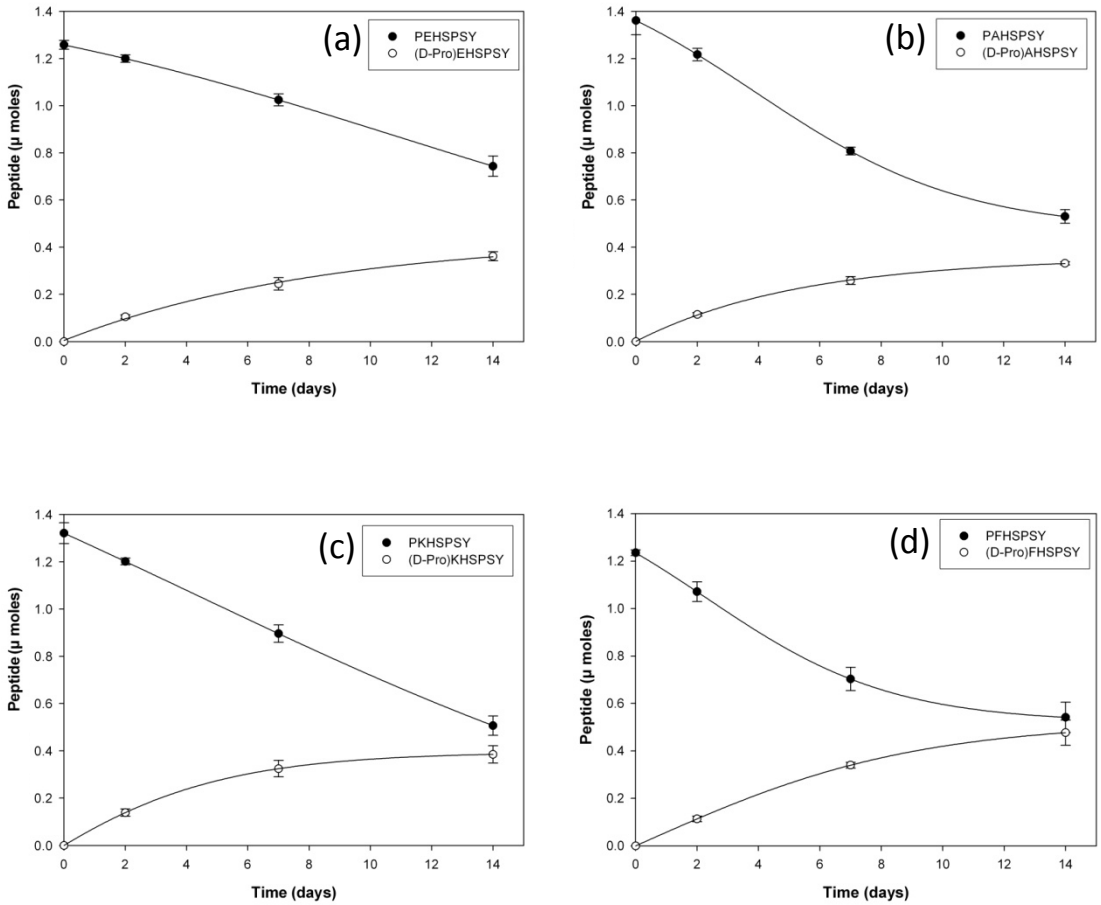

Figure 7-21: Time course of N-terminal racemisation showing (a) Loss of PEHSPSY and appearance of (D-Pro)EHSPSY, (b) loss of PAHSPSY and appearance of (D-Pro)AHSPSY, (c) loss of PKHSPSY and appearance of (D-Pro)KHSPSY and (d) loss of PFHSPSY and appearance of (D-Pro)FHSPSY. Peptides were incubated in 100mM phosphate buffer pH 7.4 at 60 °C

A comparison of the percentage conversion of each peptide to its N-terminally racemised adduct is shown in Figure 7-22. From the data it is apparent that that the penultimate amino acid has an effect on the rate of N-terminal racemisation.

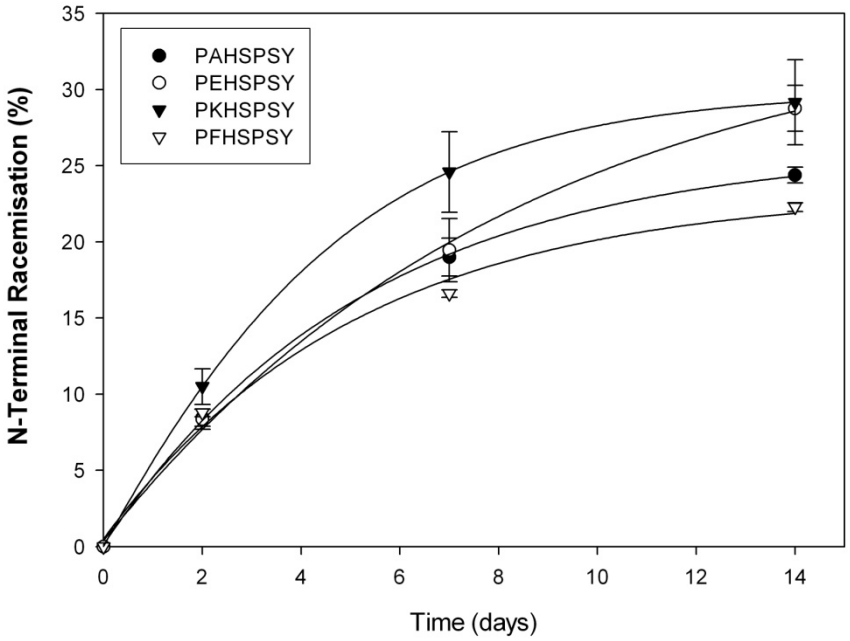

Figure 7-22: Percentage of each peptide (PAHSPSY, PEHSPSY, PKHSPSY and PFHSPSY) that underwent N-terminal racemisation following incubation in 100 mM phosphate buffer pH 7.4 at 60 °C. Percentage values were calculated as the amount (moles) of each peptide which racemised at the N-terminal residue with respect to time compared to the amount of each peptide present at T=0.

7.6 Effect of amino acid sequence on N-terminal racemisation (3' Position)

Up until now all the peptides investigated in Sections 7.3 to 7.5 were based on α-crystallin (16-21) and therefore had a His at the 3' position. It was considered necessary to investigate whether this was having an effect on the N-terminal racemisation rate. PFHSPSY and a control (PF**A**SPSY) were incubated (in triplicate) at 60 °C in 100 mM phosphate buffer pH 7.4 as per Incubation-B (Section 2.2.1).

7.6.1 Results and Discussion

Standard curves were generated and used in combination with the HPLC time point data to plot the rate of racemisation of the N-terminal Pro in each case. At each time point the triplicate results were

averaged and the rate of disappearance of the intact peptide and appearance of its N-terminal racemised adduct was plotted (Figure 7-23).

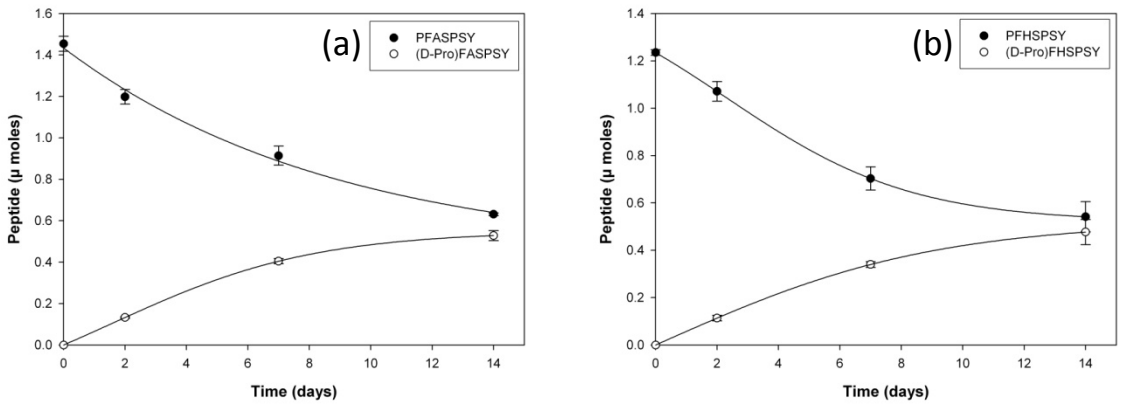

Figure 7-23: Time course of N-terminal racemisation showing (a) loss of PFASPSY and appearance of (D-Pro)FASPSY, and (b) the loss of PFHSPSY and appearance of (D-Pro)FHSPSY. Peptides were incubated in 100 mM phosphate buffer pH 7.4 at 60 °C.

A comparison of the percentage racemisation of the N-terminal Pro residue of each peptide is shown in Figure 7-24. The rate was found to be almost identical for both peptides indicating that at least for this one example having a His at the 3' position does not appear to have a significant effect on the N-terminal racemisation rate and may be ruled out as having a major effect on racemisation of the N-terminal amino acid.

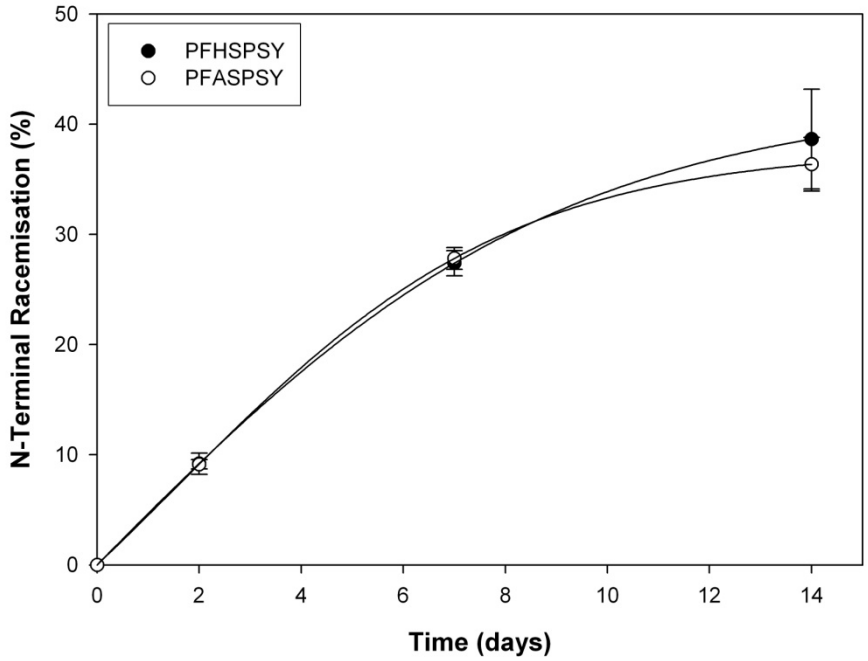

Figure 7-24: Time course of N-terminal racemisation showing the percentage of each peptide (PFHSPSY and PFASPSY) that underwent N-terminal racemisation as a function of time. Peptides were incubated in 100 mM phosphate buffer pH 7.4 at 60 °C. Percentage values were calculated as the amount (moles) of each peptide which racemised at the N-terminal residue with respect to time compared to the amount of each peptide present at T=0.

7.7 The effect of amino acid stereochemistry on the rate of racemisation

In order to investigate the effect of the enantiomeric form of the N-terminal amino acid residue on the rate of N-terminal racemisation, two sets of peptides (Table 7-2), each differing only in the stereochemistry of their N-terminal amino acids were compared. If N-terminal racemisation were being caused by simple loss and re-addition of the α proton then the rate of the forward and back reactions should be similar. The peptides were incubated (in triplicate) at 60 °C in 100 mM phosphate buffer pH 7.4 as per Incubation-B (Section 2.2.1).

Table 7-2: List of two pairs of peptides each differing only by the stereochemistry of their N-terminal residues.

Pair #1	Pair #2
(L-Pro)FHSPSY	(L-Pro)FHS(D-Pro)SY
(D-Pro)FHSPSY	(D-Pro)FHS(D-Pro)SY

7.7.1 Results and Discussion

As can be seen in Figure 7-25 the rate of racemisation of the N-terminal Pro residue in PFHSPSY compared (D-Pro)FHSPSY is significantly different.

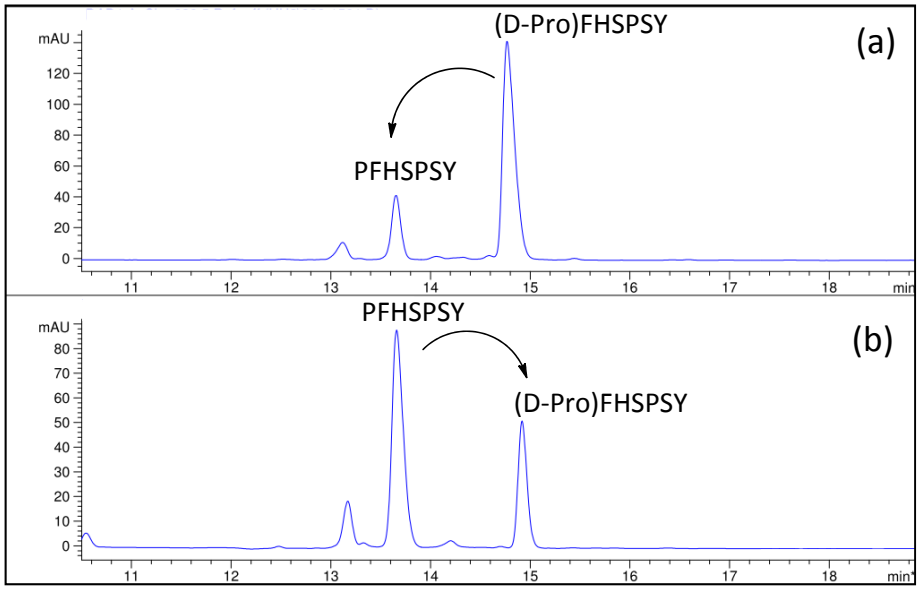

Figure 7-25: HPLC trace (280 nm) of (a) PFHSPSY day-7 time point and (b) (D-Pro)FHSPSY day-7 time point. (Peptide-Y is an additional modification whose characterisation is discussed in Chapter 8).

At each time point the triplicate results were averaged and the rate of disappearance of the intact peptide and appearance of its N-terminal racemised adduct was plotted (Figure 7-26).

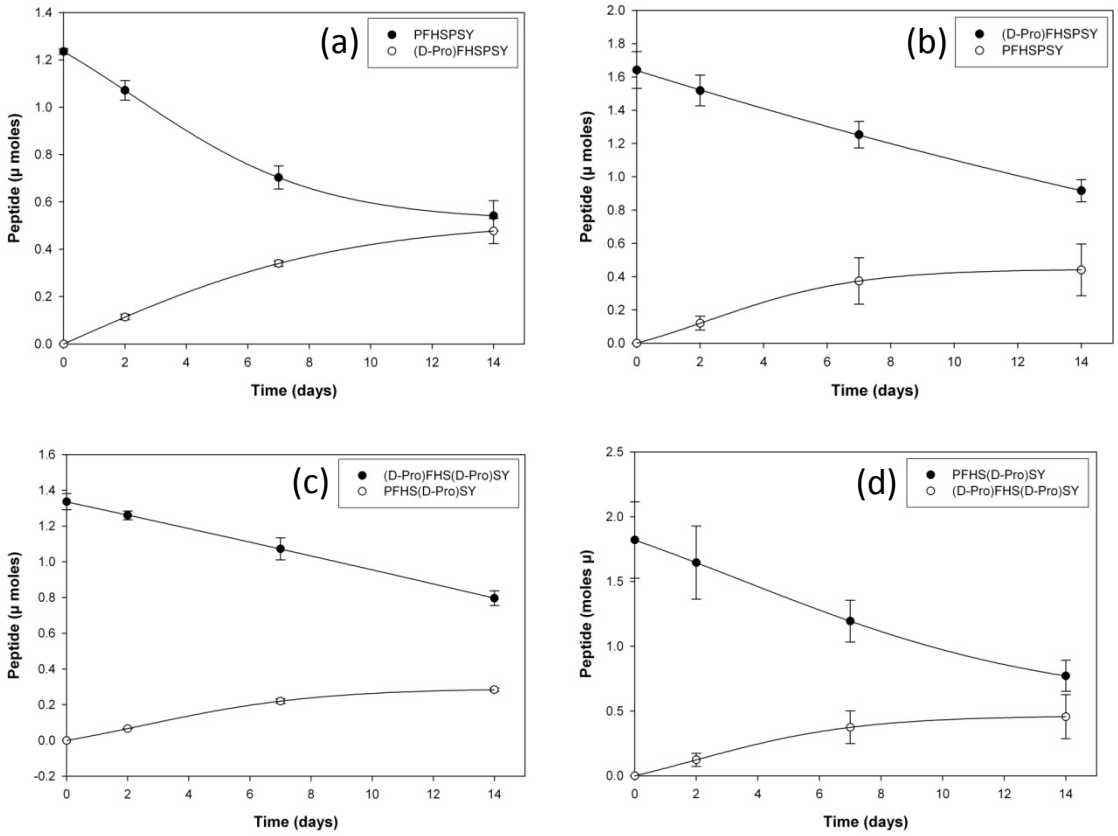

Figure 7-26: Time course of N-terminal racemisation showing (a) loss of PFHSPSY and appearance of (D-Pro)FHSPSY, (b) loss of (D-Pro)FHSPSY and appearance of PFHSPSY, (c) loss of (D-Pro)FHS(D-Pro)SY and appearance of PFHS(D-Pro)SY and (d) loss of PFHS(D-Pro)SY and appearance of (D-Pro)FHS(D-Pro)SY. Peptides were incubated in 100 mM phosphate buffer pH 7.4 at 60 °C.

A comparison of the percentage of each peptide that underwent N-terminal racemisation with respect to time was plotted in Figure 7-27 and Figure 7-28. It is apparent that both the L N-terminal amino acids peptides racemised at a significantly faster rate than the corresponding D N-terminal amino acid peptides. It seems unlikely this difference could be explained if N-terminal racemisation was occurring only *via* the simple loss / re-addition of the alpha proton. A mechanism, whereby the orientation of a D amino acid could make it less susceptible to forming a ring and hence affect the rate of racemisation is more likely and this will be discussed in more detail in Section 7.12.

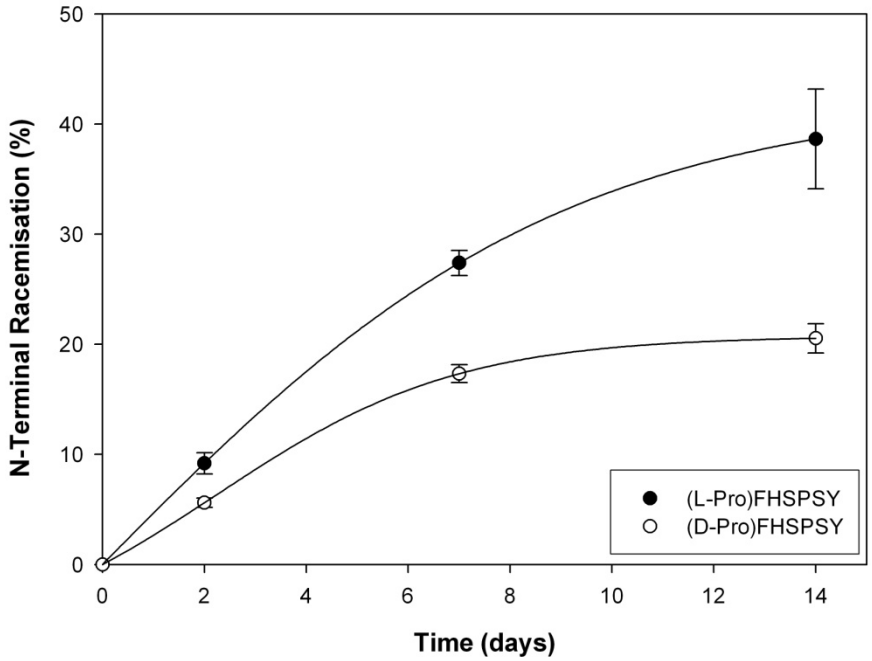

Figure 7-27: Percentage of PFHSPSY and (D-Pro)FHSPSY that underwent N-terminal racemisation. Peptides were incubated in 100 mM phosphate buffer pH 7.4 at 60 °C. Percentage values were calculated as the amount (moles) of each peptide which racemised at the N-terminal residue with respect to time compared to the amount of each peptide present at T=0.

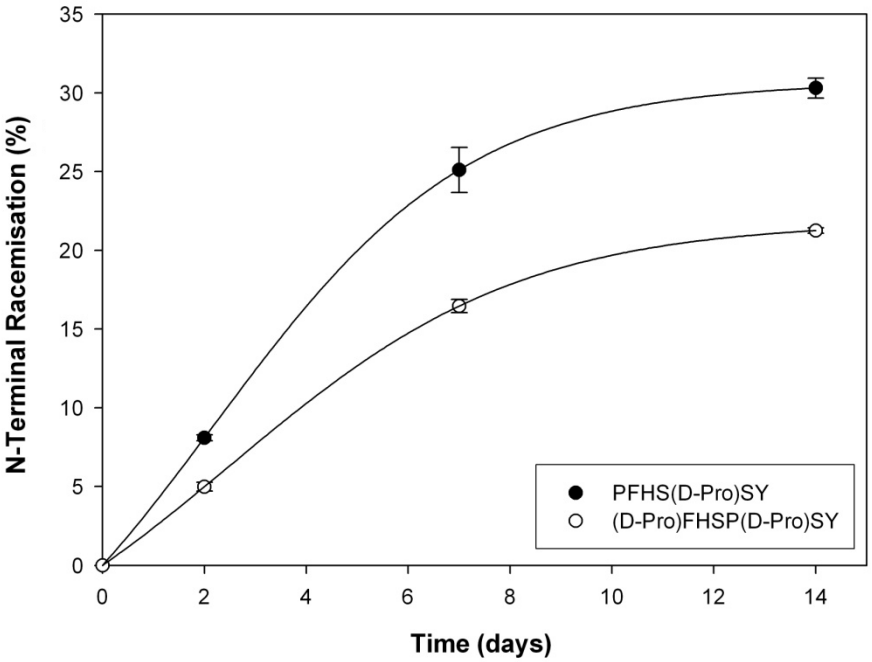

Figure 7-28: Percentage of PFHS(D-Pro)SY and (D-Pro)FHS(D-Pro)SY that underwent N-terminal racemisation. Peptides were incubated in 100 mM phosphate buffer pH 7.4 at 60 °C. Percentage values were calculated as the amount (moles) of each peptide which racemised at the N-terminal residue with respect to time compared to the amount of each peptide present at T=0.

7.8 Effect of buffer on racemisation

To examine the effect of the type of buffer on the rate of N-terminal racemisation, incubations were carried out in other buffers, all 100mM at pH 7.4. In addition to phosphate buffer, the Good's buffers HEPES and TES buffers were employed. Good's buffers are characterised by low nucleophilicity and are generally regarded as being biologically inert [248]. PFHSPSY was incubated (in triplicate) at 60 °C pH 7.4 in each buffer (phosphate, HEPES, TES) as per Incubation-B (Section 2.2.1).

7.8.1 Results and Discussion

As can be seen in Figure 7-29, racemisation of the N-terminal amino acid residue appears to be the major modification in each of the three buffers. This suggests that racemisation of the N-terminal amino acid is not markedly affected by the type of buffer. The rates of racemisation of the N-Terminal Pro residue in each buffer was plotted in Figure 7-30. It shows that the rate of racemisation of the N-terminal is initially relatively similar in all three buffers. However, by day-11 some differences were observed. The rate of N-terminal racemisation in phosphate buffer appears to slow compared to HEPES and TES. This is most likely because the rate of degradation of PFHSPSY *via* other processes is more significant in phosphate buffer and this skews the data. Evidence of this can be seen in Figure 7-29 where the phosphate buffer trace shows more evidence of earlier eluting HPLC peaks than for other buffers. This is discussed in more detail in Chapter 8.

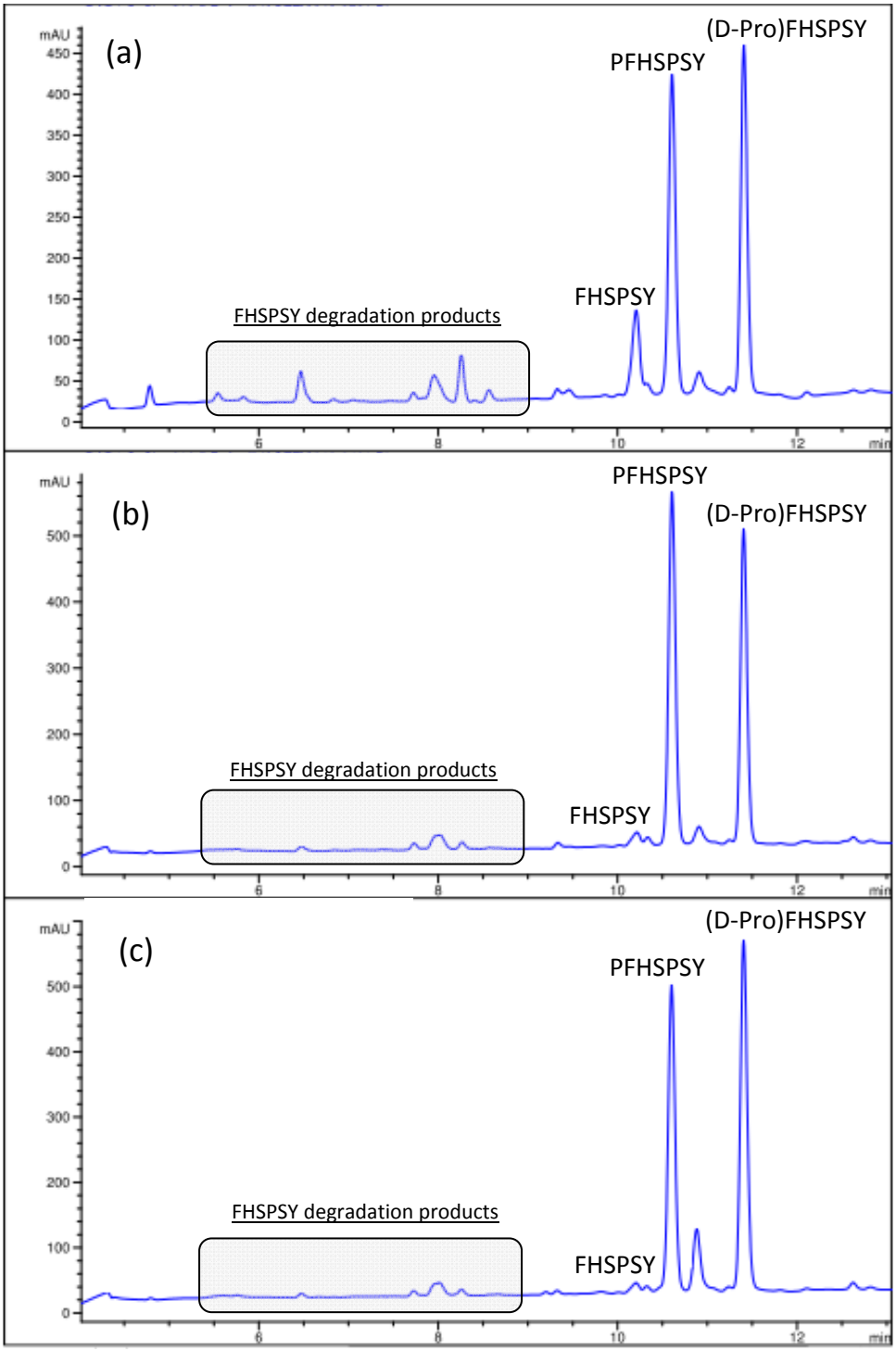

Figure 7-29: HPLC trace (280 nm) of day-11 time points following incubation of PFHSPSY in (a) phosphate buffer, (b) HEPES buffer, and (c) TES buffer at 60 °C. All buffers were 100 mM pH 7.4.

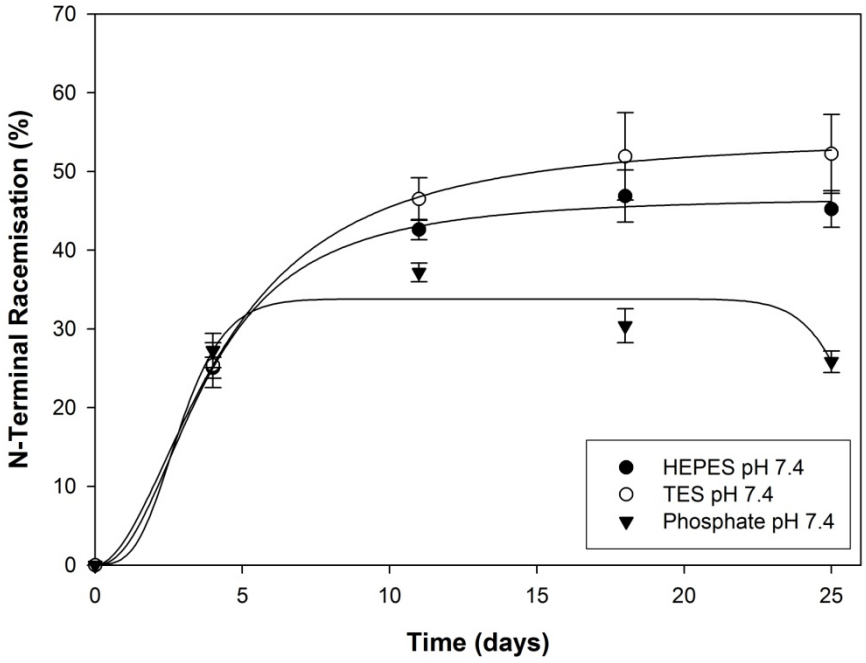

Figure 7-30: Percentage of PFHSPSY that underwent N-terminal racemisation following incubation in (a)100 mM phosphate buffer pH 7.4, (b) 100 mM TES pH 7.4 and (c) 100 mM HEPES pH 7.4 all at 60 °C. Percentage values were calculated as the amount (moles) of each peptide which racemised at the N-terminal residue with respect to time compared to the amount of each peptide present at T=0.

7.9 Effect of pH on N-terminal racemisation

In most cells, protein degradation occurs at an acidic pH in the lysosome. While N-terminal racemisation has been shown in the previous section to occur readily at neutral pH, the aim of this experiment was to investigate the effect of acidic pH on the rate of N-terminal racemisation. This may also give further insight into the mechanism. The peptide PFHSPSY was incubated (in triplicate) at 60 °C in MES buffer pH 5.4, compared to phosphate buffer pH 7.4, and characterised as per Section 2.2.2.

7.9.1 Results and Discussion

A standard curve was generated as detailed in the Materials and Methods Chapter and this was used in combination with the HPLC time point data to calculate the number of moles of each peptide that underwent N-terminal racemisation. At each time point the triplicate results were averaged and the

rate of disappearance of the intact peptide and appearance of its N-terminal racemised adduct was plotted (Figure 7-31).

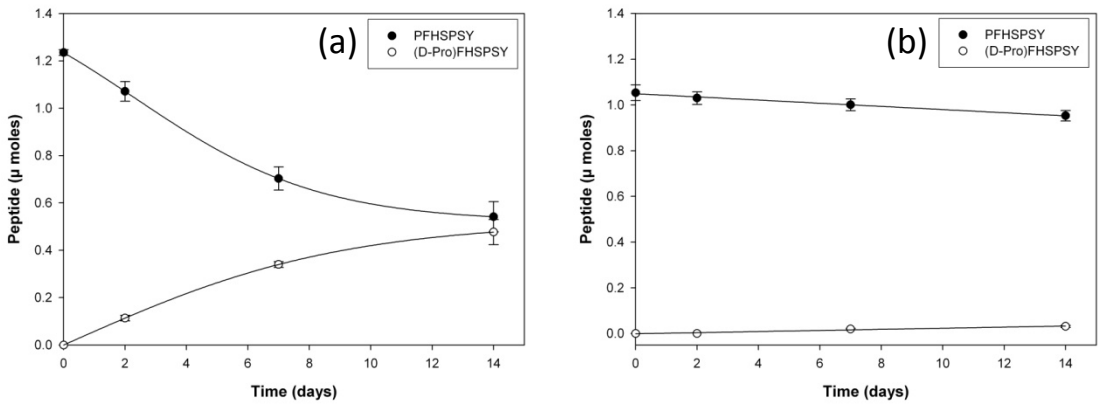

Figure 7-31: Effect of pH. Time course of N-terminal racemisation showing the loss of PFHSPSY and appearance of (D-Pro)FHSPSY following incubation in (a) 100 mM phosphate buffer pH 7.4 and (b) 100 mM MES buffer pH 5.4.

As can be seen in Figure 7-32 while N-terminal racemisation does occur at pH 5.4, the rate is markedly reduced compared to pH 7.4. The implications of this in relation to the potential mechanism of N-terminal racemisation is discussed in Section 7.12.

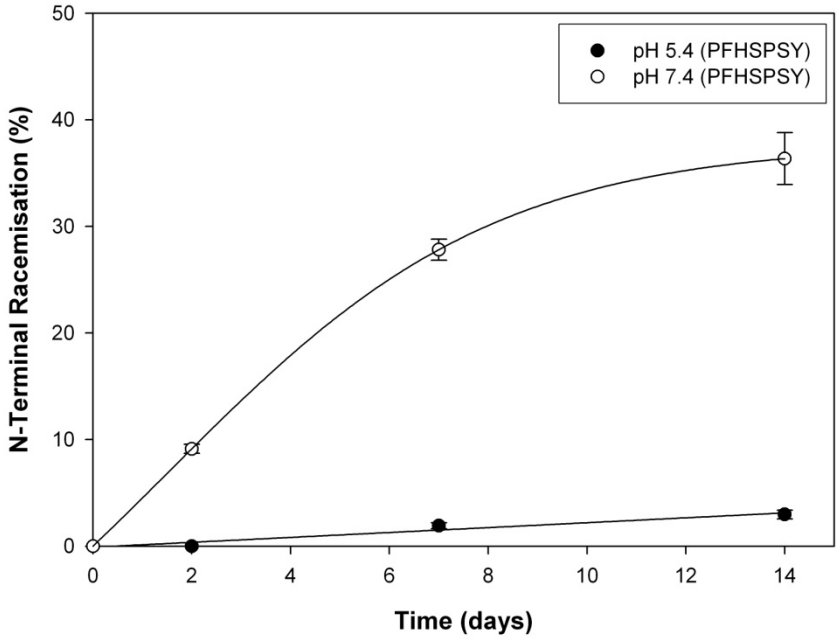

Figure 7-32: Percentage of PFHSPSY that underwent N-terminal racemisation following incubation at (a) pH 7.4 and (b) pH 5.4. Peptides were incubated in 100 mM phosphate buffer (pH 7.4) and 100 mM MES buffer (pH 5.4) at 60 °C. Percentage values were calculated as the amount (moles) of each peptide which racemised at the N-terminal residue with respect to time compared to the amount of each peptide present at T=0.

7.10 Incubation at physiological temperature

As the degradations being modelled in this thesis are proposed to occur over many decades in the lens, the use of elevated temperatures to study these processes was deemed necessary. However it also was considered important to show that these processes can occur at physiologically relevant temperatures. The model peptide PFHSPSY was incubated (in triplicate) at 37 °C in 100 mM phosphate buffer pH 7.4 and characterised as per Incubation-A (Section 2.2.1).

7.10.1 Results and Discussion

A HPLC trace showing the degradation products formed after incubation at 37 °C for 11 weeks is shown in Figure 7-33.

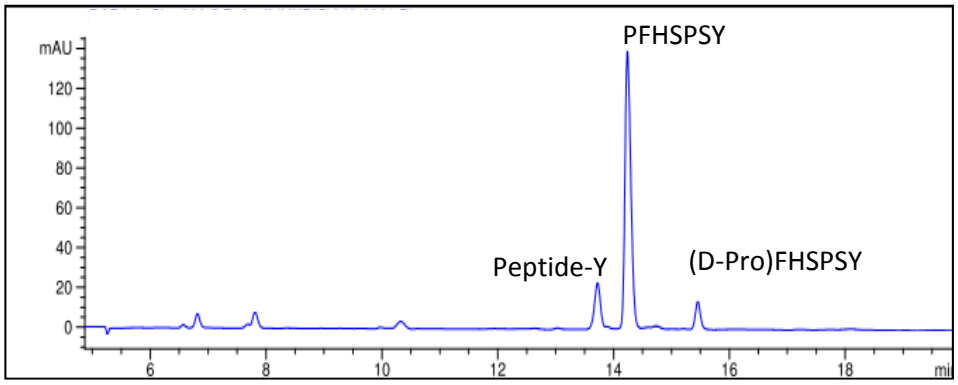

Figure 7-33: Degradation of PFHSPSY at 37 °C. A HPLC trace (280 nm) of the week-11 time point is shown. PFHSPSY was incubated in 100 mM phosphate buffer pH 7.4. Peptide-Y is characterised in Chapter-8.

The percentage of PFHSPSY that was modified *via* racemisation of its N-terminal amino acid residue is shown in Figure 7-34.

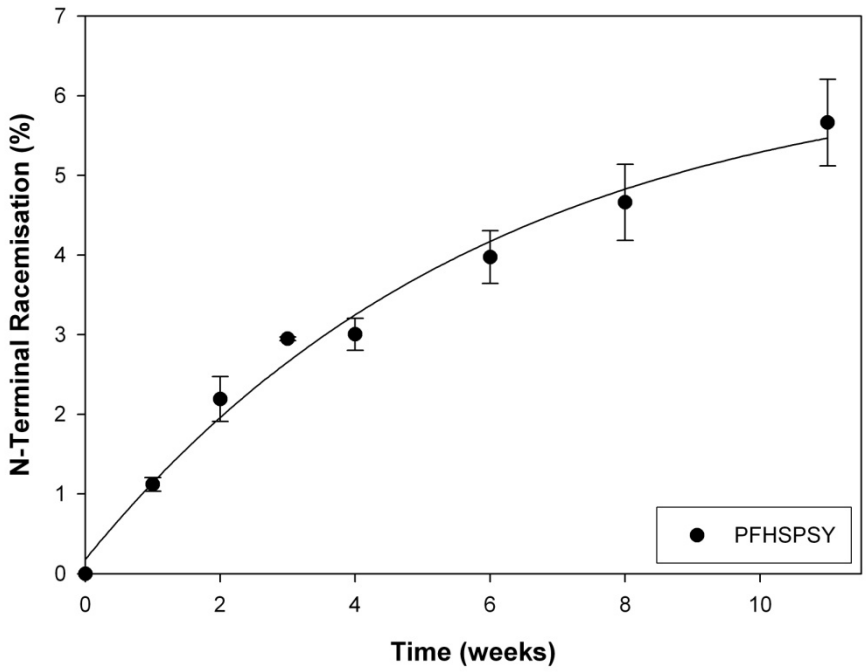

Figure 7-34: Percentage of PFHSPSY that underwent N-terminal racemisation. PFHSPSY was incubated in 100 mM phosphate buffer pH 7.4 at 37 °C. Percentage values were calculated as the amount (moles) of PFHSPSY which racemised at the N-terminal residue with respect to time compared to the amount of PFHSPSY present at T=0.

After 11 weeks at 37 °C, ~5% of PFHSPSY had racemised at the N-terminus forming (D-Pro)FHSPSY. The rate is approximately 20 times slower than at 60 °C. However, based on these results, and given that proteins in the human lens and other tissues exists for decades, it is expected that a significant amount of N-terminal racemisation of proteins with free amino terminal amino acids would occur with age.

7.11 N-terminal racemisation of a human lens protein

Having established that N-terminal racemisation of peptides can occur under physiological conditions, it was of interest to examine a known long-lived protein to determine if racemisation could be observed. Aquaporin 0 (AQP0), an abundant integral membrane protein in the lens [78, 84]

was chosen as a suitable long-lived protein to examine if age-related N-terminal racemisation could be detected. AQP0 has an N-terminal Met residue that is located within the cytosol. The sequence of AQP0 highlighting the N-terminal tryptic peptide is shown diagrammatically in Figure 7-35.

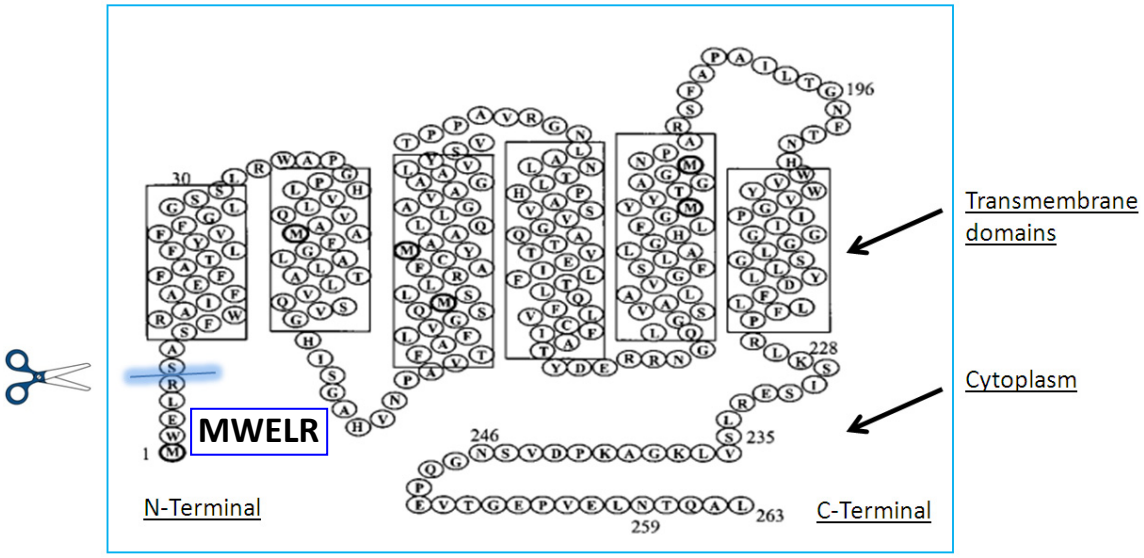

Figure 7-35: Sequence of AQP0. The N-terminal tryptic peptide is highlighted. Adapted from Schey et al. [86].

The aims of this experiment were to:

(1) To determine if a tryptic peptide corresponding to the N-terminus of AQP0 could racemise

(2) To purify AQP0 from an aged human lenses and isolate (L-Met)WELR and (D-Met)WELR (if present) using digestion with trypsin and purification *via* semi-preparative HPLC to determine if age-related N-terminal racemisation occurs in the lens.

N-terminal tryptic peptide of AQP0

The N-terminal peptide expected from the tryptic digestion of AQP0 is MWELR (Figure 7-35). To confirm that racemisation of the N-terminal residue could occur, a synthetic peptide corresponding to this sequence (MWELR) and its D-Met analogue (D-Met)WELR were incubated (in triplicate) at

60 °C in 100mM phosphate buffer pH 7.4 and characterised as per Incubation-B (Section 2.2.1). Cell membranes containing AQPO were then isolated from five human lens pairs (age range 67-69 years) which were dissected into nucleus / cortex regions. These were then digested with trypsin and characterised by ESI MS/MS and MALDI MS/MS mass spectrometry.

Results

Sample HPLC traces (280 nm) of the day-21 time-point from the incubation of MWELR and (D-Met)WELR are shown in Figure 7-36 and Figure 7-37. In each case, racemisation of the N-terminal amino acid residue was the major modification.

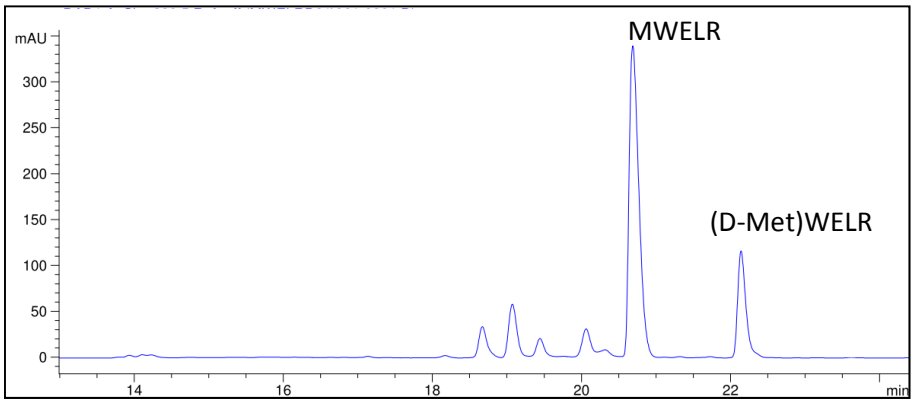

Figure 7-36: Incubation of MWELR at 60 °C. A HPLC trace (280 nm) of the day-21 time point is shown. MWELR was incubated in 100 mM phosphate buffer at pH 7.4.

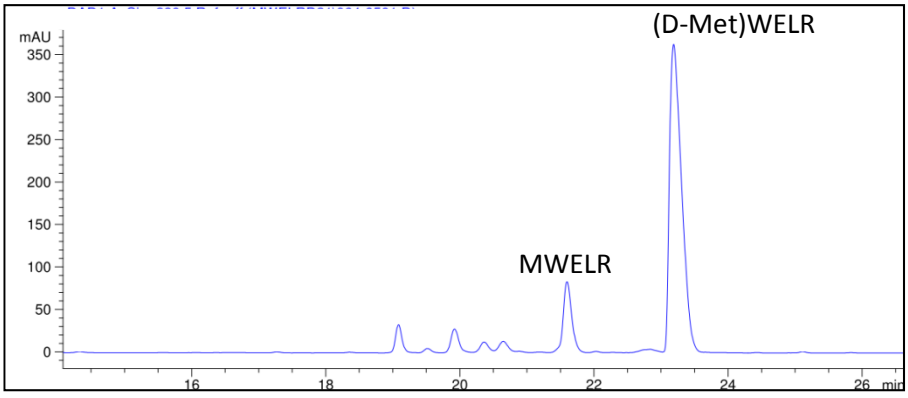

Figure 7-37: Incubation of (D-Met)WELR at 60 °C. A HPLC trace (280 nm) of the day-21 time point is shown. (D-Met)WELR was incubated in 100 mM phosphate buffer at pH 7.4.

Standard curves for each peptide were generated and used in combination with the time course data to calculate the number of moles of each peptide that underwent N-terminal racemisation (Figure 7-37).

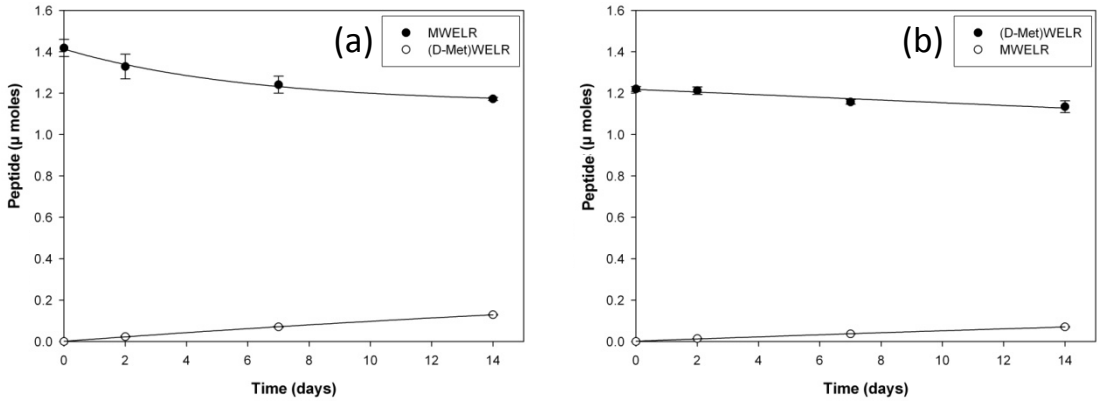

Figure 7-37: The above graphs show the (a) loss of MWELR and appearance of (D-Met)WELR and (b) loss of (D-Met)WELR and appearance of MWELR following incubation in 100 mM phosphate buffer pH 7.4 at 60 °C.

At each time point the triplicate results were averaged. The percentage of each peptide that racemised at the N-terminal residue is shown in Figure 7-38. As per Section 7.7, the L-stereoisomer again racemised faster than the D-stereoisomer.

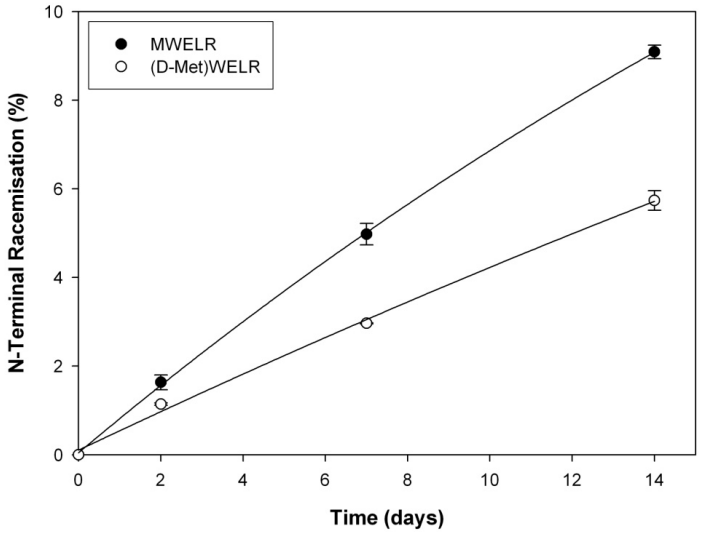

Figure 7-38: Percentage of MWELR and (D-Met)WELR that underwent N-terminal racemisation. Peptides were incubated in 100 mM phosphate buffer pH 7.4 at 60 °C. Percentage values were calculated as the amount (moles) of each peptide which racemised at the N-terminal residue with respect to time compared to the amount of each peptide present at T=0.

Figure 7-39 shows that (D-Met)WELR was also more stable to degradation following exposure to elevated temperature.

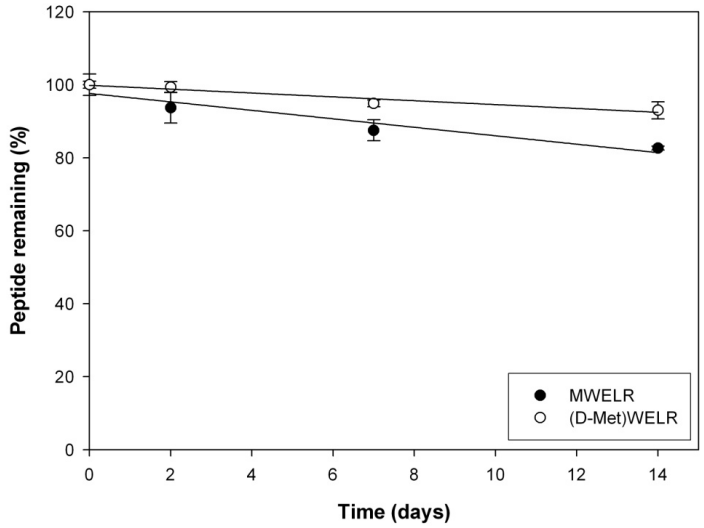

Figure 7-39: Percentage of (L-Met)WELR and (D-Met)WELR remaining with respect to time when, peptides were incubated in 100 mM phosphate buffer pH 7.4 at 60 °C. Percentage values were calculated as the amount (moles) of each peptide remaining with respect to time compared to the amount of each peptide present at T=0.

Following isolation of AQP0 from the human lens samples, digestion with trypsin and purification by semi-preparative HPLC, the following four fractions were obtained:

(1) Cortex MWELR
(2) Cortex (D-Met)WELR
(3) Nucleus MWELR
(4) Nucleus (D-Met)WELR

Analysis by MALDI mass spectrometry revealed each fraction contained an ion of 734 Da, which could correspond to MWELR / (D-Met)WELR. A sample MALDI spectrum of the Nucleus (D-Met)WELR fraction is shown in Figure 7-40.

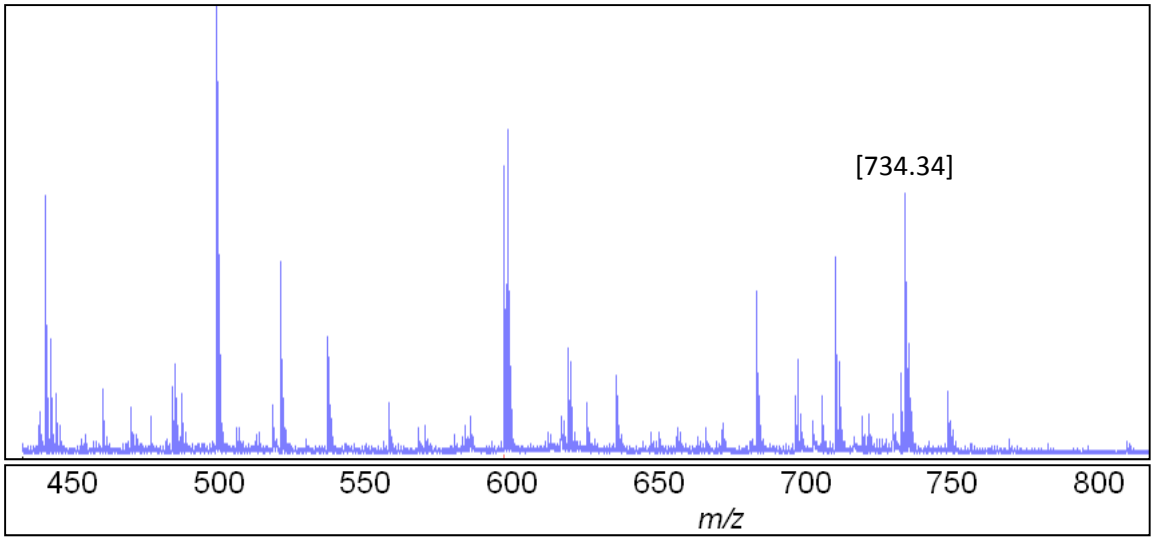

Figure 7-40: MALDI spectrum (D-Met)WELR fraction from the nucleus.

However, the presence of an ion at 734.3 Da is insufficient to prove the existence of the AQP0 N-terminal peptide. For confirmation, each fraction was analysed by MALDI MS/MS and compared to a standard of MWELR. The predicted fragmentation ions of MWELR are detailed in Figure 7-41. An example showing that the MS/MS fragmentation of the Cortex MWELR fraction, the Nucleus (D-Met)WELR fraction and a standard of MWELR are essentially identical is presented in Figure 7-42.

Amino acid	Immonium ion	β ion	β ion – H_20	Y ion	Y-H_20
M	104.05			734.37	716.35
W	159.09	318.13		603.32	585.31
E	102.06	447.17	429.16	417.25	399.23
L	86.10	560.25	542.24	288.2	
R	129.11			175.12	

Figure 7-41: Predicted fragmentation ions of MWELR.

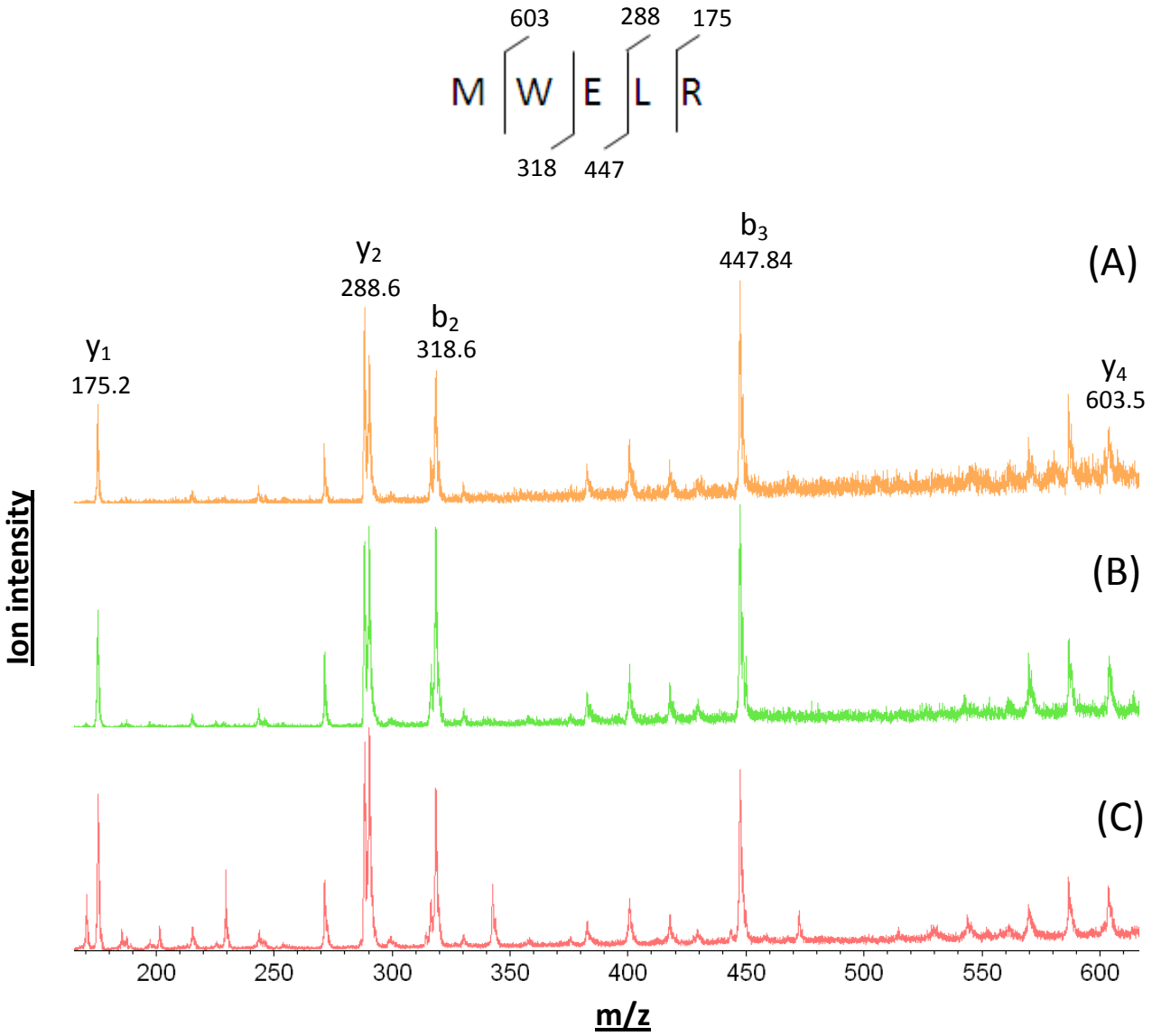

Figure 7-42: MALDI MS/MS spectra of the 734 Da ion from (A) the cortex (L-Met)WELR fraction, (B) the nucleus (D-Met)WELR fraction and (C) a standard of MWELR. Sequence ions are labelled according to Biemann's nomenclature[265]. The immonium ions for each amino acid were also detected (data not shown).

Additional information was also obtained by ESI MS/MS fragmentation of the 4 fractions at the Bioanalytical Mass Spectrometry Facility (BMSF) at the University of New South Wales, followed by positive MASCOT database assignment. An example of the MS/MS fragmentation of (D-Met)WELR from the nuclear fraction is shown in Figure 7-43.

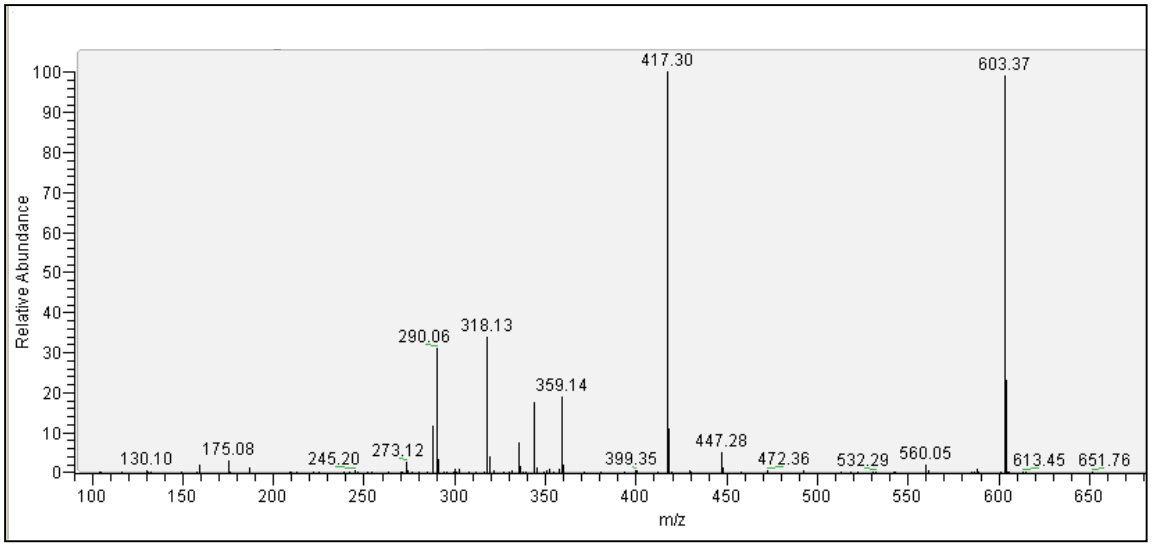

Figure 7-43: ESI MS/MS analysis of (D-Met)WELR from the nucleus. The major ions detected match those seen in the MALDI MS/MS spectrum.

Semi-quantitative analysis of the un-purified tryptic digests by ESI LC-MS/MS, and comparison with standards of MWERL and (D-Met)WELR revealed ~28% of the N-terminal of AQP0 in the nucleus of the lens was found to have racemised by age 68 (Figure 7-44) .Conversely in the cortex, which is the newer part of the lens ~13% was found to have racemised (Table 7-3).

Table 7-3: Relative racemisation of AQP0 in human lens cortex and nucleus. Lenses were aged 68 +/- 1 year.

Sample	MWELR response	D-MWELR response	L/D ratio
Nucleus	7228902	2011073	3.59
Cortex	108698515	14423522	7.54

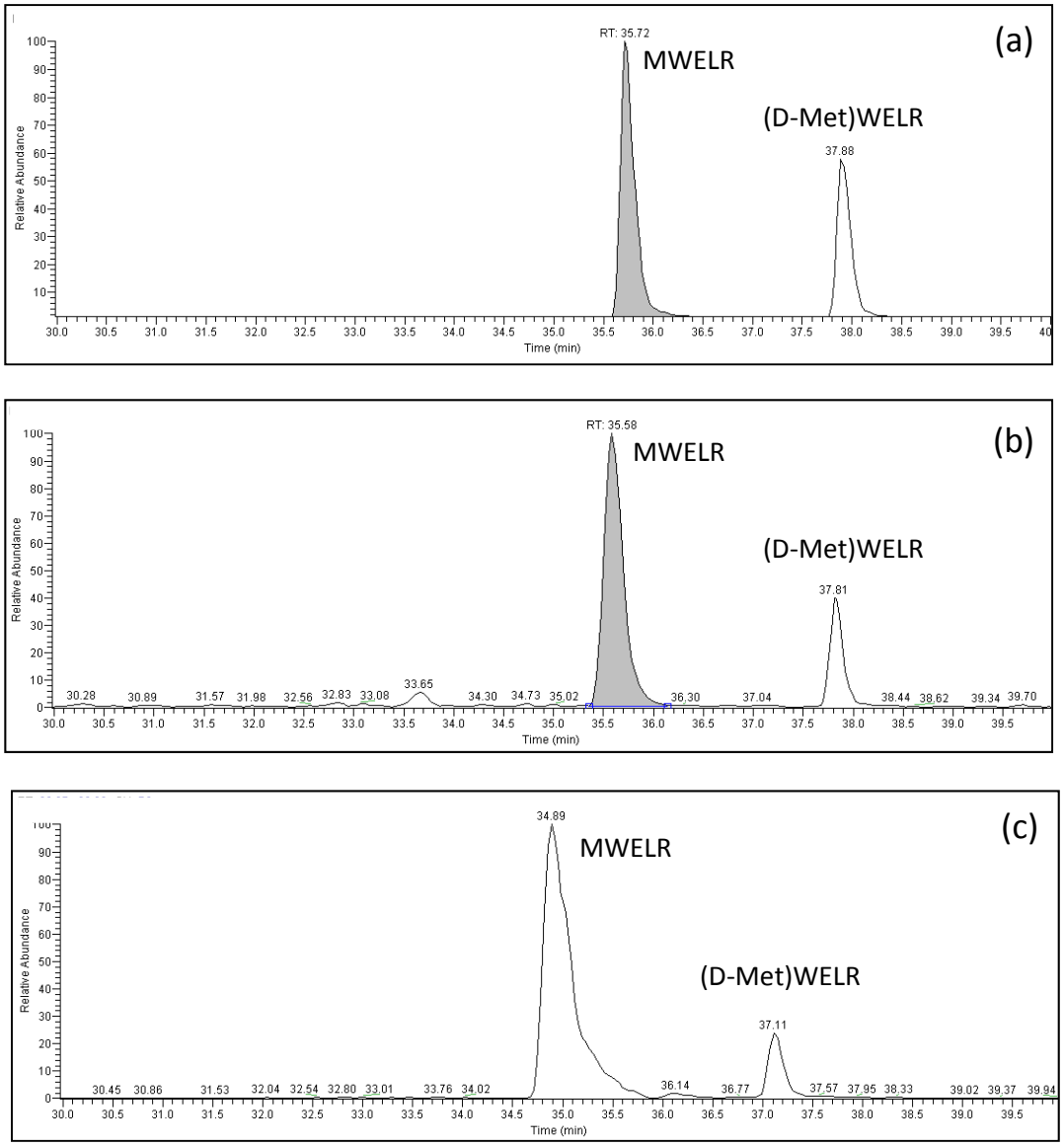

Figure 7-44: SIM [368 M+2H]$^{2+}$ taken from the ESI LC-MS of (a) Mixture of MWELR and (D-Met)WELR synthetic standards, (b) Nucleus fraction, (c) Cortex fraction. Each ion corresponding to MWELR / (D-Met)WELR in the above samples was subjected to MS/MS fragmentation and confirmed to match the fragmentation of the standards.

In terms of susceptibility to enzymatic proteolysis, it is very likely that having a D-amino acid at the N-terminus will inhibit cleavage of a long-lived protein by exopeptidases, since they are generally inactive on the D-isomers [266]. To investigate this, the stability of (L-Met)WELR and (D-Met)WELR to enzymatic degradation by leucine amino peptidase (LAP), a common lens enzyme [267] was examined. Figure 7-45 shows that (D-Met)WELR was resistant to degradation by the enzyme leucine amino peptidase (LAP) where as MWELR was completely degraded.

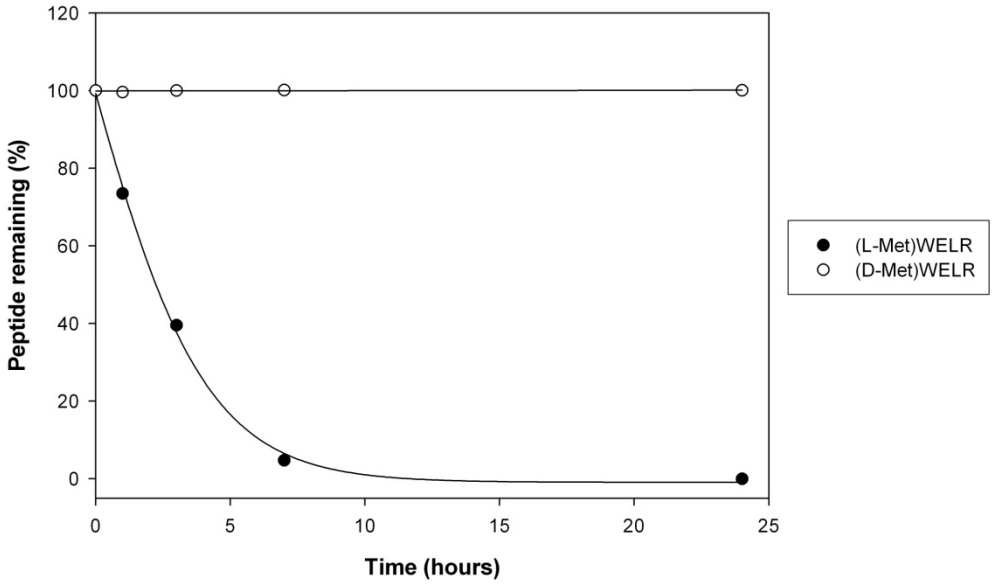

Figure 7-45: Percentage of (L-Met)WELR and (D-Met)WELR remaining with respect to time. Peptides were incubated (1mg/ml) with 1 µg leucine amino peptidase (1:1000, enzyme: substrate) in 100mM Tris buffer pH 8.5 at 30 °C. Percentage values were calculated as the amount (moles) of each peptide remaining with respect to time compared to the amount of each peptide present at T=0.

7.12 Mechanism

In this section an effort was made to propose a mechanism that could explain all of the findings observed in this chapter. Such a mechanism needs to account for the fact that:

(1) The N-terminal and penultimate residues have a significant effect on the rate of racemisation.

(2) L N-Terminal residues racemise faster than their D counterparts.

(3) N-Terminal racemisation rate is slower at pH 5.4.

For these reasons a mechanism involving a cyclic intermediate rather than simple loss / re-addition of the alpha proton of the alpha proton was proposed (

Figure 7-46).

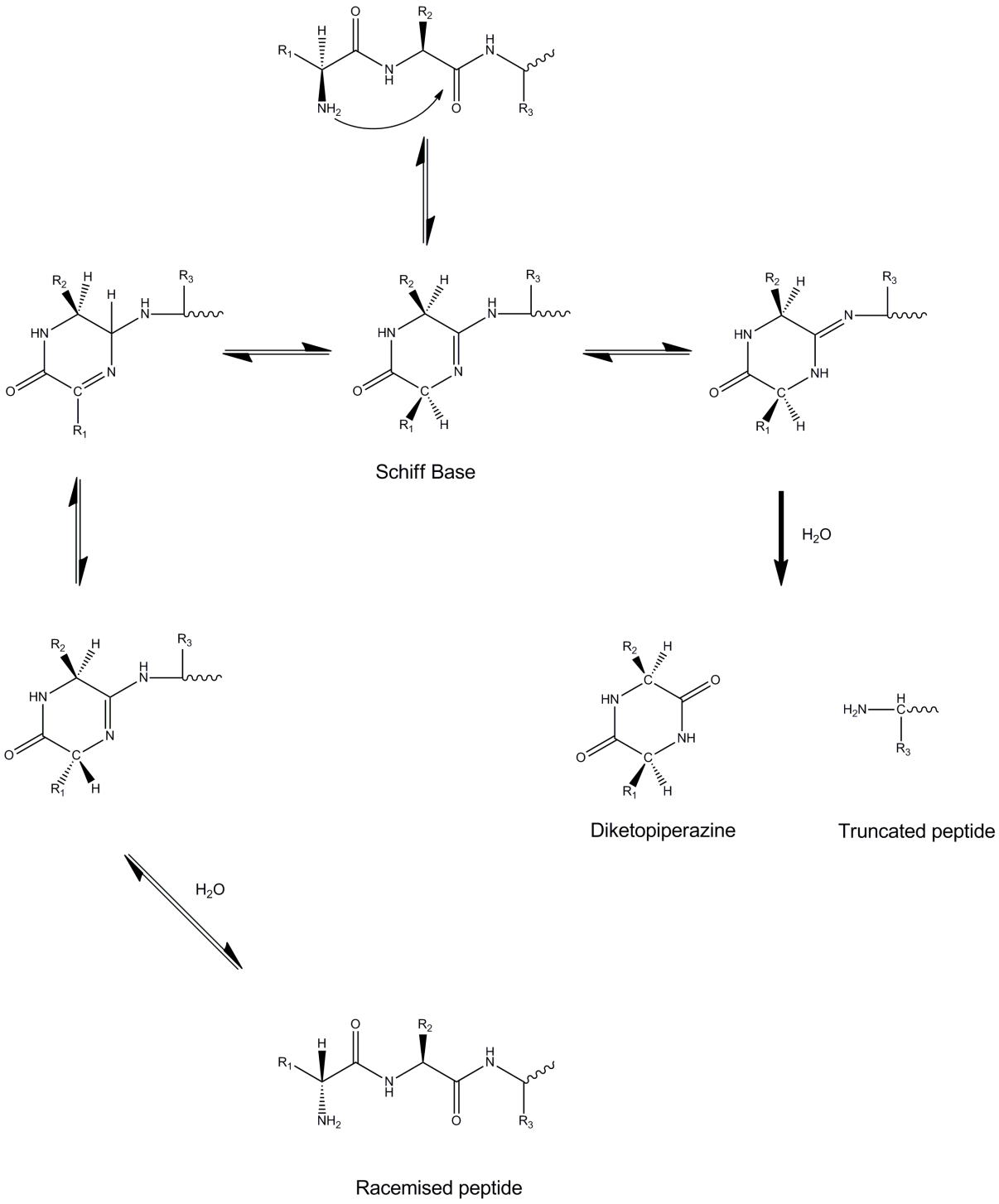

Figure 7-46: Proposed mechanism to explain racemisation of the N-terminal amino acid residue. Also shown is the pathway leading to loss of the N-terminal and penultimate amino acids as a diketopiperazine [249].

To investigate this mechanism, a peptide with a penultimate iso-Asp residue was examined. It is proposed that due to the structure of the iso-Asp residue it be much less likely to form the Schiff base described in Figure 7-47 and as a result should be less susceptible to N-terminal racemisation *via* this process. The reason for this is outlined in Figure 7-47. To test this, PFHSPSY and P(Iso-Asp)HSPSY were incubated (in triplicate) at 60 °C pH 7.4 in 100 mM phosphate buffer and characterised.

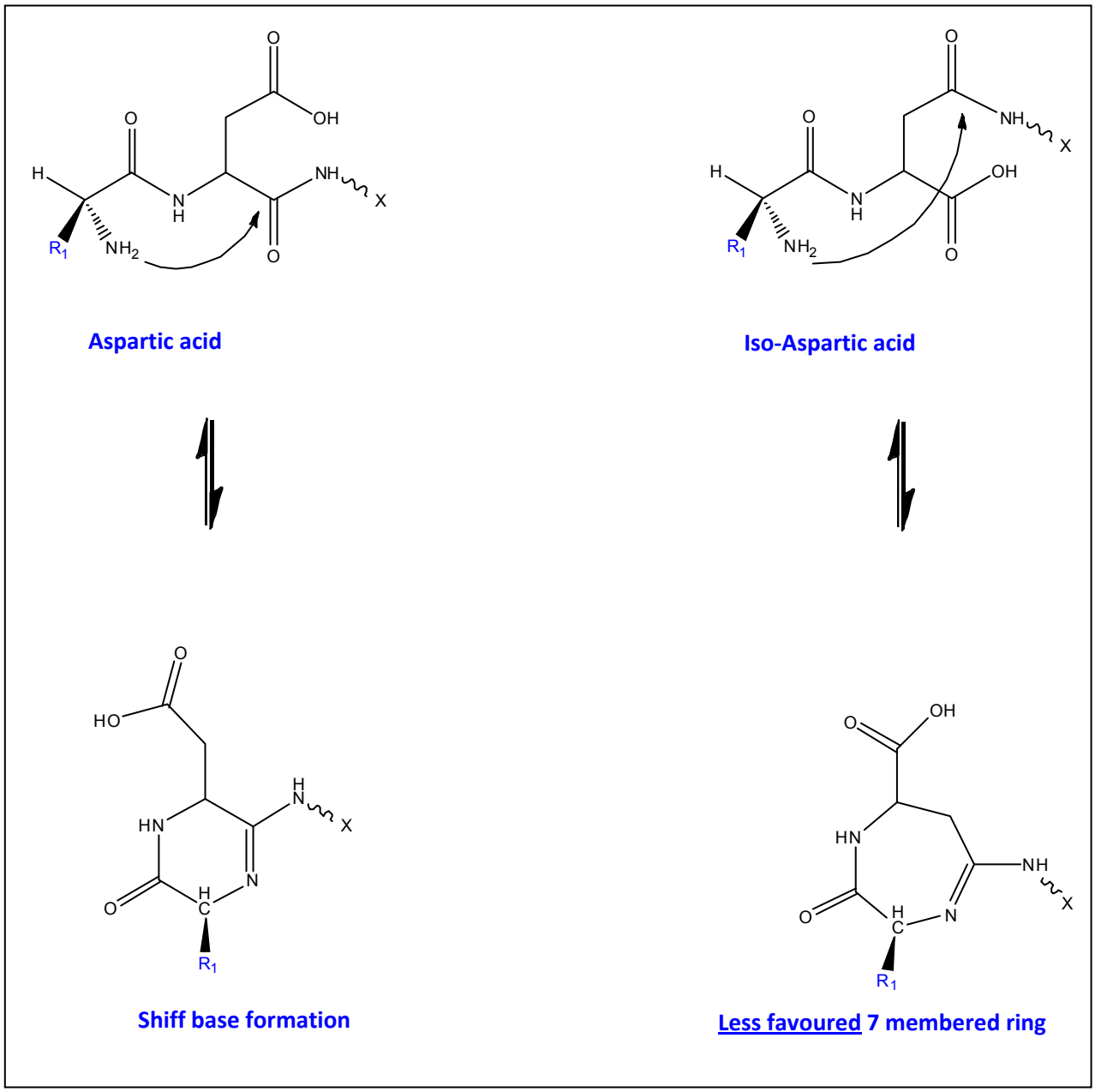

Figure 7-47: Mechanism demonstrating how a penultimate isoAsp would be less likely to participate in a ring mechanism detailed Error! Reference source not found.**, preventing/slowing N-terminal racemisation.**

7.12.1 Results and Discussion

7.12.1 Results and Discussion

As can be seen in Figure 7-48, and in contrast to the incubation of PFHSPSY, there was no evidence of N-terminal racemisation following incubation of P(iso-Asp)HSPSY for 7 days at 60 °C.

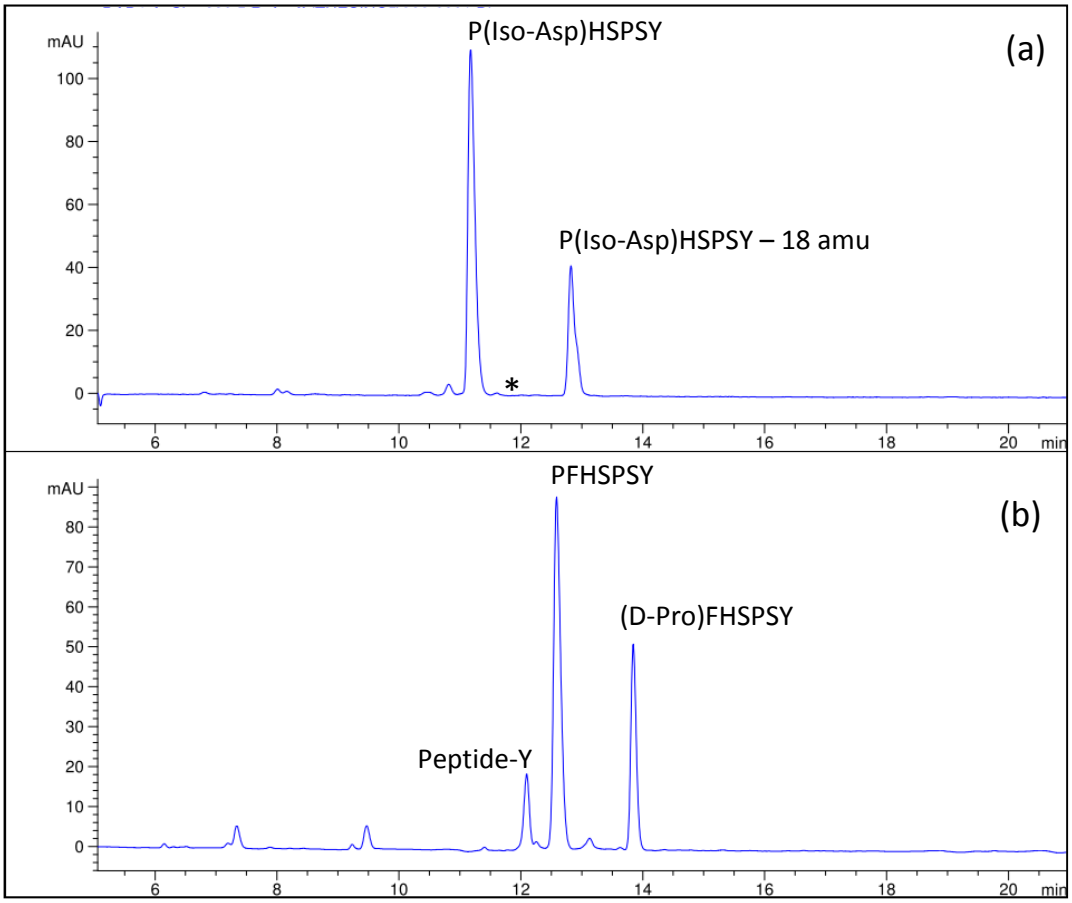

Figure 7-48: HPLC trace (280 nm) showing the degradation products formed following incubation of (a) P(Iso-Asp)HSPSY and (b) PFHSPSY in 100 mM phosphate buffer pH 7.4 at 60 °C for 7 days. The characterisation of Peptide-Y is discussed in Chapter 8. (*) represents the elution time of (D-Pro)(iso-Asp)HSPSY

The major degradation product of P(iso-Asp)HSPSY had a molecular weight of 18 amu less than P(iso-Asp)HSPSY, which may indicate the formation of the ring described in Figure 7-47. Crucially it appears that substituting the penultimate residue with iso-Asp (an amino acid that is less likely to form a ring with the N-terminal residue), has prevented, or at least significantly reduced N-terminal racemisation, strongly supporting the ring mechanism detailed in Figure 7-47 as the cause of N-

terminal racemisation. This is likely the formation of a succinimide type ring but due to time constraints the formation of a -18 Da ring will be investigated in future work.

7.13 Conclusions

This chapter investigated a novel modification where peptides were found to undergo facile racemisation of their N-terminal residues when incubated at physiological pH. It is proposed that many long lived proteins in the human body that have a free amino terminal could be subject to a similar modification. However, most long-lived proteins (e.g. crystallins) in the lens have acetylated N-termini [2] and as a result would not be subject to N-terminal racemisation. Other major lens proteins including the connexins and gamma crystallin have N-terminal Gly meaning they are also not subject to N-terminal racemisation since Gly is the only amino acid that does not exist in D and L forms [268]. However, extensive age-related truncation of lens proteins [126, 127, 196, 197] has been documented and the premise of this chapter is that following truncation, all of the resulting peptide fragments would be also subject to modifications such as N-terminal racemisation.

The results in this chapter suggest that an N-terminal Pro residue is susceptible to age-related racemisation when exposed to physiological conditions. In the case of long-lived proteins, due to the difficulties breaking down both N-terminal Pro residues and D-amino acid residues, this could lead to the accumulation of peptide fragments. It has also been shown in the literature that a substantial amount of crystallin truncation occurs at the N-terminal of Ser [128, 187]. Given the potential for N-terminal Ser residues to racemise at a comparable rate to Pro residues, there is also the potential for build up of peptide fragments with an N-terminal D-Ser residue.

While an exhaustive study was not carried out, it is apparent that amino acid residues in the penultimate position (2') had an effect on the rate of N-terminal racemisation. More importantly, it occur across a range of penultimate residues suggesting that an N-terminal residue prone to racemisation could racemise regardless of its adjoining residue. The role of the amino acid in the 3'

position does not appear be as significant. It was also demonstrated that N-terminal racemisation could occur in a range of buffers commonly used to imitate physiological conditions as well as at physiological temperatures.

Interestingly, there appears to be a clear difference between the rates of N-terminal racemisation of D residues compared to their corresponding L-residue. In all examples studied, the L stereoisomer racemised at a faster rate and this suggests that racemisation may be occurring *via* a more complex mechanism than simple loss and regain of the α proton, which should not be affected by the stereochemistry of the residue. Incubation of a model peptide with an iso-Asp residue in the penultimate position prevented N-terminal racemisation. This supports the theory that N-terminal racemisation is being caused by a ring mechanism. Further studies will be required to confirm this. A ring mechanism similar to that observed but by Sepetov et al [250], but involving the formation of a Schiff base, has been proposed. Racemisation of N-terminal residues has previously been described in the literature [250] and proposed to occur *via* the mechanism in Figure 7-49.

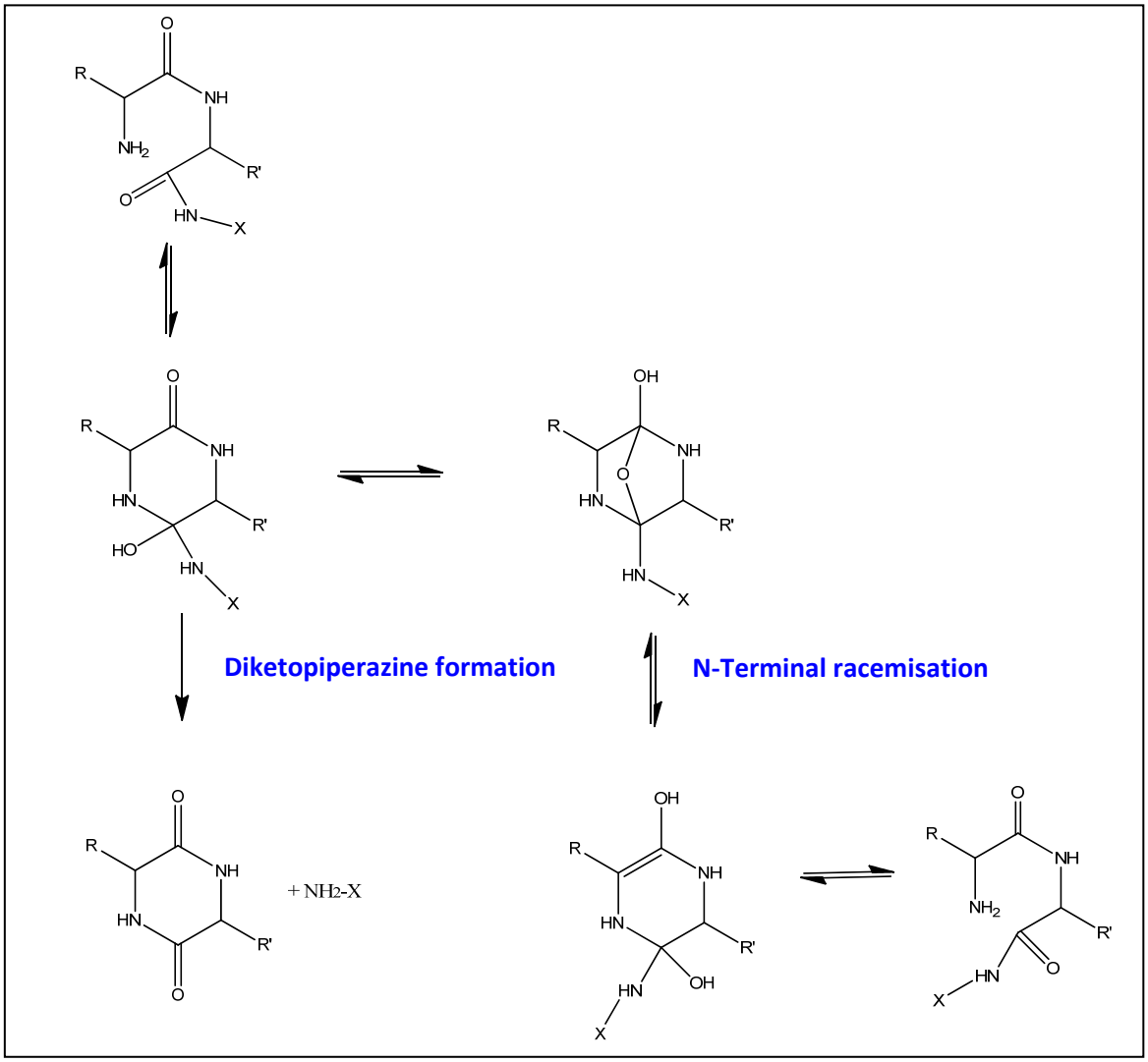

Figure 7-49: Mechanism for N-terminal racemisation proposed by Sepetov et al [246]. R^1 and R^2 = side chains of 1st and 2nd residues. X = rest of peptide.

In this mechanism, the tetrahedral intermediate, which contains a secondary amino group derived from the amide bond between the second and third amino acid residue, can potentially form a bicyclic structure by transannular attack of the newly formed hydroxyl group on the carbonyl group in the diketopiperazine like ring which could also lead to racemisation of the N-terminal residue. Previous studies have also shown that N-terminal residues are known to racemise faster due to the free amino group stabilising the carbanion [269, 270].

To investigate if N-terminal racemisation was occurring in the aged lens, the membrane protein AQP0 was examined. Evidence of N-terminal racemisation was found in both the cortex and the

nucleus of the lens. To our knowledge, this represents the first example of age-related N-terminal racemisation in the lens. The amount of N-terminal racemisation was quantified and revealed that in the nucleus, ~28% of AQP0 had undergone racemisation. Conversely only 13% of the cortex (which is the newer part of the lens) was found to have racemised. While the full consequences of this remain to be understood initial studies suggest that it may have a stabilising effect on the protein reducing its susceptibility to enzymatic and chemical degradation.

The exact consequences for proteins with D N-terminal amino acids remains to be seen, but it is known that enzymes by their nature are substrate-specific. Studies have shown that substitution of an L- amino acid with a D- amino acid in the substrate results in increased peptide stability due to resistance to enzymatic degradation [271-273]. Specific enzymes are also required to degrade peptides containing D-amino acid residues [271, 274]. In the lens, protein degradation is carried out by two major proteolytic systems, the proteasome and the lysosome [275]. Proteasomes are located in both the nucleus and the cytoplasm and their main function is to degrade unneeded or damaged proteins by proteolysis [276]. Lysosomes are a single membrane compartment containing hydrolases that perform a similar function but with enzymes optimised for an acidic pH [208].

These proteolytic enzymes can be broadly classified based on their mechanism of degradation. Endopeptidases cleave internal peptide bonds, whereas exopeptidases cleave terminal residues. An aminopeptidase is an exopeptidase that catalyses the stepwise cleavage of a single amino acid from the amino terminus of a peptide. Due to its unique structure and imide peptide bond, Pro residues are often resistant to the action of peptidases and specific Pro peptidases are required [277]. These Pro peptidases are restricted in their action in that the Pro residue must exist in a particular position in the peptide substrate before hydrolysis will take place. For example, proline iminopeptidase, requires a Pro residue at the N-terminus of a peptide while aminopeptidase P requires a Pro residue in the N-terminal penultimate position [277-279].

8 Chapter 8: Truncation at the N-Terminus

8.1 Introduction

This chapter investigated another unexpected degradation that was observed when peptides were incubated in Chapter-4. The major degradation product formed following incubation of PFHSPSY in 100 mM phosphate buffer pH 7.4 at 60 °C was N-terminally racemised (D-Pro) FHSPSY. Another degradation product of that incubation (Peptide-Y) which was not discussed in Chapter 7 was truncation of the *N*-terminal Pro residue (Figure 8-1). This chapter describes the characterisation of this modification and investigated if the loss of N-terminal Pro is a unique degradation, or if other amino acid residues could be subject to a similar truncation. Some factors were also investigated to see if *N*-terminal truncation could potentially occur in the aged human lens.

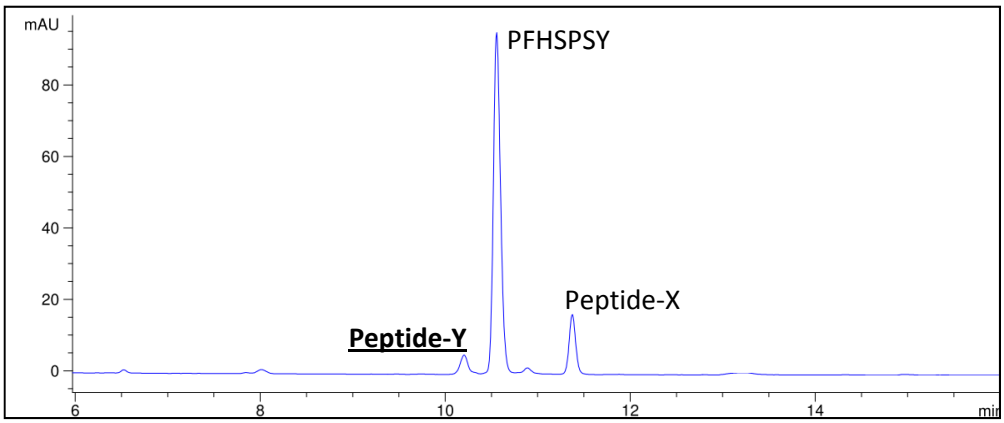

Figure 8-1: HPLC trace (280 nm) showing the formation of Peptide-Y following incubation of PFHSPSY at 60 °C. Peptide was incubated in 100 mM Phosphate buffer pH 7.4 (1 mg/ml) for 3 days.

8.2 Aim

The aim of this chapter was to examine factors which lead to truncation of a peptide at the N-terminal.

8.3 Characterisation of N-terminal truncation

PFHSPSY was incubated (in triplicate) in 100 mM phosphate buffer pH 7.4 at 60 °C and characterised as per Incubation-B (Section 2.2.1).

8.3.1 Results and Discussion

Figure 8-2 shows that two of the major products of PFHSPSY, after incubation at 60 °C, were resolved by semi-preparative HPLC.

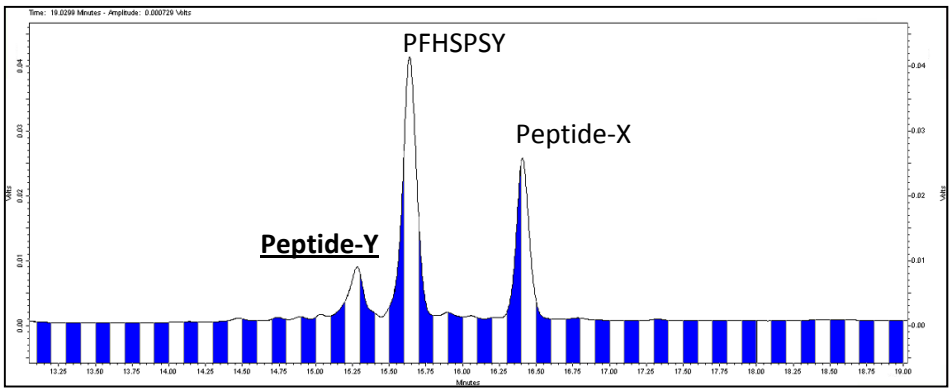

Figure 8-2: Semi preparative HPLC trace (280 nm) showing purification of Peptide-Y formed from incubation of PFHSPSY. PFHSPSY was incubated in 100 mM phosphate buffer pH 7.4 for 3 weeks at 60 °C. The alternating colours indicate the fractions which were collected.

Peptide-X was characterised and discussed in Section 7.2. Analysis of Peptide-Y by MALDI mass spectrometry (Figure 8-3) revealed a molecular ion $[M+H]^{1+}$ of 737 Da which corresponds with the molecular weight of FHSPSY suggesting the loss of the N-terminal Pro residue.

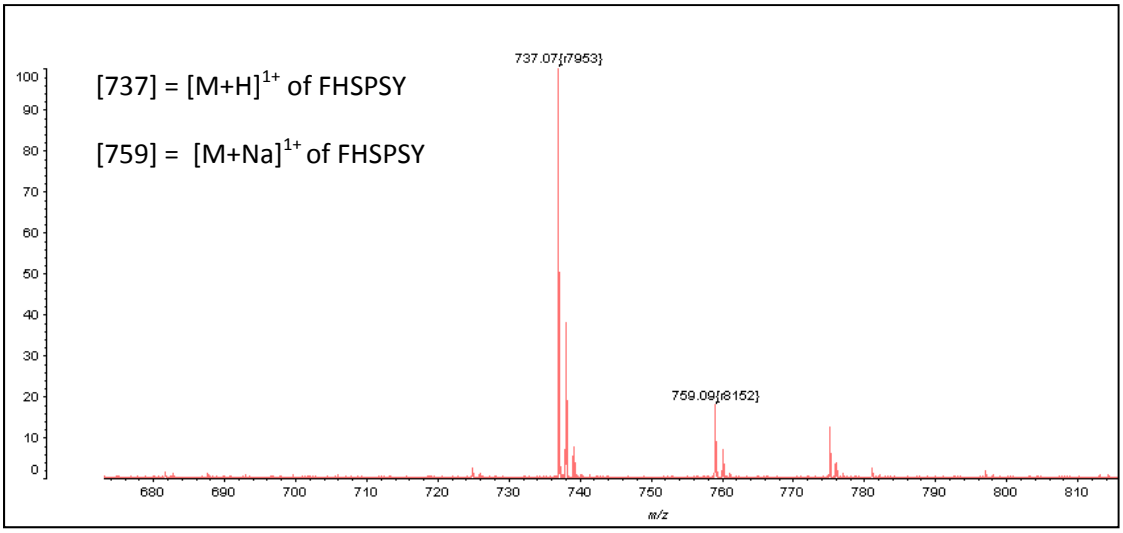

Figure 8-3: MALDI spectrum of Peptide-Y isolated from incubation of PFHSPSY in 100 mM phosphate buffer pH 7.4 at 60 °C.

Peptide-Y was also shown to have the same retention time as FHSPSY by HPLC (Figure 8-4).

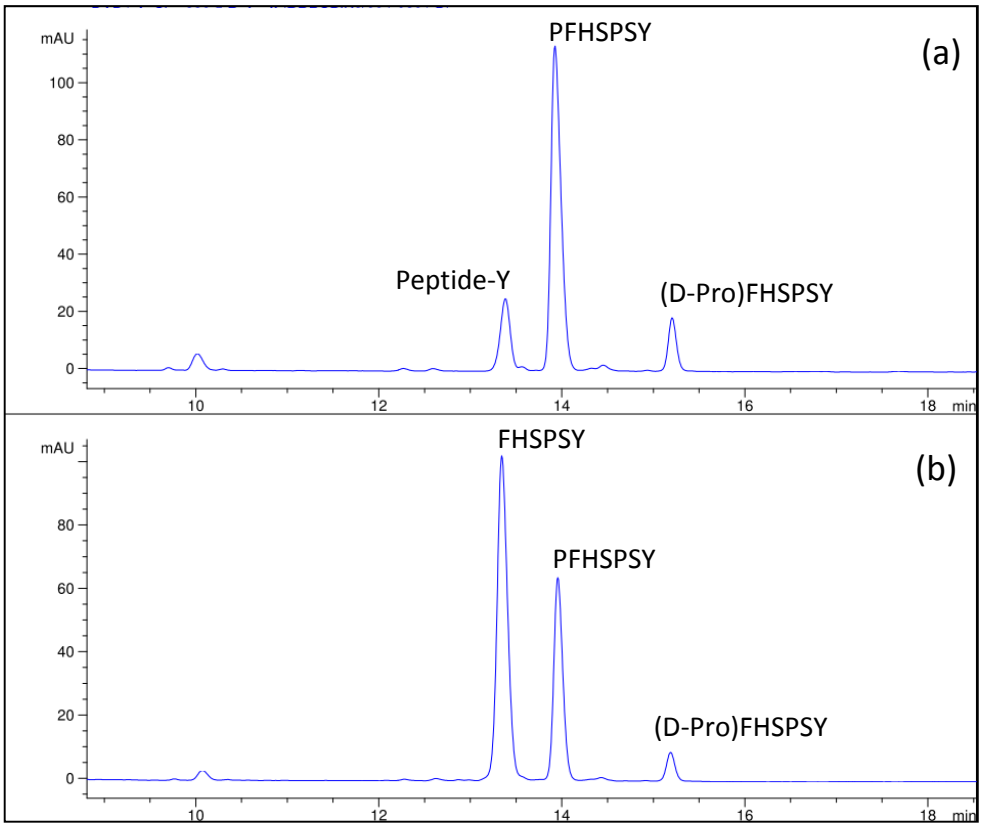

Figure 8-4: (a) HPLC trace (280 nm) of day-3 time point following incubation of PFHSPSY, (b) the same day-3 time point spiked with a commercial standard of FHSPSY.

For final confirmation, Peptide-Y was subjected to MALDI MS/MS fragmentation and compared to a standard of FHSPSY. The predicted fragmentation ions of FHSPSY are shown in Figure 8-5. As can be seen in Figure 8-6, the MS/MS fragmentation of Peptide-Y matched that of a standard of FHSPSY. This confirmed the assignment of Peptide-Y as FHSPSY, resulting from the truncation of the N-terminal Pro residue.

Seq.	#	Immon.	b	b-H2O	y	y-H2O
F	1	120.19			737.78	719.77
H	2	110.15	285.32		590.60	572.59
S	3	60.09	372.40	354.39	453.47	435.45
P	4	70.13	469.51	451.50	366.39	348.38
S	5	60.09	556.59	538.58	269.27	251.26
Y	6	136.19			182.20	

Figure 8-5: Predicted fragmentation ions of FHSPSY. The major ions present in Figure 8-6 are highlighted.

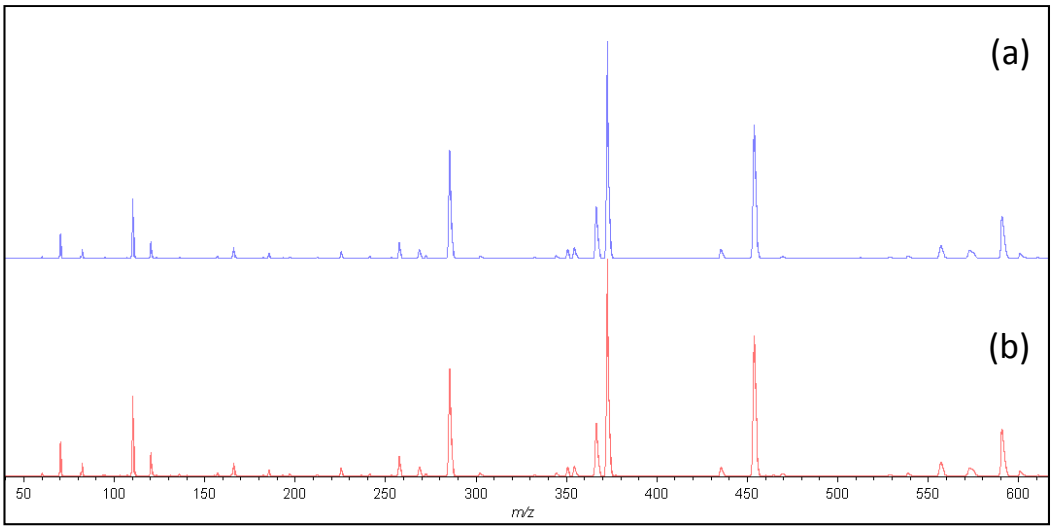

Figure 8-6: MALDI MS/MS spectra of the 737 Da ion from (a) Peptide-Y and (b) FHSPSY standard.

8.4 Effect of amino acid sequence on N-terminal truncation (1' Position)

In Section 8.3 the truncation of an *N*-terminal Pro residue following incubation at physiological pH and 60 °C was characterised. This section aimed to investigate if other residues were subject to a similar truncation, or if it is unique to Pro. Three peptides (SFHSPS, PFHSPS and AFHSPS) with

different *N*-terminal amino acids were selected. A Tyr was added to the C-terminus of each peptide to aid HPLC detection. PFHSPSY, SFHSPSY and AFHSPSY were incubated (in triplicate) at 60 °C pH 7.4 and characterised as per Incubation-B (Section 2.2.1).

8.4.1 Results and Discussion

Following truncation of the *N*-terminal residue, each of the peptides would form FHSPSY and this was used to compare the rates of truncation. A sample HPLC trace (280 nm) of a day-14 time point showing the formation of FHSPSY from PFHSPSY is shown in Figure 8-7.

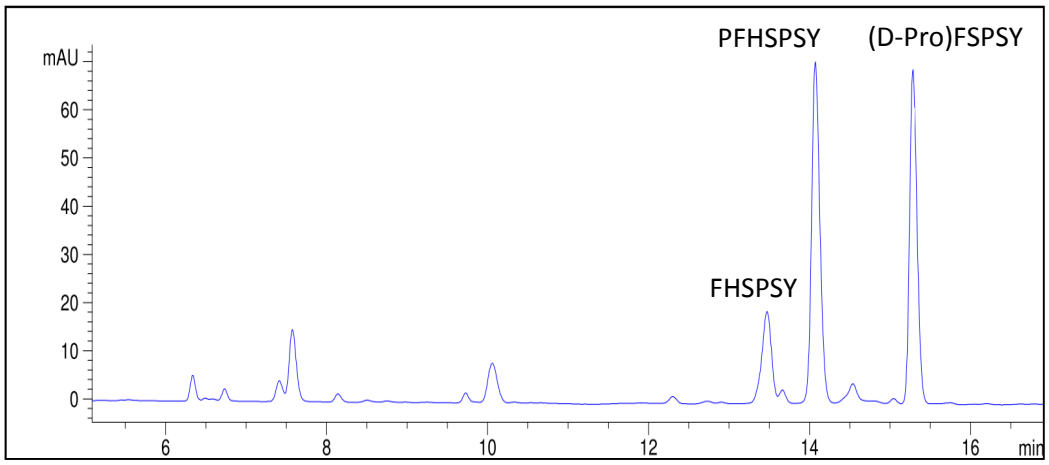

Figure 8-7: HPLC trace (280 nm) of day-7 time point showing the formation of FHSPSY following incubation of SFHSPSY. Peptide was incubated in 100 mM phosphate buffer pH 7.4 at 60 °C.

Standard curves for each peptide were generated as detailed in the Materials and Methods Chapter (Section 2.24) and these were used in combination with the HPLC time point data to calculate the number of moles of each peptide that underwent *N*-terminal truncation. The standard curve for FHSPSY is shown in Figure 8-8.

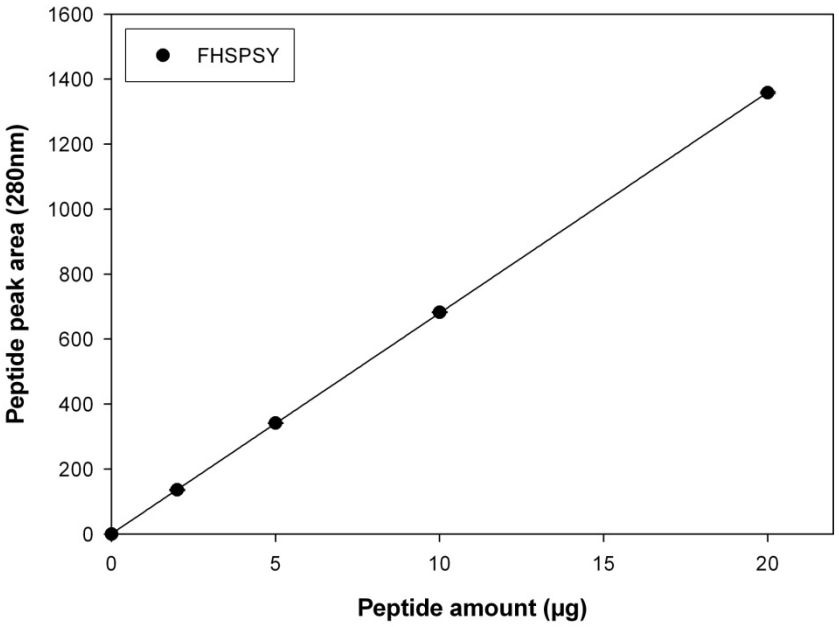

Figure 8-8: Standard curve for FHSPSY relating peak area at 280 nm to peptide amount (µg).

The HPLC results from the analysis of each incubation triplicate were averaged, points plotted +/- the SD and the rate of disappearance of the intact peptide and appearance of its truncated adduct was plotted (Figure 8-9).

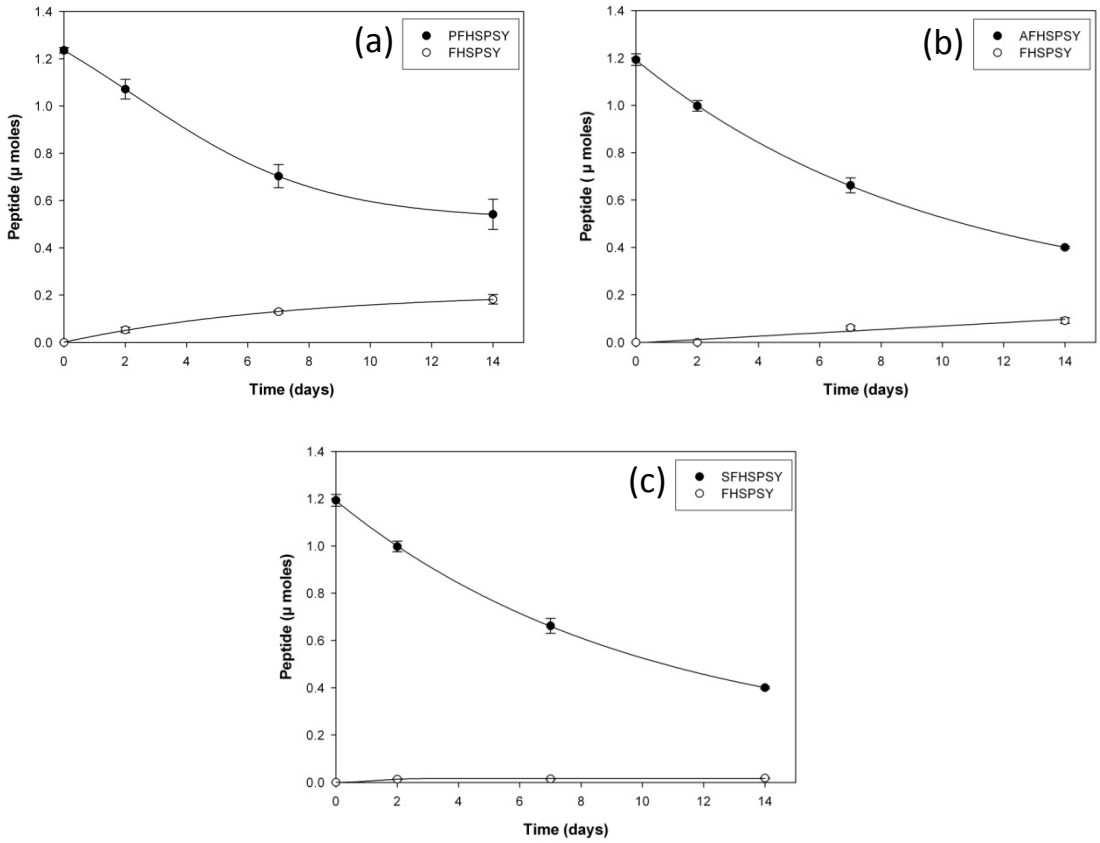

Figure 8-9: N-terminal Pro, Ala and Ser (a) Loss of PFHSPSY and appearance of FHSPSY, (b) loss of AFHSPSY and appearance of FHSPSY, (c) loss of SFHSPSY and appearance of FHSPSY. Peptides were incubated in 100 mM phosphate buffer pH 7.4 at 60 °C.

The percentage of each peptide which truncated *via* loss of the N-terminal residue to form FHSPSY is shown in Figure 8-10.

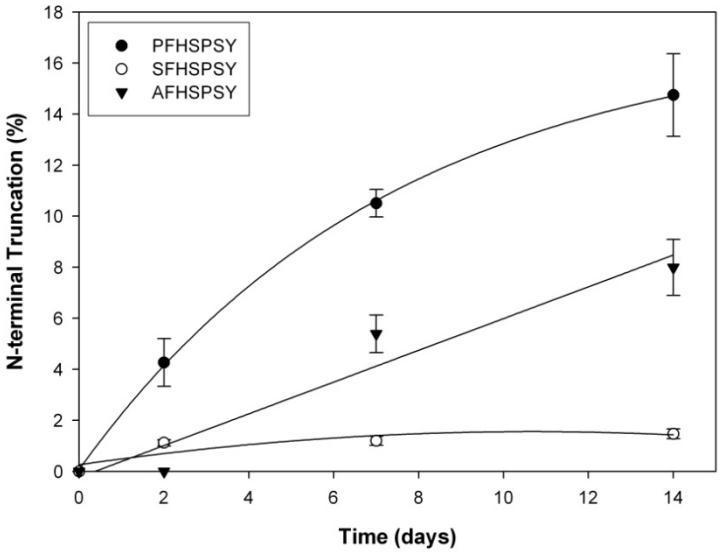

Figure 8-10: Percentage conversion of PFHSPSY, AFHSPSY and SFHSPSY to FHSPSY (truncation of N-terminal residue). Peptides were incubated in 100 mM phosphate buffer pH 7.4 at 60 °C. Percentage values were calculated as the amount (moles) of each peptide which modified *via* truncation of its N-terminal residue with respect to time compared to the amount of each intact peptide present at T=0.

The results indicate that while truncation of the N-terminal residue is not unique to Pro, there appears to be a wide range in the rate. After 2 weeks incubation at 60 °C, only ~2% of N-terminal Ser had been lost compared to ~6% of N-terminal Ala and ~14% of N-terminal Pro. One potential reason for the difference in rate is shown in Figure 8-11. SFHSPSY forms a much greater amount of HSPSY than PFHSPSY. This is likely due to the loss of an SF diketopiperazine as discussed in Chapter-6. One of the main challenges of these studies has been the fact that it is difficult to study each degradation process in isolation, but the important point is that the loss of an N-terminal residue was observed at physiological pH in each of the three peptides studied suggesting it could potentially occur in the lens.

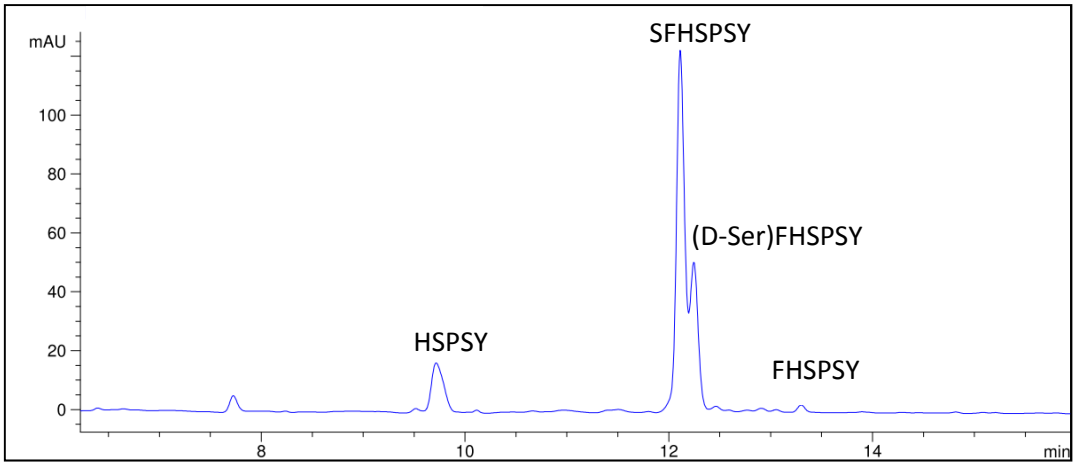

Figure 8-11: HPLC trace (280 nm) of day-7 time point showing the formation of FHSPSY following incubation of SFHSPSY. Peptide was incubated in 100 mM phosphate buffer pH 7.4 at 60 °C.

8.5 Effect of amino acid sequence on N-terminal truncation (2' Position)

To investigate the effect of the penultimate amino acid (denoted as 2') on the rate of loss of the N-terminal amino acid four related peptides were examined (Table 8-1). In each case only the residue in the penultimate position was varied. The peptides (PFHSPSY, PAHSPSY, PEHSPSY and PKHSPSY) were incubated (in triplicate) at 60°C pH 7.4 as per Incubation-B (Section 2.2.1).

Table 8-1: Four related peptides with different penultimate residues (underlined).

Peptide	Penultimate residue
P<u>F</u>HSPSY	Aromatic
P<u>A</u>HSPSY	Neutral
P<u>E</u>HSPSY	Acidic
P<u>K</u>HSPSY	Basic

8.5.1 Results and Discussion

In each case the major degradation products were identified using similar methods to those discussed in Section 8.3. A sample HPLC trace (280 nm) of a day-7 incubation time point showing the formation of AHSPSY from PAHSPSY is shown in Figure 8-12. As indicated by (*), the loss of the N-terminal residue is not the only degradation occurring in each incubation.

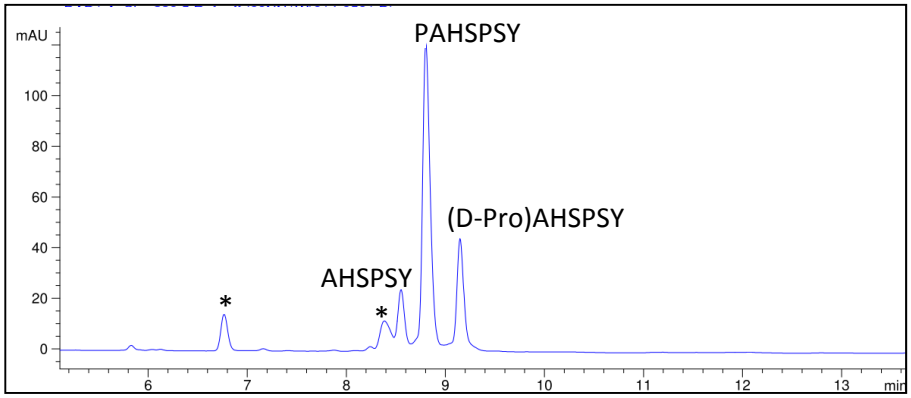

Figure 8-12: HPLC trace (280 nm) day-7 time point showing the formation of AHSPSY following incubation of PAHSPSY. Peptide was incubated in 100 mM phosphate buffer pH 7.4 at 60 °C. Degradation *via* other processes is shown by (*).

Standard curves for each peptide were generated as detailed in the Materials and Methods Chapter (Section 2.24) and these were used in combination with the HPLC data to calculate the number of moles of each peptide that underwent N-terminal truncation. At each time point the triplicate results were averaged and the rate of disappearance of the intact peptide and appearance of its N-terminally truncated adduct was plotted +/- SD (Figure 8-13).

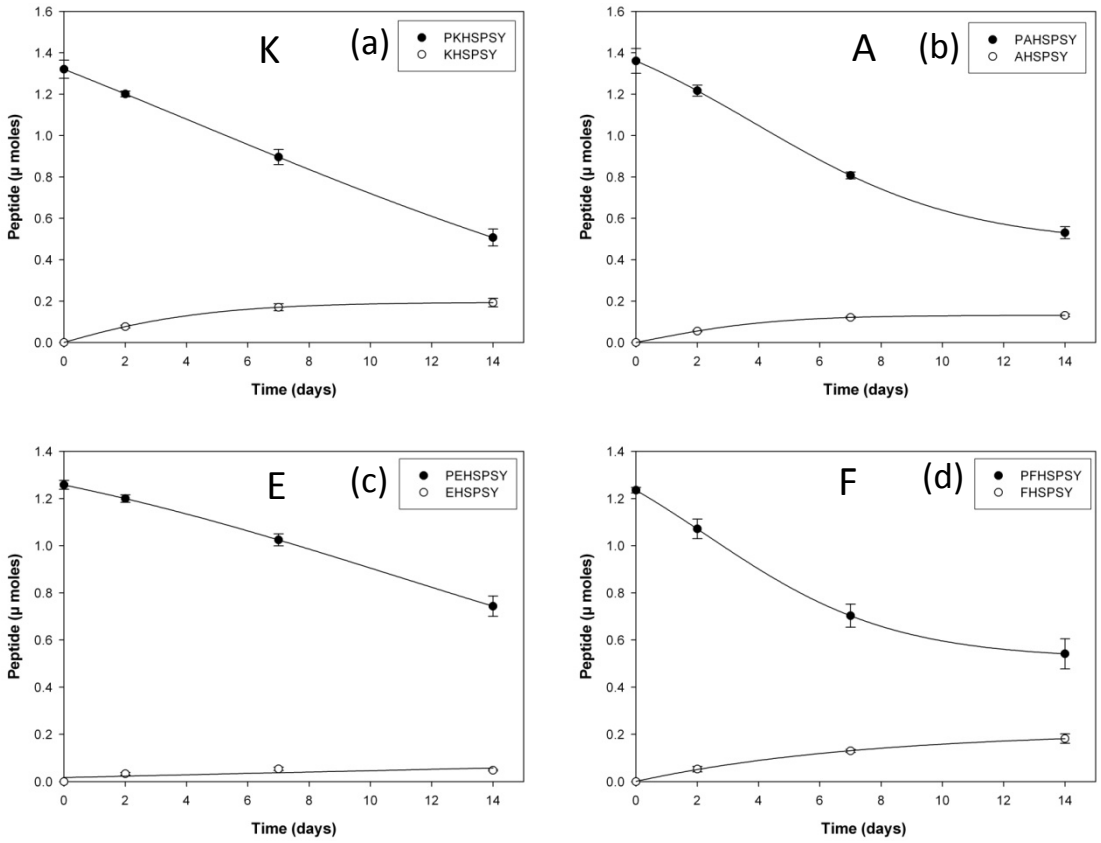

Figure 8-13: Effect of penultimate amino acid on rate of truncation of N-terminal residue. (a) Loss of PKHSPSY and appearance of KHSPSY, (b) loss of PAHSPSY and appearance of AHSPSY, (c) loss of PEHSPSY and appearance of EHSPSY and (d) loss of PFHSPSY and appearance of FHSPSY. Peptides were incubated in 100 mM phosphate buffer pH 7.4 at 60 °C.

Figure 8-14 compares the percentage of each peptide that truncated at the N-terminal Pro residue.

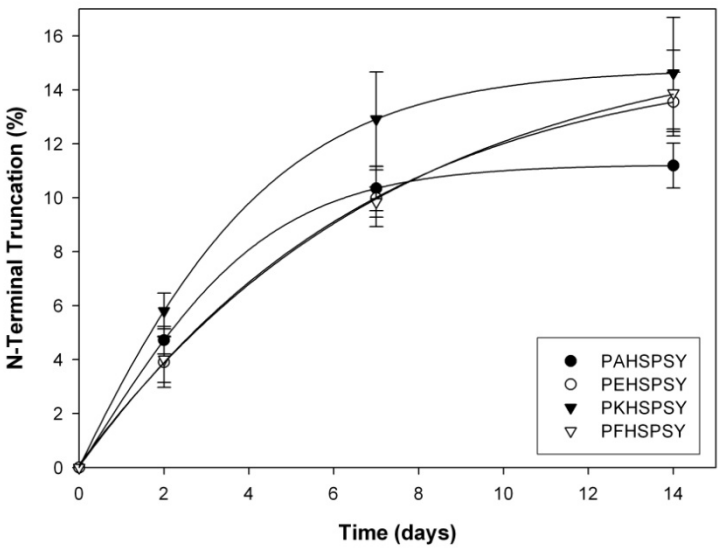

Figure 8-14: Percentage of the original peptide (PAHSPSY, PEHSPSY, PKHSPSY and PFHSPSY) that underwent truncation of its N-terminal Pro residue compared to amount present at T=0. Percentage values were calculated as the amount (moles) of each peptide which modified *via* truncation of its N-terminal residue with respect to time compared to the amount of each intact peptide present at T=0.

From the above data is appears the penultimate amino acid does affect the rate of loss of the N-terminal Pro although it is not as pronounced as the effect on the rate of the N-terminal racemisation discussed in Chapter 7. In summary, following two weeks of incubation at 60 °C (pH 7.4) the N-terminal Pro residues, regardless of the identity of the penultimate residues, were subject to a minimum of 10% truncation.

8.6 Effect of amino acid sequence on N-terminal truncation (3' Position)

As most of the peptides being investigated in Sections 8.2 and 8.4 were based on α-crystallin (16-21), and therefore had a His at the 3' position, it was necessary to investigate whether this had an effect on the loss of the N-terminal amino acid. PFHSPSY and a control peptide where His was replaced by Ala (PFHAPSY) were incubated (in triplicate) at 60 °C pH 7.4 and characterised as per Incubation-B (Section 2.2.1).

8.6.1 Results

Standard curves for each peptide and degradation product were generated as detailed in the Materials and Methods Chapter and these were used in combination with the HPLC time point data to calculate the number of moles of each peptide that underwent N-terminal truncation. At each time point the triplicate results were averaged and the rate of disappearance of the intact peptide and appearance of its N-terminally truncated adduct was plotted (Figure 8-15).

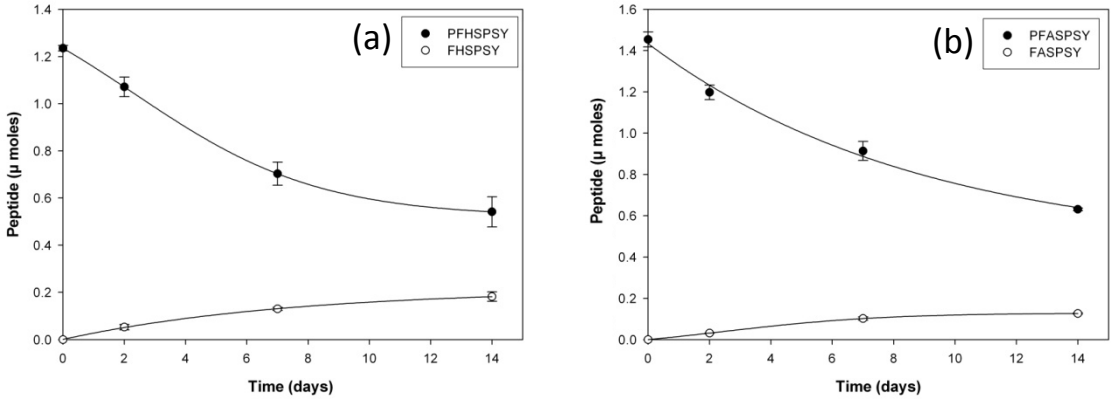

Figure 8-15: (a) Loss of PFHSPSY and appearance of FHSPSY, (b) loss of PFASPSY and appearance of FASPSY. Peptides were incubated in 100 mM phosphate buffer pH 7.4 at 60 °C.

Figure 8-16 compares the percentage of each peptide that truncated at the N-terminal Pro residue.

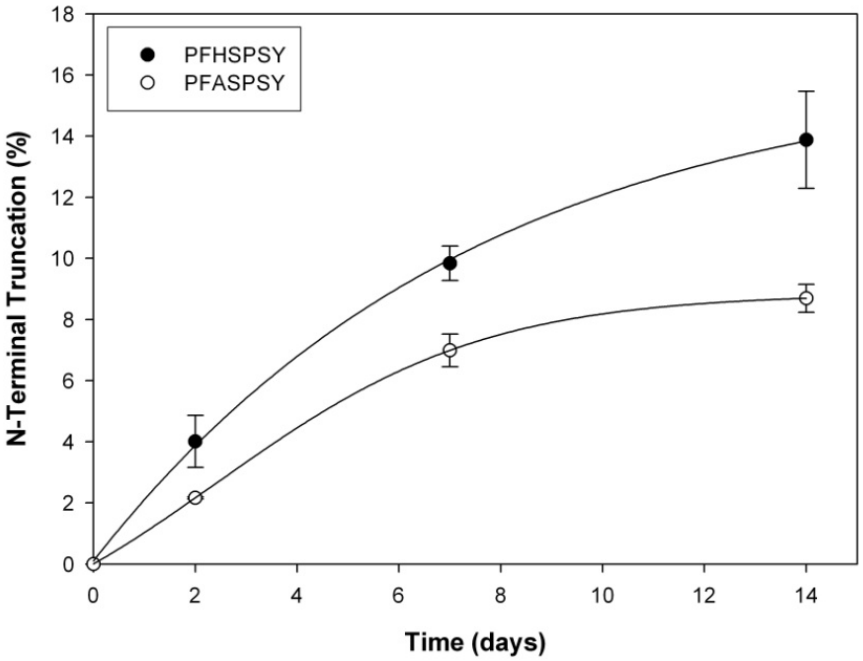

Figure 8-16: Percentage of each peptide which degraded *via* loss of the N-terminal Pro residue. Percentage values were calculated as the amount (moles) of each peptide which modified *via* truncation of its N-terminal residue with respect to time compared to the amount of each intact peptide present at T=0.

As can be seen from Figure 8-16 having a His at the 3' position appears to significantly increase the rate of N-terminal truncation. PFASPSY which does not have the basic His residue truncates at a much slower rate than PFHSPSY. This is in contrast to the minimal effect it had on the rate of N-

terminal racemisation. While this may give some indication as to the mechanism of truncation it should be noted that this difference in rate may be due to a difference in stability between the newly formed FHSPSY and FASPSY. This was investigated by separately incubating FASPSY and FHSPSY under the conditions outlined above. FASPSY degraded at approximately 3 times the rate of FHSPSY thus partially explaining the above result. One of the main challenges of these studies has been the fact that it is difficult to study each degradation process in isolation. This is due to the degradation products also being unstable under the incubation conditions.

8.7 Effect of amino acid stereochemistry on truncation rate

In Section 7.7 N-terminal stereoisomers of Pro were shown to racemise at different rates. To investigate if the same was true for N-terminal truncation, the four peptides in Table 8-2 were incubated (in triplicate) at 60 °C pH 7.4 and characterised as per Incubation-B in (Section 2.2.1).

Table 8-2: List of the two peptide pairs to be examined. Each pair differs only by the stereochemistry of their N-terminal residue.

Pair #1	Pair #2
(L-Pro)FHSPSY	(L-Pro)FHS(D-Pro)SY
(D-Pro)FHSPSY	(D-Pro)FHS(D-Pro)SY

8.7.1 Results and Discussion

As can be seen in Figure 8-17, the rate of truncation of the N-terminal Pro residue in PFHSPSY compared (D-Pro)FHSPSY is markedly different.

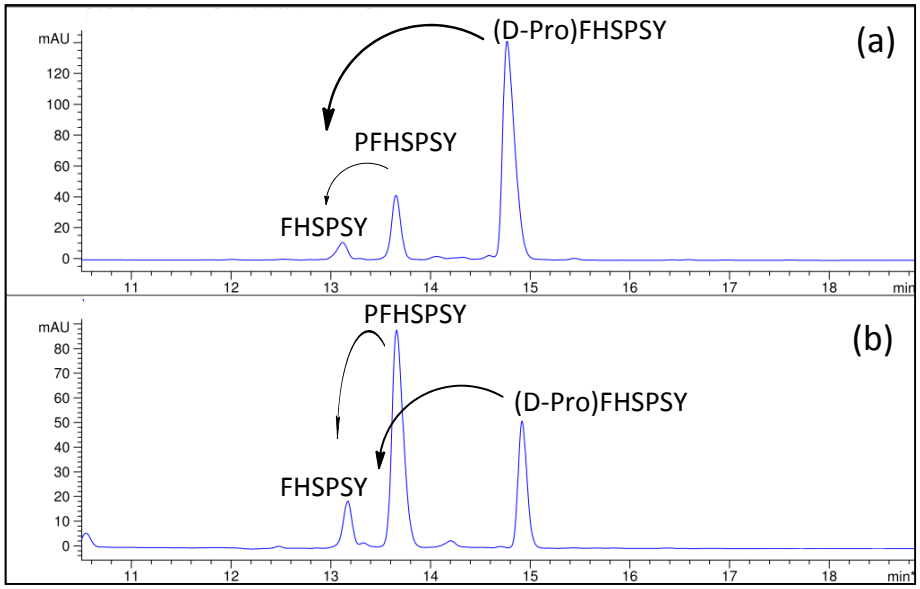

Figure 8-17: HPLC trace (280 nm) of (a) PFHSPSY day-7 time point and (b) (D-Pro)FHSPSY day-7 time point. (Peptide-Y is an additional modification whose characterisation is discussed in Chapter-8).

At each time point the triplicate results were averaged and the rate of disappearance of the intact peptide and appearance of its N-terminally truncated adduct was plotted (Figure 8-18).

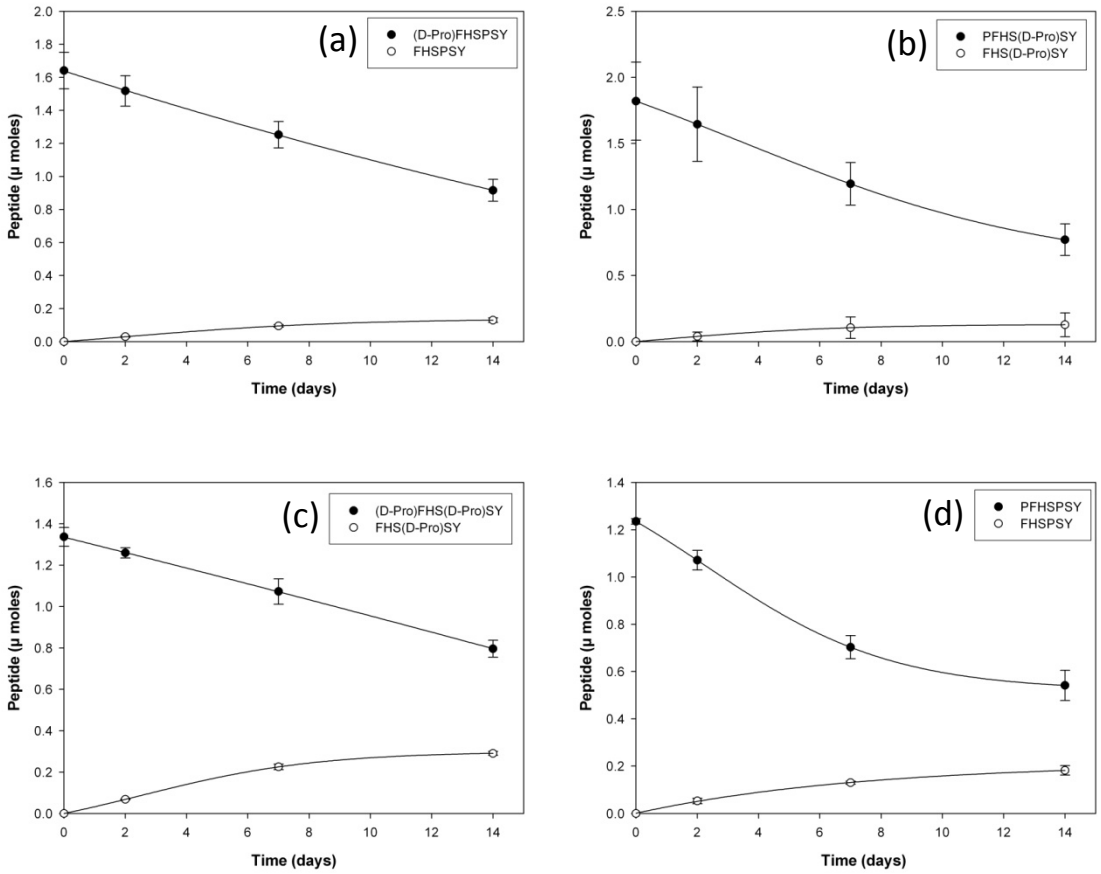

Figure 8-18: (a) Loss of PFHSPSY and appearance of FHSPSY, (b) loss of (D-Pro)FHSPSY and appearance of FHSPSY, (c) loss of PFHS(D-Pro)SY and appearance of FHS(D-Pro)SY and (d) loss of (D-Pro)FHS(D-Pro)SY and appearance of FHS(D-Pro)SY. Peptides were incubated in 100 mM phosphate buffer pH 7.4 at 60 °C the above graphs show.

A comparison of the percentage of N-terminal truncation of PFHSPSY and (D-Pro)FHSPSY was plotted in Figure 8-19 and the percentage rate of N-terminal truncation of PFHS(D-Pro)SY and (D-Pro)FHS(D-Pro)Y was plotted in Figure 8-20.

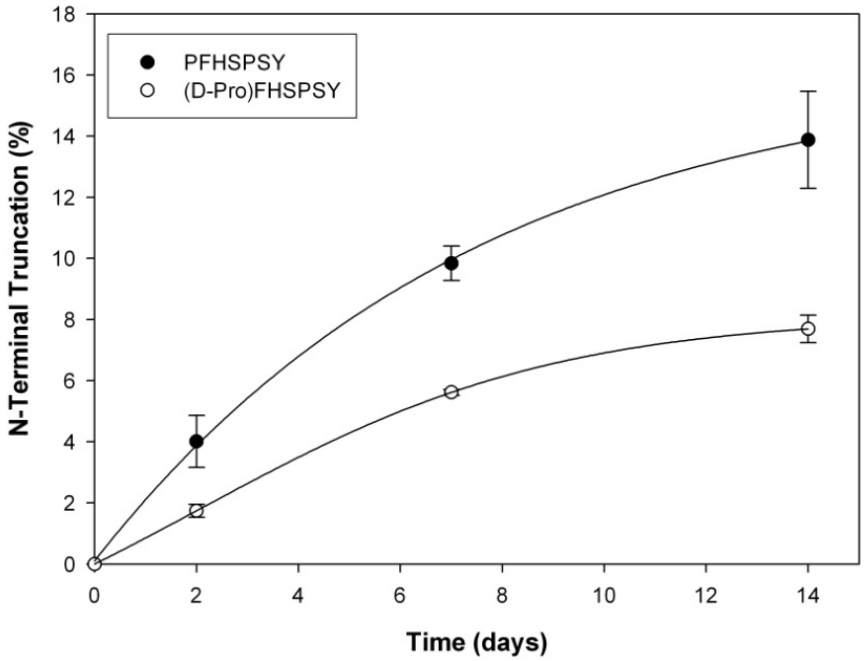

Figure 8-19: Percentage of PFHSPSY and (D-Pro)FHSPSY which degraded *via* loss of an N-terminal Pro residue. Percentage values were calculated as the amount (moles) of each peptide which modified *via* truncation of its N-terminal residue with respect to time compared to the amount of each intact peptide present at T=0.

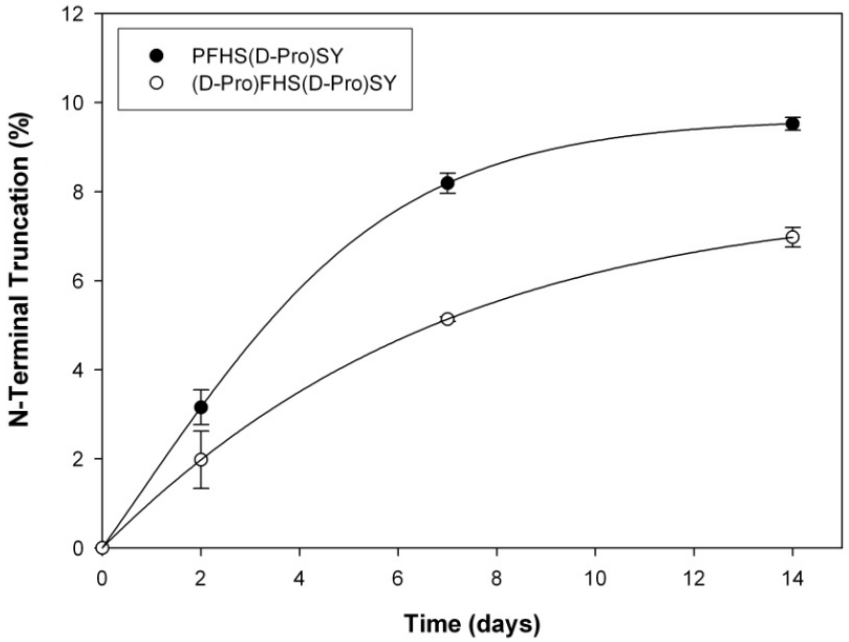

Figure 8-20: Percentage of PFHS(D-Pro)SY and (D-Pro)FHS(D-Pro)Y which degraded *via* loss of an N-terminal Pro residue. Percentage values were calculated as the amount (moles) of each peptide which modified *via* truncation of its N-terminal residue with respect to time compared to the amount of each intact peptide present at T=0.

As can be seen in the above figures there is a significant difference in the rate of N-terminal truncation between D-Pro and L-Pro. In PFHSPSY vs (D-Pro)FHSPSY the L-form of Pro truncates at a faster rate than the D-form. Similar results are seen in comparing PFHS(D-Pro)SY and (D-Pro)FHS(D-Pro)Y. The reasons for this are as yet unclear.

8.8 Effect of buffer type on N-terminal truncation rate.

Phosphate buffer has been shown to act as a nucleophile [246, 247] and it is possible that this may be causing truncation of the N-terminal residue. To examine this, peptide incubations were a carried out in other buffers, at pH 7.4. The Good's buffers HEPES and TES were chosen for comparison. Good's buffers are characterised by low nucleophilicity and are generally regarded as being biologically inert [248]. PFHSPSY was incubated (in triplicate) at 60 °C pH 7.4 in each buffer (phosphate, HEPES, TES) and characterised as per Incubation-B (Section 2.2.1).

8.8.1 Results and Discussion

A sample HPLC trace (280 nm) of the day-11 time-point from each incubation is shown in Figure 8-21.

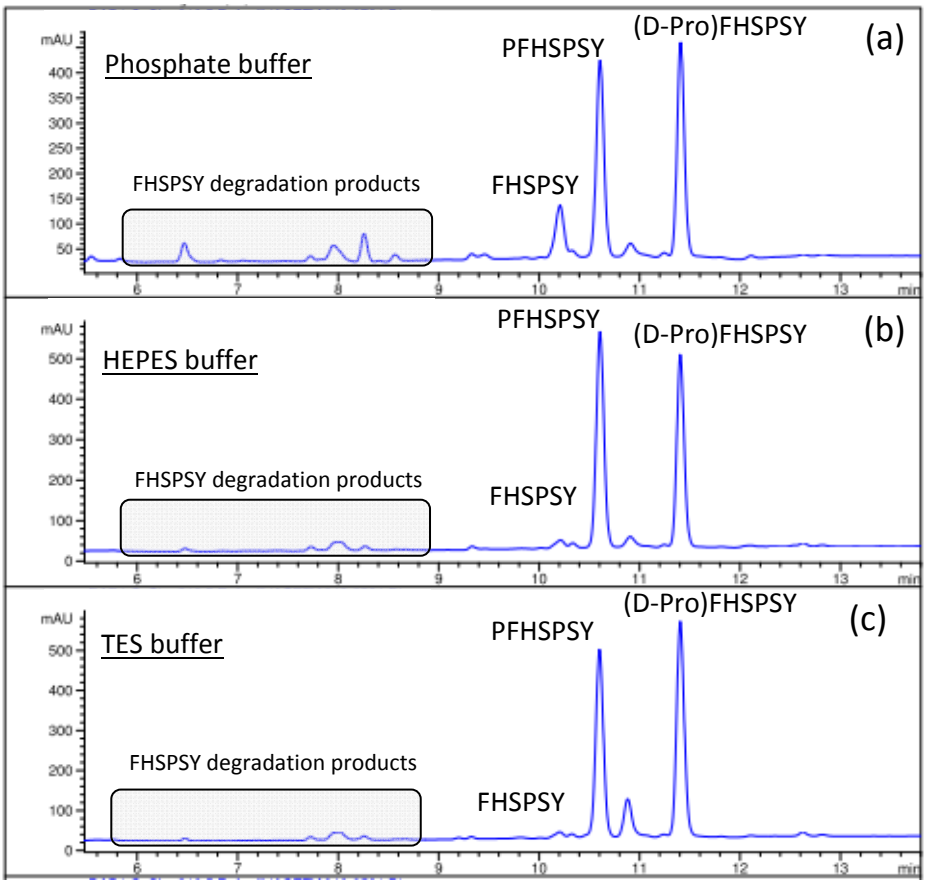

Figure 8-21: HPLC trace (280 nm) of the day-11 time-point from the incubation of PFHSPSY in (a) phosphate buffer, (b) HEPES buffer and (c) TES buffer. Peptides were incubated at 60 °C and all buffers were pH 7.4.

The standard curves generated for Section 8.3 were used in combination with the HPLC time point data to plot the rate of truncation of the N-terminal Pro in each buffer. The percentage truncation of the N-Terminal Pro in each buffer was plotted in Figure 8-22.

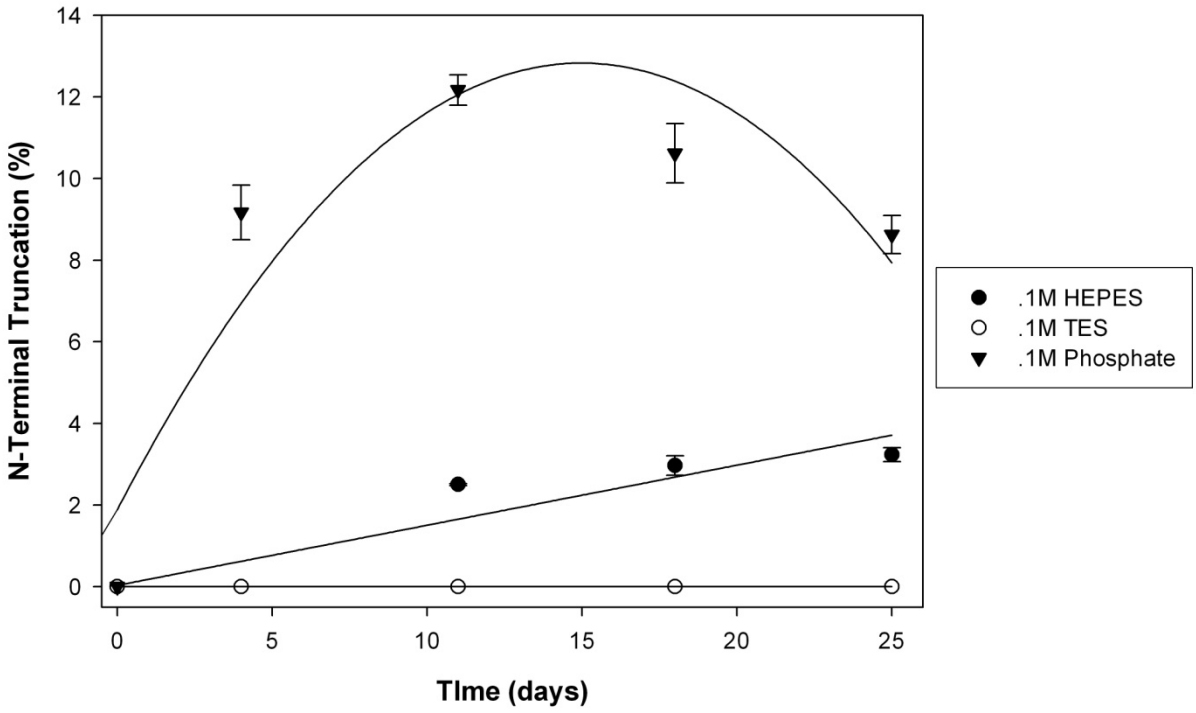

Figure 8-22: Percentage of PFHSPSY which degraded *via* loss of a N-terminal Pro residue when incubated in (a) phosphate buffer, (b) HEPES buffer and (c) TES buffer. All peptides were incubated at 60 °C and all buffers were 100 mM pH 7.4. Percentage values were calculated as the amount (moles) of each peptide which modified *via* truncation of its N-terminal residue with respect to time compared to the amount of each intact peptide present at T=0.

As can be seen above there is a significant difference in the rate of N-terminal truncation between the three buffers. Both of the Goods buffers showed relatively little N-terminal truncation compared to the phosphate buffer. These results suggest that one factor contributing to loss of the N-terminal residue may be the nucleophilicity of phosphate buffer [246, 247]. It is also possible that trace metal ions in the phosphate buffer could be involved in the N-terminal truncation and this was examined in Section 8.8.

The decrease in the apparent amount of N-terminal truncation (FHSPSY) seen in the phosphate buffer towards the later time points is due to further degradation of the N-terminally truncated product FHSPSY. Figure 8-23 shows that when FHSPSY was separately incubated under the same conditions it was subject to further degradation.

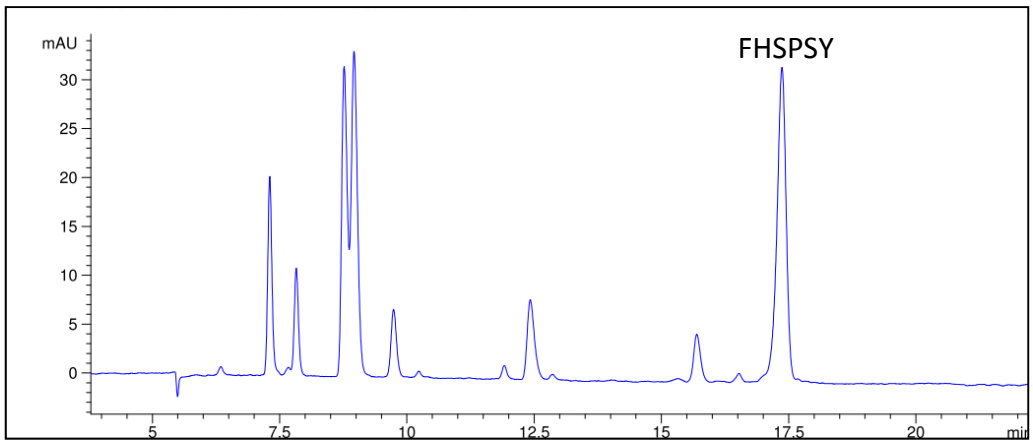

Figure 8-23: Degradation of FHSPSY when incubated separately under the same conditions (100 mM phosphate buffer pH 7.4, 60 °C).

8.9 Effect of metal ions on N-terminal truncation

As N-terminal truncation occurred at a reduced rate in HEPES and TES buffers compared to phosphate, it was proposed that trace metal ions could be involved. This is because it is well known that phosphate contains significant levels of trace metal ions [280]. To investigate this, incubations were carried out in phosphate buffer in the presence of EDTA which is a known metal chelator. PFHSPSY and PFHSPSY containing 1 mM EDTA were incubated (in triplicate) at 60 °C pH 7.4 and characterised as per Incubation-B (Section 2.2.1).

8.9.1 Results and Discussion

The standard curves generated for Section 8.3 were used in combination with the HPLC time point data to plot the rate of truncation of the N-terminal Pro in each buffer. The percentage truncation of the N-Terminal Pro in each buffer was plotted in Figure 8-24.

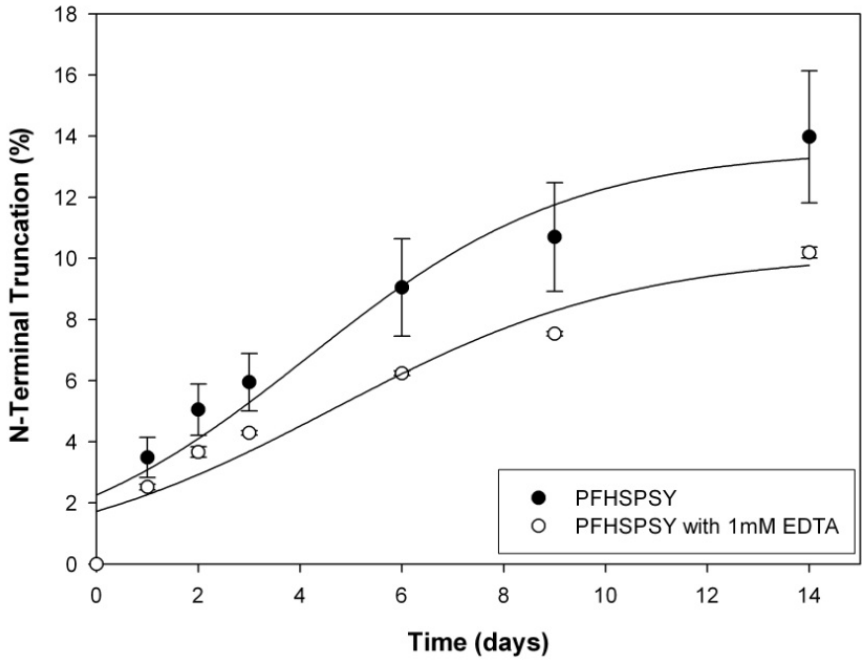

Figure 8-24: Percentage of PFHSPSY which degraded *via* loss of a N-terminal Pro residue when incubated with, and without, EDTA. Peptides were incubated in 100 mM phosphate buffer pH 7.4 at 60 °C. Percentage values were calculated as the amount (moles) of each peptide which modified *via* truncation of its N-terminal residue with respect to time compared to the amount of each intact peptide present at T=0.

The data show that there was a decrease in the rate and extent of N-terminal truncation in the EDTA incubation which implies one of two possibilities:

(1) The N-terminal truncation is being caused / catalysed by trace metals present in buffer.

(2) EDTA is interfering with other processes involved in the N-terminal racemisation.

Further investigation into this matter is required.

8.10 Effect of buffer pH on N-terminal truncation

While N-terminal truncation has been shown to occur at neutral pH it was the aim of this experiment to investigate the effect of acidic pH on the rate of N-terminal truncation. PFHSPSY was incubated (in triplicate) at 60 °C in MES buffer pH 5.4 and characterised as per Incubation-B (Section 2.2.1).

8.10.1 Results and Discussion

The standard curve for PFHSPSY generated for Section 8.3 was used in combination with the HPLC time point data to calculate the percentage of PFHSPSY that underwent N-terminal truncation. At each time point the triplicate results were averaged and the rate of disappearance of the intact peptide and appearance of its N-terminally truncated adduct was plotted (Figure 8-25).

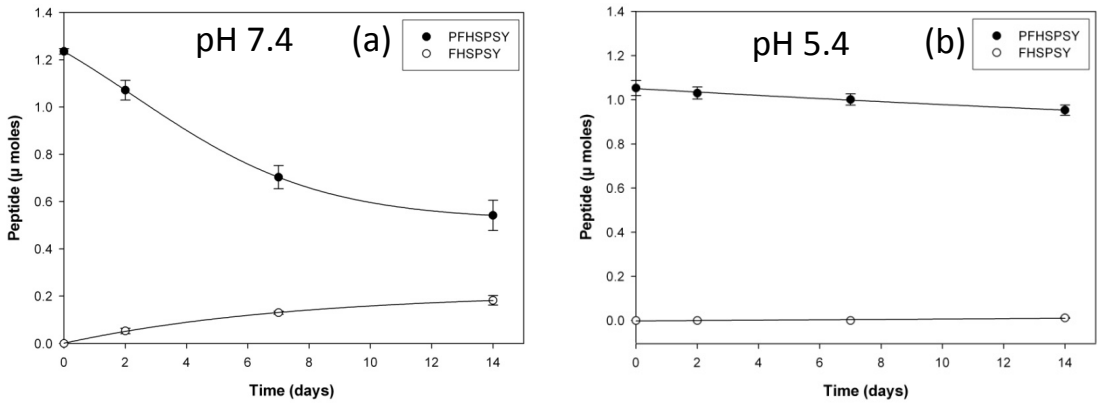

Figure 8-25: Loss of PFHSPSY and appearance of FHSPSY when incubated in (a) phosphate buffer pH 7.4, (b) MES buffer pH 5.4. All buffers were 100 mM and all peptides were incubated at 60 °C.

As can be seen in Figure 8-26 the rate of N-terminal truncation was markedly reduced in MES buffer (pH 5.4) compared to phosphate buffer (pH 7.4). However combining these results with those obtained in Section 8.7 shows that minimal N-terminal truncation occurs in TES buffer (pH 7.4) and in MES buffer (pH 5.4). This suggests that truncation of an N-terminal amino acid residue may be increased by the nucleophilicity of phosphate buffer [246, 247].

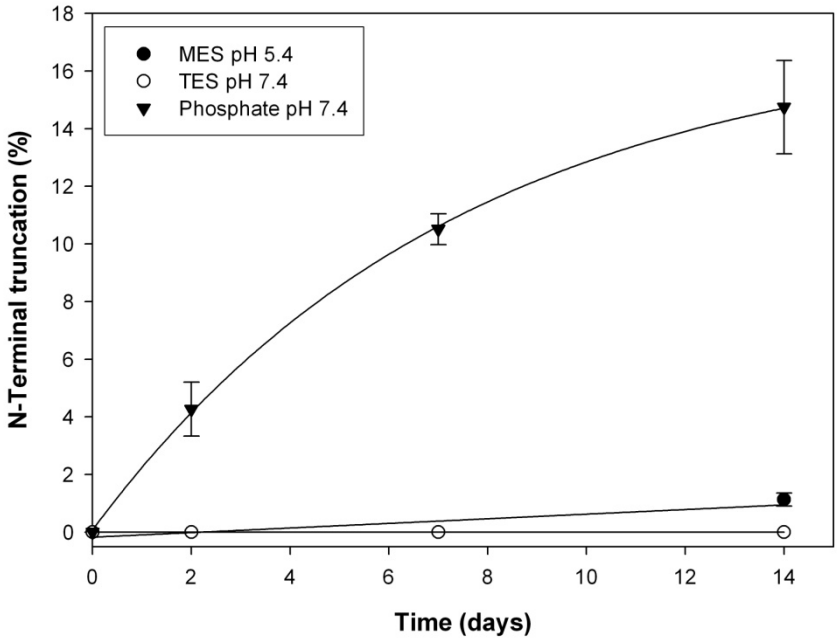

Figure 8-26: Percentage of PFHSPSY which degraded *via* loss of a N-terminal Pro residue when incubated in (a) MES buffer pH 5.4, TES buffer pH 7.4 and (c) phosphate buffer pH 7.4. All buffers were 100 mM and all peptides were incubated at 60 °C. Percentage values were calculated as the amount (moles) of each peptide which modified *via* truncation of its N-terminal residue with respect to time compared to the amount of each intact peptide present at T=0.

8.11 Incubation at physiological temperature

As the degradations being studied in this thesis are expected to occur slowly over many years the use of elevated temperatures to study these processes was deemed necessary. However, as with N-terminal racemisation it was considered important to show that N-terminal truncation could occur at physiological temperature. PFHSPSY was incubated (in triplicate) at 37 °C pH 7.4 and characterised as per Incubation-A (Section 2.2.1).

8.11.1 Results and Discussion

The percentage of PFHSPSY that underwent N-terminal truncation at physiological temperature was calculated as per Section 8.3. As can be seen from Figure 8-27, N-terminal truncation does occur at physiological temperature. Interestingly although it occurs at a lower rate, it occurs approximately

three times faster than N-terminal racemisation which is in contrast to the results at 60 °C where N-terminal racemisation is the faster reaction. The reasons for this are as yet unknown.

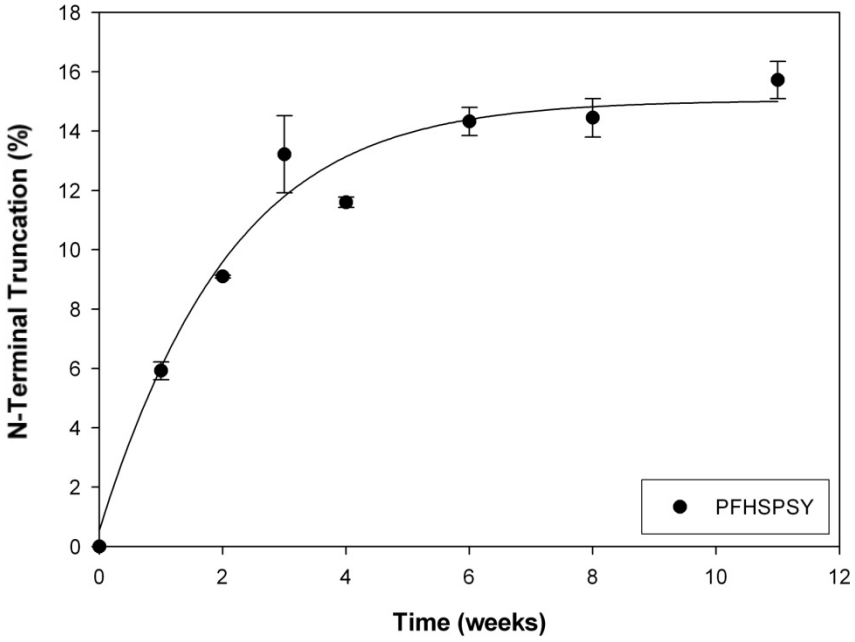

Figure 8-27: Incubation at physiological temperature. Percentage of PFHSPSY which degraded *via* loss of a N-terminal Pro residue. PFHSPSY was incubated in 100 mM phosphate buffer pH 7.4 at 37 °C . Percentage values were calculated as the amount (moles) of PFHSPSY which modified *via* truncation of its N-terminal residue with respect to time compared to the amount of PFHSPSY present at T=0.

8.12 Conclusions

This chapter investigated the potential for peptides to degrade *via* truncation of their N-terminal residue. While an exhaustive study was not carried out, it was revealed that different amino acids truncate at substantially different rates. N-terminal Pro truncated at almost twice the rate of N-terminal Ser and about four times the rate of an N-terminal Ala. The effect of the penultimate amino acid residue was also studied and while a difference was noted it was less pronounced in truncation than its effect on the rate of N-terminal racemisation.

When the effect of the amino acid in the 3' position was examined, having a His in the 3' position compared to an Ala appeared to increase the rate of N-terminal truncation, but this finding turned out to be mainly due to the differing degradation rates of the resulting peptides. A consistent

feature was that N-terminal truncation was shown to occur with a range of N-terminal and penultimate amino acid residues.

pH affected the rate of N-terminal truncation. While it occurred readily in phosphate buffer at pH 7.4, minimal N-terminal truncation was found to occur in MES buffer pH 5.4. In contrast to N-terminal racemisation where the choice of buffer had a minimal effect, the rate of N-terminal truncation was also greatly affected by the choice of buffer. The rate was significantly reduced when buffers other than phosphate were used. Studies have shown that phosphate can act as a nucleophile [246, 247] and this may be the most likely explanation of these results.

Impurities in the phosphate buffer such as trace metal ions may contribute and this was investigated by comparing incubations with and without a metal chelator (EDTA). The rate of N-terminal truncation was reduced when EDTA was present indicating that metals may play a role in the truncation mechanism. It is also possible that EDTA interfered with whatever mechanism is causing the N-terminal truncation.

As was found with N-terminal racemisation (Chapter-7) there also appears to be a difference between the rate of N-terminal truncation of a peptide with a D-Pro residue compared to its corresponding L-Pro residue. N-terminal L residues truncated at a faster rate than N-terminal D residues. The reasons for this are not yet understood and further investigation is warranted. If this holds true for proteins then racemisation of the N-terminal residue of a long lived protein would delay its degradation by other non-enzymatic processes.

Crucially N-terminal truncation was also shown to occur under physiological conditions (pH 7.4 and 37 °C) and given the presence of both phosphate buffer and metal ions [281] in the cytosol of the lens it seems possible that sequential truncation of the N-terminal residue could occur in aged lens protein which have free amino terminals. Recent publications by Su et al [187] have described the accumulation of low molecular weight crystallin fragments in the lens. Many of these exhibit a

"laddering" type effect with the loss of sequential amino acid residues from the N-terminal, similar to that observed with the model peptides studied in this chapter.

9 Chapter 9: Section-C Overview (UV filter)

9.1 Introduction

The lenses of humans and other primates contain low molecular weight compounds that act as filters by absorbing UV light in the 300–400 nm region [282, 283]. These tryptophan based metabolites prevent UV-induced photo damage to the retina [284]. Commonly used animal models such as rats and mice appear to be poor choices for the study of UV filters. In addition to seeing UV light and lacking UV filter compounds, their lenses are also unlike human lenses in many other respects [151]. Due to the similarity of the UV filters present in the thirteen-lined ground squirrel [166] to those found in man, this species has been proposed as a suitable animal model for investigating the effects of UV radiation on cataract, and other ocular diseases, thought to involve exposure to light.

Work published by other members of the Truscott group [166] showed that N-acetly 3-hydroxy-kynurenine and N-acetyl-kynurenine were the major UV filters found in the lens of the thirteen-lined ground squirrel. However an additional UV filter which is not found in the human lens and whose structure remains to be elucidated was also isolated. It was of interest to determine the structure of this unknown UV filter.

9.2 Aim:

(1) Elucidate the structure of this unknown UV filter (UV-X) by utilizing a range of analytical techniques including mass spectrometry, and NMR spectroscopy.

10 Chapter 10: UV filter

Work published by other members of the Truscott group in collaboration with Giblin's group [166] showed that *N*-acetly 3-hydroxy-kynurenine and *N*-acetyl-kynurenine are the major UV filters found in the lens of the thirteen-lined ground squirrel (Figure 10-1). However, an additional UV filter that is not found in the human lens and whose structure remains to be elucidated was also isolated (UV-X). The structure of this compound, designated UV-X, was of interest due to the similarity of the squirrel lens UV filter content, to that found in the human lens. Another unknown UV filter, (Peak-2 in Figure 10-1) was shown to have the same molecular weight and MS/MS fragmentation as UV-X. While Peak-2 has been speculated to be a stereoisomer of UV-X, due to its low relative concentration, at this stage only UV-X was examined.

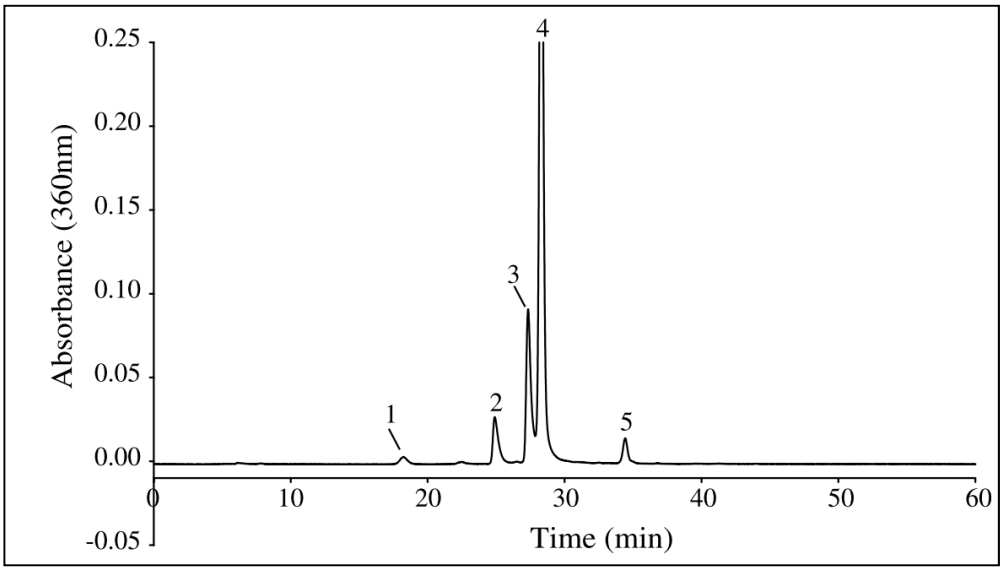

Figure 10-1: HPLC trace of UV-absorbing compounds present in the lens of the thirteen-lined ground squirrel. Lenses were extracted in ethanol prior to analysis. Peak identity is as follows: (1) 3OHKyn, (2) Unknown A, (3) UV-X, (4) *N*-acetyl-3OHKyn; (5) *N*-acetyl-Kyn. Adapted from [166].

The squirrel lenses were extracted [166], purified by semi preparative HPLC and analysed by mass spectrometry and NMR spectroscopy as per the Materials and Methods Chapter (Section 2.27).

10.1 Mass spectrometry analysis

Results

The exact molecular ion of UV-X was initially determined as 346.1391 $[M+H]^{1+}$ using high resolution mass spectrometry. Excalibur software (Thermo Fisher Scientific) was then used to calculate the closest empirical formula to this molecular weight. It revealed $C_{17}H_{20}O_5N_3$ as the closest match and the only possibility within the 2 ppm margin of error. However at this stage a number of potential empirical formulas outside of the 2 ppm range were not ruled out.

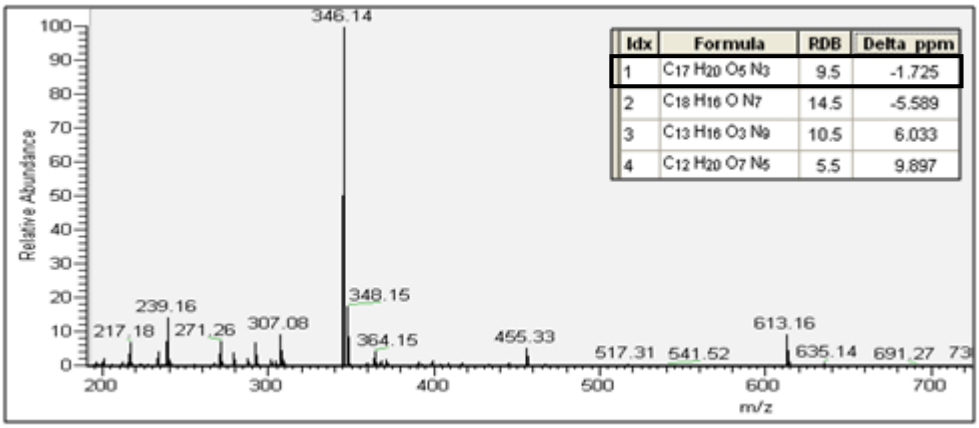

Figure 10-2: High resolution mass spectrometry analysis of UV-X revealed the most likely empirical formula as $C_{17}H_{20}O_5N_3$.

Analysis by high resolution MS/MS showed (Figure 10-3) that the 346.14 $[M+H]^{1+}$ ion fragmented to an ion m/z 287.1 with the neutral loss of C_2H_5NO. This is very likely represents loss of H_2NCOCH_3 from an acetyl group [285].

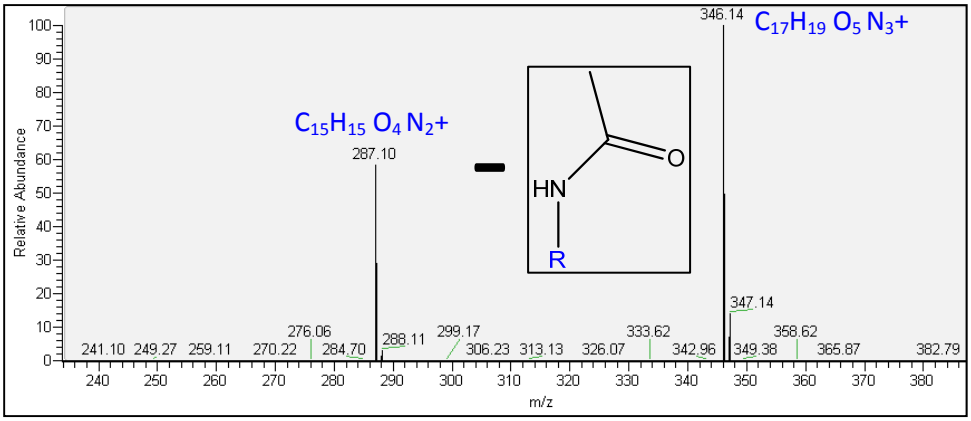

Figure 10-3: High resolution MS/MS fragmentation of UV-X 346.14 $[M+H]^{1+}$ ion.

Fragmentation of the m/z 287.10 ion (Figure 10-4) revealed further neutral losses of CO, (OH• + CO) and C_5H_5NO.

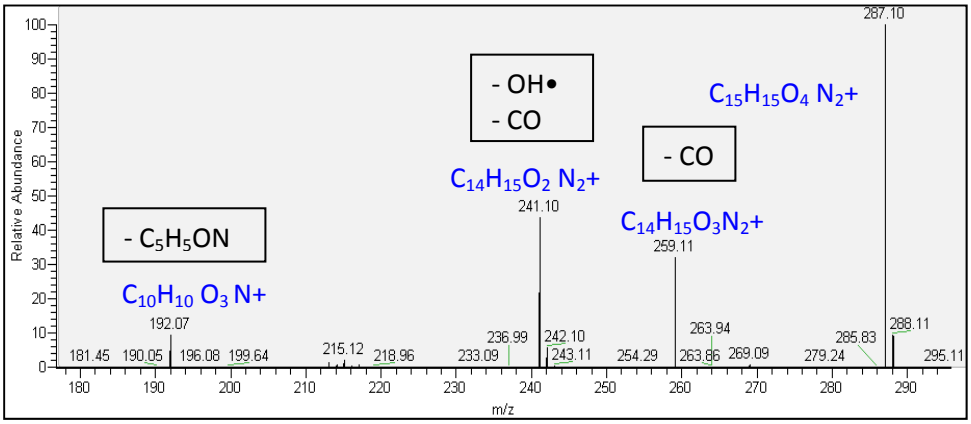

Figure 10-4: High resolution fragmentation of UV-X m/z 287.10 ion.

The spontaneous loss of a CO molecule, indicated by the direct fragmentation of m/z 287.1 ion to m/z 259.1 was difficult to explain mechanistically based on a typical Kynurenine based UV filter structure (Figure 10-5). Carboxylic acids fragment *via* loss of a CO molecule, but this must be preceded by the loss of an OH radical [286].

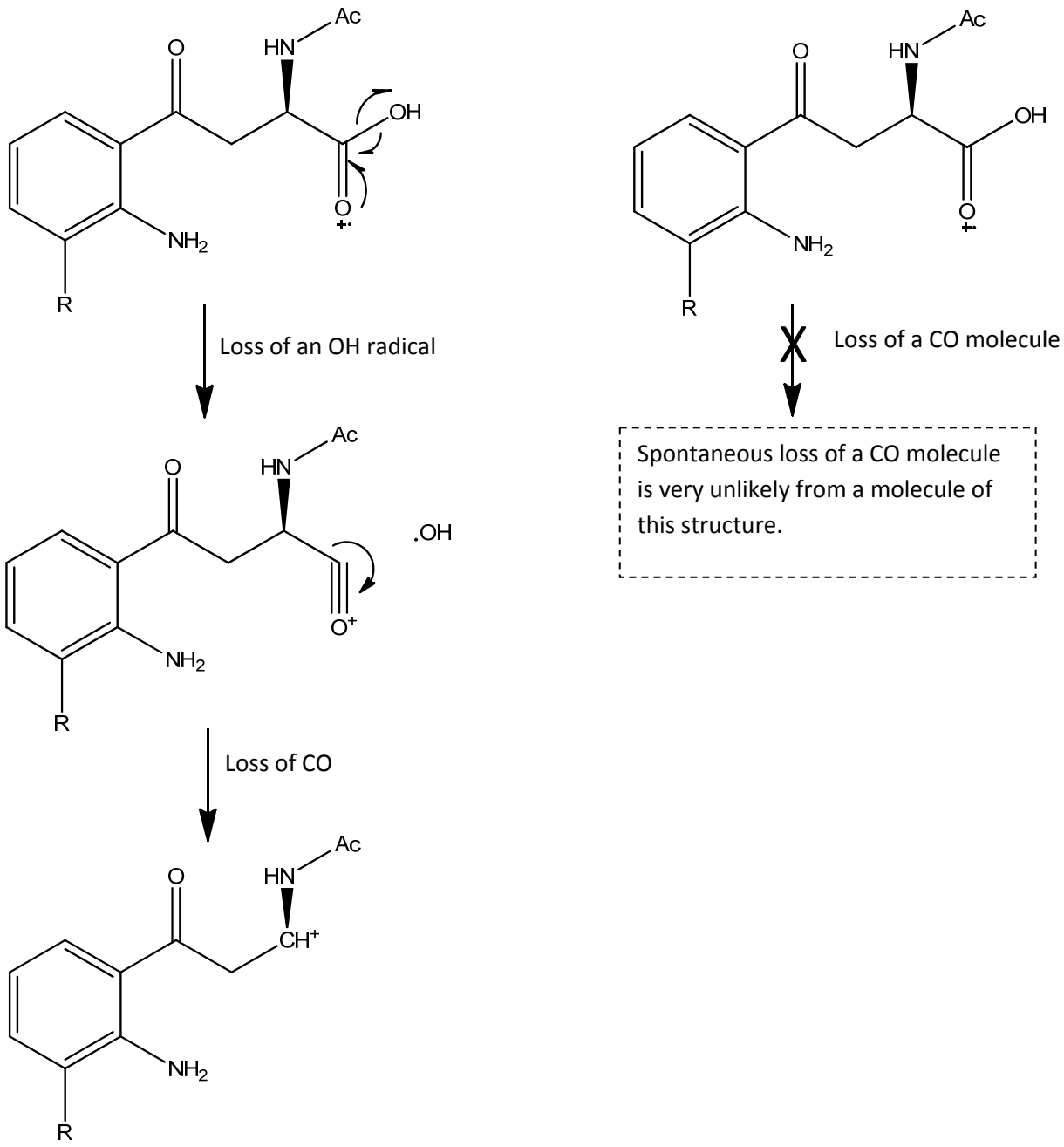

Figure 10-5: (a) Mechanism showing α-cleavage of the carboxylic acid by MS/MS spectrometry from a typical UV filter leading to loss of a CO molecule, which is preceded by loss of an OH radical. (b) Spontaneous loss of a CO molecule without the loss preceding loss of and OH radical or other group is very unlikely to occur in a typical UV filter. Ac = Acetyl group, R = H (for Kyn) and R=OH (for 3OH Kyn).

In addition to the apparent "spontaneous" loss of a CO molecule there an example of a typical carboxylic fragmentation pattern present in UV-X. This is seen in Figure 10-4 where the m/z 287.1 ion at fragments to m/z 241.1, first *via* the expected loss of OH• and then *via* the loss of a CO molecule, suggesting that UV-X likely contains at least one carboxylic acid.

Functional groups that can spontaneously lose a CO molecule following MS/MS fragmentation include phenols [287] and some lactones [288, 289]. However fragmentation of *N*-acetyl 3OHKyn [166] does not show evidence of a neutral loss of CO from the phenol ring, thus suggesting that it should not occur in UV-X should it contain a similar phenol group. The fact that a spontaneous loss of a CO molecule was occurring as readily as the fragmentation of a carboxylic acid from UV-X suggested that the molecular ion may be incorrect. Examining the mass spectrum of the crude UV-X sample once again, revealed the presence of an ion at m/z 364.1. High resolution MS analysis of this ion determined it differed from the ion at m/z 346.1 by a water molecule (i.e. H_2O) with an empirical formula of $C_{17}H_{22}O_6N_3$.

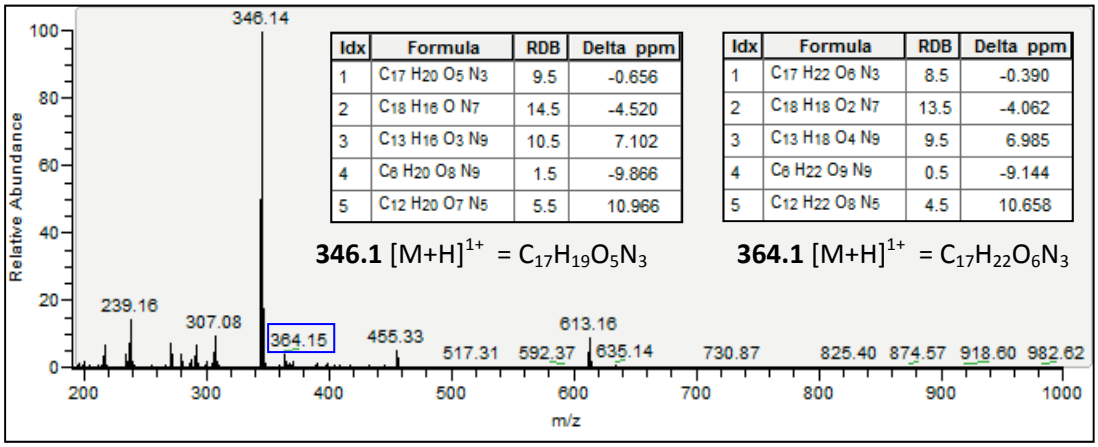

Figure 10-6: High resolution MS analysis of UV-X highlighting the additional ion at 364.1 $[M+H]^{1+}$ as the correct molecular ion.

This ion was initially thought to be an additional impurity present in UV-X [166], but it now appears more likely that it is the true molecular ion of UV-X. The molecular ion of a carboxylic acid is usually observed, but often in low abundance due to facile loss of a water molecule [290, 291]. Additional

evidence came from the analysis of Peak-2 in Figure 10-1 by mass spectrometry. Due to its different retention time by HPLC but identical MS/MS fragmentation pattern, it is proposed to be a stereoisomer of UV-X. If the m/z 364.1 ion was from an impurity in UV-X, then it was very unlikely Peak-2 would contain a similar impurity. Analysis of the high resolution mass spectrum of Peak-2 (Figure 10-7) showed it also contained an m/z 364.1 ion. Based on this, it was proposed that the apparent "spontaneous" loss of a CO molecule was actually a combined loss of two moieties (OH• + CO) suggesting the presence of a second carboxylic acid group in UV-X.

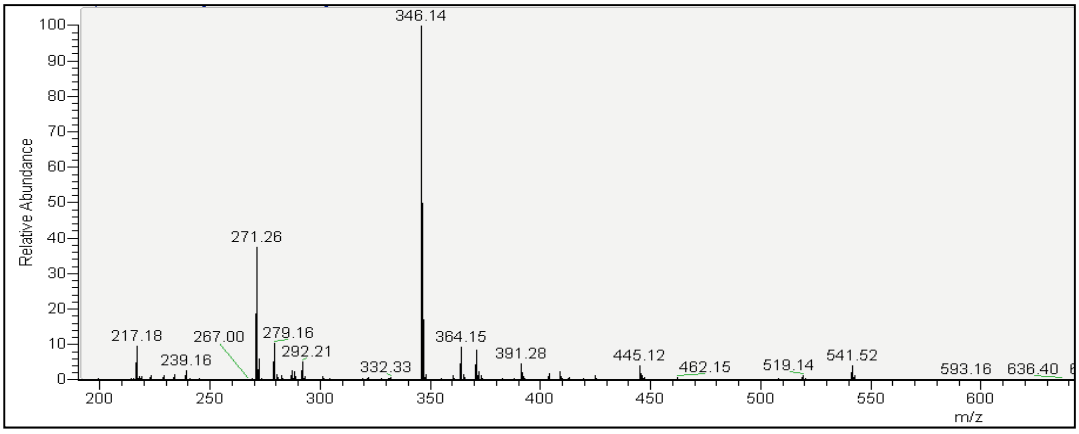

Figure 10-7: High resolution MS analysis of Peptide-2 highlighting the presence of an m/z 364.1 ion.

Fragmentation of the m/z 259.08 ion (Figure 10-8) formed an ion at m/z 242, which is a loss of an OH radical. Looking back at Figure 10-4, this confirmed that the m/z 241.10 ion was formed directly from the m/z 287.10 ion and not as a result of further fragmentation of the m/z 259.08 ion. There were also losses of C_5H_5ON and (OH• + CO).

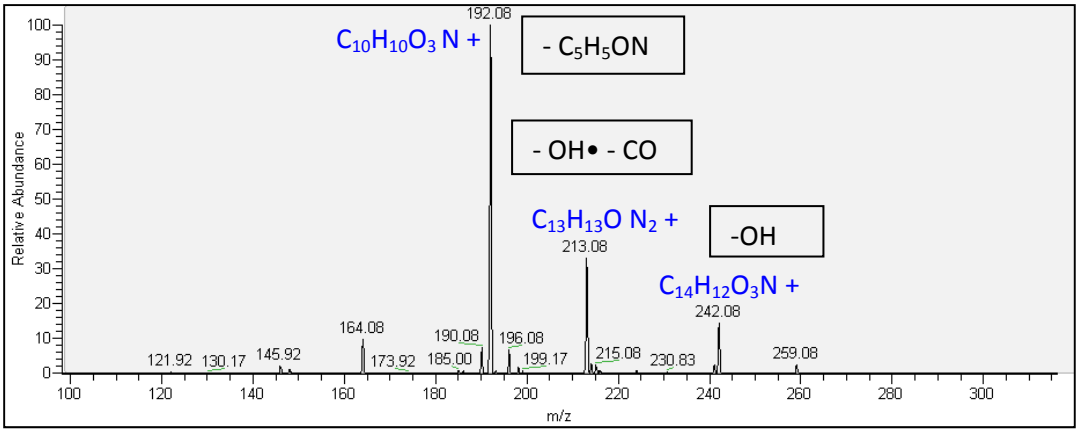

Figure 10-8: Fragmentation of UV-X m/z 259.08 ion.

Fragmentation of 241.08 $[M+H]^{1+}$ revealed further losses of CO and an OH radical.

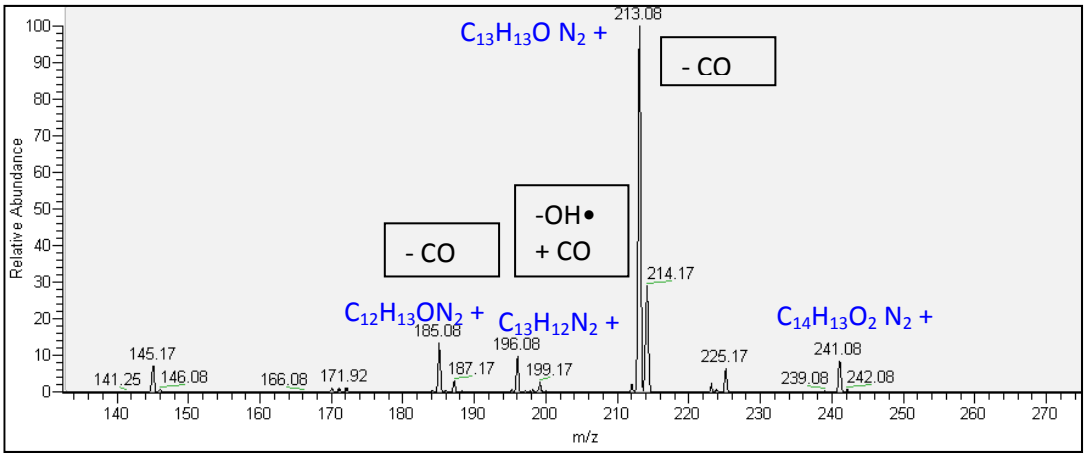

Figure 10-9: Fragmentation of UV-X m/z 241.08 ion.

A summary of the major fragmentation pathways of UV-X is shown in Figure 10-10.

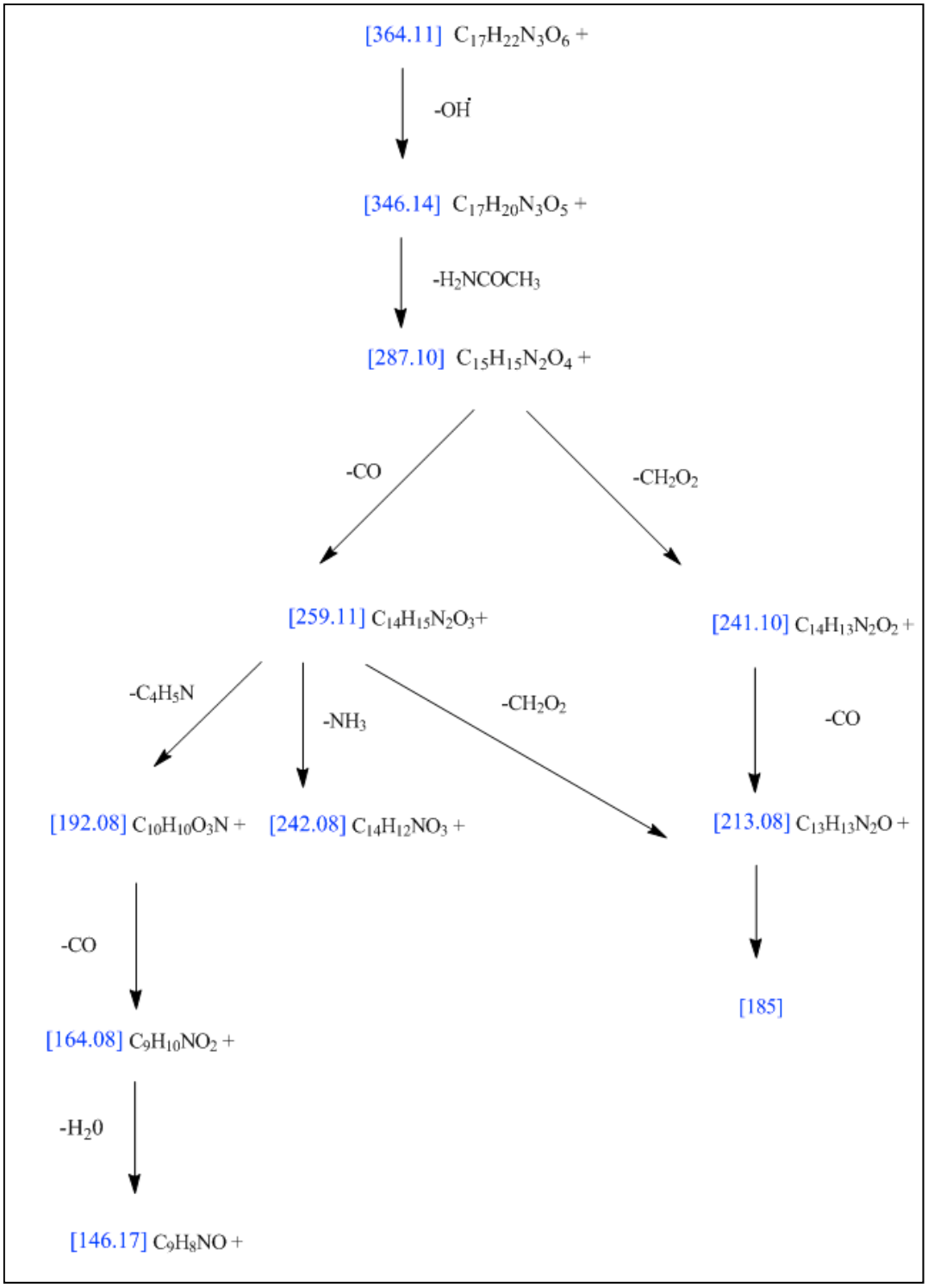

Figure 10-10: Summary of major fragmentation pathways of UV-X.

The facile neutral loss of a C_2H_5ON suggests the presence of an NH-acetyl group. Additionally the loss of (H_2O + CO) was indicative of a carboxylic acid (Figure 10-11).

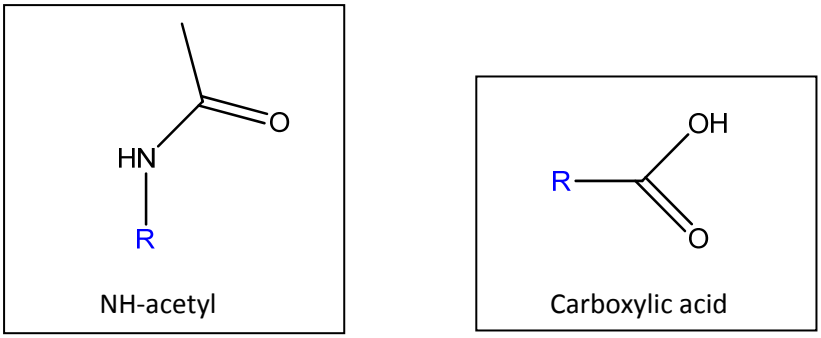

Figure 10-11: Functional groups of UV-X consistent with a UV filter such as *N*-acetyl 3OHKyn. (R ≠ H).

Both of these are also major fragmentation pathways of *N*-acetyl 3OH Kyn and *N*-acetyl Kyn [166, 292].The structural similarities of UV-X with *N*-acetyl 3OH Kyn suggested by MS/MS mass spectrometry are highlighted in blue in Figure 10-12.

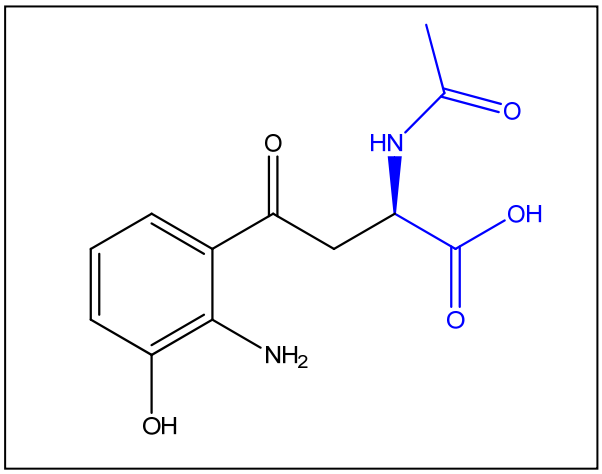

Figure 10-12: Structure of N-Acetyl 3OH Kyn. The similarities with UV-X are highlighted in blue.

The loss of a second carboxylic acid (OH• and CO), C_4H_5N and C_5H_5NO are not consistent with a typical UV filter and were assigned part of the "modified" portion of the structure (Figure 10-13).

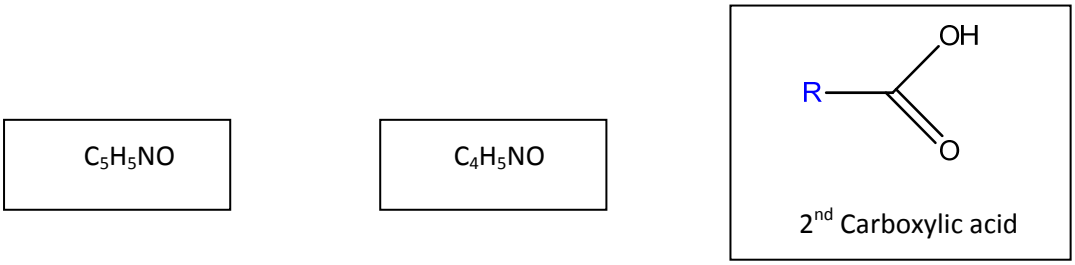

Figure 10-13: Functional groups of UV-X not consistent with a UV filter such as Acetyl 3OH Kyn. Structures are indicative only. Isomers of above structures are possible.

10.2 NMR analysis

NMR analysis was used to gain further structural information. 1D ^{1}H, 2D ^{1}H-TOCSY ^{13}C-^{1}H HSQC and ^{13}C HMBC scans were performed as detailed in the Materials and Methods Chapter. The NMR data is shown in Figures 1-11 to 1-16. The amount of sample available for analysis (< 100 µg) was right at the detection limits for 2D and ^{13}C carbon NMR spectroscopy and even using reduced volume 100 µl shigemi tubes to enhance the sample concentration, it still presented challenges.

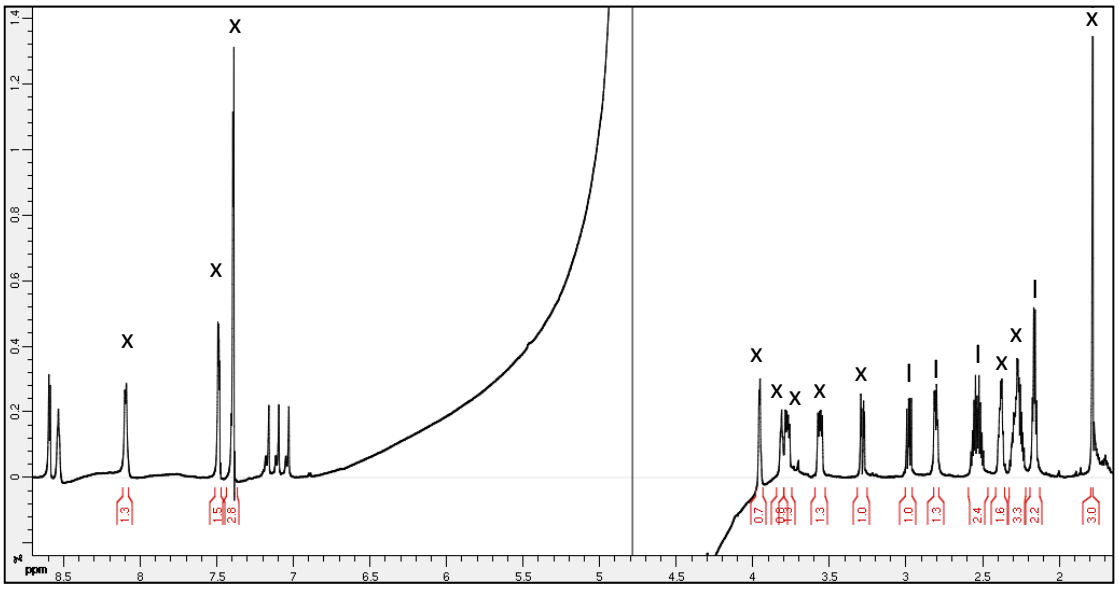

Figure 10-14: Integrated ^{1}H NMR spectrum of UV-X showing assignment of each peak as either UV-X(x) or the impurity (I).

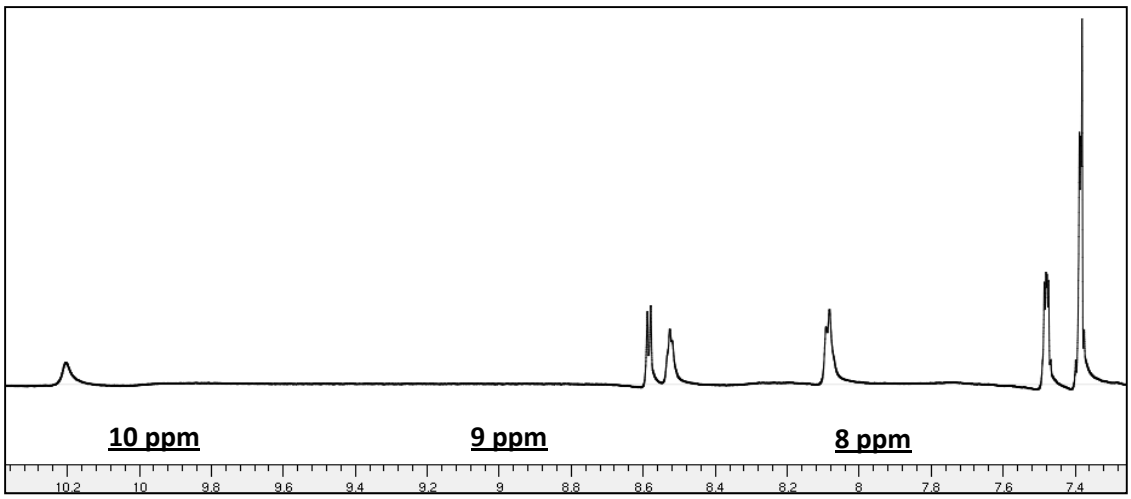

Figure 10-15: ^{1}H NMR spectrum (10.5 ppm to 7.3 ppm).

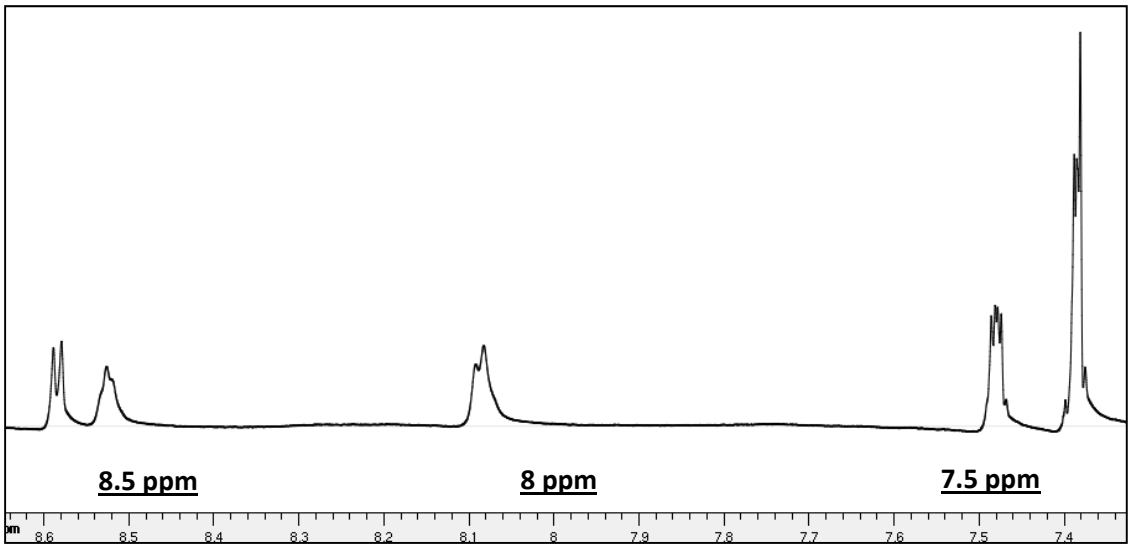

Figure 10-16: ^{1}H NMR spectrum (8.5 ppm to 7.3 ppm).

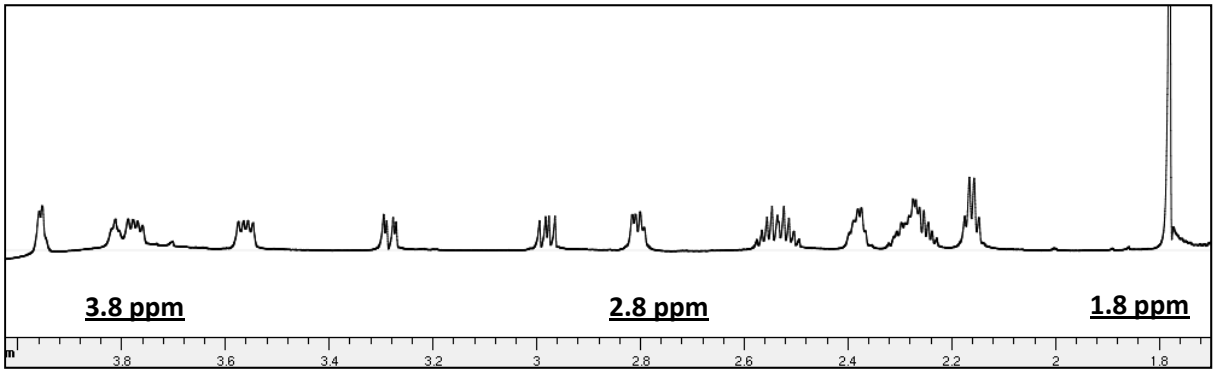

Figure 10-17: ^{1}H NMR spectrum (4 ppm to 1.7 ppm).

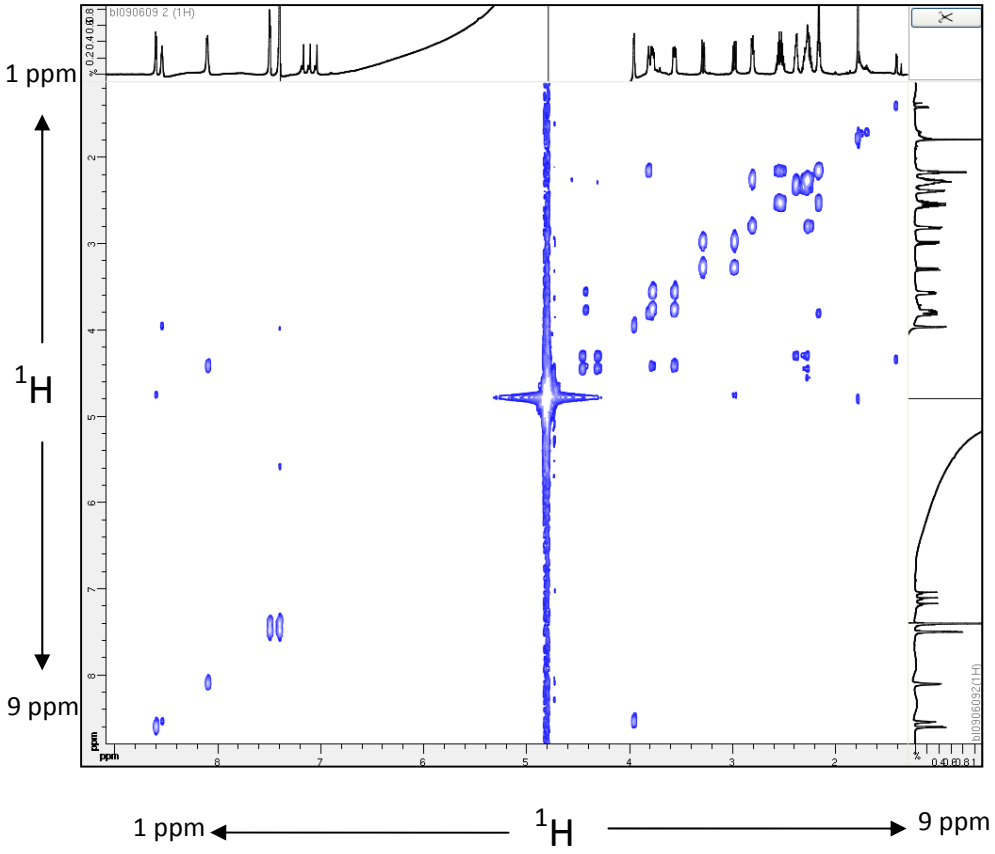

Figure 10-18: COSY spectrum (1 ppm to 9 ppm).

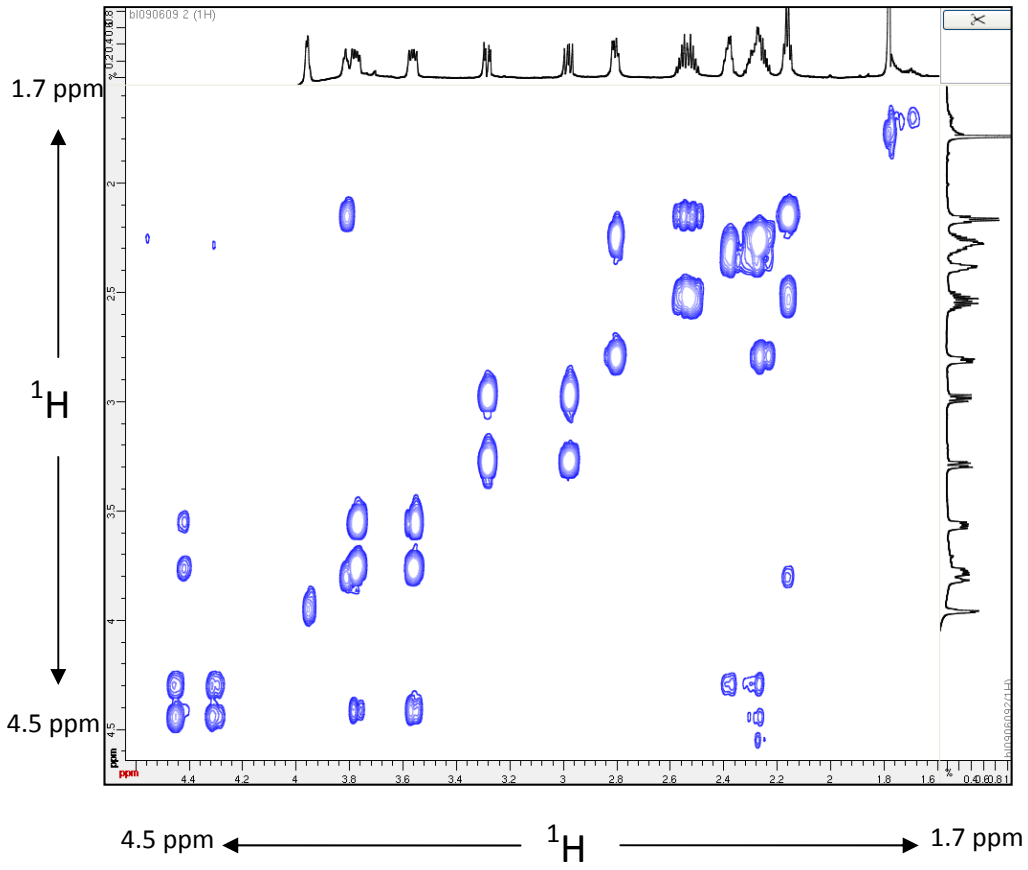

Figure 10-19: COSY spectrum (1.7 ppm to 4 ppm).

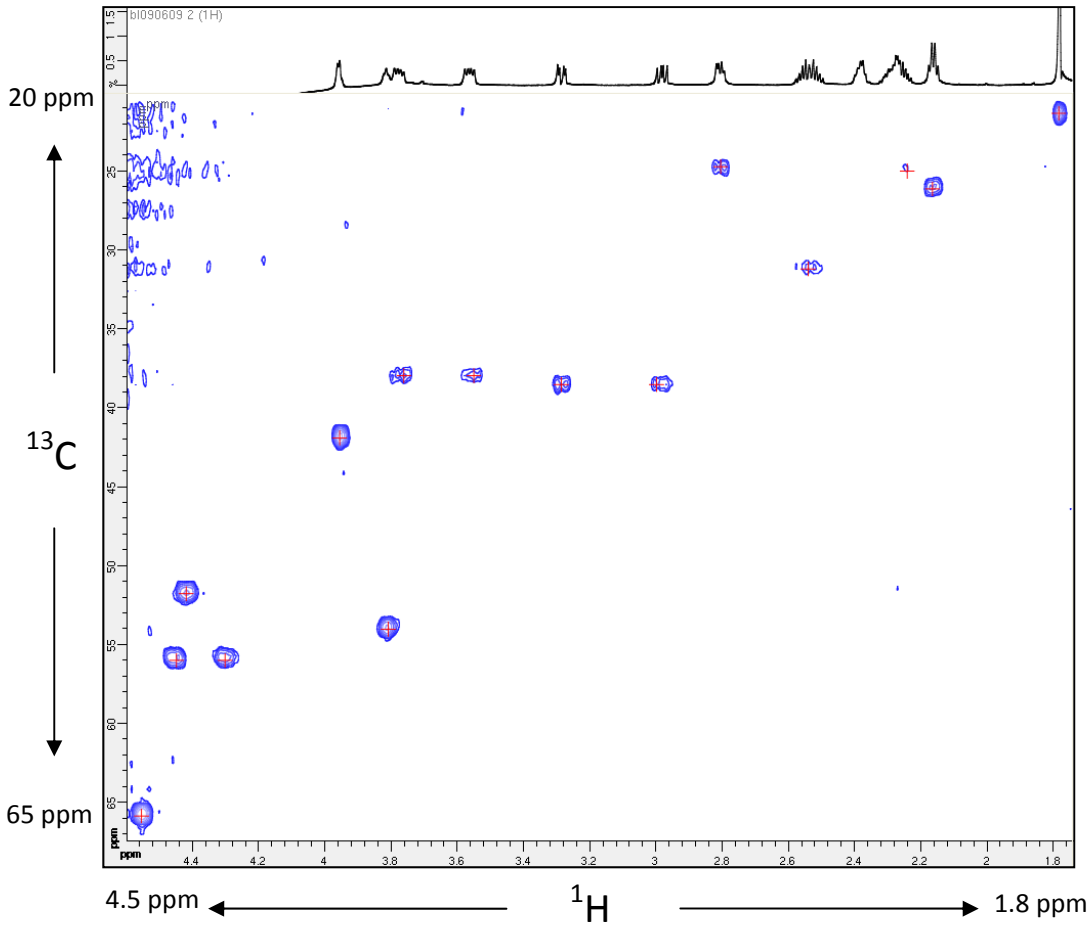

Figure 10-20: HSQC spectrum.

Upon examining the NMR data one thing that became apparent was that while UV-X eluted as one peak by HPLC, it actually contained two compounds in the ratio of 1: 1.3. This was determined by the relative integration of the various proton peaks (Figure 10-14). Analysis by ultra pressure liquid performance chromatography (UPLC) was then done to see if the two compounds could be resolved. Figure 10-21 shows the UPLC trace (219 nm) indicating that two compounds (Peak-A and Peak-B) were resolved (the peak at 0.2 minutes is part of the solvent front and not considered). 219 nm was chosen as both compounds absorbed in this region.

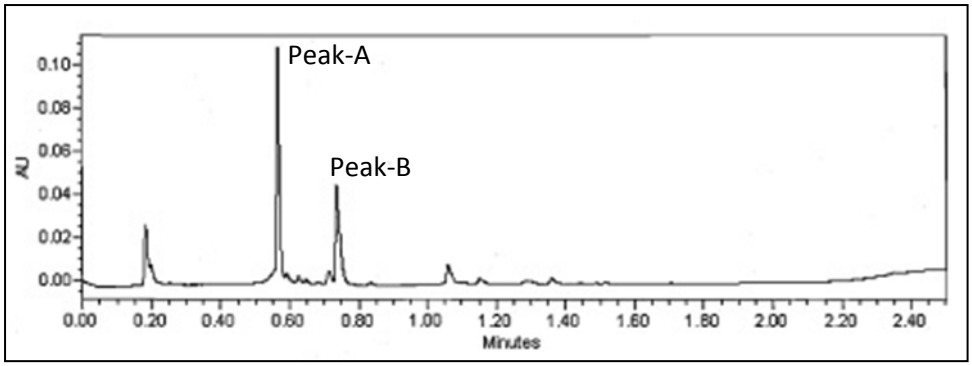

Figure 10-21: UPLC trace (219 nm) showing the resolution of two compounds.

An evaporative light scattering detector (ELSD) was also used to obtain an accurate ratio of the amount of Peak-A compared to Peak-B. It revealed that Peak-A and Peak-B were present in the ratio of 1: 1.3, which was comparable to the NMR data.

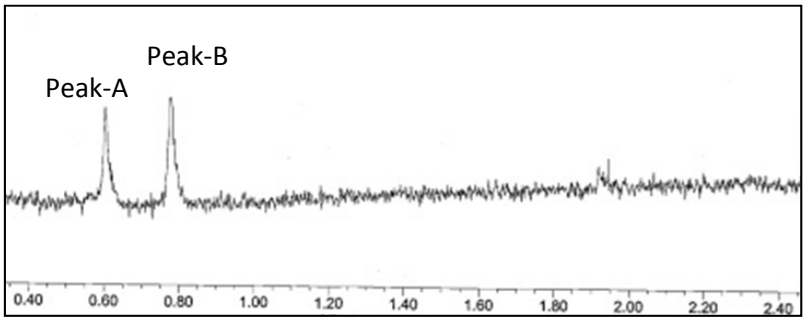

Figure 10-22: ELSD trace showing Peak-A and Peak-B present in the ratio of 1: 1.3.

The UV absorbance profiles of Peak-A and Peak-B are shown in Figure 10-23.

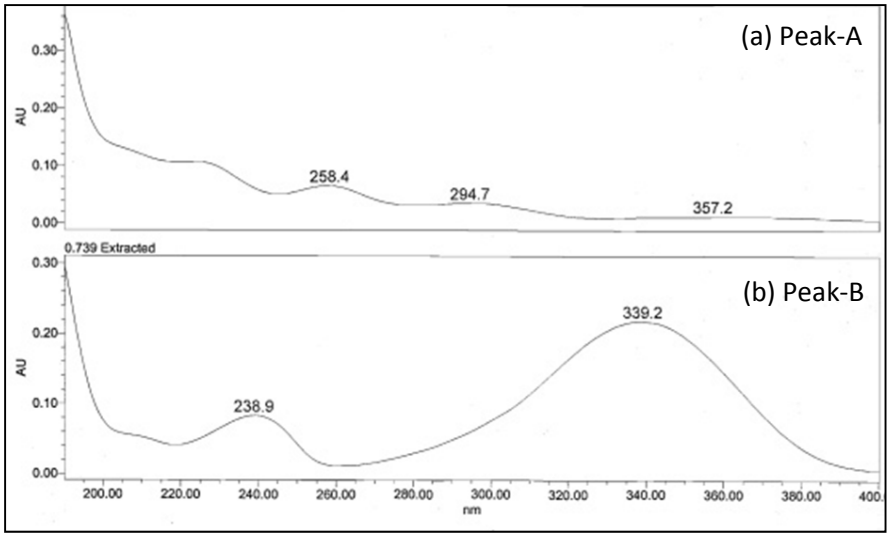

Figure 10-23: UV absorbance profile of (a) Peak-A and (b) Peak-B.

Peak B absorbed strongly in the ~340 nm range which is slightly lower than a typical UV filter such as Kyn and 3OHKyn which have an absorbance maximum of approximately 365 nm [282].This suggests some modification of the chromophoric structure of UV-X compared to a typical UV filter. Based on its UV absorbance profile, Peak-A was likely not a UV filter and its structure was therefore not further investigated. Unfortunately, it was not possible to purify the two compounds using the UPLC, so the NMR data was processed using the mixture.

The next step was to assign the NMR data to the empirical formula ($C_{17}H_{21}O_6N_3$) calculated from the mass spectrometric analysis of UV-X. While a range of 2D NMR experiments were obtained it was difficult to decipher the structural detail from each experiment in isolation. Instead the focus was to use the data to generate structures of various fragments of UV-X and then try and piece them together. For reasons that will be explained in more detail throughout the chapter, UV-X was considered as 3 fragments. The first fragment being the portion that has major similarities to a typical Kyn UV filter. The second fragment being the “aromatic” portion of the molecule and the third fragment being the “modified” portion of the UV filter, which was regarded as likely the addition of some other molecule to a known UV filter.

10.2.1 Fragment-1

As shown previously in

Figure 10-3 and Figure 10-4, the MS/MS data revealed part of the structure of UV-X had similarities with *N*-acetyl 3OHKyn. This fragment of the molecule was chosen as a good starting point and the NMR data was used to determine if other functional groups present in *N*-acetyl 3OH Kyn could be accounted for in UV-X. Analysis of the HSQC spectra (Figure 10-20) revealed two proton signals at 3.55 ppm (dd) and 3.75 ppm (dd) that correlated to a carbon at 38 ppm, strongly suggesting a methylene (CH_2) with two diastereotopic protons. In addition, a proton signal at 4.41 ppm correlated by HSQC to a carbon at 51.8 ppm, indicating a methine (CH). The methine at 4.41 ppm also had a COSY correlation (Figure 10-18) to the methylene. These correlations are indicated diagrammatically in Figure 10-24 and Figure 10-25.

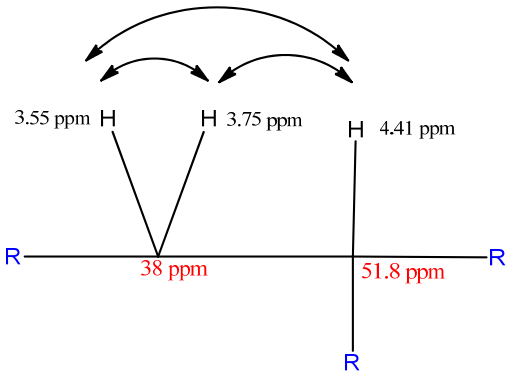

Figure 10-24: COSY correlations. (R ≠ H) .

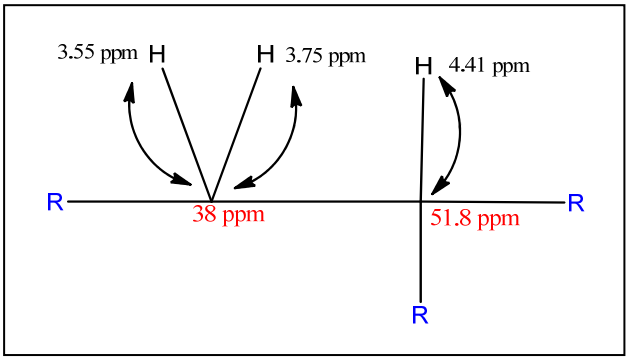

Figure 10-25: HSQC correlations. (R ≠ H).

The methine at 4.41 ppm also had a COSY (Figure 10-26) correlation with a proton signal at 8.09 ppm. The proton at 8.09 ppm did not have a HSQC signal (Figure 10-27), meaning it was not attached to a carbon atom. The methine at 4.41 ppm had a HMBC correlation to a carbon at 173 ppm, consistent with a carbonyl of an amide. Based on the fact that the mass spectra showed the loss of an *N*-acetyl group and the fact that the major UV lens filter found in the squirrel lens also had an *N*-acetyl, this group was assigned as the most likely option.

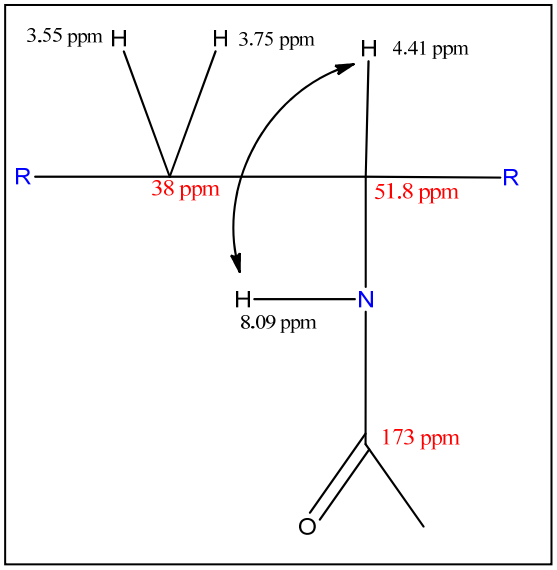

Figure 10-26: COSY correlation to NH. (R ≠ H).

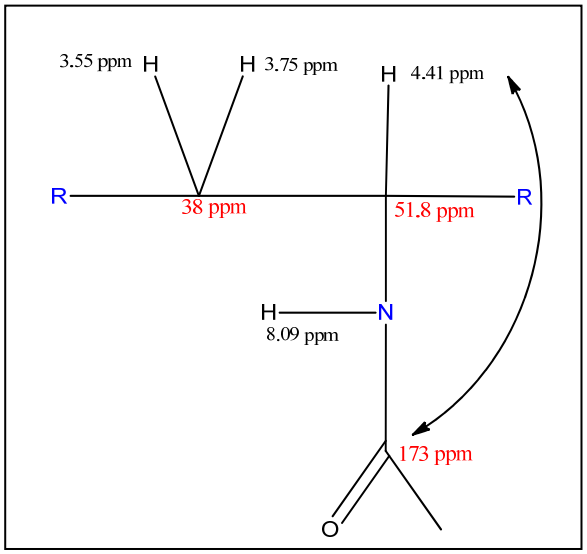

Figure 10-27: HMBC correlation to carbonyl group from N-acetyl.

The mass spectral fragmentation data revealed the presence of two carboxylic acids in UV-X. The methylene protons (3.55/3.75 ppm) had a HMBC correlation to a carbonyl at 176 ppm, which is within the expected range for a carboxylic acid. Given the similarity of this part of the structure to a typical UV filter, the following connectivity (Figure 10-28) was proposed.

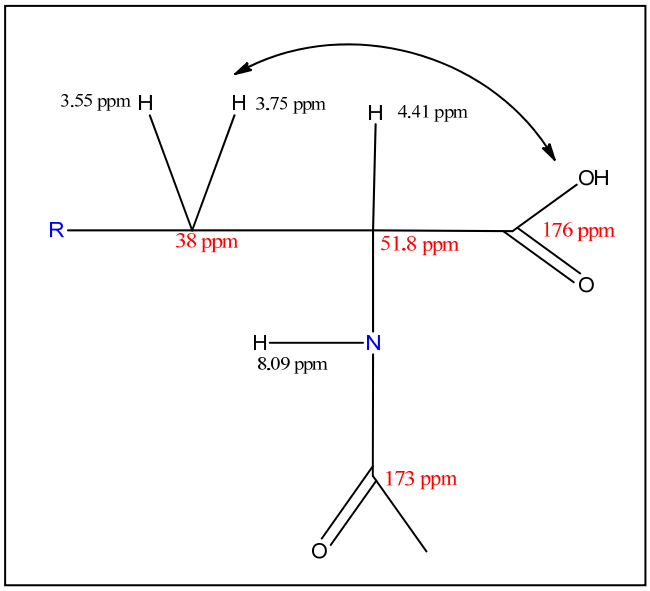

Figure 10-28: HMBC correlation to carboxylic acid.

Figure 10-29 shows the structural fragments confirmed by MS/MS and NMR in blue and the additional information provided by NMR alone in red. However, expected HMBC correlation between the methylene (3.55/3.75 ppm) and the methine (4.41 ppm) protons with a carbonyl at ~200 ppm (black arrows in Figure 10-29) were not observed. Standards of 3OHKyn were analysed by NMR using the same experimental conditions and showed that this correlation is readily detected should the carbonyl be present. Clearly the first major difference between UV-X and a conventional Kyn-based UV filter is the lack or modification of this carbonyl group in UV-X.

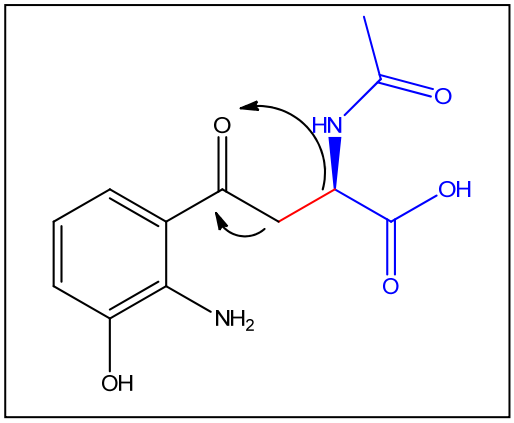

Figure 10-29: Similarities of UV-X to *N*-acetyl 3OH Kyn. The structure confirmed by MS/MS and NMR is shown in blue and the additional information provided by NMR alone is shown in red. The expected HMBC correlations shown with arrows were not observed.

10.2.2 Fragment-2

Due to its UV absorbance profile and its similarity to other UV filters it was deemed likely that UV-X contained an aromatic ring of some kind. Figure 10-30 shows a magnified section of the HSQC spectrum highlighting the aromatic region.

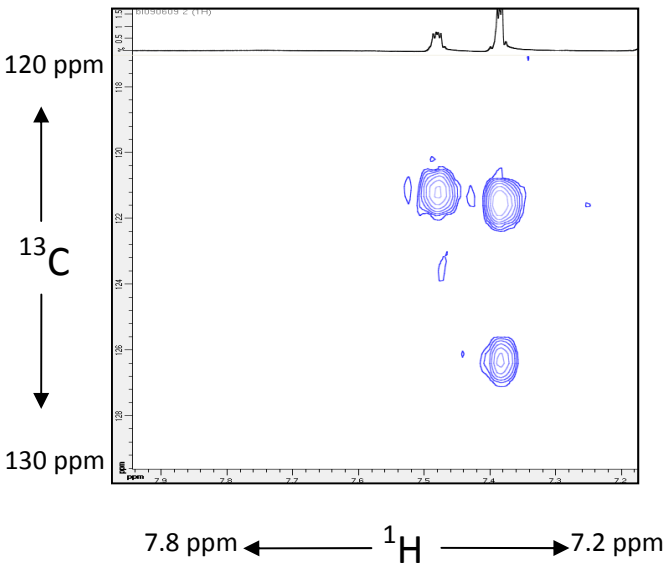

Figure 10-30: Aromatic region of UV-X from HSQC spectrum.

The presence of two ^{1}H peaks in this region (with an integration of 3), and the corresponding three ^{13}C signals seen in Figure 10-30, suggested three aromatic protons present in UV-X. Given the other structural similarities to UV filters seen in Fragment-1, the most likely scenario is a tri-substituted aromatic six membered ring. For this to be true, 3 additional carbon atoms must be observed in the HMBC spectrum, since a peak in a HMBC spectrum that is not present in the HSQC spectrum represents a carbon atom that does not have a hydrogen atom attached.

Figure 10-31 shows an overlay of the HSQC and HMBC spectra where the pink correlations represent the HSQC signals and the blue represent the HMBC signals. Only five unique aromatic carbons (*) in total were observed.

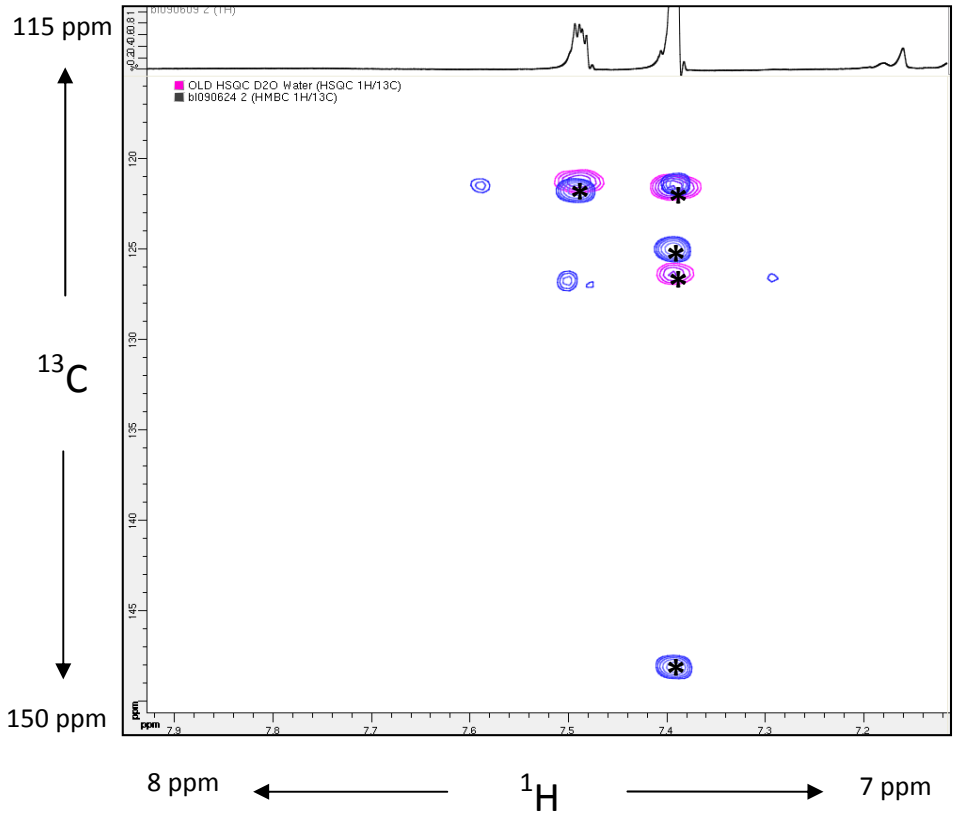

Figure 10-31: Overlay of HMBC and HSQC spectrum of aromatic region of UV-X. Unique carbon atoms are indicated by (*).

Four of the aromatic carbons had a chemical shift in the region of 120 – 128 ppm, with the remaining carbon having a chemical shift of 148 ppm, indicating that it may be attached to a nitrogen or oxygen [293]. At this point it was speculated that the sixth carbon signal was too weak to

be seen due to the limited amount of sample that was available for analysis. A potential structure for fragment-2 is shown in Figure 10-32.

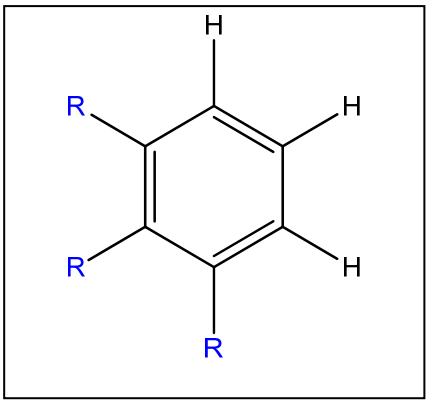

Figure 10-32: Aromatic ring of UV-X. (R ≠ H).

Given the abundance of *N*-acetyl 3OHKyn in the squirrel lens, a possible structure of the aromatic ring is shown in Figure 10-33.

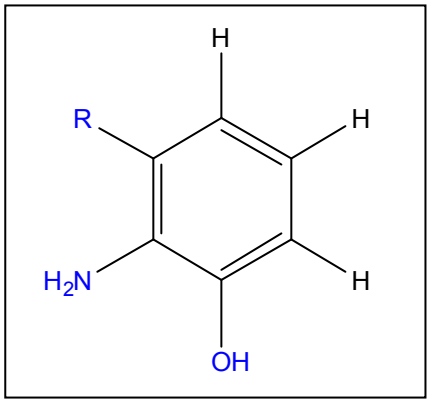

Figure 10-33: Possible aromatic ring of UV-X. R = rest of UV filter.

However there are a number of inconsistencies with the NMR spectra of UV-X that suggest the ring structure may be more complex (Figure 10-34). The coupling of the three protons in 3OH Kyn adopt the expected (d, dd, d) splitting pattern, but while UV-X also contains a tri-substituted ring, it is markedly different to that of 3OH Kyn. This may be due to the coincidental overlapping of two of the three protons in UV-X.

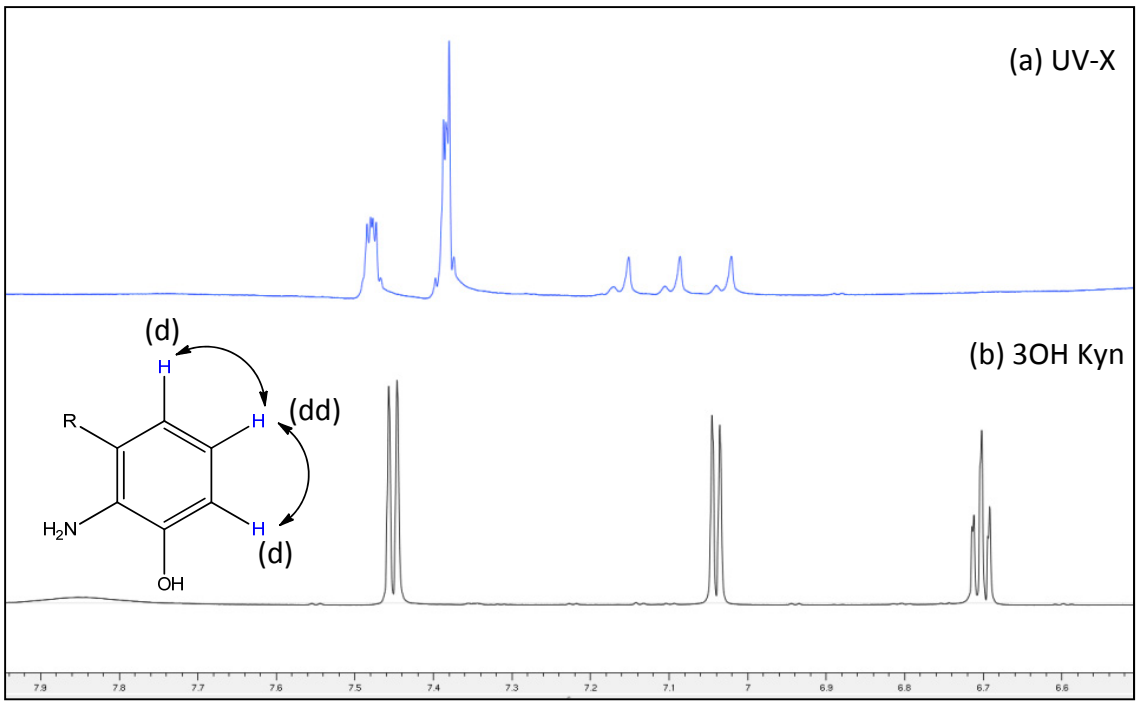

Figure 10-34: ^{1}H NMR spectra of the aromatic region of (a) UV-X and (b) 3OH Kyn showing the splitting patterns. (d) = doublet, (dd) = doublet of doublets.

Of the six aromatic carbons in 3OHKyn, four carbons had chemical shift in the 116 to 126 ppm region, which accounted for the three aromatic methine carbons and the quaternary carbon that links the aromatic ring to the rest of the UV filter (R in Figure 10-34). The carbons attached to the OH (phenolic) and amino group had chemical shifts in the 140 to 144 ppm region. Conversely UV-X showed four carbon signals n the ~ 116 to 126 ppm region and only one carbon signal with a chemical shift of 148 ppm, consistent with attachment to the OH or amino group. No other carbon signal was observed in the aromatic region. This suggested either the amino or phenolic group was missing, or modified, or simply overlaid with the other signal.

A phenolic group can be observed by ^{1}H NMR but due to chemical exchange it is often too broad to distinguish, so the fact that a broad peak was not observed in the proton spectra of UV-X was not sufficient evidence to rule out its presence. Additionally, should an amino group be present, its typical chemical shift would be in the ~5 ppm region, which would be swamped by the water suppression peak, so again it was not able to be ruled out at this stage.

10.2.3 Fragment-3

Fragment-3 was the most crucial piece of the puzzle. With Fragment- 1 and Fragment-2 bearing reasonable similarities to other UV filters, it was Fragment-3 that would define the unique structure of UV-X. Initial indications from the MS/MS fragmentation showing the neutral loss of C_4H_5N and C_5H_5NO suggested a 5 or 6 membered nitrogen containing ring. It is known from the mass spectrometry data that Fragment-3 also contained a carboxylic acid. The connectivity was assembled by mapping out the COSY and HMBC correlations indicated in Figure 10-35 and Figure 10-36. As can be seen, the structure proposed is a five membered nitrogen containing ring that connects to the rest of UV-X at two points indicated by R and R'.

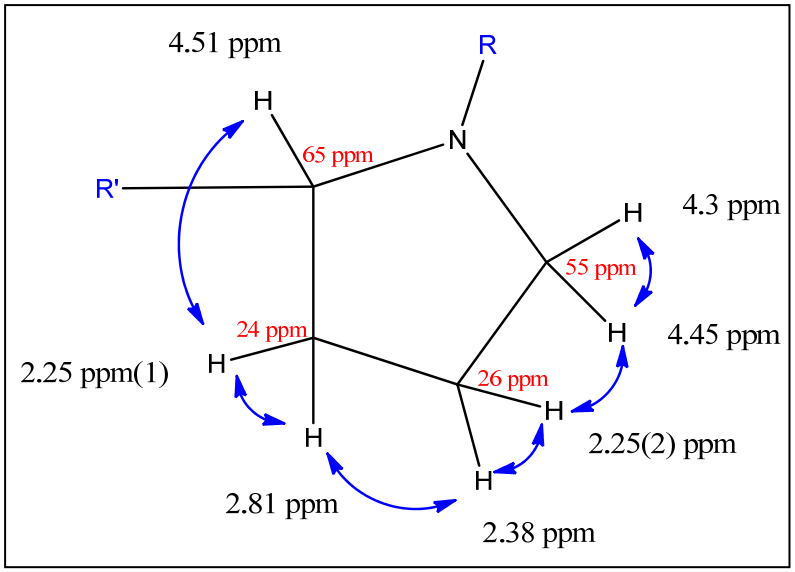

Figure 10-35: COSY correlations of UV-X fragment 3. (R and R' ≠ H).

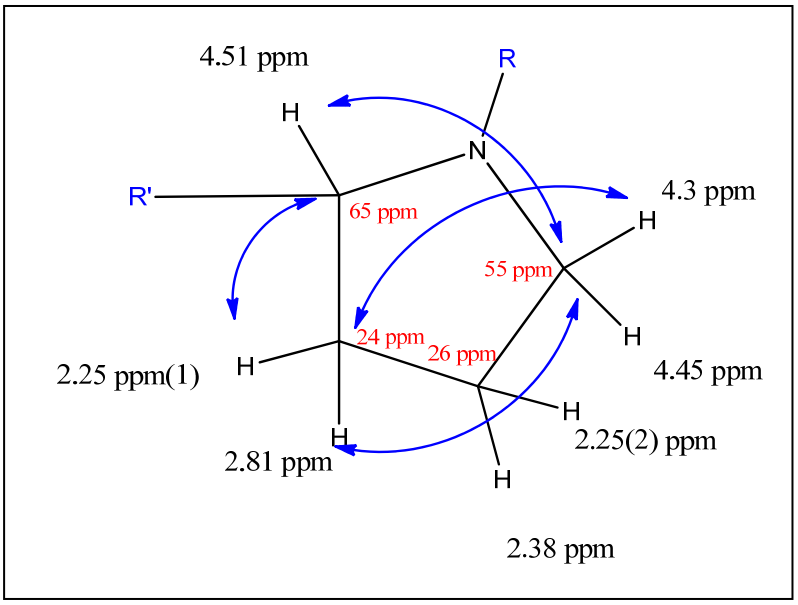

Figure 10-36: Major HMBC correlations of UV-X fragment 3. (R and R' ≠H).

10.3 Acid hydrolysis of UV-X

To help in the structural elucidation, it was decided to subject UV-X to acid hydrolysis (as per Section 2.4) to see if it was a hydrolysable compound and able to form characterisable fragments.

10.3.1 Results

Figure 10-37 show a HPLC trace of the products formed following incubation of UV-X in HCl at 100 °C for 2.5 hours. Two new products that absorbed at 360 nm were detected. Unfortunately analysis of these products by ESI mass spectrometry was not successful. This may have been due to salt contamination.

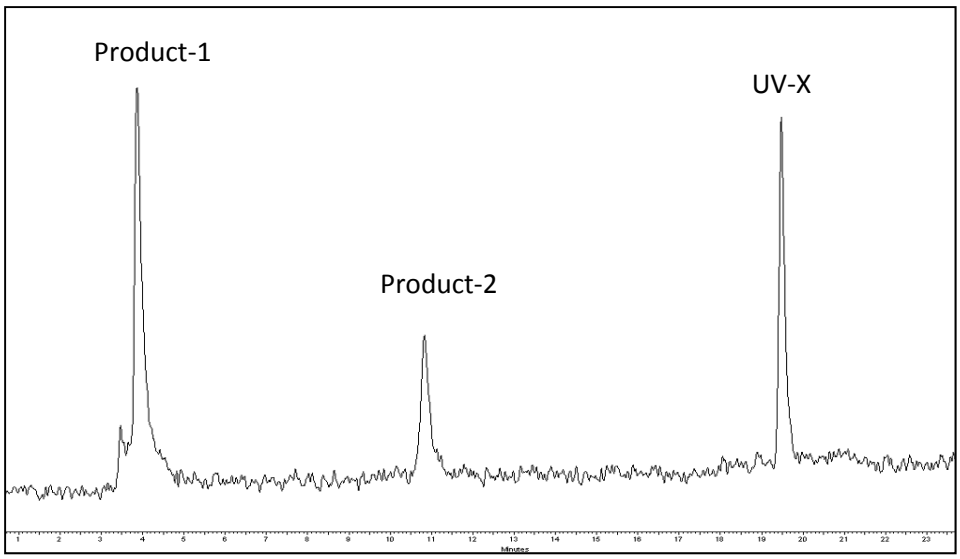

Figure 10-37: HPLC trace (360 nm) of the products formed following incubation of UV-X in 6M HCl at 100 °C for 2.5 hours.

10.4 Assembling the structure

With the basic structures of the 3 fragments assigned, the final challenge was to connect them together in way that agreed with the NMR and MS/MS observations.

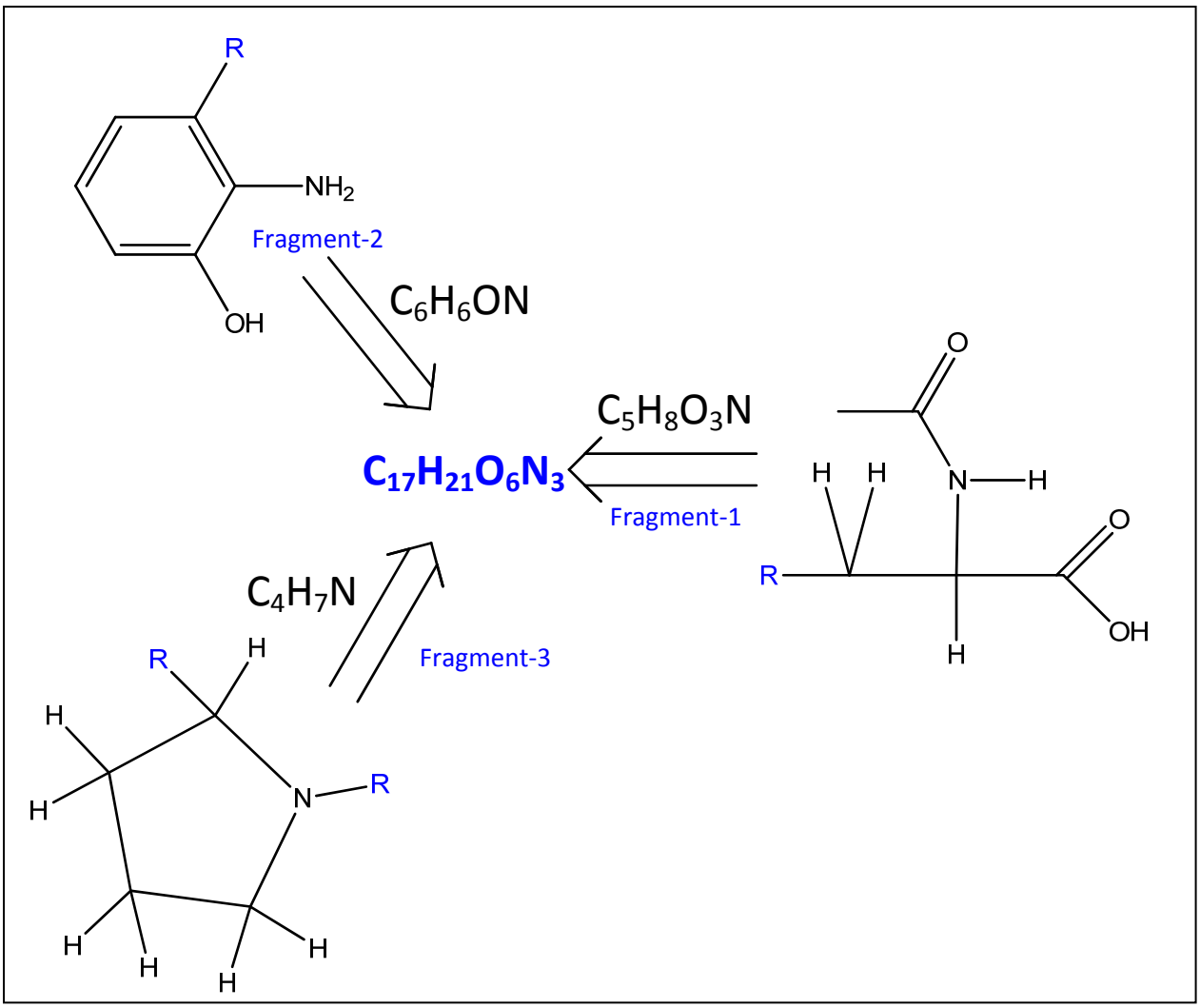

Figure 10-38: Diagram showing the assembly of the three fragments of UV-X. (R ≠ H). The three fragments above plus and additional C_2O_2 make up UV-X ($C_{17}H_{21}O_6N_3$).wa

The key structural information used to assemble the pieces of UV-X are:

(1) The carbonyl connecting Fragment-1 and the aromatic ring (Fragment-2) in a typical UV filter was missing or modified.

(2) Each of the three fragments had a HMBC correlation with a carbon at 176 ppm, which must be the carbon that connects the fragments.

(3) Fragment-3 had a HMBC correlation with a carbon at 167 ppm that was most likely a carboxylic acid given the mass spectrometry data revealed the presence of a second carboxylic acid.

In consultation with Professor Peter Karuso of Macquarie University the following has been proposed as the most likely UV-X structure.

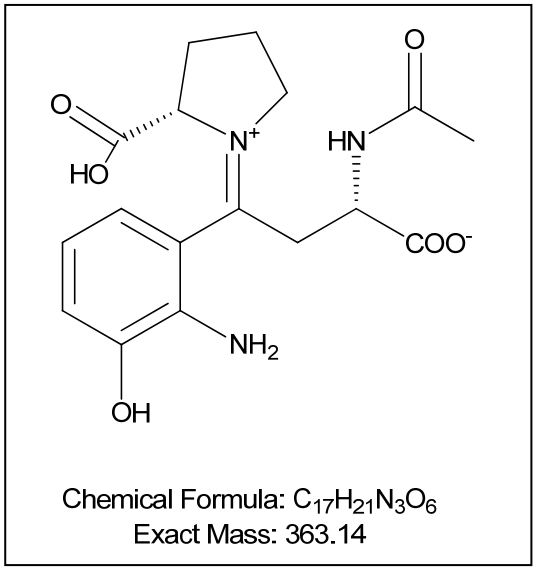

Figure 10-39: Proposed structure of UV-X.

10.5 Incubation studies

Due to time constraints it was not possible to attempt the synthesis of UV-X but it was speculated that it may potentially form from the direct addition of Pro to *N*-acetyl 3OH Kyn. While no data on the free amino acid content in the lens of the thirteen-lined ground squirrel is available, Pro is the most abundant free amino acid in the human and bovine lens [294]. Additionally, while the pK_{aH} value of Pro is comparable to that of Ala, its nucleophilic reactivity has been shown to be greater than that of all other amino acids, with the exception of cysteine, by several orders of magnitude

[295]. For this reason it was speculated that it may be possible to form UV-X by directly incubating *N*-acetyl 3OH Kyn with Pro at physiological pH as detailed in the Materials and Methods Chapter (Section 2.24).

10.5.1 Results

As can be seen in Figure 10-40, incubation of *N*-acetyl 3OHKyn either with or without Pro in 100mM phosphate buffer pH 7.4 did not show any evidence of forming an adduct matching the retention time of UV-X. Interestingly though, incubation of *N*-acetyl 3OHKyn in the presence of Pro appeared to make *N*-acetyl 3OHKyn more stable than when it was incubated in buffer alone. The reasons for this are as yet unknown and due to time constraints this will have to be investigated in future work.

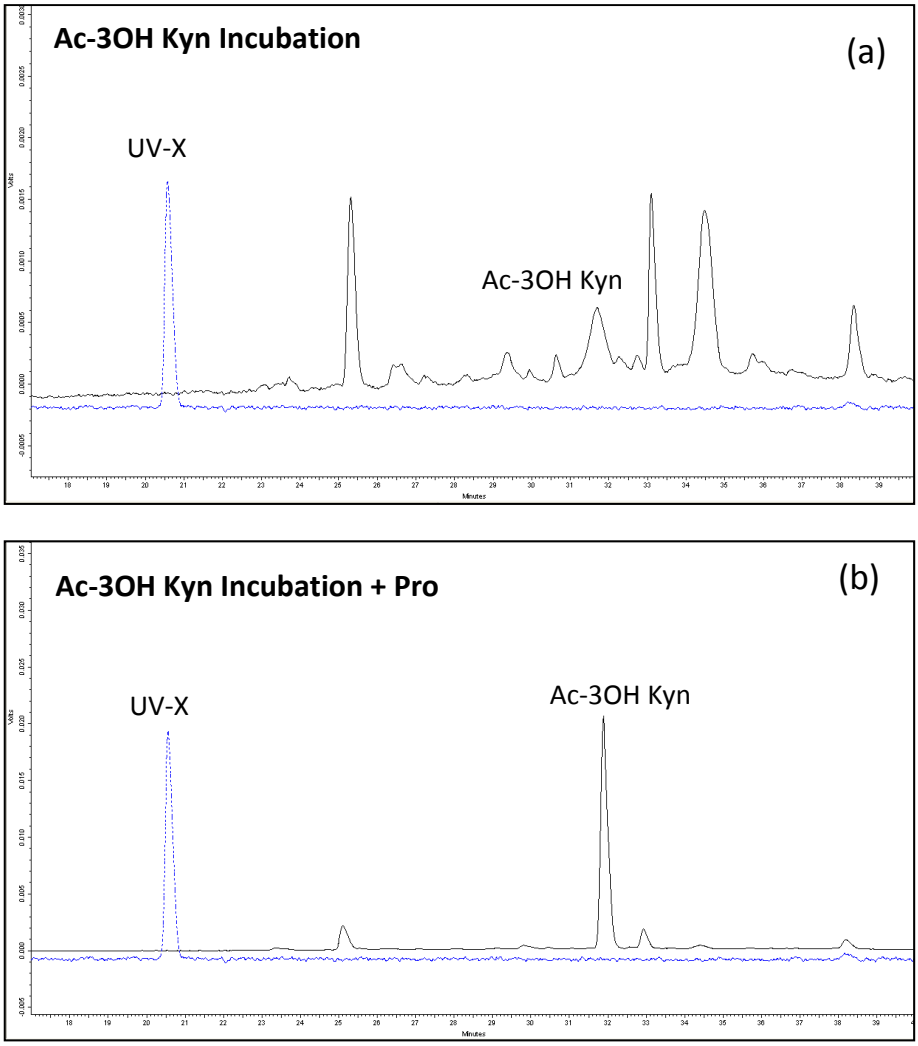

Figure 10-40: HPLC spectra (360 nm) of day-5 time point from (a) Ac- 3OHKyn incubation and (b) Ac-3OHKyn incubated with 10 equiv of Pro. Incubations were in 100 mM phosphate buffer pH 7.4 at 60 °C. An overlay showing the expected retention time of UV-X is shown with a blue dotted line.

10.6 Conclusions and future work

The proposed structure of UV-X correlated with all aspects of the MS and MS/MS data. It also correlated with the vast majority of the NMR data and given the small amounts available for analysis, inconsistencies were not surprising. While it was not possible to absolutely confirm the structure of UV-X, a number of key experiments are planned for future work that will hopefully provide the necessary additional proof. The first proposed experiment will involve the reduction of UV-X. One proposed method (based on Palmieri et al [296]) was used to reduce a similar molecule to

UV-X (Figure 10-41) with $NaBH_4$. $NaBH_4$ is a reducing agent and it should lead to the reduction of an imine bond should it be present in UV-X. This would then be easily detected by a difference of +2 Da following analysis by mass spectrometry, thus confirming the presence of an imine. In addition the UV spectrum should change substantially.

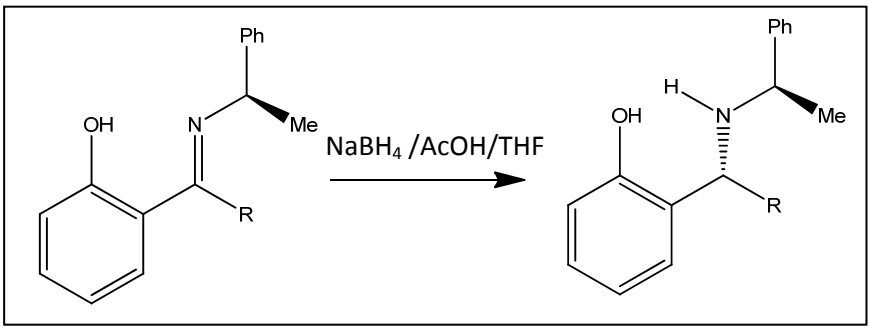

Figure 10-41: Reduction of imine bond using $NaBH_4$. Adapted from Palmieri et al [296].

The second proposed experiment will involve the incubation of N-acetyl 3OHKyn and Pro under conditions which promote the formation of an imine bond. One example by Yang et al uses microwave energy to directly form an imine *via* the reaction of a ketone and amine under solvent free conditions [297]. Another possibility involves the use of a Lewis acid catalyst in an apolar solvent, that should promote the formation of an imine bond [298].

11 Chapter 11: Conclusions

The age-dependent degradation of long-lived proteins in human lenses has been implicated in a range of ocular conditions including presbyopia and age-related nuclear cataract (ARNC) [299]. Denaturation of old proteins appears to result from the intrinsic instability of certain amino acids, and while some of these modifications have been documented, it is likely more remain to be elucidated. Research into the fundamental causes of these age-related conditions is essential so that non-surgical, cost effective treatment options can be developed. Understanding this process is also important for other age-related diseases [1]. The aim of this thesis was to investigate some of these degenerative reactions by incubating model peptides under physiologically relevant pHs, while using elevated temperatures to simulate the extended periods that long-lived lens proteins are exposed to.

The aim of Section-A of this thesis was to investigate the mechanism behind the apparent spontaneous truncation of long-lived lens proteins at the N-terminus of Ser residues. As age-related racemisation of Ser residues is also observed in the lens, it was proposed that these two modifications may be the result of a linked mechanism analogous to that of Asn. Model peptides based on lens αB-crystallin sequences were incubated at physiological pH and non-enzymatic truncation at the N-terminal of Ser, analogous to that seen in the lens, was demonstrated.

Additionally racemisation of internal Ser residues was shown to occur under the same conditions. However, exposure to elevated temperatures for extended periods was required to induce these modifications. While further studies are necessary, the results in this thesis suggest that these two modifications do not occur *via* a linked mechanism. The strongest evidence for this was that when the Ser OH group was blocked, truncation at the N-terminal of Ser was reduced but significant racemisation still occurred.

Another explanation of Ser racemisation was investigated by examining the potential for phosphoser (pSer) residues to form dehydroalanine (DHA) *via* beta elimination. It was proposed that addition of a water molecule to DHA could result in the formation of D- Ser. However, the results in this thesis suggest that this does not occur. While DHA was demonstrated to form at physiological pH, its stability, combined with the lack of any D-Ser formation, ruled out the addition of water to DHA as a cause of Ser racemisation.

The generation of DHA residues from pSer peptides at physiological pH does support the possibility of it occurring in long-lived proteins. Studies have shown that the prevalence of pSer groups in dentin phosphoproteins, which are long lived proteins found in teeth, decreases linearly with age [222, 223]. Additionally the location of pSer residues in some of the major long lived lens proteins has recently been characterised [224, 225]. Should the loss of phosphate groups from these proteins proceed in a similar manner to the model peptide studied in this thesis, then it is certainly conceivable that a significant amount of DHA could result. Reaction of these DHA residues with thiols and amines side chains may explain some of the non disulfide cross linking known to occur in aged lens protein [204, 214].

Section-B of this thesis examined a range of modifications at the N-termini of peptides, which were initially observed as side reactions that occurred when model peptides were incubated for Section-A. Diketopiperazine (dkp) formation involves the cleavage of a cyclic lactam from the N-terminus of a peptide. While the formation of a dkp has been shown to be a side reaction in peptide synthesis, to our knowledge it has been little studied in any detail as a degradation pathway of long-lived proteins. To address this, the potential for truncated lens crystallin fragments to further degrade *via* this process was examined.

For peptides with a penultimate Pro residue, degradation *via* dkp formation was shown to readily proceed, even at physiological temperatures. A number of other peptides that did not have a penultimate Pro residue were shown to degrade in a similar manner, although elevated temperature

was required. Based on the results in this thesis it is certainly conceivable that long-lived proteins, with a free amino terminus would be susceptible to degradation *via* dkp formation.

The second modification examined in this section was the novel racemisation of the N-terminal amino acid. This was shown to readily occur under physiological conditions and with several amino acid residues. An interesting finding in relation to this was that L-amino acids consistently racemised faster than their D- amino acid counterparts. As this and other findings could not be explained by simple loss and re-addition of the alpha proton, a novel mechanism involving the formation of a cyclic Schiff base was proposed.

This concept was then expanded to determine if long-lived proteins could be susceptible to similar modifications. It was found that 28% of the N-terminal Met residue of AQPO, isolated from the nucleus of five lens pairs (ages 67-69) had racemised. Conversely only 13% of the cortex (which is the newer part of the lens) N-terminal residue was found to have racemised. These results may have significant implications for other long-lived proteins found in the lens and also for those in other tissues e.g. the brain and heart. While the exact consequences are yet to be investigated, preliminary analysis confirmed that a D- amino acid at the N-terminus is less susceptible to enzymatic degradation, thus potentially playing a protective role.

The final modification examined in Section-B was the loss of the N-terminal amino acid residue. While this was also demonstrated to occur under physiological conditions across a range of N-terminal amino acids, the data does suggest that it may be accelerated by phosphate buffer. Phosphate buffer has been shown to behave as a nucleophile and incubation of peptides in buffers other than phosphate resulted in a significant reduction (or elimination) of this modification. However it is important to note that the lens contains sodium phosphate and it is still possible that this could occur in long-lived proteins.

Recent publications have described the accumulation of low molecular weight crystallin fragments in the lens. Many of these exhibit a “laddering” type effect with the loss of sequential amino acid residues from the N-terminal, similar to that observed with the model peptides studied in this chapter.

Section-C of this thesis involved the purification and characterisation of a new UV filter found in the lens of the thirteen-lined ground squirrel. Its structure was of interest due to the lens of the thirteen-lined ground squirrel having a similar UV filter composition to that found in the human lens. As mentioned in the introduction chapter of this thesis, UV filters are subject to age-related modifications e.g. oxidation or deamination. An interesting feature of the major UV filters found in the lens of the thirteen-lined ground squirrel is that they contain an acetyl group on the non aromatic amine. This prevents deamination from occurring, thus preventing the UV filter from binding to lens proteins through its side chain.

Due to the small quantities available for analysis, this study proved extremely challenging. Despite this, a potential structure that agrees with the majority of the analytical data has been proposed. Attempts were made to synthesise the compound but due to time constraints this will need to done at a later stage. The structure of the unknown UV filter is described as a proline adduct of N-acetyl 3OH Kynurenine, produced *via* the formation of an imine between the proline nitrogen and the carbonyl of the UV filter. Future work will involve synthesis of the proposed UV filter to assess if it is the correct structure.

The major challenge with many of the experiments detailed in this thesis was that it was usually not possible to study each modification in isolation. Often the modifications were competing reactions and this made accurate quantification difficult. It is important to note that one aim of this thesis was to demonstrate the potential for these modifications to occur under physiological conditions rather than to provide an accurate account of the rates. Another challenge was that while the use of elevated temperatures has often been used to simulate the effects ageing, it could be argued that

some of these modifications may not occur at 37 °C. Where possible this was examined by using physiological temperature, but due to the decades that long-lived proteins exist before displaying many age-related modifications, this was often not practical. It should also be recognised that conditions in the test tube are not the same as those in the cell. In cells proteins, membranes and other metabolites are present that may facilitate some reactions.

The modifications studied in this thesis may have implications for a wide range of long-lived proteins [1] . In addition to the lens, long-lived proteins are found at many other sites in the human body e.g. the brain, the heart. This thesis suggests that analysis of other long-lived proteins for evidence of age-related N-terminal racemisation and other modifications is certainly warranted. Further analysis into the potential of DHA residues to form protein cross links is also of interest. An overview of the modifications studied in this thesis and their relationship to each other is shown in Figure 11-1. It is likely that rather than one specific modification, many of the age-related conditions are the result of a combination of these and other modifications. Understanding more about these processes is crucial to our understanding of the aging process, and may be an important step towards finding a solution to the many age-related conditions.

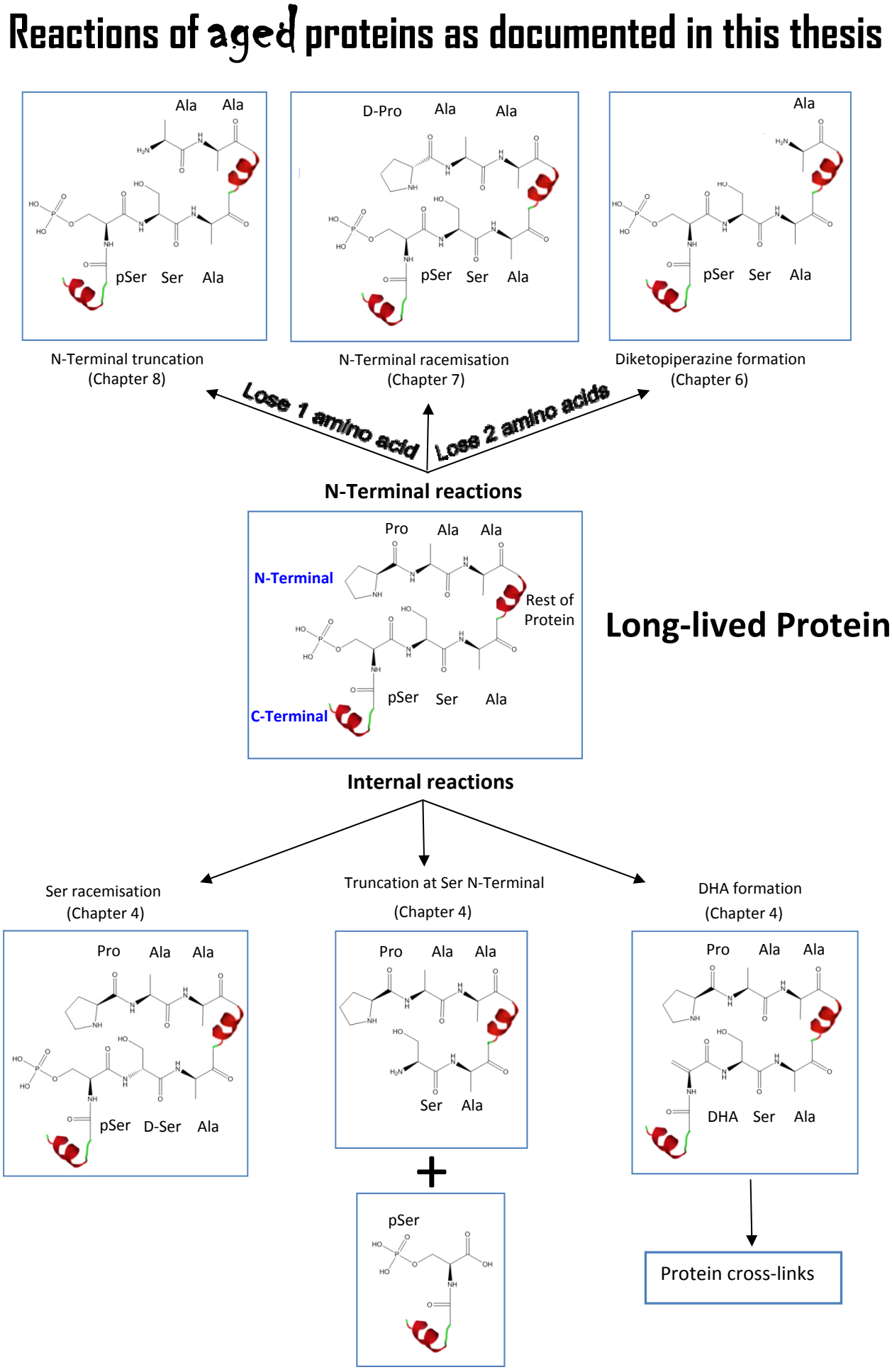

Figure 11-1: Overview of modifications studied in this thesis

References:

1. Truscott, R.J.W., *Are ancient proteins responsible for the age-related decline in health and fitness?* Rejuvenation Res., 2010. **13**: p. 83-89.
2. Su, S.-P., J.D. McArthur, R.J.W. Truscott, and J.A. Aquilina, *Truncation, cross-linking and interaction of crystallins and intermediate filament proteins in the aging human lens.* Biochim. Biophys. Acta,, 2011. **1814**(5): p. 647-656.
3. Gordois, A., L. Pezzullo, and H. Cutler, *The global economic cost of visual impairment.* Access Economics, 2010.
4. Access Economics, *The Economic Impact of Vision Loss in Australia in 2009.* 2010. **2010a**.
5. West, S., *Epidemiology of cataract: accomplishments over 25 years and future directions.* Ophthalmic Epidemiol., 2007. **14**(4): p. 173-178.
6. Brian, G. and H. Taylor, *Cataract blindness – challenges for the 21st century.* Bulletin of the World Health Organization, 2001. **79**: p. 249-256.
7. Australian Institute of Health and Welfare, *http://www.aihw.gov.au/mediacentre/2005/mr20050722.cfm*. 2005.
8. Michael, R. and A.J. Bron, *The ageing lens and cataract: a model of normal and pathological ageing.* Philos T Roy Soc B, 2011. **366**(1568): p. 1278-1292.
9. Taylor, H.R., *Epidemiology of age-related cataract.* Eye (Lond), 1999. **13 (Pt 3b)**: p. 445-8.
10. Toh, T.Y., J. Morton, J. Coxon, and M.J. Elder, *Medical treatment of cataract.* Clin Experiment Ophthalmol, 2007. **35**(7): p. 664-671.
11. Owsley, C., G. McGwin, K. Scilley, C.A. Girkin, J.M. Phillips, and K. Searcey, *Perceived barriers to care and attitudes about vision and eye care: focus groups with older African Americans and eye care providers.* Invest Ophthalmol Vis Sci, 2006. **47**: p. 2797-802.
12. Snellingen, T., B.R. Shrestha, M.P. Gharti, J.K. Shrestha, M.P. Upadhyay, and R.P. Pokhrel, *Socioeconomic barriers to cataract surgery in Nepal: the South Asian cataract management study.* Br J Ophthalmol, 1998. **82**: p. 1424-8.
13. Garry, B. and T. Hugh, *Cataract blindness – challenges for the 21st century.* Bulletin of the World Health Organization, 2001. **79**(3).
14. Congdon, N.G., D.S. Friedman, and T. Lietman, *Important causes of visual impairment in the world today.* JAMA, 2003. **290**: p. 2057-60.
15. WebMD. *http://www.webmd.com/eye-health/picture-of-the-eyes*. 2012 [cited 2012 27th March].
16. Opthobook. *http://www.ophthobook.com/*. 2012 [cited 2012 3rd July].
17. Harding, J.J., *Cataract: biochecmistry, epidemiology and pharmacology.* Chapman and Hall, 1991.
18. Harding, J.J., *Lens* 1997: Chapman & Hall. 94-134.
19. *http://www.photobiology.info/Roberts.html*. [cited 2012 9th March].
20. Bassnett, S., J.R. Kuszak, L. Reinisch, H.G. Brown, and D.C. Beebe, *Intercellular communication between epithelial and fiber cells of the eye lens.* J Cell Sci, 1994. **107 (Pt 4)**: p. 799-811.
21. Lee, A., J.S. Morrow, and V.M. Fowler, *Caspase remodeling of the spectrin membrane skeleton during lens development and aging.* J. Biol. Chem., 2001. **276**: p. 20735-20742.
22. Shestopalov, V.I. and S. Bassnett, *Expression of autofluorescent proteins reveals a novel protein permeable pathway between cells in the lens core.* J. Cell Sci., 2000. **113**: p. 1913-1921.
23. Lynnerup, N., H. Kjeldsen, S. Heegaard, C. Jacobsen, and J. Heinemeier, *Radiocarbon dating of the human eye lens crystallines reveal proteins without carbon turnover throughout life.* PLoS One, 2008. **3**(1): p. e1529.

24. Bloemendal, H., *The vertebrate eye lens. A useful system for the study of fundamental biological processes on a molecular level.* Science, 1977. **197**(4299): p. 127-138.
25. Strenk, S.A., L.M. Strenk, and J.F. Koretz, *The mechanism of presbyopia.* Prog Retin Eye Res, 2005. **24**: p. 379-93.
26. Helmholtz, H.V., *Accomodation of the eyes.* Graefes Arch Clin Exp Ophthalmol, 1855. **1**: p. 1-70.
27. Strenk, S.A., J.L. Semmlow, L.M. Strenk, P. Munoz, J. Gronlund-Jacob, and J.K. DeMarco, *Age-related changes in human ciliary muscle and lens: a magnetic resonance imaging study.* Invest Ophthalmol Vis Sci, 1999. **40**: p. 1162-9.
28. Fagerholm, P.P., B.T. Philipson, and B. Lindstrom, *Normal human lens - the distribution of protein.* Exp Eye Res, 1981. **33**: p. 615-20.
29. Fisher, R.F. and B.E. Pettet, *Presbyopia and the water content of the human crystalline lens.* J. Physiol., 1973. **234**(2): p. 443-447.
30. Bloemendal, H., W. de Jong, R. Jaenicke, N.H. Lubsen, C. Slingsby, and A. Tardieu, *Ageing and vision: structure, stability and function of lens crystallins.* Prog Biophys Mol Bio, 2004. **86**(3): p. 407-485.
31. Bron, A.J., G.F. Vrensen, J. Koretz, G. Maraini, and J.J. Harding, *The ageing lens.* Ophthalmologica, 2000. **214**(1): p. 86-104.
32. Santhoshkumar, P., M. Raju, and K.K. Sharma, *αA-Crystallin Peptide SDRDKFVIFLDVKHF accumulating in aging lens impairs the function of alpha crystallin and induces lens protein aggregation.* PLoS ONE, 2011. **6**(4): p. e19291.
33. Usha P, A., *Crystallins in the eye: Function and pathology.* Prog Retin Eye Res, 2007. **26**(1): p. 78-98.
34. Delaye, M. and A. Tardieu, *Short-range order of crystallin proteins accounts for eye lens transparency.* Nature, 1983. **302**(5907): p. 415-417.
35. Benedek, G.B., J. Pande, G.M. Thurston, and J.I. Clark, *Theoretical and experimental basis for the inhibition of cataract.* Prog Retin Eye Res, 1999. **18**(3): p. 391-402.
36. de Jong, W.W., W. Hendriks, J.W.M. Mulders, and H. Bloemendal, *Evolution of eye lens crystallins: the stress connection.* Trends Biochem. Sci., 1989. **14**(9): p. 365-368.
37. Groenen, P.J.T.A., K.B. Merck, J.W.W. De, and H. Bloemendal, *Structure and modifications of the junior chaperone α-crystallin. From lens transparency to molecular pathology.* Eur. J. Biochem., 1994. **225**: p. 1-19.
38. Horwitz, J., *Alpha-crystallin.* Exp Eye Res, 2003. **76**(2): p. 145-153.
39. Peschek, J., N. Braun, T.M. Franzmann, Y. Georgalis, M. Haslbeck, S. Weinkauf, and J. Buchner, *The eye lens chaperone α-crystallin forms defined globular assemblies.* Proc. Nat. Acad. Sci., 2009.
40. Ma, Z., S.R.A. Hanson, K.J. Lampi, L.L. David, D.L. Smith, and J.B. Smith, *Age-related changes in human lens crystallins identified by HPLC and mass spectrometry.* Exp Eye Res, 1998. **67**(1): p. 21-30.
41. Horwitz, J., M.P. Bova, L. Ding, D.A. Haley, and P.L. Stewart, *Lens α-crystallin: Function and structure.* Eye, 1999. **13**(3b): p. 403-408.
42. Kato, K., H. Shinohara, N. Kurobe, S. Goto, Y. Inaguma, and K. Ohshima, *Immunoreactive αA crystallin in rat non-lenticular tissues detected with a sensitive immunoassay method.* Biochim. Biophys. Acta, Protein Struct. Mol. Enzymol., 1991. **1080**: p. 173-80.
43. Bhat, S.P. and C.N. Nagineni, *αB subunit of lens-specific protein α-crystallin is present in other ocular and non-ocular tissues.* Biochem. Biophys. Res. Commun., 1989. **158**: p. 319-25.
44. Iwaki, T., A. Kume-Iwaki, and J.E. Goldman, *Cellular distribution of alpha B-crystallin in non-lenticular tissues.* J Histochem Cytochem, 1990. **38**: p. 31-9.
45. de Jong, W.W., G.-J. Caspers, and J.A.M. Leunissen, *Genealogy of the α-crystallin—small heat-shock protein superfamily.* International Journal of Biological Macromolecules, 1999. **22**(3-4): p. 151-162.

46. Carver, J., A. Rekas, D. Thorn, and M. Wilson, *Small heat-shock proteins and clusterin: Intra- and extracellular molecular chaperones with a common mechanism of action and function?* IUBMB Life, 2003. **55**: p. 661-668.
47. Horwitz, J., *Alpha-crystallin can function as a molecular chaperone.* Proc. Natl. Acad. Sci. U. S. A., 1992. **89**(21): p. 10449-10453.
48. Laganowsky, A., J.L.P. Benesch, M. Landau, L. Ding, M.R. Sawaya, D. Cascio, Q. Huang, C.V. Robinson, J. Horwitz, and D. Eisenberg, *Crystal structures of truncated alphaA and alphaB crystallins reveal structural mechanisms of polydispersity important for eye lens function.* Protein Sci. **19**(5): p. 1031-1043.
49. Bagneris, C., O.A. Bateman, C.E. Naylor, N. Cronin, W.C. Boelens, N.H. Keep, and C. Slingsby, *Crystal structures of α-crystallin domain dimers of αB-crystallin and Hsp20.* J. Mol. Biol., 2009. **392**(5): p. 1242-1252.
50. Lubsen, N.H., H.J.M. Aarts, and J.G.G. Schoenmakers, *The evolution of lenticular proteins: the β- and γ-crystallin super gene family.* Prog. Biophys. Mol. Biol., 1988. **51**: p. 47-76.
51. Andley, U.P., *Crystallins in the eye: function and pathology.* Prog. Retinal Eye Res., 2007. **26**: p. 78-98.
52. van Montfort, R.L.M., O.A. Bateman, N.H. Lubsen, and C. Slingsby, *Crystal structure of truncated human βB1-crystallin.* Protein Science, 2003. **12**(11): p. 2606-2612.
53. Hanson, S.R.A., D.L. Smith, and J.B. Smith, *Deamidation and disulfide bonding in human lens γ-crystallins.* Exp. Eye Res., 1998. **67**: p. 301-312.
54. Ueda, Y., M.K. Duncan, and L.L. David, *Lens proteomics: the accumulation of crystallin modifications in the mouse lens with age.* Invest Ophthalmol Vis Sci, 2002. **43**: p. 205-15.
55. Den, D.J.T., R.J.M. Moormann, N.H. Lubsen, and J.G.G. Schoenmakers, *Concerted and divergent evolution within the rat γ-crystallin gene family.* J. Mol. Biol., 1986. **189**: p. 37-46.
56. Lampi, K.J., Z. Ma, M. Shih, T.R. Shearer, J.B. Smith, D.L. Smith, and L.L. David, *Sequence analysis of βA3, βB3, and βA4 crystallins completes the identification of the major proteins in young human lens.* J. Biol. Chem., 1997. **272**(4): p. 2268-2275.
57. Scharf, J., A. Dovrat, and D. Gershon, *Defective superoxide-dismutase molecules accumulate with age in human lenses.* Graefe's Arch. Clin. Exp. Ophthalmol., 1987. **225**: p. 133-6.
58. Charlton, J.M. and R. van Heyningen, *Glucose 6-phosphate dehydrogenase in the mammalian lens.* Exp Eye Res, 1971. **11**(2): p. 147-60.
59. Dovrat, A., J. Scharf, and D. Gershon, *Glyceraldehyde 3-phosphate dehydrogenase activity in rat and human lenses and the fate of enzyme molecules in the aging lens.* Mech Ageing Dev, 1984. **28**(2-3): p. 187-91.
60. Zhu, X., A. Korlimbinis, and R.J.W. Truscott., *Age-dependent denaturation of enzymes in the human lens: A paradigm for organismic aging?* Rejuvenation Res., 2010. **13**(5): p. 553-560.
61. Borchman, D. and M.C. Yappert, *Lipids and the ocular lens.* J. Lipid Res., 2010. **51**: p. 2473-2488.
62. Hughes, J.R., J.M. Deeley, S.J. Blanksby, F. Leisch, S.R. Ellis, R.J.W. Truscott, and T.W. Mitchell, *Instability of the cellular lipidome with age.* Age (Dordr).
63. Byrdwell, W.C. and D. Borchman, *Liquid chromatography/mass-spectrometric characterization of sphingomyelin and dihydrosphingomyelin of human lens membranes.* Ophthalmic Res., 1997. **29**: p. 191-206.
64. Deeley, J.M., J.A. Hankin, M.G. Friedrich, R.C. Murphy, R.J.W. Truscott, T.W. Mitchell, and S.J. Blanksby, *Sphingolipid distribution changes with age in the human lens.* J. Lipid Res., 2010. **51**(9): p. 2753-2760.
65. Borchman, D., M.C. Yappert, and M. Afzal, *Lens lipids and maximum lifespan.* Exp. Eye Res., 2004. **79**: p. 761-768.
66. Singer, S.J. and G.L. Nicolson, *The fluid mosaic model of the structure of cell membranes.* Science, 1972. **175**(4023): p. 720-731.

67. Yappert, M.C., M. Rujoi, D. Borchman, and D.B. DuPre, *Dihydrosphingomyelin in Primate Lens Membranes: Correlation with Lens Growth.* Invest. Ophthalmol. Vis. Sci., 2003. **44**(5): p. 4480-.
68. Iwata, J.L., L.G. Bardygula-Nonn, T. Glonek, and J.V. Greiner, *Interspecies comparisons of lens phospholipids.* Curr Eye Res, 1995. **14**: p. 937-41.
69. Deeley, J.M., T.W. Mitchell, X.J. Wei, J. Korth, J.R. Nealon, S.J. Blanksby, and R.J.W. Truscott, *Human lens lipids differ markedly from those of commonly used experimental animals.* Biochim. Biophys. Acta,, 2008. **1781**(6-7): p. 288-298.
70. Taylor, V.L., K.J. al-Ghoul, C.W. Lane, V.A. Davis, J.R. Kuszak, and M.J. Costello, *Morphology of the normal human lens.* Invest Ophthalmol Vis Sci, 1996. **37**: p. 1396-410.
71. Bok, D., J. Dockstader, and J. Horwitz, *Immunocytochemical localization of the lens main intrinsic polypeptide (MIP26) in communicating junctions.* J. Cell Biol., 1982. **92**: p. 213-20.
72. Verkman, A.S., J. Ruiz-Ederra, and M.H. Levin, *Functions of aquaporins in the eye.* Prog. Retinal Eye Res., 2008. **27**: p. 420-433.
73. Goodenough, D.A., J.A. Goliger, and D.L. Paul, *Connexins, connexons, and intercellular communication.* Annu. Rev. Biochem., 1996. **65**: p. 475-502.
74. Liu, J., J. Xu, S. Gu, B.J. Nicholson, and J.X. Jiang, *Aquaporin 0 enhances gap junction coupling via its cell adhesion function and interaction with connexin 50.* J Cell Sci. **124**(2): p. 198-206.
75. Yang, B. and A.S. Verkman, *Water and glycerol permeabilities of aquaporins 1-5 and MIP determined quantitatively by expression of epitope-tagged constructs in Xenopus oocytes.* J. Biol. Chem., 1997. **272**: p. 16140-16146.
76. Chandy, G., G.A. Zampighi, M. Kreman, and J.E. Hall, *Comparison of the water transporting properties of MIP and AQP1.* J. Membr. Biol., 1997. **159**: p. 29-39.
77. Nemeth-Cahalan, K.L. and J.E. Hall, *pH and calcium regulate the water permeability of aquaporin 0.* J. Biol. Chem., 2000. **275**: p. 6777-6782.
78. Zampighi, G.A., S. Eskandari, and M. Kreman, *Epithelial organization of the mammalian lens.* Exp. Eye Res., 2000. **71**: p. 415-435.
79. Mathias, R.T., G. Riquelme, and J.L. Rae, *Cell to cell communication and pH in the frog lens.* J Gen Physiol, 1991. **98**: p. 1085-103.
80. Gonen, T., Y. Cheng, J. Kistler, and T. Walz, *Aquaporin-0 membrane junctions form upon proteolytic cleavage.* J. Mol. Biol., 2004. **342**: p. 1337-1345.
81. Berry, V., P. Francis, S. Kaushal, A. Moore, and S. Bhattacharya, *Missense mutations in MIP underlie autosomal dominant "polymorphic" and lamellar cataracts linked to 12q.* Nat. Genet., 2000. **25**: p. 15-17.
82. Shiels, A., S. Bassnett, K. Varadaraj, R. Mathias, K. Al-Ghoul, J. Kuszak, D. Donoviel, S. Lilleberg, G. Friedrich, and B. Zambrowicz, *Optical dysfunction of the crystalline lens in aquaporin-0-deficient mice.* Physiol. Genomics, 2001. **7**: p. 179-186.
83. Fotiadis, D., L. Hasler, D.J. Muller, H. Stahlberg, J. Kistler, and A. Engel, *Surface tongue-and-groove contours on lens MIP facilitate cell-to-cell adherence.* J. Mol. Biol., 2000. **300**: p. 779-789.
84. Ball, L.E., D.L. Garland, R.K. Crouch, and K.L. Schey, *Post-translational modifications of aquaporin 0 (AQP0) in the normal human lens: spatial and temporal occurrence.* Biochemistry, 2004. **43**: p. 9856-9865.
85. Korlimbinis, A., Y. Berry, D. Thibault, K.L. Schey, and R.J.W. Truscott, *Protein aging: Truncation of aquaporin 0 in human lens regions is a continuous age-dependent process.* Exp. Eye Res., 2009. **88**: p. 966-973.
86. Schey, K.L., M. Little, J.G. Fowler, and R.K. Crouch, *Characterization of human lens major intrinsic protein structure.* Invest Ophthalmol Vis Sci, 2000. **41**: p. 175-82.
87. Shiels, A., J.M. King, D.S. Mackay, and S. Bassnett, *Refractive defects and cataracts in mice lacking lens intrinsic membrane protein-2.* Invest Ophthalmol Vis Sci, 2007. **48**: p. 500-8.

88. Arneson, M.L. and C.F. Louis, *Structural arrangement of lens fiber cell plasma membrane protein MP20.* Exp. Eye Res., 1998. **66**: p. 495-509.
89. Chen, T., X. Li, Y. Yang, A.G. Erdene, and R.L. Church, *Does lens intrinsic membrane protein MP19 contain a membrane-targeting signal?* Mol. Vision, 2003. **9**: p. 735-746.
90. Tenbroek, E., M. Arneson, L. Jarvis, and C. Louis, *The distribution of the fiber cell intrinsic membrane proteins MP20 and connexin46 in the bovine lens.* J. Cell Sci., 1992. **103**: p. 245-57.
91. Gonen, T., P. Donaldson, and J. Kistler, *Galectin-3 is associated with the plasma membrane of lens fiber cells.* Invest Ophthalmol Vis Sci, 2000. **41**: p. 199-203.
92. Grey, A.C., M.D. Jacobs, T. Gonen, J. Kistler, and P.J. Donaldson, *Insertion of MP20 into lens fibre cell plasma membranes correlates with the formation of an extracellular diffusion barrier.* Exp Eye Res, 2003. **77**: p. 567-74.
93. Gong, X., C. Cheng, and C.-h. Xia, *Connexins in lens development and cataractogenesis.* J. Membr. Biol., 2007. **218**: p. 9-12.
94. Yeager, M., V.M. Unger, and M.M. Falk, *Synthesis, assembly and structure of gap junction intercellular channels.* Curr Opin Struct Biol, 1998. **8**: p. 517-24.
95. Beyer, E.C., J. Kistler, D.L. Paul, and D.A. Goodenough, *Antisera directed against connexin43 peptides react with a 43-kD protein localized to gap junctions in myocardium and other tissues.* J. Cell Biol., 1989. **108**: p. 595-605.
96. Rong, P., X. Wang, I. Niesman, Y. Wu, L.E. Benedetti, I. Dunia, E. Levy, and X. Gong, *Disruption of Gja8 (α8 connexin) in mice leads to microphthalmia associated with retardation of lens growth and lens fiber maturation.* Development (Cambridge, U. K.), 2002. **129**: p. 167-174.
97. Sellitto, C., L. Li, and T.W. White, *Connexin50 is essential for normal postnatal lens cell proliferation.* Invest Ophthalmol Vis Sci, 2004. **45**: p. 3196-202.
98. Mathias, R.T., T.W. White, and X. Gong, *Lens gap junctions in growth, differentiation, and homeostasis.* Physiol Rev, 2010. **90**(1): p. 179-206.
99. Fleishman, S.J., V.M. Unger, M. Yeager, and N. Ben-Tal, *A calpha model for the transmembrane α helices of gap junction intercellular channels.* Mol. Cell, 2004. **15**(6): p. 879-888.
100. Perng, M.-D., Q. Zhang, and R.A. Quinlan, *Insights into the beaded filament of the eye lens.* Exp. Cell Res., 2007. **313**: p. 2180-2188.
101. Ramaekers, F.C.S., L.G. Poels, P.H.K. Jap, and H. Bloemendal, *Simultaneous demonstration of microfilaments and intermediate-sized filaments in the lens by double immunofluorescence.* Exp. Eye Res., 1982. **35**: p. 363-9.
102. Geisler, N. and K. Weber, *Isolation of polymerization-competent vimentin from porcine eye lens tissue.* FEBS Lett., 1981. **125**: p. 253-6.
103. Kibbelaar, M.A., A.M.E. Selten-Versteegen, I. Dunia, E.L. Benedetti, and H. Bloemendal, *Actin in mammalian lens.* Eur. J. Biochem., 1979. **95**: p. 543-9.
104. Ramaekers, F.C.S. and H. Bloemendal. *Cytoskeletal and contractile structures in lens cell differentiation*. 1981: Wiley.
105. Sandilands, A., A.R. Prescott, J.M. Carter, A.M. Hutcheson, R.A. Quinlan, J. Richards, and P.G. FitzGerald, *Vimentin and CP49/filensin form distinct networks in the lens which are independently modulated during lens fiber cell differentiation.* J. Cell Sci., 1995. **108**: p. 1397-406.
106. Hood, B.D., B. Garner, and R.J.W. Truscott, *Human lens coloration and aging: evidence for crystallin modification by the major ultraviolet filter, 3-hydroxy-kynurenine O-β-D-glucoside.* J. Biol. Chem., 1999. **274**: p. 32547-32550.
107. Bova, L.M., M.H. Sweeney, J.F. Jamie, and R.J. Truscott, *Major changes in human ocular UV protection with age.* Invest Ophthalmol Vis Sci, 2001. **42**: p. 200-5.

108. Botting, N.P., *Chemistry and neurochemistry of the kynurenine pathway of tryptophan metabolism.* Chem. Soc. Rev., 1995. **24**(6): p. 401-412.
109. Heyningen R, V., *Fluorescent glucoside in the human lens.* Nature (London), 1971. **230**: p. 393-4.
110. Wood, A.M. and R.J.W. Truscott, *UV filters in human lenses: Tryptophan catabolism.* Exp. Eye Res., 1993. **56**: p. 317-25.
111. Wood, A.M. and R.J.W. Truscott, *Ultraviolet filter compounds in human lenses: 3-Hydroxykynurenine glucoside formation.* Vision Res., 1994. **34**: p. 1369-74.
112. Truscott, R.J.W., A.M. Wood, J.A. Carver, M.M. Sheil, G.M. Stutchbury, J.L. Zhu, and G.W. Kilby, *A new UV-filter compound in human lenses.* FEBS Letters, 1994. **348**(2): p. 173-176.
113. Mizdrak, J., P.G. Hains, R.J. Truscott, J.F. Jamie, and M.J. Davies, *Tryptophan-derived ultraviolet filter compounds covalently bound to lens proteins are photosensitizers of oxidative damage.* Free Radic Biol Med, 2008. **44**(6): p. 1108-19.
114. Dillon, J. and S.J. Atherton, *Time resolved spectroscopic studies on the intact human lens.* Photochem. Photobiol., 1990. **51**: p. 465-8.
115. Dillon, J., R.H. Wang, and S.J. Atherton, *Photochemical and photophysical studies on human lens constituents.* Photochem. Photobiol., 1990. **52**: p. 849-54.
116. Davies, M.J. and R.J.W. Truscott, *Photo-oxidation of proteins and its role in cataractogenesis.* J. Photochem. Photobiol., B, 2001. **63**: p. 114-125.
117. Hooi, M. and R. Truscott, *Racemisation and human cataract. D-Ser, D-Asp/Asn and D-Thr are higher in the lifelong proteins of cataract lenses than in age-matched normal lenses.* AGE, 2011. **33**(2): p. 131-141.
118. Masters, P.M., J.L. Bada, and J. Samuel Zigler, *Aspartic acid racemisation in the human lens during ageing and in cataract formation.* Nature, 1977. **268**(5615): p. 71-73.
119. Fujii, N., L.J. Takemoto, S. Matsumoto, K. Hiroki, D. Boyle, and M. Akaboshi, *Comparison of aspartic acid content in alpha A-crystallin from normal and age-matched cataractous human lenses.* Biochem. Biophys. Res. Commun., 2000. **278**(2): p. 408-413.
120. Lowenson, J. and S. Clarke, *Does the chemical instability of aspartyl and asparaginyl residues in proteins contribute to erythrocyte aging? The role of protein carboxyl methylation reactions.* Blood Cells, 1988. **14**(1): p. 103-117.
121. Helfman, P.M., J.L. Bada, and M.Y. Shou, *Considerations on the role of aspartic acid racemization in the aging process.* Gerontology, 1977. **23**(6): p. 419-425.
122. Fujii, N., K. Satoh, K. Harada, and Y. Ishibashi, *Simultaneous stereoinversion and isomerization at specific aspartic acid residues in αA-crystallin from human lens.* J. Biochem., 1994. **116**: p. 663-9.
123. Groenen, P.J.T.A., M.J.P. van Dongen, C.E.M. Voorter, H. Bloemendal, and W.W. de Jong, *Age-dependent deamidation of alpha B-crystallin.* FEBS Letters, 1993. **322**(1): p. 69-72.
124. Radkiewicz, J.L., H. Zipse, S. Clarke, and K.N. Houk, *Accelerated racemization of aspartic acid and asparagine residues via succinimide intermediates: An ab initio theoretical exploration of mechanism.* J. Am. Chem. Soc., 1996. **118**(38): p. 9148-9155.
125. Voorter, C.E., W.A. de Haard-Hoekman, P.J. van den Oetelaar, H. Bloemendal, and W.W. de Jong, *Spontaneous peptide bond cleavage in aging alpha-crystallin through a succinimide intermediate.* J. Biol. Chem., 1988. **263**(35): p. 19020-19023.
126. Srivastava, O.P. and K. Srivastava, *beta B2-crystallin undergoes extensive truncation during aging in human lenses.* Biochem. Biophys. Res. Commun, 2003. **301**(1): p. 44-49.
127. Srivastava, O.P., *Truncation of lens crystallins.* Invest Ophthalmol Vis Sci., 2000. **41**(4): p. I10-I10.
128. Santhoshkumar, P., P. Udupa, R. Murugesan, and K.K. Sharma, *Significance of Interactions of low molecular weight crystallin fragments in lens aging and cataract formation.* J. Biol. Chem., 2008. **283**: p. 8477-8485.

129. Takemoto, L. and S. Gopalakrishnan, *Alpha-A crystallin: quantitation of C-terminal modification during lens aging.* Curr Eye Res, 1994. **13**(12): p. 879-83.
130. Scharf, J., A. Dovrat, and M. Nahir, *Localization of denatured enzyme molecules in rat lenses.* Br J Exp Pathol, 1988. **69**(3): p. 339-43.
131. Truscott, R.J.W. and X. Zhu, *Prog Retin Eye Res.* Progress in Retinal and Eye Research, 2010. **29**(6): p. 487-499.
132. Lampi, K.J., J.T. Oxford, H.P. Bachinger, T.R. Shearer, L.L. David, and D.M. Kapfer, *Deamidation of human βB1 alters the elongated structure of the dimer.* Exp. Eye Res. , 2001. **72**(3): p. 279-288.
133. Kelley, M.J., L.L. David, N. Iwasaki, J. Wright, and T.R. Shearer, *α-Crystallin chaperone activity is reduced by calpain II in vitro and in selenite cataract.* J. Biol. Chem., 1993. **268**(25): p. 18844-18849.
134. Feng, J., D.L. Smith, and J.B. Smith, *Human lens β-crystallin solubility.* J Biol Chem, 2000. **275**(16): p. 11585-11590.
135. Takemoto, L. and T. Emmons, *Age-dependent deamidation of the major intrinsic polypeptide from lens membranes.* Curr Eye Res, 1991. **10**(9): p. 865-9.
136. De, J.W.W., K.F.S.M. Van, and H. Bloemendal, *Intracellular carboxy-terminal degradation of the αA chain of α-crystallin.* Eur. J. Biochem., 1974. **48**: p. 271-6.
137. Van, K.F.S.M., W. Willems-Thijssen, and H.J. Hoenders, *Intracellular degradation and deamidation of α-crystallin subunits.* Eur. J. Biochem., 1976. **66**: p. 477-83.
138. Lyons, B., J. Jamie, and R. Truscott, *Spontaneous cleavage of proteins at serine residues.* Int. J. Pept. Res. Ther. , 2011. **17**(2): p. 1-5.
139. Robinson, A.B., *Evolution and the distribution of glutaminyl and asparaginyl residues in proteins.* Proc. Nat. Acad. Sci. U. S. A., 1974. **71**: p. 885-88.
140. Harding, J.J., *Nonenzymic covalent posttranslational modification of proteins in vivo.* Adv. Protein Chem., 1985. **37**: p. 247-334.
141. Miesbauer, L.R., X. Zhou, Z. Yang, Y. Sun, D.L. Smith, and J.B. Smith, *Post-translational modifications of water-soluble human lens crystallins from young adults.* J. Biol. Chem., 1994. **269**(17): p. 12494-12502.
142. Kamei, A., T. Hamaguchi, N. Matsuura, and K. Masuda, *Does post-translational modification influence chaperone-like activity of α-crystallin? Study on phosphorylation.* Biol. Pharm. Bull., 2001. **24**: p. 96-99.
143. Van, B.M.A.M., S.E.A. Hoogakker, J.J. Harding, and J.W.W. De, *The influence of some post-translational modifications on the chaperone-like activity of α-crystallin.* Ophthalmic Res., 1996. **28**: p. 32-38.
144. Huang, C.-H., Y.-T. Wang, C.-F. Tsai, Y.-J. Chen, J.-S. Lee, and S.-H. Chiou, *Phosphoproteomics characterization of novel phosphorylated sites of lens proteins from normal and cataractous human eye lenses.* Mol. Vision, 2011. **17**: p. 186-198.
145. Giblin, F.J., *Glutathione: a vital lens antioxidant.* J. Ocul. Pharmacol. Ther., 2000. **16**: p. 121-135.
146. Reddy, V.N., *Glutathione and its function in the lens - an overview.* Exp. Eye Res., 1990. **50**: p. 771-8.
147. Shang, F., M. Lu, E. Dudek, J. Reddan, and A. Taylor, *Vitamin C and vitamin E restore the resistance of GSH-depleted lens cells to H2O2.* Free Radic Biol Med, 2003. **34**(5): p. 521-30.
148. Graham, K.S., C.C. Reddy, and R.W. Scholz, *Reduced glutathione effects on α-tocopherol concentration of rat liver microsomes undergoing NADPH-dependent lipid peroxidation.* Lipids, 1989. **24**(11): p. 909-914.
149. Harding, J.J., *Free and protein-bound glutathione in normal and cataractous human lenses.* Biochem. J., 1970. **117**: p. 957-60.
150. Boscia, F., I. Grattagliano, G. Vendemiale, T. Micelli-Ferrari, and E. Altomare, *Protein oxidation and lens opacity in humans.* Invest Ophthalmol Vis Sci, 2000. **41**: p. 2461-5.

151. Truscott, R.J.W., *Age-related nuclear cataract-oxidation is the key.* Exp. Eye Res., 2005. **80**: p. 709-725.
152. Varma, S.D., P.S. Devamanoharan, and S.M. Morris, *Prevention of cataracts by nutritional and metabolic antioxidants.* Crit. Rev. Food Sci. Nutr., 1995. **35**: p. 111-29.
153. Truscott, R.J. and R.C. Augusteyn, *The state of sulphydryl groups in normal and cataractous human lenses.* Exp Eye Res, 1977. **25**: p. 139-48.
154. Truscott, R.J.W. and R.C. Augusteyn, *Changes in human lens proteins during nuclear cataract formation.* Exp. Eye Res., 1977. **24**: p. 159-70.
155. Cheng, R., B. Lin, and B.J. Ortwerth, *Rate of formation of AGEs during ascorbate glycation and during aging in human lens tissue.* Biochim. Biophys. Acta, Mol. Basis Dis., 2002. **1587**: p. 65-74.
156. Linetsky, M., E. Shipova, R. Cheng, and B.J. Ortwerth, *Glycation by ascorbic acid oxidation products leads to the aggregation of lens proteins.* Biochim. Biophys. Acta, , 2008. **1782**: p. 22-34.
157. Ortwerth, B.J. and P.R. Olesen, *Ascorbic acid-induced crosslinking of lens proteins: evidence supporting a maillard reaction.* Biochim. Biophys. Acta, Protein Struct. Mol. Enzymol., 1988. **956**: p. 10-22.
158. Coghlan, S.D. and R.C. Augusteyn, *Changes in the distribution of proteins in the aging human lens.* Exp. Eye Res., 1977. **25**: p. 603-11.
159. Ecroyd, H. and J.A. Carver, *Crystallin proteins and amyloid fibrils.* Cell. Mol. Life Sci., 2009. **66**: p. 62-81.
160. Horwitz, J., T. Emmons, and L. Takemoto, *The ability of lens alpha crystallin to protect against heat-induced aggregation is age-dependent.* Curr Eye Res, 1992. **11**(8): p. 817-22.
161. Parker, N.R., A. Korlimbinis, J.F. Jamie, M.J. Davies, and R.J. Truscott, *Reversible binding of kynurenine to lens proteins: potential protection by glutathione in young lenses.* Invest Ophthalmol Vis Sci, 2007. **48**(8): p. 3705-13.
162. Taylor, L.M., A.J. Andrew, J.F. Jamie, and R.J.W. Truscott, *UV Filter Instability: Consequences for the Human Lens.* Exp. Eye Res., 2002. **75**: p. 165-175.
163. Aquilina, J.A., J.A. Carver, and R.J. Truscott, *Polypeptide modification and cross-linking by oxidized 3-hydroxykynurenine.* Biochemistry, 2000. **39**: p. 16176-84.
164. Stutchbury, G.M. and R.J.W. Truscott, *The modification of proteins by 3-hydroxykynurenine.* Exp. Eye Res., 1993. **57**: p. 149-55.
165. Korlimbinis, A., P.G. Hains, R.J. Truscott, and J.A. Aquilina, *3-Hydroxykynurenine oxidizes alpha-crystallin: potential role in cataractogenesis.* Biochemistry, 2006. **45**(6): p. 1852-60.
166. Hains, P.G., M.F. Simpanya, F. Giblin, and R.J. Truscott, *UV filters in the lens of the thirteen lined ground squirrel (Spermophilus tridecemlineatus).* Exp Eye Res, 2006. **82**(4): p. 730-7.
167. Duane, *Normal values of the accommodation at all ages.* J. Am. Med. Assoc, 1912. **59**: p. 3.
168. Truscott, R.J., *Presbyopia. Emerging from a blur towards an understanding of the molecular basis for this most common eye condition.* Exp. Eye Res., 2009. **88**: p. 241-247.
169. Harocopos, G.J., Y.-B. Shui, M. McKinnon, N.M. Holekamp, M.O. Gordon, and D.C. Beebe, *Importance of vitreous liquefaction in age-related cataract.* Invest Ophthalmol Vis Sci, 2004. **45**: p. 77-85.
170. Heys, K.R., S.L. Cram, and R.J.W. Truscott, *Massive increase in the stiffness of the human lens nucleus with age: the basis for presbyopia?* Mol Vis, 2004. **10**: p. 956-63.
171. Glasser, A. and M.C. Campbell, *Presbyopia and the optical changes in the human crystalline lens with age.* Vision Res, 1998. **38**: p. 209-29.
172. Koretz, J.F. and G.H. Handelman, *How the human eye focuses.* Sci Am, 1988. **259**: p. 92-9.
173. Roy, D. and A. Spector, *Absence of low-molecular-weight alpha crystallin in nuclear region of old human lenses.* Proc. Natl. Acad. Sci. U. S. A., 1976. **73**: p. 3484-7.
174. Sheppard, A.L. and L.N. Davies, *In vivo analysis of ciliary muscle morphologic changes with accommodation and axial ametropia.* Invest Ophthalmol Vis Sci, 2011. **51**(12): p. 6882-9.

175. Schwartz, B., *Enviromental temperature and the occular temperature gradient.* Arch Ophthalmol, 1965. **74**: p. 237-43.
176. Miranda, M.N., *The geographic factor in the onset of presbyopia.* Trans Am Ophthalmol Soc, 1979. **77**: p. 603-21.
177. Sweeney, M.H.J. and R.J.W. Truscott, *An impediment to glutathione diffusion in older normal human lenses: a possible precondition for nuclear cataract.* Exp. Eye Res., 1998. **67**: p. 587-595.
178. Moffat, B.A., K.A. Landman, R.J.W. Truscott, M.H.J. Sweeney, and J.M. Pope, *Age-related changes in the kinetics of water transport in normal human lenses.* Exp. Eye Res., 1999. **69**: p. 663-669.
179. Young, R.W., *Age-Related cataract.* New York : Oxford University Press, 1991.
180. Chylack, L.T., Jr., J.K. Wolfe, D.M. Singer, M.C. Leske, M.A. Bullimore, I.L. Bailey, J. Friend, D. McCarthy, and S.Y. Wu, *The Lens Opacities Classification System III. The Longitudinal Study of Cataract Study Group.* Arch Ophthalmol, 1993. **111**(6): p. 831-6.
181. Sparrow, J.M., A.J. Bron, N.A. Brown, W. Ayliffe, and A.R. Hill, *The Oxford Clinical Cataract Classification and Grading System.* International Ophthalmology, 1986. **9**(4): p. 207-25.
182. Pirie, A., *Color and solubility of the proteins of human cataracts.* Invest Ophthalmol Vis Sci., 1968. **7**(6): p. 634-650.
183. McCarty, C.A., B.N. Mukesh, C.L. Fu, and H.R. Taylor, *The epidemiology of cataract in Australia.* Am J Ophthalmol, 1999. **128**: p. 446-65.
184. Taylor, H.R., *Eye care for the future: the Weisenfeld lecture.* Invest Ophthalmol Vis Sci, 2003. **44**: p. 1413-8.
185. Harding, J.J. and H.R. van, *Drugs, including alcohol, that act as risk factors for cataract, and possible protection against cataract by aspirin-like analgesics and cyclopenthiazide.* Br J Ophthalmol, 1988. **72**: p. 809-14.
186. Minassian, D.C., P. Rosen, J.K. Dart, A. Reidy, P. Desai, M. Sidhu, S. Kaushal, and N. Wingate, *Extracapsular cataract extraction compared with small incision surgery by phacoemulsification: a randomised trial.* Br J Ophthalmol, 2001. **85**(7): p. 822-9.
187. Su, S.P., J.D. McArthur, and J.A. Aquilina, *Localization of low molecular weight crystallin peptides in the aging human lens using a MALDI mass spectrometry imaging approach.* Exp Eye Res, 2010. **91**(1): p. 97-103.
188. Gouras, P. and B. Ekesten, *Why do mice have ultra-violet vision?* Exp Eye Res, 2004. **79**(6): p. 887-892.
189. Thomas, M.R. and E.K. O'Shea, *An intracellular phosphate buffer filters transient fluctuations in extracellular phosphate levels.* Proceedings of the National Academy of Sciences of the United States of America, 2005. **102**(27): p. 9565-70.
190. Cohen, L. and A. Gusev, *Small molecule analysis by MALDI mass spectrometry.* Anal. Bioanal. Chem., 2002. **373**(7): p. 571-586.
191. Goodlett, D.R., P.A. Abuaf, P.A. Savage, K.A. Kowalski, T.K. Mukherjee, J.W. Tolan, N. Corkum, G. Goldstein, and J.B. Crowther, *Peptide chiral purity determination: hydrolysis in deuterated acid, derivatization with Marfey's reagent and analysis using high-performance liquid chromatography-electrospray ionization-mass spectrometry.* J. Chromatogr., A, 1995. **707**(2): p. 233-244.
192. Piotto, M., V. Saudek, and V. Sklenář, *Gradient-tailored excitation for single-quantum NMR spectroscopy of aqueous solutions.* J. Biomol. NMR, 1992. **2**(6): p. 661-665.
193. Hains, P.G. and R.J. Truscott, *Age-dependent deamidation of lifelong proteins in the human lens.* Invest Ophthalmol Vis Sci, 2010. **51**(6): p. 3107-14.
194. Robinson, N.E. and A.B. Robinson, *Deamidation of human proteins.* Proc. Natl. Acad. Sci. U. S. A., 2001. **98**(22): p. 12409-12413.
195. Wilmarth, P.A., S. Tanner, S. Dasari, S.R. Nagalla, M.A. Riviere, V. Bafna, P.A. Pevzner, and L.L. David, *Age-related changes in human crystallins determined from comparative analysis*

of post-translational modifications in young and aged lens: does deamidation contribute to crystallin insolubility? J. Proteome Res., 2006. **5**(10): p. 2554-66.
196. Takemoto, L.J., *Identification of the in vivo truncation sites at the C-terminal region of alpha-A crystallin from aged bovine and human lens.* Curr Eye Res, 1995. **14**(9): p. 837-41.
197. Harrington, V., S. McCall, S. Huynh, K. Srivastava, and O. Srivastava, *Crystallins in water soluble-high molecular weight protein fractions and water insoluble protein fractions in aging and cataractous human lenses.* Mol Vis, 2004. **10**(61): p. 476-489.
198. Su, S.P., B. Lyons, M. Friedrich, J.D. McArthur, X. Song, D. Xavier, J.A. Aquilina, and R.J. Truscott, *Molecular signatures of long-lived proteins: Autolytic cleavage adjacent to serine residues.* Aging Cell, 2012. **10.1111/j.1474-9726.2012.00860.x [doi]**.
199. Scharf, J., A. Dovrat, and D. Gershon, *Defective superoxide-dismutase molecules accumulate with age in human lenses.* Graefes Arch Clin Exp Ophthalmol, 1987. **225**(2): p. 133-6.
200. Clarke, S., *Propensity for spontaneous succinimide formation from aspartyl and asparaginyl residues in cellular proteins.* Int. J. Pept. Protein Res., 1987. **30**(6): p. 808-821.
201. Mills, K.V. and H. Paulus, *Biochemical mechanisms of intein-mediated protein splicing.* Nucleic Acids Mol. Biol., 2005. **16**: p. 233-255.
202. Ueno, K., T. Ueda, K. Sakai, Y. Abe, N. Hamasaki, M. Okamoto, and T. Imoto, *Evidence for a novel racemization process of an asparaginyl residue in mouse lysozyme under physiological conditions.* Cell Mol Life Sci, 2005. **62**(2): p. 199-205.
203. Ebbers, E.J., G.J.A. Ariaans, J.P.M. Houbiers, A. Bruggink, and B. Zwanenburg, *Controlled racemization of optically active organic compounds: prospects for asymmetric transformation.* Tetrahedron, 1997. **53**(.): p. 9417-9476.
204. Linetsky, M., J.M.W. Hill, R.D. LeGrand, and F. Hu, *Dehydroalanine crosslinks in human lens.* Exp. Eye Res., 2004. **79**: p. 499-512.
205. Hooi, M.Y.S., M.J. Raftery, and R.J.W. Truscott, *Age-dependent racemization of serine residues in a human chaperone protein.* Protein Science, 2013. **22**(1): p. 93-100.
206. Braun, N., M. Zacharias, J. Peschek, A. Kastenmuller, J. Zou, M. Hanzlik, M. Haslbeck, J. Rappsilber, J. Buchner, and S. Weinkauf, *Multiple molecular architectures of the eye lens chaperone alphaB-crystallin elucidated by a triple hybrid approach.* Proceedings of the National Academy of Sciences of the United States of America, 2011. **108**(51): p. 20491-6.
207. Johansson, D.G.A., G. Wallin, A. Sandberg, B. Macao, J. Aqvist, and T. Hard, *Protein autoproteolysis: Conformational strain linked to the rate of peptide cleavage by the pH dependence of the N-O-acyl shift reaction.* J. Am. Chem. Soc., 2009. **131**(27): p. 9475-9477.
208. Cuervo, A.M. and J.F. Dice, *When lysosomes get old.* Exp Geront, 2000. **35**(2): p. 119-131.
209. Luzio, J.P., P.R. Pryor, and N.A. Bright, *Lysosomes: fusion and function.* Nat Rev Mol Cell Biol, 2007. **8**(8): p. 622-632.
210. Sudhakar Reddy, G., G. Vanita Reddy, and G. Gill Smith, *The effect of Ni(II), Zn(II), Cu(II), Co(II) and Pd(II) ions on racemisation of hydroxy α amino acids.* Inorganica Chimica Acta, 1989. **166**(1): p. 55-58.
211. Erie, J.C., J.A. Butz, J.A. Good, E.A. Erie, M.F. Burritt, and J.D. Cameron, *Heavy metal concentrations in human eyes.* Am J Ophthalmol, 2005. **139**(5): p. 888-893.
212. Cozzone, A.J., *Post-translational modification of proteins by reversible phosphorylation in prokaryotes.* Biochimie, 1998. **80**(1): p. 43-48.
213. Schey, K.L. and Z. Wang, *Thioether modifications at phosphorylation sites in aged human lens proteins*, in *ARVO 2012*. 2012.
214. Linetsky, M. and R.D. LeGrand, *Glutathionylation of lens proteins through the formation of thioether bond.* Mol. Cell. Biochem., 2005. **272**: p. 133-144.
215. Byford, M.F., *Rapid and selective modification of phosphoserine residues catalysed by Ba2+ ions for their detection during peptide microsequencing.* Biochem J, 1991. **280 (Pt 1)**: p. 261-5.

216. Biernat, J. and E.-M. Mandelkow, *The Development of Cell Processes Induced by tau Protein Requires Phosphorylation of Serine 262 and 356 in the Repeat Domain and Is Inhibited by Phosphorylation in the Proline-rich Domains.* Mol. Biol. Cell, 1999. **10**(3): p. 727-740.
217. MacCoss, M.J., W.H. McDonald, A. Saraf, R. Sadygov, J.M. Clark, J.J. Tasto, K.L. Gould, D. Wolters, M. Washburn, A. Weiss, J.I. Clark, and J.R. Yates, 3rd, *Shotgun identification of protein modifications from protein complexes and lens tissue.* Proc Natl Acad Sci U S A, 2002. **99**(12): p. 7900-5.
218. Kato, K., Y. Inaguma, H. Ito, K. Iida, I. Iwamoto, K. Kamei, N. Ochi, H. Ohta, and M. Kishikawa, *Ser-59 is the major phosphorylation site in alphaB-crystallin accumulated in the brains of patients with Alexander's disease.* J Neurochem, 2001. **76**(3): p. 730-6.
219. Younis, I.R., M. Elliott, C.J. Peer, A.J.L. Cooper, J.T. Pinto, G.W. Konat, M. Kraszpulski, W.P. Petros, and P.S. Callery, *Dehydroalanine analog of glutathione: An electrophilic busulfan metabolite that binds to human glutathione S-transferase A1-1.* J. Pharmacol. Exp. Ther., 2008. **327**(3): p. 770-776.
220. Jones, G.P., D.E. Rivett, and D.J. Tucker, *The reaction of biogenic amines with proteins.* J. Sci. Food Agric., 1981. **32**(8): p. 805-812.
221. Zanuy, D., J. Casanovas, and C. Alemán, *The conformation of dehydroalanine in short homopeptides: molecular dynamics simulations of a 6-residue chain.* Biophys. Chem., 2002. **98**(3): p. 301-312.
222. Cloos, P.A.C. and A.L. Jensen, *Age-related de-phosphorylation of proteins in dentin: A biological tool for assessment of protein age.* Biogerontology, 2000. **1**(4): p. 341-356.
223. Masters, P.M., *In vivo decomposition of phosphoserine and serine in noncollagenous protein from human dentin.* Calcif Tissue Int, 1985. **37**(3): p. 236-41.
224. Schey, K.L., L.E. Ball, R.K. Crouch, and D.L. Garland, *The distribution of phosphorylated and posttranslationally modified aquaporin 0 within the normal human lens.* Invest. Ophthalmol. Vis. Sci., 2003. **44**(5): p. 4483-.
225. Huang, C.H., Y.T. Wang, C.F. Tsai, Y.J. Chen, J.S. Lee, and S.H. Chiou, *Phosphoproteomics characterization of novel phosphorylated sites of lens proteins from normal and cataractous human eye lenses.* Mol. Vis., 2011. **17**: p. 186-198.
226. Shapira, R., K.D. Wilkinson, and G. Shapira, *Racemization of individual aspartate residues in human myelin basic protein.* J Neurochem, 1988. **50**(2): p. 649-54.
227. Savas, J.N., B.H. Toyama, T. Xu, J.R. Yates, and M.W. Hetzer, *Extremely long-lived nuclear pore proteins in the rat brain.* Science. **335**(6071): p. 942.
228. McCudden, C.R. and V.B. Kraus, *Biochemistry of amino acid racemization and clinical application to musculoskeletal disease.* Clin Biochem, 2006. **39**(12): p. 1112-30.
229. Hooi, M.Y. and R.J. Truscott, *Racemisation and human cataract. D-Ser, D-Asp/Asn and D-Thr are higher in the lifelong proteins of cataract lenses than in age-matched normal lenses.* Age 2010. **DOI 10.1007/s11357-010-9171-7**.
230. Powell, J.T., N. Vine, and M. Crossman, *On the accumulation of D-aspartate in elastin and other proteins of the ageing aorta.* Atherosclerosis, 1992. **97**(2-3): p. 201-208.
231. Charlton, J.M. and R. Van Heyningen, *Glucose 6-phosphate dehydrogenase in the mammalian lens.* Exp. Eye Res., 1971. **11**: p. 147-60.
232. Alcala, J., M. Katar, G. Rudner, and H. Maisel, *Human beta crystallins: regional and age related changes.* Curr. Eye Res., 1988. **7**: p. 353-9.
233. Shih, M., K.J. Lampi, T.R. Shearer, and L.L. David, *Cleavage of β-crystallins during maturation of bovine lens.* Mol. Vision, 1998. **4**: p. No pp. given Article 4.
234. Berbers, G.A.M., W.A. Hoekman, H. Bloemendal, J.W.W. De, T. Kleinschmidt, and G. Braunitzer, *Homology between the primary structures of the major bovine β-crystallin chains.* Eur. J. Biochem., 1984. **139**: p. 467-79.

235. Radzicka, A. and R. Wolfenden, *Rates of uncatalyzed peptide bond hydrolysis in neutral solution and the transition state affinities of proteases.* J. Am. Chem. Soc., 1996. **118**: p. 6105-6109.
236. Goolcharran, C. and R.T. Borchardt, *Kinetics of diketopiperazine formation using model peptides.* J. Pharm. Sci., 1998. **87**: p. 283-288.
237. Skwierczynski, R.D. and K.A. Connors, *Demethylation kinetics of aspartame and L-phenylalanine methyl ester in aqueous solution.* Pharm. Res., 1993. **10**: p. 1174-80.
238. Purdie, J.E. and N.L. Benoiton, *Piperazinedione formation from esters of dipeptides containing glycine, alanine, and sarcosine. Kinetics in aqueous solution.* J. Chem. Soc., Perkin Trans. 2, 1973: p. 1845-52.
239. Capasso, S., A. Vergara, and L. Mazzarella, *Mechanism of 2,5-Dioxopiperazine formation.* J. Am. Chem. Soc., 1998. **120**: p. 1990-1995.
240. Lundquist, J.T.I.V. and J.C. Pelletier, *Improved solid-phase peptide synthesis method utilizing α-azide-protected amino acids.* Org. Lett., 2001. **3**: p. 781-783.
241. Borsuk, K., D.F.L. Van, I.F. Eggen, K.P.B.W. Ten, A. Petersen, and F.P.J.T. Rutjes, *Application of substituted 2-(trimethylsilyl)ethyl esters to suppress diketopiperazine formation.* Tetrahedron Lett., 2004. **45**: p. 3585-3588.
242. Straub, J.A., A. Akiyama, P. Parmar, and G.F. Musso, *Chemical pathways of degradation of the bradykinin analog, RMP-7.* Pharm. Res., 1995. **12**: p. 305-8.
243. Gu, L. and R.G. Strickley, *Diketopiperazine formation, hydrolysis, and epimerization of the new dipeptide angiotensin-converting enzyme inhibitor RS-10085.* Pharm. Res., 1987. **4**: p. 392-7.
244. Battersby, J.E., W.S. Hancock, E. Canova-Davis, J. Oeswein, and B. O'Connor, *Diketopiperazine formation and N-terminal degradation in recombinant human growth hormone.* Int. J. Pept. Protein Res., 1994. **44**: p. 215-22.
245. Chaves, J.M., K. Srivastava, R. Gupta, and O.P. Srivastava, *Structural and functional roles of deamidation and/or truncation of N- or C-termini in human alpha A-Crystallin.* Biochemistry, 2008. **47**(38): p. 10069-10083.
246. Gill, M.S., A.A. Neverov, and R.S. Brown, *Dissection of nucleophilic and general base roles for the reaction of phosphate with p-nitrophenyl thiolacetate, p-nitrophenyl thiolformate, and phenyl thiolacetate.* J Org Chem, 1997. **62**(21): p. 7351-7357.
247. Good, N.E., G.D. Winget, W. Winter, T.N. Connolly, S. Izawa, and R.M. Singh, *Hydrogen ion buffers for biological research.* Biochemistry, 1966. **5**(2): p. 467-77.
248. Ferguson, W.J., K.I. Braunschweiger, W.R. Braunschweiger, J.R. Smith, J.J. McCormick, C.C. Wasmann, N.P. Jarvis, D.H. Bell, and N.E. Good, *Hydrogen ion buffers for biological research.* Anal. Biochem., 1980. **104**(2): p. 300-310.
249. Steinberg, S.M. and J.L. Bada, *Peptide decomposition in the neutral pH region via the formation of diketopiperazines.* J. Org. Chem., 1983. **48**(13): p. 2295-2298.
250. Sepetov, N.F., M.A. Krymsky, M.V. Ovchinnikov, Z.D. Bespalova, O.L. Isakova, M. Soucek, and M. Lebl, *Rearrangement, racemization and decomposition of peptides in aqueous solution.* Pept Res, 1991. **4**: p. 308-13.
251. Goolcharran, C., J.L. Cleland, R. Keck, A.J.S. Jones, and R.T. Borchardt, *Comparison of the rates of deamidation, diketopiperazine formation, and oxidation in recombinant human vascular endothelial growth factor and model peptides.* PharmSci, 2000. **2**(1): p. No pp. given.
252. Smith, G.G. and T. Sivakua, *Mechanism of the racemization of amino acids. Kinetics of racemization of arylglycines.* J. Org. Chem., 1983. **48**(5): p. 627-634.
253. Friedman, M., *Chemistry, nutrition, and microbiology of D-amino acids.* J. Agric. Food Chem., 1999. **47**(9): p. 3457-3479.
254. Hayashi, R. and I. Kameda, *Decreased proteolysis of alkali-treated protein: Consequences of racemisation in food processing.* J. Food Sci., 1980. **45**(5): p. 1430-1431.

255. Shen, S.-j., H.G. Floss, H. Kumagai, H. Yamada, N.E.K. Soda, S.A. Wasserman, and C. Walsh, *Mechanism of pyridoxal phosphate-dependent enzymatic amino-acid racemization.* Journal of the Chemical Society, Chemical Communications, 1983. **0**(2): p. 82-83.
256. Floros, J.D., H.Y. Wetzstein, and M.S. Chinnan, *Chemical (NaOH) peeling as viewed by scanning electron microscopy: pimiento peppers as a case study.* J. Food Sci., 1987. **52**(5): p. 1312-1316.
257. Masters Patricia, M. and M. Friedman, *Amino acid racemization in alkali-treated food proteins*, in *Chemical Deterioration of Proteins*. 1980, AMERICAN CHEMICAL SOCIETY. p. 165-194.
258. Friebe, S., B. Hartrodt, K. Neubert, and G.J. Krauss, *High-performance liquid chromatographic separation of cis-trans isomers of proline-containing peptides. II.Fractionation in different cyclodextrin systems.* J. Chromatogr., A, 1994. **661**(1-2): p. 7-12.
259. Grathwohl, C. and K. Wuethrich, *NMR studies of the rates of proline cis-trans isomerization in oligopeptides.* Biopolymers, 1981. **20**(12): p. 2623-33.
260. Stewart, W.E. and T.H. Siddall, III, *Nuclear magnetic resonance studies of amides.* Chem. Rev., 1970. **70**(5): p. 517-51.
261. Lu, K.P., G. Finn, T.H. Lee, and L.K. Nicholson, *Prolyl cis-trans isomerization as a molecular timer.* Nat Chem Biol, 2007. **3**(10): p. 619-629.
262. Wüthrich, K., *NMR of Proteins and Nucleic acids.* Wiley New York, 1986.
263. Schubert, M., D. Labudde, H. Oschkinat, and P. Schmieder, *A software tool for the prediction of Xaa-Pro peptide bond conformations in proteins* J. Biomol. NMR, 2002. **24**(2): p. 149-154.
264. Howarth, O.W. and D.M. Lilley, *C-13 NMR of peptides and proteins.* Progr. NMR Spectr, 1978. **12**(1).
265. Biemann, K. and H.A. Scoble, *Characterization by tandem mass spectrometry of structural modifications in proteins.* Science, 1987. **237**(4818): p. 992-998.
266. Smith, E.L. and D.H. Spackman, *Leucine aminopeptidase.* J. Biol. Chem., 1955. **212**(1): p. 271-299.
267. Taylor, A., T. Surgenor, D.K.R. Thomson, R.J. Graham, and H. Oettgen, *Comparison of leucine aminopeptidase from human lens, beef lens and kidney, and hog lens and kidney.* Exp Eye Res., 1984. **38**(3): p. 217-229.
268. Beyer, E.C., G.M. Lipkind, J.W. Kyle, and V.M. Berthoud, *Structural organization of intercellular channels II. Amino terminal domain of the connexins: sequence, functional roles, and structure.* Biochim. Biophys. Acta, 2011. **1818**(8): p. 1823-1830.
269. Bada, J.L., *Amino acid racemization dating of fossil bones.* Annu. Rev. Earth Planet. Sci., 1985. **13**: p. 241-68.
270. Smith, G.G. and R.C. Evans. *The effect of structure and conditions on the rate of racemization of free and bound amino acids*. 1980: Wiley.
271. Paquet, A., W.C. Thresher, B.S. Harold, E. Swaisgood, and G.L. Catignani, *Syntheses and digestibility determination of some epimeric tripeptides occurring in dietary proteins.* Nutr. Res. (N. Y.), 1985. **5**(8): p. 891-901.
272. Tugyi, R., K. Uray, D. Ivan, E. Fellinger, A. Perkins, and F. Hudecz, *Partial d-amino acid substitution: Improved enzymatic stability and preserved Ab recognition of a MUC2 epitope peptide.* Proc. Natl. Acad. Sci. U. S. A., 2005. **102**(2): p. 413-418.
273. Powell, M., T. Stewart, L. Otvos, L. Urge, F. Gaeta, A. Sette, T. Arrhenius, D. Thomson, K. Soda, and S. Colon, *Peptide stability in drug development. II. Effect of single amino acid substitution and glycosylation on peptide reactivity in human serum.* Pharm. Res., 1993. **10**(9): p. 1268-1273.
274. Asano, Y., A. Nakazawa, Y. Kato, and K. Kondo, *Properties of a novel D-stereospecific aminopeptidase from Ochrobactrum anthropi.* J. Biol. Chem., 1989. **264**(24): p. 14233-14239.
275. Chondrogianni, N. and E.S. Gonos, *Proteasome dysfunction in mammalian aging: Steps and factors involved.* Exp Geront., 2005. **40**(12): p. 931-938.

276. Viteri, G., G. Carrard, I. Birlouez, E. Silva, and B. Friguet, *Age-dependent protein modifications and declining proteasome activity in the human lens.* Arch Biochem Biophys
2004. **427**(2): p. 197-203.
277. Yoshimoto, T., D. Tsuru, and R. Walter, *Proline-specific peptidases.* Wiss. Beitr. - Martin-Luther-Univ. Halle-Wittenberg, 1984. **46**: p. 194-217.
278. Mentlein, R., *Proline residues in the maturation and degradation of peptide hormones and neuropeptides.* FEBS Lett., 1988. **234**: p. 251-6.
279. Heymann, E. and R. Mentlein, *Complementary action of dipeptidyl peptidase IV and aminopeptidase M in the digestion of β-casein.* J. Dairy Res., 1986. **53**: p. 229-36.
280. Patton, C., S. Thompson, and D. Epel, *Some precautions in using chelators to buffer metals in biological solutions.* Cell Calcium, 2004. **35**: p. 427-431.
281. Fan, X., J. Zhang, M. Theves, C. Strauch, I. Nemet, X. Liu, J. Qian, F.J. Giblin, and V.M. Monnier, *Mechanism of lysine oxidation in human lens crystallins during aging and in diabetes.* J Biol Chem, 2009. **284**(50): p. 34618-27.
282. Heyningen R, V. *Glucoside of 3-hydroxykynurenine and other fluorescent compounds in the human lens*. 1973: Assoc. Sci. Publ.
283. Cooper, G.F. and J.G. Robson, *The yellow colour of the lens of man and other primates.* J Physiol, 1969. **203**(2): p. 411-7.
284. Zigman, S. and T. Paxhia, *The nature and properties of squirrel lens yellow pigment.* Exp Eye Res, 1988. **47**(6): p. 819-24.
285. Franz, N., L. Menin, and H.A. Klok, *A post-modification approach to peptide foldamers.* Org Biomol Chem, 2009. **7**(24): p. 5207-18.
286. Downard, K., *Mass Spectrometry: A Foundation Course*. 2004: Royal Society of Chemistry. 210 pp.
287. Beynon, J.H., G.R. Lester, and A.E. Williams, *Some specific molecular rearrangements in the mass spectra of organic compounds.* J. Phys. Chem., 1959. **63**(11): p. 1861-1868.
288. Wang, Y., L.-y. Gao, Y.-p. Wu, and L. Sun, *Analysis of six statins by electrospray ion trap mass spectrometry.* Zhipu Xuebao, 2010. **31**(6): p. 368-375.
289. Crotti, A.n.E.M., T. Fonseca, H. Hong, J. Staunton, S.r.E. Galembeck, N.P. Lopes, and P.J. Gates, *The fragmentation mechanism of five-membered lactones by electrospray ionisation tandem mass spectrometry.* Int. J. Mass Spectrom., 2004. **232**(3): p. 271-276.
290. Smith, R.M., *Neutral Losses and Ion Series*, in *Understanding mass spectra: A basic approach*. 2005, John Wiley & Sons, Inc. p. 121-149.
291. Silverstein, R.M., F.X. Webster, and D.J. Kiemle, *Spectrometric identification of organic compounds (7th Edition)*, John Wiley & Sons.
292. Vazquez, S., R.J.W. Truscott, R.A. J., A. Weimann, and M.M. Sheil, *A study of kynurenine fragmentation using electrospray tandem mass spectrometry.* J. Am. Soc. Mass Spectrom., 2001. **12**(7): p. 786-794.
293. Pretsch, E., P. Bühlmann, and M. Badertscher, *Structure determination of organic compounds - tables of spectral data (4th Edition)*, Springer - Verlag.
294. Cioli, S. and V. D'Arrigo, *Free amino acids in the normal and cataractous bovine and human lens capsule and lens.* Ophthalmologica, 1976. **173**(6): p. 505-12.
295. Brotzel, F., Y.C. Chu, and H. Mayr, *Nucleophilicities of primary and secondary amines in water.* J. Org. Chem., 2007. **72**(10): p. 3679-3688.
296. Palmieri, G., *Synthesis of enantiopure 2-hydroxybenzylamines by stereoselective reduction of 2-imidoylphenols. Application in the catalytic enantioselective addition of diethylzinc to aldehydes.* Eur. J. Org. Chem., 1999: p. 805-811.
297. Yang, H.J., W.H. Sun, Z.L. Li, and Z. Ma, *The rapid synthesis of Schiff-base without solvent under microwave irradiation.* Chin. Chem. Lett., 2002. **13**: p. 3-6.

298. Nugent, T.C. and M. El-Shazly, *Chiral amine synthesis. Recent developments and trends for enamide reduction, reductive amination, and imine reduction.* Adv. Synth. Catal., 2010. **352**: p. 753-819.
299. Truscott, R.J. and X. Zhu, *Presbyopia and cataract: a question of heat and time.* Prog Retin Eye Res, 2010. **29**(6): p. 487-99.